


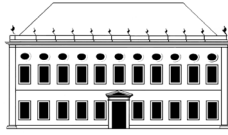
J. S. Redinha
J. da Providência
A. J. C. Varandas
Editors



Quantal Aspects
in Chemistry and Physics

*A tribute to the memory of
Professor Couceiro da Costa*

(Página deixada propositadamente em branco)



D O C U M E N T O S



COORDENAÇÃO EDITORIAL

Imprensa da Universidade de Coimbra
Email: imprensauc@ci.uc.pt
URL: http://www.uc.pt/imprensa_uc
Vendas online: <http://livrariadaimpresa.com>

CONCEPÇÃO GRÁFICA

António Barros

PAGINAÇÃO E PROGRAMAÇÃO (La)TeX

Pedro Caridade

IMPRESSÃO E ACABAMENTO

Publidis

ISBN

978-989-26-0094-9

ISBN Digital

978-989-26-0240-0

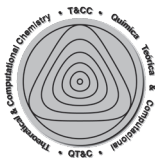
DOI

<http://dx.doi.org/10.14195/978-989-26-0240-0>

DEPÓSITO LEGAL


324861/11

OBRA PUBLICADA COM O APOIO DE:



Theoretical & Computational Chemistry
Universidade de Coimbra

J. S. Redinha
J. da Providência
A. J. C. Varandas
Editors



uantal Aspects
in Chemistry and Physics

A tribute to the memory of
Professor Couceiro da Costa

(Página deixada propositadamente em branco)



Alvin Karpis

(Página deixada propositadamente em branco)

CONTENTS

Forward	9
Honouring Professor Ruy Couceiro da Costa	
<i>E. R. de Arantes e Oliveira</i>	11
A homage to Professor Ruy Couceiro da Costa	
<i>H. S. C. Madeira</i>	13
Professor Couceiro da Costa: The pionner in the teaching of quantum chemistry in Portugal	
<i>J. Simões Redinha</i>	15
Spontaneous symmetry breaking in quantum physics	
<i>J. da Providência</i>	33
The interpretation of quantum mechanics revisited	
<i>Fernando M. S. Silva Fernandes</i>	45
Adiabatic approximation and related issues including topological implications	
<i>A. J. C. Varandas</i>	79

The quantum aspects of proteins and their biological function	
<i>H. G. Bohr</i>	133
Computational proteomics	
<i>Irina S. Moreira, Natercia F. Bras, Alexandra T. P. Carvalho, Nuno M. F. S. A. Cerqueira, Daniel F. Dourado, Marta A. S. Perez, Antonio J. M. Ribeiro, Sergio F. Sousa, Pedro A. Fernandes, and Maria J. Ramos</i>	181
Computational thermochemistry: Accurate estimation and prediction of molecular thermochemical parameters	
<i>Victor M. F. Morais</i>	221
Creating metamaterials at the nano-scale	
<i>J. M. Pacheco and C. L. Reis</i>	257

FORWARD

Some professors left their names intimately associated to the progress of their Schools. Due to their intelligence, exceptional human qualities and devotion to science, as well as deep insight on the role of the latter in future developments, they became reference personalities for future generations. In this context, it is a pleasure to remember Couceiro da Costa, an outstanding professor of Chemistry at the University of Coimbra from 1920 to 1955.

When Couceiro da Costa joined the university, science in Portugal was plagued with many problems that hindered modernization: poor research centers, outdated installations, reduced teaching and research staff, and severe budget constraints. During eighteen years as Head of the Chemistry Department, he did a wonderful job hoping to overcome all such difficulties.

A committee of three Professors of the University of Coimbra and members of the Academia das Ciências de Lisboa, two of them former students of Couceiro da Costa (a chemist, J. S. Redinha, and a physicist, J. da Providência) as well as A. J. C. Varandas, Professor of Theoretical Chemistry, decided to embrace the initiative of organizing a meeting to honor the old master. They imagined that the most significant way of so doing would be by bringing together contemporary reknown scientists to discuss recent progress in a field that was once pioneered by him in Portugal. Entitled “Quantal Aspects in Chemistry and Physics” this meeting is hoped to bring his name before the younger generations, since quantum mechanics and statistical thermodynamics are about the two dearest topics among the ones that he cultivated. Only he could have had then the capacity to follow the development of such matters and be aware of their impact

in the scientific preparation of future university generations.

The meeting “Quantal Aspects in Chemistry and Physics” took place at the Academia das Ciências de Lisboa on the 27th of November, 2009. The invited lecturers are from chemistry, physics and mathematics departments of different Portuguese universities and from the Technical University of Denmark. Their lectures are compiled in the present volume.

The success of this initiative has only been possible owing to the goodwill and help of the president of the Academia das Ciências de Lisboa, Prof. Arantes e Oliveira who welcomed this initiative from its inception, the rector of the University of Coimbra, Prof. Seabra Santos for his encouragement, and the vice-Rector Prof. Henrique Madeira for his participation at the Meeting. Thanks are also due to the head of the Department of Chemistry of the University of Coimbra, Prof. Formosinho Simões. The organizing committee is also indebted to the speakers for their valuable contributions. A final word to acknowledge the editorial care of Dr. Pedro Caridade in the preparation of this volume. The Imprensa da Universidade de Coimbra is also thanked for the publication of the present proceedings.

The Editors

1. HONOURING PROFESSOR RUY COUCEIRO DA COSTA

E. R. de Arantes e Oliveira

Academia das Ciências de Lisboa, Portugal

Eminent Academicians

Ladies and Gentlemen

The idea of organizing a Symposium to pay tribute to Professor Ruy Couceiro da Costa, now long deceased, started with a group of members of our Academy from the University of Coimbra.

Prof. Couceiro da Costa, carried out his professional life in Coimbra, where he had the great merit of introducing very early the teaching in the University of subjects, such as classical and quantum statistical mechanics, nowadays quantum mechanics, and the theory of the chemical bond, which at that time were very recent topics.

He did this very early, both in terms of his brilliant university career, and in the actual evolution of the noble sciences which he cultivated. Quantal Aspects of Chemistry and Physics were, in fact, still little known within the international scientific community when he introduced them into those courses for which he was responsible.

Perhaps because he died young, Ruy Couceiro da Costa never came to be elected as a member of the Academy of Sciences. He left, however, a galaxy of former pupils who decided, in recognition of how much they owe to him, to propose this homage as a contribution to the programme of academic activities

of the Class of Sciences of the ACL in the current year of 2009.

The Symposium held today does not follow, either in the formal or real sense, the traditional practice in the Academies of recently elected full academicians praising their predecessors in the chairs which they will occupy. Nor should it be considered as an activity of the University of Coimbra carried out outside that institution.

Instead, this should be considered as a tribute to an unforgettable professor whose memory the prestige of the Coimbra nucleus in the heart of the Academy of Sciences of Lisbon has made it possible to honor at the national level.

This is all I intend to say and explain.

With that, I will now give the floor to the eminent Academician Professor Simões Redinha, in whom I wish to greet all those involved in the organization of this event, and with the certainty that this homage by remarkable pupils of such a distinguished master will merely go into more depth than my own feelings.

Prof. E. R. de Arantes e Oliveira

President of the Academy of Sciences of Lisbon

27th November 2009

2. A HOMAGE TO RUY COUCEIRO DA COSTA

H. S. C. Madeira

University of Coimbra, Portugal

“Yo soy yo y mi circunstancia”. In the words of Ortega y Gasset, if we look at the work and legacy of Professor Couceiro da Costa many decades after his departure, this implies that we understand his time and circumstances. Professor Couceiro da Costa was Professor of Chemistry in the University of Coimbra from 1925 to 1955. It is not hard to imagine the difficulties and material deficiencies for teaching and research in Chemistry in the first decades of last century. Whilst it is certain that Professor Couceiro da Costa contributed to resolve these material problems, particularly during the almost two decades in which he was Director of the Department of Chemistry, his greatest contribution, seen from this distance, is to have instilled in Coimbra the modern view of a University. He believed in Chemistry and Physics, and defended and practiced the view of the prime role of the creation of knowledge, through research and teaching of the most up-to-date problems, as the element which distinguishes the great Universities, while his action also contributed, through example, to the modernization of the University in other areas.

Time, the great evaluator, assures us that this belated tribute to Professor Couceiro da Costa is entirely fair and warranted. The Rectory of the University of Coimbra is pleased and proud to be associated with this initiative of the Academia de Ciências de Lisboa, proposed by three members of that illustrious Academy, all eminent Professors of the University of Coimbra: Professor José

Simões Redinha, Professor João da Providência and Professor António Varandas. The form used for this tribute, through a meeting of distinguished scientists to debate current problems of “Quantal Aspects in Chemistry and Physics”, subscribes to the attitude of modernity which Professor Couceiro da Costa cultivated, and which is seen as the great factor of progress through the scientific research at the vanguard of knowledge. The resulting production of this book, containing the communications presented and discussed in the meeting, provides the most long lasting form to pay tribute to Professor Couceiro da Costa, and to become aware of his pioneering role in the teaching of theoretical chemistry in Portugal.

It is always an act of greatness to recognize publicly the merit and contributions of others. However, it is also an act of humility, a clear manifestation, as we know that progress is a long chain of individual contributions. If looking back allows us to see clearly, as Professor Couceiro da Costa emphasized through his vision of a modern University which teaches and carries out research into the problems of its era, following his inspirational example it is good to look to the present and the future, and increasingly recognize at the appropriate time, the contributors who are around us. Science has, after all, through the peer group evaluation and recognition the guaranty of the quality of its results.

Prof. Henrique Santos do Carmo Madeira
Vice-Rector of the University of Coimbra

3. PROFESSOR COUCEIRO DA COSTA: THE PIONNER IN THE TEACHING OF QUANTUM CHEMISTRY IN PORTUGAL

J. Simões Redinha*

Department of Chemistry, University of Coimbra

3.1 Couceiro da Costa: The scientist

Ruy Gustavo Couceiro da Costa graduated in Physico-Chemical Sciences with high honours at the University of Coimbra in 1922. During his studies, he proved he had a bright mind with a special aptitude to science. In 1920, he was invited to join the chemical staff of the University of Coimbra as an assistant lecturer. Soon he displayed a propensity to interpret chemistry in both physical and mathematical grounds and an ability to delve deeply into scientific concepts. He was awarded his PhD in 1927 and in 1936 he was appointed professor of physical chemistry, a subject taught in the last year of the chemical graduate courses.

His PhD thesis was prepared in the *Chemical Physics Department of the Hydrological Institute of the College of France* and in the *Department of Chemistry of the University of Coimbra*. It deals with the analysis of gases emanated from Portuguese mineral water springs. Experimentation is the dominant feature of the work. Delicate glass blowing manipulations were involved to make the apparatus and devices used in the sampling, separation, identification and quantification of the components of the gaseous mixtures.

In those days, besides a thesis, the candidate for the doctorate degree had to propose three topics of chemistry and three of physics to be defended in

*Email address: jsredinha@netcabo.pt

the examination. The subjects chosen by Couceiro da Costa were theoretical open questions of utmost importance at the time. The pieces of work presented in his PhD examination showed immediately his scientific qualities: a talent to do experimental and theoretical research, a belief in both of these scientific approaches and his pleasure to undertake either of them. As an empiricist, he considered experiment the root of knowledge. Nevertheless he thought that generalisation could only be taken following a mathematical model as the inductive way. At the end of the lecture that he was invited to deliver on the commemoration of the 50th anniversary of the *Real Sociedad Española de Física y Química*, in 1953, he said: “The problems require quantitative solutions, otherwise we fall into the arbitrariness, which means the loss of prestige of theory.”

It is not common to find someone who so easily take off the ‘lab jack’ after finishing a fine experiment and held the slide rule – the calculation tool of the time – to establish the theoretical explanation for the results or devise a new theory for a subject, popular at the time.

At a glance, the publications of Couceiro da Costa, considering their dispersion throughout the analytical and physical chemistry fields, may appear as resulting from pure serendipity. This though would not be quite correct. Indeed, he had three aims in mind while planning his research: to rationalise concepts based on inadequate scientific grounds, to closely follow the frontiers reached by the progress of science or use science to serve the society, contributing to the progress of industry and human welfare. And, underlying these aims, were the concepts that teaching should result in the student receiving a solid and modern scientific preparation and the idea that the knowledge and university laboratories should be put at the service of the country that pays for them.

The application of thermodynamics to the study of the distillation and crystallisation of a two-components liquid mixtures and the theorization of the analytical titration procedures illustrate the first aim. In the former paper, $P - x$ and $T - x$ diagrams for liquid-vapor and liquid-solid binary systems were interpreted from the work performed by van't Hoff machines (a piston pump closed by a membrane permeable only to one of the components) in a thermodynamic cycle

formed by two isotherms and two adiabatic operations. The different types of theoretical diagrams explained the curves obtained from the experimental data.

The second paper referred to above deals with the theoretical interpretation of the volumetric techniques of the analytical chemistry. The analytical procedure is equated in terms of the equilibria occurring in solution and the properties with physical meaning are given by the derivatives of the deduced function in the different points of the titration.

The thixotropy of the vanadium pentoxide, published in 1934, is an up-to-date review of the colloidal state, in which he included research of his authorship. Colloids were known from Graham in 1860 who coined the name. However, until the end of the 19th century, colloidal solutions were considered as systems of enigmatic behavior compared with that of true solutions. The discovery of the role they played in aspects related with life, industry, etc., and the invention of new instruments increased the interest in this field. The research was initiated in inorganic colloids and was extended later to organic species. By the 1920s, about half of the papers submitted to *The Journal of Physical Chemistry* were related with the colloidal state. Between 1947 and 1951, this journal adopted the designation *The Journal of Physical and Colloid Chemistry*. It returned to the original name with the launching of periodicals especially dedicated to the matter. The work of Couceiro da Costa was of topical interest at the time.

Another evidence of his awareness about the recent acquisitions of science is the paper on the quantum mechanics in the prediction of chemical activity, published in 1954, after a conference given in Lisbon before the *Portuguese Chemical Society*.

During the period between the two world wars, great progress was achieved in theoretical organic chemistry. Famous chemists left their names linked to the electronic interpretation of the structure and reactions of organic compounds, especially in U.K. This scientific movement and the importance of the matter led to the appearance of a new discipline which was called "Physical Organic Chemistry" after the title of Hammett's monograph that was published in 1940.

Two British chemists gave impressive contributions for this success: Robert Robinson and C. K. Ingold. Ingold published his theory in vol. 5 of *The Chemical Reviews* (1934) in a paper entitled “The mechanism of an electronic theory of organic reactions”. This theory gave rise to a controversy that lasted for years. A heated debate with Robinson became famous because it was a struggle between two influential scientists. Ingold was accused of plagiarism of Robinson’s pioneering work published in 1926 in *Journal of the Chemical Society*.

The controversy abated and by 1939 Ingold’s ideas gained general acceptance. “Structure and mechanism in organic chemistry”, published by Ingold in 1953, one of the four hundred and forty three publications authored or coauthored by him, was a reference book for decades.

The paper of Couceiro da Costa addressed the prediction of reactions between hydrocarbons with nucleophilic, electrophilic and radical molecular groups. He used quantum mechanics as research method. The effects of resonance, orientation in substituted benzene compounds and π -complexes were discussed. The main aim of his work was to show the potentialities of the molecular orbital theory in predicting reactions. It is a modern piece of work, both in respect to the focused topic and the novelty of the method employed. To underline the power of the quantal methods in relation to the older electronic theories he added the remark that the success of Ingold and Robinson with so modest data available, as to the values for dipole moments and refractivities was only possible because both were gifted scientists.

Besides aspects of pure chemistry, Couceiro da Costa published some papers on the composition and the evolution of the physical properties of mineral waters with time. He did very fine work on the trace analysis of metals using colorimetry, absorption spectrophotometry and atomic emission spectrometry in the early days of the development of physical methods of analytical chemistry. The laboratory methods he used were not applications of standard techniques, but rather procedures settled on physical chemical grounds, improving their analytical selectivity and sensitivity.

Backroft (1867, 1953), the influential American scientist, president of the

American Electrochemical Society and of the American Chemical Society, founder of the Journal of Physical Chemistry and its editor for decades, divided scientists into two groups: diligent “accumulators” and inspired “guessers”. Couceiro da Costa was included in the later category.

3.2 Couceiro da Costa: The head of the Department of Chemistry

In 1937, Couceiro da Costa was appointed head of his department. A lot of difficulties were waiting for him: poor, almost inexistent research activity, antiquated and exiguous installations, and insufficient financing for equipment, chemicals and journals. His predecessor, Prof. Egas Pinto Basto, did not accept the situation of the department and it was him who took the first steps to improve the situation. But, he died early. It was Couceiro da Costa who gave effectively the decisive contribution to the progress of the department. New graduates were sent abroad with scholarships to do research in English and American universities, where most of them got a PhD degree. Upon their return to Portugal, they carried on their research programs, giving rise to research teams which guided students and young graduates towards science.

Meanwhile, the teaching and research laboratories were equipped with modern instruments, purchased with money from different public and private funds. The library subscribed to the most important chemical journals published worldwide. Old volumes, sometimes complete collections of the subscribed periodicals were acquired. The library grew from a room that kept a few textbooks to an excellent teaching and research support facility. The scientific panorama of the department changed.

In spite of the efforts made to install research, teaching was also considered the most important university function. There was not so much concern in preparing the students for problem-solving, but rather to give them a good chemical preparation on both theoretical and laboratory sides. The main goal of university teaching was effectively the education of the mind for science.

In Portugal, the authorities responsible for education never believed in the role of science in human progress. Thus, the fraction of GNP allocated to higher

education and to R&D was always insufficient. With Couceiro da Costa, the budget increased substantially. Despite his prestige and the circle of influential acquaintances he fought hard to overcome the difficulties caused by the shortage of funds. Once being accused of being too ambitious, he argued: "It is quite natural to intend that our laboratories are at least similar to the most modest ones of advanced countries; with this income we are quite far from this goal."

The laboratories of the Faculty of Sciences dated from the end of the 18th century. The evolution of science, the increasing number of courses and chairs, the growing number of students made these laboratories quite unsatisfactory to meet these demands. The old *Laboratorio Chimico* was one of the first to be built especially for chemistry, in the eighteenth century. It was a beautiful edifice of magnificent architecture, but too narrow for the modern chemical activity. Instruments occupied all corners; the journals were kept in bookcases covering the walls of the lecture theater and all along the corridors. A new laboratory was, in fact, desperately needed.

In 1934, the government decided to reinstall the University of Coimbra, building new edifices and modernising some others. Couceiro da Costa devoted himself with great enthusiasm to the planning of new installations. He visited various European universities to collect information on laboratories and on the organization of recent departments of chemistry. Unfortunately, he did not assist in the construction, but he left the outline of a new laboratory large enough to be used as a chemical laboratory for the time being. The available area of the new building is 16000 m² over a total of six floors. Before the reduced number of chemistry students today it is considered by some people as being too big; the reality is that the university and the country is not proceeding in the correct way so as to bring more students to science.

In 1952, he faced a new challenge with respect to laboratory installations and, once again, he overcame it. Among the criticism of many, the approval of a few, and the indifference of the majority, Portugal decided to introduce the study of nuclear science to the university. In October of that year, the *Comissão Provisória de Energia Nuclear do Instituto de Alta Cultura* was created. In its

program was scheduled the foundation of research centers associated to the universities. Couceiro da Costa could not lose this opportunity, all the more because he had been an ardent supporter of this project. However, it was not possible to install something else in the old edifice, and the new one would not be ready in time. Therefore, in a quite a short time, he built an annex with a few rooms equipped to carry out work with radioactive materials (*Centro de Estudos de Química Nuclear e Radioquímica*) in the landscaped space at the side entrance of the *Laboratorio Chimico*.

This extension of the main building was pulled down recently to install what is called *Museu da Ciência e da Técnica da Universidade de Coimbra*. It had no value from an architectural point of view, but it was really an historical document. Its place is now just an open air space.

3.3 Couceiro da Costa: The professor of physical chemistry

Aside from a few other chemical courses, Couceiro da Costa taught during his career two subjects: “inorganic chemistry” and “physical chemistry”. The former was taught in the first year of the undergraduate chemical courses and it was really an introduction to the study of chemistry. The program gave a good grounding in chemical fundamentals without using much mathematics. The latter, taught in the last year of the degree, was a deep interpretation of chemistry as science. The syllabus of “physical chemistry” was devised at the time of the development of this discipline. To get a better idea about his merit as a lecturer, it is useful to revisit the most important steps in the awakening of this chemical method.

Chemistry is a branch of science that had to travel a long journey before getting the statute of a scientific discipline. In this context, science is understood as a body of knowledge that, through observation/perception, induction and deduction reasoning, establishes laws able to explain the natural world. The history of chemistry is indeed rather peculiar insofar as the chemical phenomena accompanying very closely the life of man from the very beginning, took a long time to reach the status of mature science. It remained for millennia as a set of

separate acquirements and techniques but without a theoretical matrix joining them together.

In spite of the progress of experimental chemistry during the first scientific revolution (17th-18th centuries), this situation remained unaltered. Lavoisier's work contributed very little to change that. Chemists, physicists and philosophers noted this imperfection. Kant, in the *Metaphysische Anfangsgründe der Naturwissenschaft* (1786) and in the preface of the 2nd edition of *Kritik der Reinen Vernunft* (1787) characterised chemistry as a set of very useful techniques but not as a true science, because the deductive method could not be applied to the subject matter of chemistry. Later, Maxwell criticised the deficiency of rigor, clearness and abstraction in chemistry. In Helmholtz's opinion, it was not advanced rationally.

Chemistry and physics grew separately but by the middle 1800's both disciplines started to converge. Since the 17th century, heat became an important concept in natural philosophy. It was related with the power generated by the steam machines that later propelled the industrial revolution. In chemistry, heat produced transformations of matter like calcination, hardly understood. Thus, it was natural that scientists raised the questions about the nature of heat.

In the first half of the 19th century, two theories found audience. One admitted that heat was matter. It appeared in phlogiston as matter of a substance determining all chemical transformations. Lavoisier tabled heat as an element, the caloric. Carnot considered the caloric as matter able to produce work while moving from a hot to a cold reservoir. In contrast, the kinetic theory admitted that heat was the result of particle motions, atoms and molecules. The development of thermodynamics proved that heat was, in fact, a manifestation of energy.

With the discovery of the second law of thermodynamics, in 1850, and its enunciate in terms of entropy, 15 years later, thermodynamics was established. Gibbs, in his renowned work "On the Equilibrium of Heterogeneous Substances", published in 1878, adapted thermodynamics to the interpretation of chemical systems. The work of Gibbs remained largely unknown for a long

time because it appeared in the modest *Journal of the Connecticut Academy of Sciences* and was written in difficult mathematical terms. The great European scientists: Maxwell, van der Waals, van't Hoff and Le Châtelier, were deeply impressed as soon as they made acquaintance with Gibbs' monumental work and became its most active promoters.

Thermodynamics was then applied to the chemical phenomena, being the first approach of physical chemistry. In 1887, Ostwald and van't Hoff launched the *Zeitschrift für Physikalische Chemie*, the first journal specially dedicated to the new discipline.

Physical chemistry grew rapidly in sciences related with chemistry and by the turn of the century its study was part of the university curricula. In Portugal, it was introduced in the university as a one semester course in 1911. At the time, it was also created another semester course dedicated to the study of thermodynamics.

In the United States, the importance of theoretical and practical physical chemistry was soon perceived. This gave rise to a movement to qualify people in this field. Many graduates were sent to good research centers in Europe. Paris, Leipzig, Heidelberg and Berlin received American chemists in short visits or in longer stays to run research projects. From 1889 to 1904, forty two American graduates attended Ostwald laboratories in Leipzig. When they returned to their country, many of them became influential lecturers and research leaders. As a corollary of this intense activity, a journal dedicated to physical chemistry, *The Journal of Physical Chemistry*, was launched by the American Chemical Society in 1896.

Lewis, an old student of Leipzig, went back to MIT in America and in 1912 was invited to lead the California Institute of Technology (CALTECH). Some colleagues and students followed him and in a few years CALTECH left the position of a modest institute and became one of the best world research centers. One of the most active areas at the time in CALTECH was thermodynamics. In 1923 Lewis and one of the colleagues who came with him from MIT, Randall, wrote the concise and comprehensive book, "Thermodynamics and Free Energy of

Chemical Substances”, which became a reference in chemical thermodynamics. This book was a valuable agent to make the Gibbs’ work known amongst scientists.

The kinetic theory of heat was not forgotten. Various scientists tried to explain the properties of ideal gases by mechanics. They did not succeed until Maxwell, who in 1860 was able to establish a distribution law of the particles against velocity at a given temperature. The theory based on the mechanics and statistics explained various properties of the gases such as pressure, free mean path, viscosity and diffusion.

However, the triumph of Maxwells’ theory was not the interpretation of the behavior of the gases but rather for being the first with a new approach to interpret the physico-chemical phenomena, latter called statistical physics or statistical mechanics. This science allows the determination of the macroscopic properties of matter from the information taken from the microscopic properties, atoms or molecules. The publication of Maxwells’ work called the attention of Boltzmann and both, in friendly concurrence, improved the previous theory and obtained a more general distribution law, which was known as the Maxwell-Boltzmann distribution law.

Boltzmann progressed his research trying to establish a link between mechanics and thermodynamics. He attempted to base the second law of thermodynamics on mechanical grounds. From the mechanical statistical treatment of more complex gaseous systems under an external force field he derived the famous H function, which had the particularity to decrease with time, and tended to a constant value as the system approached the stationary state. Boltzmann admitted then that H was related to the entropy. The H theorem was the mechanical version of the second law. He set up the equation $S = k \ln W$, relating the entropy with the number of microstates of the system under consideration.

The apparent contradiction for the explanation of irreversibility by mechanics, gave rise to opened and inflamed discussions that did not affect the foundations of statistical thermodynamics.

Gibbs, in 1902, cut-off the links of the statistical physics with the primitive

roots as systems of particles with certain properties and developed it as rational mechanics. With Gibbs, statistical mechanics was complete in classical terms, applicable to any system, and ready to receive the new mechanics that was coming.

Late in the 19th century, physicists were attempting to interpret the distribution law for the thermal radiation emitted by a hot body. The Rayleigh-Jeans equation accounted for the experimental results at long wavelengths (low temperatures) but failed to explain the spectrum at short wavelengths. In this region, classical physics predicted a thermal emission of a hot body at an infinite rate (ultraviolet catastrophe). In the University of Berlin there was an active group working on this subject, among them, Max Planck. He obtained an equation able to explain the full spectrum of the thermal radiation emitted by a black body. In the deduction of this law he admitted that the radiation was in thermal equilibrium with a set of harmonic oscillators. The results could only be explained considering that the energy of each oscillator would be given by the equation, $E = nb\nu$, where n is an integral number, h a universal constant later called after him and ν the frequency of the radiation. That is, the energy of each oscillator was quantized being $h\nu$ the quantum of energy. It is very likely that Planck did not become aware of the importance of his quantum theory that he announced to the Berlin Physical Society on 14th of December of 1900. He took it as being some sort of mathematical trick that enable him to explain the results observed for the black-body radiation. He did not realize that it was a turning point in the history of the physics.

Hertz discovered that the light was capable to eject electrons from metals (1887) and Leonard in 1902 observed that the maximum value of the energy of the electrons was related to the frequency of the radiation. The latter author also verified that the effect is observed only at frequencies above a certain limit, and further that the threshold frequency was different for every metal. According to classical electromagnetism the energy of the ejected electrons should be dependent not on the frequency but rather on its intensity. Three years later, Einstein interpreted the photoelectric effect; part of the kinetic energy of a quantum of

the radiation was transferred to the electron of the target which acquires enough energy to leave the metal. The quantum, $h\nu$, of the radiation was called by Einstein, photon. The radiation behaves as a wave and sometimes as a particle. The idea of light quanta contradicted the wave theory from the Maxwells' equation.

The wave-particle duality gave rise to great controversies and quarrels, which ended in 1924 with Broglies' investigation. The French physicist proved that effectively an electromagnetic wave corresponds to a corpuscle and the corpuscles, as electrons, behave as a wave. He deduced an equation relating the velocity, v , of an electron of mass, m , with the corresponding wavelength, $\lambda = h/(mv)$. Davidson and Gurner obtaining diffraction patterns using electrons confirmed the De Broglies' theory experimentally.

Meanwhile (1913) Bohr had the stroke of genius to apply the quantum theory to the atom. Inspired in the periodic law of Mendeleev, according to which a determined energy level could only contain a certain number of electrons, he developed his well-known atomic model, based on the quantum theory.

A puzzle for the scientists of that time was to explain why the orbiting electron did not loose energy and fall towards the nucleus as predicted by the classical electromagnetic theory. The Bohr atom explained the emission spectrum of the hydrogen but was not able to interpret the spectra of multi-electron elements. Refinements were added to the Bohr model as proposed by Sommerfeld and Broglie. The latter admitted that an electron in an orbit could be considered as a wave around the nucleus and will only be observed in the situation that permits a standing wave.

With de Broglie, the old quantum theory was at the end after standing for twenty-five years as an opened question. However, it produced a rich harvest for the second phase of the development of quantum mechanics. Heisenberg announced the discovery of this theory in 1925 in a paper published in *Zeitschrift für Physik*. He founded it in a rather unfamiliar form for physicists, the matrix mechanics. Six months after Heisenberg's paper, Schrödinger published in *Annalen der Physik* a different version of the theory describing the quantum state of the electron by a wave function. Soon, it was realised that both versions were

equivalent, which means that the quantum mechanics was discovered twice in six months time.

Quantum mechanics was a wonderful creation of outstanding physicists, gifted and privileged minds with credentials in mathematics and physics and knowledge of chemistry. Chemistry, with its roots in the microscopic world, took advantage of it and experimented, making great progress during the development of the theory. A new science was developed in the chemical field and the progress was such that by 1940s it gave birth to Quantum Chemistry, also called Theoretical Chemistry. Physical Chemistry had then three research methods available to the study of systems at equilibrium: thermodynamics, statistical mechanics and quantum mechanics.

The academic career of Couceiro da Costa (1920-1955) elapsed during the development of the physical chemistry. When he arrived at the University of Coimbra, chemical thermodynamics was a recent method applied to chemistry, statistical mechanics were just taking its first steps, quantum statistical and quantum mechanics were in development.

By the 1920s, physics passed over the greatest crisis of its history due to the conflicts between quantum theory, Newtonian mechanics and Maxwellian electromagnetism. Causality, a fundamental scientific assumption that passed untouched through the development of the statistical mechanics, was to be renounced to the understanding of the new ideas and facts. Complementarity, in some aspects, accepted principles of the classical physics while rejected them in some others.

Before this situation, it is surprising as a young man that had just arrived at university was capable of recognising the importance of the revolution and who followed it closely. Soon, he introduced these new ideas at the undergraduate level what is an assertion of his idea on the aim of university teaching that it was to prepare the students for the forthcoming world. To do this, the professor has to lead his students to the scientific frontiers of knowledge.

Making a plea to my memory and with the collaboration of my colleague Professor J. Providência, both old students of Couceiro da Costa, we reproduced

the topics of the program of “physical chemistry” from 1937s on and we present it in Appendix I. This program was taught when the first books of quantum chemistry were just being published.

3.4 Couceiro da Costa: The man

Couceiro da Costa was born in January of 1901 in Praia (Cabo Verde) in a distinguished family. His father was magistrate and diplomat and when the republican regime rose to power he was appointed governor of the Portuguese-India State. His maternal uncle was professor of chemistry in the University of Coimbra. He began his schooling in India and finished it in Portugal with distinction (19 in 20). He obtained his degree at the University of Coimbra in 1922 with honours. Still a student, he was invited to join the university as an assistant lecturer and obtained his doctoral degree in 1927. In 1934, he was promoted to full professor and held the cathedra of “physical chemistry”. Three years later, he was appointed head of the Department of Chemistry, a post that he held until his death in 1955, at the age of fifty four. He married Maria Helena Wittnich Carrisso in 1938 and they had a son and a daughter.

Couceiro da Costa was a kind and educated man. He was tender-hearted with human problems, keenly interested in the professional situation of assistants and technical staff. His jovial nature made him a wonderful fellow worker and a friend although keeping the deferential barriers created by his prestige and personality. The pleasant atmosphere he created in the Department of Chemistry was also characterised by deep respect to ethical principles, justice and dedication to the university cause.

A social-minded person, he enjoyed a break late in the afternoon to have coffee with his colleagues. This was an opportunity to talk about the work in progress, science or just to comment on the affairs of every day life. His opinion always deserved to be listened to.

He was quite rigorous in what to the laboratory work is concerned. He used to say that a student that was not well-prepared would never be a skilful experimenter. For those, experience does not teach; on the contrary, it just made

the faults more apparent.

When someone did his job negligently he lost his temper and reacted immediately. Soon though, he forgot the incident and proceeded calmly with what he was doing. He did not bear any grudges.

The intellectual achievements never overshadowed his natural simplicity and education. He was approachable by the qualified students and encouraged them to take an academic career. To get a place to work with him was an honour given his reputation and rigorous selection criteria. The daily work with him was a permanent lesson. When he discovered something rather interesting in the work he had in hand he called his collaborators and with great enthusiasm explained what he had just found. I have never met someone with such a deep critical insight into the fundamental concepts of chemistry.

Appendix 1 Program of the physical chemistry course taught by Couceiro da Costa in the 1940s

- *Classical statistical mechanics*: Phase space, Liouville's theorem. Statistical equilibrium. Maxwell-Boltzmann distribution law. Mean values in statistical distribution. Principles of the energy equipartition. Axioms of Gibbs statistical mechanics.
- *Quantum statistics*: Indistinguishability of identical particles. Quantum statistics: Bose-Einstein and Fermi-Dirac statistics. Comparison of the three statistics. Examples of Bose-Einstein and Fermi-Dirac systems. Electron gas in metals. Heat capacity of solids. Real gases. Quantum statistics in the resolution of apparent discrepancies between theory and experiment.
- *Statistical thermodynamics*: Entropy and probability. Boltzmann's H theorem. Partition functions: translational, rotational and vibrational partition functions. Monoatomic and diatomic molecules.
- *Quantum mechanics*: Quantum theory. The Bohr-Sommerfeld atom and the primitive quantum theory. Hamilton-Jacobi theory of integrable systems. Quantum mechanics: de Broglie, Heisenberg, Schrodinger. Inter-

pretation of the wave function. The theory of the chemical bond. The hydrogen molecular ion and hydrogen molecule. Heitler and London theory of the chemical bond

Appendix 2 Selecta Bibliográfica de Ruy Gustavo Couceiro da Costa

- “Aplicação da Termodinâmica ao estudo da destilação e cristalização fracionadas”, *Revista de Química Pura e Aplicada* III Série – II Ano, 28-37 (1926).
- “Análise dos gases espontâneos das nascentes de águas minerais”, *Dissertação de doutoramento* (Imprensa da Universidade, Coimbra, Portugal, 1927).
- *Teses de Física e Química* que se propõe defender no exame de Doutoramento Ruy Gustavo Couceiro da Costa.

Química:

- I. *O facto de os electrólitos fortes se afastarem da lei de Guldberg e Waage não invalida a teoria de Arrhenius.*
- II. *A pressão e a temperatura podem considerar-se propriedades específicas.*
- III. *A dissolução, susceptível de saturação, é um fenómeno químico.*

Física:

- I. A teoria das ondulações do éter é insuficiente.
 - II. A pressão osmótica não pode ser explicada pelo bombardeamento, geralmente admitido, da membrana semi-permeável.
 - III. A formação de soluções coloidais, de partículas sólidas, é contrária ao segundo princípio da termodinâmica. (Imprensa da Universidade, Coimbra, Portugal, 1927).
- “Estudo teórico da extracção e teoria da lavagem”, *Revista de Química Pura e Aplicada* III Série – V Ano, 34-38 (1930).
 - “Tixotropia do pentóxido de vanádio”, *Dissertação do concurso a professor*

- catedrático, *Revista da Faculdade de Ciências* (Coimbra) **5**, 478-637 (1934).
- “Considerações sobre alguns métodos potenciométricos de análise”, *O Instituto* **89**, 342-349 (1935).
 - “Considerações sobre a curva de neutralização dos ácidos”, *O Instituto* **89**, 393-409 (1935).
 - “Dosagem microquímica do tálio” (Tipografia da Atlântida, Coimbra, Portugal, 1936).
 - “Dosagem do estanho nas cassiterites”, *Revista da Faculdade de Ciências* (Coimbra) **6**, 5-19 (1936).
 - “Programa das Instalações da Faculdade. III. Laboratório Químico”, *Revista da Faculdade de Ciências* (Coimbra) **18**, 175-183 (1949).
 - “Determinação do pH, conductibilidade e potencial de oxidação duma água mineral na emergência”, Comunicação ao *XIII Congresso Luso-Espanhol para o Progresso das Ciências*, Lisboa, Tomo IV, 3^a Secção, 145-146 (1950).
 - “Precipitação dos sulfuretos dos metais do 2^o grupo da Análise Química Inorgânica” (trabalho realizado de colaboração com Fernando Luís de Moraes Zamith), *Comunicação ao XIII Congresso Luso-Espanhol para o Progresso das Ciências*, Lisboa, Tomo IV, 3^a Secção, 147-150 (1950).
 - “Determinação de pH, potencial de oxidação-redução e conductibilidade das águas de Salus e Vidago. Evolução dessas grandezas com o tempo. Mecanismo da evolução das águas”, *Publicações do Instituto de Climatologia e Hidrologia da Universidade de Coimbra* **XII**, 65-76 (1951).
 - “Desgaseificação e gaseificação das águas de Salus e Vidago”, *Publicações do Instituto de Climatologia e Hidrologia da Universidade de Coimbra* **XII**, 77-85 (1951).
 - “Conceito de oxidação-redução. Aplicação à hidrologia”, Conferência na *III Reunião da Sociedade Portuguesa de Hidrologia Médica*, Coimbra (1952); *Clínica, Higiene e Hidrologia* **XIX**, 108-110 (1953).

- “Estudo teórico de algumas reacções químicas”, Dissertação inaugural, Oviedo (1953); *Las Ciências de Madrid* **XIX**, nº 3, 609-626 (1953).
- “Dosagem espectrofotométrica de amoníaco vestigiário pela reacção de Nessler”, Comunicação apresentada nas comemorações das bodas de ouro da *Real Sociedad Española de Física y Química* (1953); *Anales de Física y Química* Tomo L(B), 325-328 (1954).
- “Estudo da dosagem espectrofotométrica do fluoretião em pequenas quantidades, pelo alizarino-sulfonato de sódio”, Comunicação apresentada nas comemorações das bodas de ouro da *Real Sociedad Española de Física y Química* (1953); *Anales de Física y Química* Tomo L(B), 799-808 (1954).
- “A Mecânica quântica na previsão da actividade química”, *Revista da Faculdade de Ciências* (Lisboa) **III**, 2^a Série B, 197-226 (1954).

4. SPONTANEOUS SYMMETRY BREAKING IN QUANTUM PHYSICS¹

J. da Providência*

CFT, Department of Physics, University of Coimbra, Coimbra, Portugal

Following a classification due to Sir Rudolf Peierls, two possible types of spontaneously broken symmetries are discussed, namely, *spontaneously broken symmetry of first kind*, when a symmetric ground state is degenerate with an asymmetric one, and *spontaneously broken symmetry of second kind*, when the ground state belongs to a representation of the relevant symmetry group other than the identical one. *Symmetry breaking approximation* is also considered. In this case, in order to take into account in a simple manner important correlations between the particles of the system, a symmetric ground state of a quantal system is described by an approximation method which violates the symmetry. However, great care should then be exerted in order to insure that the approximation scheme does not break the symmetry to such an extent that the relevant physical properties are distorted. Color superconductivity is an example of such a case which is here discussed in detail.

A novel BCS-type formalism is constructed in the framework of a schematic QCD inspired quark model, having in mind the description of color symmetrical superconducting states. The physical properties of the BCS vacuum (average numbers of quarks of different colors) remain unchanged under an arbitrary color rotation. In the usual approach to color superconductivity, the pairing correlations affect only the quasi-particle states of two colors, the single particle states of the third color remaining unaffected by the pairing correlations. As a consequence, the average numbers of quarks depend apparently on the color, which is an unphysical and undesirable feature. The $SU(3)$ symmetry should not be violated to such an extent. In the theory of color symmetrical superconductivity here proposed, the pairing correlations affect symmetrically the quasi-particle states of the three colors so that vanishing net color-charge is automatically insured. It is found that the ground state energy of the color symmetrical sector of the Bonn model is well approximated by the average energy of the color symmetrical superconducting state proposed here.

¹Talk based on joint work with H. Bohr and C. Providência

*Email address: providencia@teor.fis.uc.pt

4.1 Introduction

It is in general expected that the invariance properties of the Hamiltonian of an arbitrary quantum system are shared by its ground state. However, in some situations, this expectation is not realized. We say then that a *spontaneous symmetry breaking* occurs. Rudolf Peierls [1] refers to *spontaneous symmetry breaking of first kind* when the ground state is symmetric and is also degenerate, or almost degenerate, with states of a different symmetry. Then, linear combinations of states with different symmetries may arise as a consequence of small perturbations inherent to the processes of preparation or measurement. This is the case of optically active molecules, such as sugar. The two non-stationary asymmetric forms will very slowly transform into one another, in the course of time.

According to Peierls, a *broken symmetry of second kind* occurs when the ground state belongs to a representation of the relevant symmetry group, other than the identical one. This form of symmetry breaking is present in a ferromagnet which may be regarded as a lattice of N atoms each one possessing a spin s , the forces between spins showing a tendency to align them. The total spin is Ns and may point in practically any direction. Thus, the ferromagnet is not isotropic, contrary to the Hamiltonian. Here, the relevant symmetry group is the rotation group of the spin, that is, the group $SU(2)$.

Peierls refers to *broken symmetry approximation* when, in order to incorporate important correlations, it is convenient to resort to approximations which break some relevant symmetry of the Hamiltonian. This is the case of the shell-model (a translation leaves the Hamiltonian invariant, but the shell-model breaks this symmetry) and of superconductivity (the global gauge symmetry, which insures the conservation of the number of electrons, is broken by the BCS state). The symmetry is broken by the approximation used to describe the physical state, but not by the physical state itself.

Since the invention of Quantum Chromo-Dynamics (QCD) as the rigorous theory of the strong interaction, it has been generally accepted that quark and gluon fields are the building blocks of nuclear structure, in the framework of

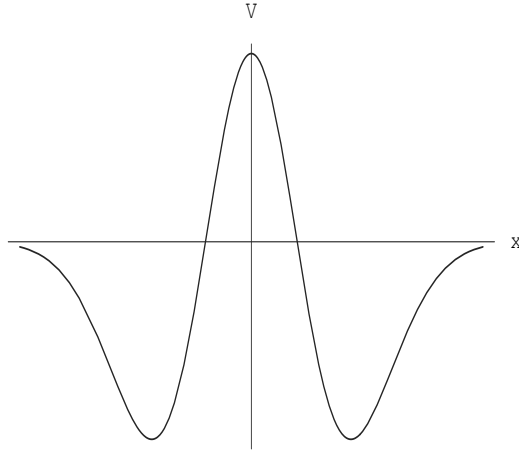


Figure 4.1. The double well potential $V(x)$ in quantum mechanics

QCD field theory. The color quantum number is associated with the $SU(3)$ symmetry which characterizes this theory. The phase equilibrium of hadronic matter is a topic of great current interest of particular relevance to astrophysics. When the density of hadronic matter reaches high values, that is, values which are several times higher than the nuclear density at equilibrium, a great diversity of phases is expected, namely: restoration of chiral symmetry, deconfinement, and color superconductivity. Chiral symmetry is the characteristic symmetry of QCD according to which the helicity of the Dirac fermions with zero mass is a Lorentz invariant. A nucleon is a small cavity, or bag, confining three quarks of different colors. The quark mass is dynamically generated, almost entirely, through a mechanism which is analogous to the Higgs mechanism and is associated with the spontaneous breakdown of chiral symmetry. As the density increases, the nucleonic bags begin to overlap and end up by getting dissolved, so that the quarks become free. Due to the complexity of the theory, it is extremely difficult, if not impossible, to obtain reliable results directly from QCD. It is therefore usual to resort to effective models such as the Nambu-Jona-Lasinio (NJL) model [2–4]. These models assume that the gluonic degrees of freedom produce an attractive two-body force between the quarks, which, effectively, replaces the gluons. Since this force is attractive, it originates the phenomenon of color superconduct-

ivity, which is analogous to the corresponding superconductivity effect familiar from condensed matter physics and is described as the formation of Cooper pairs, according to the Bardeen-Cooper-Schrieffer (BCS) theory. At present, it is generally accepted that QCD exhibits, at high densities, color superconductivity induced by the phenomenon of Cooper instability. Color superconductivity is supposed to be realized in hadronic matter at extremely high densities, several times the normal nuclear density, which is expected to be found, for instance, in the interior of neutron stars. The color superconducting phase of quark matter, described by the BCS formalism, breaks color symmetry. On the other hand, this symmetry, being a form of gauge symmetry, is not actually broken by the physical state. The breakdown of the $SU(3)$ symmetry by the approximation method is the price one has to pay in order to account for important correlations which are responsible for the superconducting property. However, great care should then be exerted in order to insure that the approximation scheme does not break the symmetry to such an extent that the relevant physical properties are distorted. This fact imposes important restrictions on the BCS formalism which should therefore be used with caution. It is important to identify and discard spurious unphysical states, belonging to representations other than the identical one, which, unavoidably, will artificially emerge.

Effective models have been used with success to investigate the properties of hadronic matter and to obtain a qualitative picture of the phase diagram [5]. Recently, the color superconducting phase has been investigated by many authors in the framework of the BCS approach. Quarks move freely in the deconfined phase, but this phase remains a singlet of the color $SU(3)$ group, since, as remarked, a gauge symmetry can not be spontaneously broken [8].

A BCS state $|\Phi\rangle$ describes a colorless physical state if $N_1 = N_2 = N_3$, where N_i denotes the number of quarks with color i , which means that

$$\langle\Phi|S_{\lambda_3}|\Phi\rangle = \langle\Phi|S_{\lambda_8}|\Phi\rangle = 0. \quad (4.1)$$

Here, S_{λ_k} denotes the $SU(3)$ generator associated with the de Gell-Mann matrix λ_k , that is, $S_{\lambda_3} \propto N_1 - N_2$, $S_{\lambda_8} \propto N_1 + N_2 - 2N_3$. Nevertheless, the condition (4.1)

is not enough to ensure that $|\Phi\rangle$ is physically acceptable. Since, as observed, the $SU(3)$ symmetry cannot be broken, the physical content of the several states which, by a color rotation, are obtained from a given physically acceptable BCS state, must be the same. Unphysical spurious states, belonging to irreducible representations which are different from the identical one, are invariably exhibited by the effective models which are found in the literature. It is very important to ensure that the performed calculations are not invalidated by those undesirable states. Let U_c denote an arbitrary color rotation, *i.e.*, $U_c = \exp \sum_{k=1}^8 ix_k S_{\lambda_k}$, being x_k real and arbitrary parameters. The state $|\Phi\rangle$ must be equivalent to the rotated state $U_c|\Phi\rangle$, for any U_c , as far as expectation values of physical observables are concerned, *i.e.*, the physical properties associated with $|\Phi\rangle$ must be the same as those associated with $U_c|\Phi\rangle$. Thus, condition (4.1) must be replaced by condition

$$\langle \Phi | U_c^\dagger S_{\lambda_3} U_c | \Phi \rangle = \langle \Phi | U_c^\dagger S_{\lambda_8} U_c | \Phi \rangle = 0,$$

for an arbitrary U_c , which implies

$$\langle \Phi | S_{\lambda_k} | \Phi \rangle = 0, \quad k = 1, 2, \dots, 8. \quad (4.2)$$

This is the condition a state $|\Phi\rangle$ must satisfy in order to be physically meaningful. If only condition (4.1) is imposed, and not condition (4.2), the BCS state $|\Phi\rangle$ may not be equivalent to the state $U_c|\Phi\rangle$. If this happens, it will belong to an $SU(3)$ representation which is not the identical one, and this is physically unacceptable. In [9], it is shown that the condition (4.2) may be easily implemented. In the next section, the construction of a BCS state which is suitable to describe a color singlet, is illustrated in the framework of a convenient schematic model.

4.2 A schematic $SU(3)$ pairing model

At present, it is, in general, admitted that nuclear structure is based on quark and gluon fields, in the framework of QCD field theory. An interesting model (in spite of well known drawbacks) concerning that viewpoint is the Bonn model proposed by Petry *et al.* [11]. This model describes the nucleus as an MIT bag,

that is, a set of free quarks bound together by an external pressure. By introducing a decisive pairing force that suppresses unphysical degeneracies of the quark system, many features of nuclear physics are reasonably well accounted for by that model.

The quark model proposed by H. R. Petry *et al.* [11] is defined by the Hamiltonian

$$H = G \sum_{j=1}^3 A_j^\dagger A_j, \quad (4.3)$$

where

$$A_1^\dagger = \sum_{m>0} (c_{2m}^\dagger c_{3\bar{m}}^\dagger + c_{2\bar{m}}^\dagger c_{3m}^\dagger), \quad \bar{\bar{m}} = m. \quad (4.4)$$

In Eq. (4.3), $G < 0$ is the coupling constant and the expressions for A_2^\dagger, A_3^\dagger , are obtained by circular permutation of the indices 1, 2, 3. In Eq. (4.4), c_{im}^\dagger are quark creation operators and the indices i and m denote, respectively, the color and the remaining single particle quantum numbers. The state obtained from m by time reversal, in a generalized sense, is denoted by $\bar{\bar{m}}$.

Color superconductivity has been applied in [9] to the description of the ground state of the Bonn model, which in general is not color symmetric. Indeed, although H has $SU(3)$ symmetry, its eigenstates are not necessarily $SU(3)$ singlets. Since, from the point of view of hadronic physics, the sectors which belong to other representations than the singlet one are not acceptable, the study of the color symmetrical sector is particularly interesting. The generators of color $U(3)$ read

$$S_{kl} = \sum_m c_{km}^\dagger c_{lm} = \sum_{m>0} (c_{km}^\dagger c_{lm} + c_{k\bar{m}}^\dagger c_{l\bar{m}}).$$

A state $|\Phi\rangle$ is a color singlet if it satisfies the following condition

$$S_{kl}|\Phi\rangle = 0, \quad k \neq l, \quad S_{kk}|\Phi\rangle = \lambda|\Phi\rangle, \quad k = 1, 2, 3. \quad (4.5)$$

Let us consider the general BCS state.

$$|\Phi\rangle = \exp \sum_{j=0}^3 \left(K \sum_{0 < m \leq \Omega'} A_{jm}^\dagger + \bar{K} \sum_{\Omega' < m \leq \Omega} A_{jm} \right) |0_{\Omega'}\rangle,$$

where

$$|0_{\Omega'}\rangle = \left(\prod_{j=1}^3 \prod_{\Omega' < m \leq \Omega} c_{jm}^\dagger c_{jm}^\dagger \right) |0\rangle,$$

and

$$A_{1m}^\dagger = (c_{2m}^\dagger c_{3\bar{m}}^\dagger + c_{2\bar{m}}^\dagger c_{3m}^\dagger).$$

The expressions for $A_{2m}^\dagger, A_{3m}^\dagger$, are obtained by circular permutation of the indices 1, 2, 3. This state is color neutral in the sense that $\langle \Phi | \hat{N}_1 | \Phi \rangle = \langle \Phi | \hat{N}_2 | \Phi \rangle = \langle \Phi | \hat{N}_3 | \Phi \rangle$, where the quark number operators read

$$\hat{N}_j = \sum_j c_{jm}^\dagger c_{jm}, \quad j = 1, 2, 3.$$

The parameters K, \tilde{K} are real. We denote by 2Ω the level degeneracy for a fixed color, that is, the totality of eigenstates pertaining to all quantum numbers beyond color. It is convenient to introduce the notation $\langle W \rangle = \langle \Phi | W | \Phi \rangle / \langle \Phi | \Phi \rangle$. If $\Omega' = \Omega$, the quark number $N = \langle \hat{N}_1 + \hat{N}_2 + \hat{N}_3 \rangle$ satisfies $0 \leq N \leq 4\Omega$. If $\Omega' = 0$, the quark number N satisfies $4\Omega \leq N \leq 6\Omega$. The state vector $|\Phi\rangle$ has obviously zero net color charge, but it is not color symmetrical, that is, it does not fulfil the condition (4.5). However, K, \tilde{K} may be chosen so that $|\Phi\rangle$ is color symmetrical in the average, in the sense that (4.2) is satisfied. We observe that

$$\begin{aligned} c_{1m}|\Phi\rangle &= K(c_{2\bar{m}}^\dagger - c_{3\bar{m}}^\dagger)|\Phi\rangle, & c_{1\bar{m}}|\Phi\rangle &= K(c_{2m}^\dagger - c_{3m}^\dagger)|\Phi\rangle, & 0 < m \leq \Omega', \\ c_{1m}^\dagger|\Phi\rangle &= -\tilde{K}(c_{2\bar{m}} - c_{3\bar{m}})|\Phi\rangle, & c_{1\bar{m}}^\dagger|\Phi\rangle &= -\tilde{K}(c_{2m} - c_{3m})|\Phi\rangle, & \Omega' < m \leq \Omega. \end{aligned} \quad (4.6)$$

These relations are crucial. They are straightforward consequences of the commutation relations

$$\begin{aligned} \left[c_{1p}, \left(K \sum_{0 < m \leq \Omega'} A_{jm}^\dagger + \tilde{K} \sum_{\Omega' < m \leq \Omega} A_{jm} \right) \right] &= K(c_{2\bar{p}}^\dagger - c_{3\bar{p}}^\dagger), & 0 < p \leq \Omega', \\ \left[c_{1p}^\dagger, \left(K \sum_{0 < m \leq \Omega'} A_{jm}^\dagger + \tilde{K} \sum_{\Omega' < m \leq \Omega} A_{jm} \right) \right] &= -\tilde{K}(c_{2\bar{p}} - c_{3\bar{p}}), & \Omega' < p \leq \Omega. \end{aligned}$$

From (4.6) it follows that the BCS vacuum $|\Phi\rangle$ is annihilated by the operators

$$\begin{aligned} d_{1m} &= c_{1m} - K(c_{2\bar{m}}^\dagger - c_{3\bar{m}}^\dagger), & d_{1\bar{m}} &= c_{1\bar{m}} - K(c_{2m}^\dagger - c_{3m}^\dagger), & 0 < m \leq \Omega', \\ d_{1m} &= c_{1m}^\dagger + \tilde{K}(c_{2\bar{m}} - c_{3\bar{m}}), & d_{1\bar{m}} &= c_{1\bar{m}}^\dagger + \tilde{K}(c_{2m} - c_{3m}), & \Omega' < m \leq \Omega. \end{aligned} \quad (4.7)$$

The expressions for d_{2m} , d_{3m} , $d_{2\bar{m}}$, $d_{3\bar{m}}$, are obtained by circular permutation of the indices 1, 2, 3. These operators characterize the so-called Bogoliubov quasi-particles. The transformation in Eq. (4.7) is not canonical, since $\{d_{im}, d_{jm}^\dagger\} \neq \delta_{ij}$, but the corresponding canonical transformation, which is not needed for the present purpose, may be easily obtained. We observe that the contractions $\langle c_{im}^\dagger c_{jm} \rangle$, $i \neq j$, are independent of i, j . Similarly the contractions $\langle c_{jm}^\dagger c_{jm} \rangle$, are independent of j .

If $0 < m \leq \Omega'$, we easily find that

$$\langle c_{im}^\dagger c_{jm} \rangle = \langle c_{i\bar{m}}^\dagger c_{j\bar{m}} \rangle = -\frac{K^2}{1+3K^2}, \quad i \neq j, \quad \langle c_{jm}^\dagger c_{jm} \rangle = \langle c_{j\bar{m}}^\dagger c_{j\bar{m}} \rangle = \frac{2K^2}{1+3K^2}.$$

If, on the other hand, $\Omega' < m \leq \Omega$, we have

$$\langle c_{im}^\dagger c_{jm} \rangle = \langle c_{i\bar{m}}^\dagger c_{j\bar{m}} \rangle = \frac{\tilde{K}^2}{1+3\tilde{K}^2}, \quad i \neq j, \quad \langle c_{jm}^\dagger c_{jm} \rangle = \langle c_{j\bar{m}}^\dagger c_{j\bar{m}} \rangle = 1 - \frac{2\tilde{K}^2}{1+3\tilde{K}^2}.$$

Thus, we obtain

$$\langle S_{ij} \rangle = -2\Omega' \frac{K^2}{1+3K^2} + 2(\Omega - \Omega') \frac{\tilde{K}^2}{1+3\tilde{K}^2}, \quad i \neq j. \quad (4.8)$$

By conveniently choosing K, \tilde{K} , we may insure that Eq. (4.2) is satisfied, so that the BCS vacuum $|\Phi\rangle$ represents a color singlet. We recall that the $SU(3)$ generators S_λ associated with the Gell-Mann matrices λ_j read

$$\begin{aligned} S_{\lambda_1} &= S_{21} + S_{12}, & S_{\lambda_2} &= i(S_{21} - S_{12}), & S_{\lambda_3} &= S_{11} - S_{22}, \\ S_{\lambda_4} &= S_{31} + S_{13}, & S_{\lambda_5} &= i(S_{31} - S_{13}), & S_{\lambda_6} &= S_{32} + S_{23}, \\ S_{\lambda_7} &= i(S_{32} - S_{23}), & S_{\lambda_8} &= \frac{1}{\sqrt{3}}(S_{11} + S_{22} - 2S_{33}). \end{aligned}$$

The state $|\Phi\rangle$ satisfies automatically (4.1), which is very convenient, but is not sufficient. Indeed, (4.1) remains valid when we replace $|\Phi\rangle$ by $U_c|\Phi\rangle$, for an arbitrary color rotation U_c , only if (4.2) is further implemented.

Next we compute the contractions $\langle c_{2m} c_{1\bar{m}} \rangle = \langle c_{3m} c_{2\bar{m}} \rangle = \langle c_{1m} c_{3\bar{m}} \rangle = \langle c_{2\bar{m}} c_{1m} \rangle = \langle c_{3\bar{m}} c_{2m} \rangle = \langle c_{1\bar{m}} c_{3m} \rangle =: D_m$, where D_m is real. We find

$$D_m = \frac{K}{1+3K^2}, \quad \text{for } 0 < m \leq \Omega'; \quad D_m = \frac{\tilde{K}}{1+3\tilde{K}^2}, \quad \text{for } \Omega' < m \leq \Omega.$$

We are now able to compute the energy expectation value

$$\frac{\mathcal{E}}{G} = \sum_{j=1}^3 \frac{\langle \Phi | A_j^\dagger A_j | \Phi \rangle}{\langle \Phi | \Phi \rangle}.$$

Let $p = \Omega'/\Omega$, $q = 1 - p = (\Omega - \Omega')/\Omega$. Define $\theta, \tilde{\theta}$ such that $\sqrt{3}K/\sqrt{1+3K^2} = \sin \theta$, $1/\sqrt{1+3K^2} = \cos \theta$, $\sqrt{3}\tilde{K}/\sqrt{1+3\tilde{K}^2} = \sin \tilde{\theta}$, $1/\sqrt{1+3\tilde{K}^2} = \cos \tilde{\theta}$. Then, having in mind (4.8), the color symmetry constraint $\langle S_{ij} \rangle = 0$, $i \neq j$, reduces to

$$p \cos 2\theta - q \cos 2\tilde{\theta} = p - q.$$

The main contribution to the energy expectation value comes from the square of the expectation values $\langle A_1 \rangle = \langle A_2 \rangle = \langle A_3 \rangle = \Omega(p \sin 2\theta + q \sin 2\tilde{\theta})/\sqrt{3}$, which involve contractions of the form $\langle cc \rangle$. The corresponding constrained extremum occurs for $\cos 2\theta = -\cos 2\tilde{\theta} = p - q$, $\sin 2\theta = \sin 2\tilde{\theta} = \sqrt{1 - (p - q)^2}$, so that, in the leading order, we have

$$\frac{\mathcal{E}}{G} \approx \Omega^2(1 - (p - q)^2).$$

In terms of the variables $\theta, \tilde{\theta}$, the number of quarks reads

$$N = 6\Omega \left[p \frac{1 - \cos 2\theta}{3} + q \left(1 - \frac{1 - \cos 2\tilde{\theta}}{3} \right) \right].$$

At the extremum, $N = 6\Omega q$, and

$$\frac{\mathcal{E}}{G} \approx \Omega^2 \left[1 - \left(1 - \frac{N}{3\Omega} \right)^2 \right].$$

To complete the calculation of \mathcal{E}/G we must add the small corrections coming from the neglected contractions of the form $\langle c^\dagger c \rangle$.

In terms of $\theta, \tilde{\theta}$, we have

$$\langle c_{jm}^\dagger c_{jm} \rangle = \langle c_{j\bar{m}}^\dagger c_{j\bar{m}} \rangle = \frac{1}{3}(1 - \cos 2\theta), \quad \text{for } 0 < m \leq \Omega',$$

$$\langle c_{jm}^\dagger c_{jm} \rangle = \langle c_{j\bar{m}}^\dagger c_{j\bar{m}} \rangle = 1 - \frac{1}{3}(1 - \cos 2\tilde{\theta}), \quad \text{for } \Omega' < m \leq \Omega.$$

At the extremum, $\langle c_{jm}^\dagger c_{jm} \rangle = \langle c_{j\bar{m}}^\dagger c_{j\bar{m}} \rangle = 2q/3$, for $0 < m \leq \Omega'$, $\langle c_{jm}^\dagger c_{jm} \rangle = \langle c_{j\bar{m}}^\dagger c_{j\bar{m}} \rangle = (1 + 2q)/3$, for $\Omega' < m \leq \Omega$. Finally, the ground state energy of the color symmetrical super-conducting phase reads,

$$\frac{\mathcal{E}}{G} = \frac{N}{9} \left(6\Omega - N + 1 + \frac{4N}{3\Omega} \right), \quad 0 \leq N \leq 6\Omega. \quad (4.9)$$

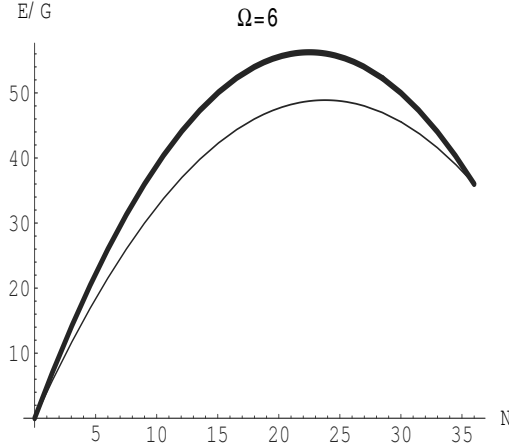


Figure 4.2. ground state energy of the color symmetrical sector versus the quark number, for $\Omega = 6$. Thick line: exact result according to (4.10); thin line: color symmetrical BCS estimate according to (4.9). Since $G < 0$, the upper curve lies below in energy, in agreement with Ritz theorem.

Using the Schwinger type representation of $su(4)$, formulated in terms of appropriate boson operators, which was developed by Yamamura *et al.* [12], the color symmetrical sector of the Bonn model has been characterized in [13]. There, the exact ground state energy of the color symmetrical sector was found to read

$$\frac{\mathcal{E}}{G} = \frac{N}{3} \left(2\Omega + 3 - \frac{N}{3} \right), \quad 0 \leq N \leq 6\Omega. \quad (4.10)$$

It is interesting to compare Eqs. (4.9) and (4.10). This is done, in Figure 4.2.

4.3 Conclusions

Following a classification due to Sir Rudolf Peierls, two possible types of spontaneously broken symmetries have been discussed, namely, spontaneously broken symmetry of first kind, when a symmetric ground state is degenerate with an asymmetric one, and spontaneously broken symmetry of second kind, when the ground state belongs to a representation of the relevant symmetry group other than the identical one. Symmetry breaking approximation may also be considered. In this case, in order to take into account in a simple manner important correlations, a symmetric ground state of a quantal system is described

by an approximation method which violates the symmetry. However, great care should then be exerted in order to insure that the approximation scheme does not break the symmetry to such an extent that physical properties are distorted. Color superconductivity is an example of such a case which is here discussed in detail.

We have constructed a BCS-type formalism, based on a conveniently generalized Bogoliubov transformation, which is appropriate to describe color symmetrical superconducting states of quark matter. It is found that the ground state energy of the color symmetrical sector of the Bonn model is well approximated by the average energy of the color symmetrical superconducting state proposed here and it is easily seen that the color symmetric BCS result becomes closer to the exact one while Ω increases.

It should be emphasized that the present approach automatically ensures vanishing net color charge, even if (4.2) is not imposed. Condition (4.2) is important because most field theoretic models contain sectors which belong to other color $SU(3)$ representations than the color singlet one. Such sectors are therefore unphysical and should be discarded.

References

- [1] R. Peierls, J. Phys. A: Math. Gen. **24**, 5273 (1991).
- [2] Y. Nambu, G. Jona-Lasinio, Phys. Rev. **122**, 345 (1961); Phys. Rev. **124**, 246 (1961).
- [3] S. P. Klevanky, Rev. Mod. Phys. **64**, 649 (1992).
- [4] T. Hatsuda and T. Kunihiro, Phys. Rep. **247**, 221 (1994).
- [5] M. Buballa, Phys. Rep. **407**, 205 (2005).
- [6] M. Alford, K. Rajagopal and F. Wilczek, Phys. Lett. B **422** 247 (1998); Nucl. Phys. B **537**, 443 (1999).
- [7] M. G. Alford, K. Rajagopal, T. Shaefer, A. Schmitt, Rev. Mod. Phys. **80**, 1455 (2008).
- [8] S. Elitzur, Phys. Rev. D **12**, 3978 (1975).
- [9] H. Bohr and J. da Providência, J. Phys. A: Math. Theor. **41**, 405202 (2008).

- [10] H. Bohr, C. Providência and J. da Providência, Eur. Phys. J. A **41**, 355 (2009); Eur. Phys. Lett. **89**, 42001 (2010).
- [11] H. R. Petry, H. Hofstaedt, S. Merk, K. Bleuler, H. Bohr and K. S. Narain, Phys. Lett. B **159**, 363 (1985).
- [12] M. Yamamura, T. Kuriyama, A. Kunihiro, Prog. Theor. Phys. **104**, 385 (2000).
- [13] C. Providência, J. da Providência, F. Cordeiro, M. Yamamura, S. Nishiyama and Y. Tsue, Ann. Phys. **324**, 1666 (2009).

5. THE INTERPRETATION OF QUANTUM MECHANICS REVISITED

Fernando M. S. Silva Fernandes*

Centre for Molecular Sciences and Materials, Department of Chemistry and
Biochemistry, Faculty of Sciences, University of Lisboa, Portugal

The foundations and meaning of quantum theory became a central issue to Albert Einstein and Niels Bohr since the onset of their impassioned debate in the 1920s, enriched by the contributions of many other distinguished scientists and philosophers. The questions are not settled down at all, despite the great achievements of the theory, its impressive accordance with experiment and predictive power. The fundamental and technological applications range from cosmology to biology, with the development of invaluable instruments and the design of new materials.

Is quantum mechanics a complete or an incomplete theory? Is there an objective reality independent of the observer or is the reality created by the measurements? Are hidden-variable theories justifiable? Is there a quantum theory founded in a local-causal and non-linear approach that formally contains the orthodox linear theory as a special case? Can such a formulation unify classical and quantum physics? Are Heisenberg's uncertainty relations valid in all cases?

Here, the subject is addressed as an adaptation of our contribution to the Colloquium "*Quantal aspects in Chemistry and Physics. A tribute in memory of Professor Ruy Couceiro da Costa*" held at Academia das Ciências de Lisboa, November 27, 2009.

Ruy Couceiro da Costa (1901-1955), University of Coimbra, was one of the first professors and researchers to apply and teach quantum mechanics at Portuguese universities. The above questions presumably crossed his mind as they do pervade, presently, the minds of teachers and researchers interested in the interpretation, philosophy and epistemology of quantum theory.

5.1 Introduction

The roots of quantum theory, originated in the 19th century by Gustav

*Email address: fsilva@fc.ul.pt

Kirchoff's challenge on the black body radiation, were definitely launched between 1900 and 1925. Experiments and first theoretical models on the behaviour of light and material particles recognized that: (i) light is emitted or absorbed, and constituted, by photons of energy $E = \hbar\omega$ (Planck - Einstein's relation), where \hbar is the reduced Planck constant and ω the time frequency; (ii) atomic energies are quantized, *i.e.*, when an atom "jumps" from an energy level E_i to another E_f it emits or absorbs a photon, $E_f - E_i = \hbar\omega$ (Bohr-Sommerfeld models); (iii) to a photon or material particle with momentum, p , is associated a wave number (space frequency) $k = 2\pi/\lambda$, such that $p = \hbar k$ (de Broglie's relation); (iv) some atomic emission lines split, in the presence of a magnetic field, into well distinct lines (Zeeman's effect); and (v) each electron "orbit" can contain only two electrons (early form of Pauli's exclusion principle underlying the Periodic Table structure).

Classical wave theory and classical mechanics are unable to rationalize the evident wave-particle duality either for light or material particles. The Bohr-Sommerfeld models, though remarkable steps forward, are essentially based on classical mechanics with the introduction of rather *ad hoc* quantum rules, and do not describe most of the atomic and molecular properties. Thus, a well-founded theory was needed to reproduce all known experimental results in such a way that quantum numbers and rules turned out naturally, *i.e.*, without *ad hoc* assumptions.

Since 1925 many quantum formulations were achieved, starting with Heisenberg, Born, Jordan's *matrix mechanics* (1925) and Schrödinger's *wave mechanics* (1926) which, apparently different, were proved to be equivalent by Schrödinger and, independently, by Dirac. However, these formulations are spinless, not fully explaining Zeeman's effect and other spectroscopic details.

Pauli introduced the *spin matrices* (1927) into Schrödinger's time dependent equation, though well-aware that the introduction of spin in such a way was rather *ad hoc*. It is noteworthy that Ralph Kronig firstly, and Uhlenbeck and Goudsmit later, had anticipated the existence of electronic spin in 1925. Curiously, Kronig was much discouraged on the proposal by Pauli who later

regretted it.

Between 1928 and 1933, Dirac, based on special relativity, developed a *relativistic quantum theory*, from which spin came out naturally, reproducing Zeeman's effect. Besides, the positron was predicted whose real existence Carl Anderson confirmed experimentally by 1933.

These achievements constitute what is known as the *first quantization*. Yet, an extension to a *second quantization* was still needed to account for the interaction of matter and radiation that Dirac's theory was unable to accommodate. It requires the quantization of fields so that particles turn out as the *quanta of non-classical fields*, allowing the creation and annihilation of quanta in different types of interaction. This is the scope of *quantum field theories*, particularly of *quantum electrodynamics* (Bethe, Tomonaga, Schwinger, Feynman, Dyson, ...) developed since 1948, a very successful theory that reproduces the experimental value of the "g-factor", for example, with an outstanding accuracy.

Further on, *gauge and renormalization group theories* (Yang, Mills, Glashow, Salam, Weinberg, Kadanoff, Fisher, Wilson, Gell-Mann, ...) extended quantum field formulations to atomic nuclei (with their "coloured" quarks and gluons), giving birth to *quantum chromodynamics* aiming at the understanding of a myriad of elementary particles and the unification of fundamental forces.

Despite all these great achievements, the gravitation problem still remained. Presently, *superstrings theory* (Green, Schwarz, Witten, ...) appears as the "jewel of the crown" for it attempts the full unification of quantum mechanics and general relativity as well as of the whole physics, what underlies the "dreams of a final theory".

Quantum theories gave rise to a remarkable progress in chemistry and physics, predicting, with great accuracy, the properties of molecules, atoms, nuclei, elementary particles, chemical and nuclear reactions. The mechanisms of the universal forces are unravelled by means of their mediating "particles" and symmetries. The fundamental and technological applications range from cosmology to biology, with the development of invaluable instruments and the design of new materials.

Simultaneously, quantum theory challenges the classical reasoning concerned with causality, determinism, locality and objective reality, shaking the philosophy, ontology and epistemology of science. In this context, since the 1950's, hidden-variable theories were proposed (Bohm, Bell, ...) aiming to recover some of the classical views and experimentally pitting them against the orthodox quantum standpoint.

Recently, the linearity, non-locality and non-causal realm of the orthodox quantum theory has again been questioned. In 2003, José Croca proposed a new approach, based on de Broglie's "pilot wave" idea and radically changing the non-local Fourier ontology of the orthodox quantum theory to a *local wavelet analysis*. A non-linear equation was established and generalized uncertainty relations were derived which, in special cases, lead to Schrödinger's equation and Heisenberg's relations.

5.2 Orthodox Interpretation

Niels Bohr was one of the most brilliant physicists of the 20th century. The model for the hydrogen atom, the interpretation of quantum theory, the proposal for the uranium enrichment in the 235-isotope and the foundation of the Copenhagen school were, among others, the pillars of Bohr's huge influence in the scientific and philosophical communities all over the world.

As for the theory interpretation, the chief ideas were put forward in the 1920's through the complementary principle and the onset of his debate with Albert Einstein. Bohr, with the contributions of Heisenberg and Pauli, was for certain the precursor of the so-called "Copenhagen or orthodox interpretation" that is, presently, the "standard" for the majority of teachers and researchers [1–4]. It should be noted, however, that Bohr's own ideas and the Copenhagen interpretation are frequently taken as being the same. This is not strictly true. For instance, Bohr avoided the postulate of wave function "collapse" that is central to the Copenhagen interpretation which, in its present form, is essentially based on von Neumann's mathematical formulation [4, 5]. We shall use indistinctly the terms "orthodox" and "Copenhagen" just to convey the standard

interpretation and distinguish it from other theories and interpretations such as hidden-variables, many-worlds and non-linear formulations.

Let's then outline the orthodox fundamentals:

- To a free particle with sharp momentum p , and energy E , is associated a *monochromatic harmonic wave* such that $p = \hbar k$ and $E = \hbar\omega$.
- Wave and particle concepts are mutually exclusive, though complementary to rationalize the experimental observations.
- The state $|\Psi\rangle$ of a particle with sharp position, x_0 , is described by the Fourier expansion:

$$|\Psi\rangle = \delta(x - x_0) = \hbar^{-1/2} \int_{-\infty}^{+\infty} \exp(-ix_0 p_x/\hbar) \exp(ix p_x/\hbar) dp_x \quad \Delta x = 0$$

where $\delta(x - x_0)$ is the Dirac delta function, $\exp(ix p_x/\hbar)$ the eigenfunctions of the momentum operator and Δx the indeterminacy of the position.

In this case, p_x and E are undefined. There exists, however, a set of simultaneous possibilities (the eigenvalues of the momentum operator), each one only really *attributable* through measurements. By means of very many repeated measurements of the momentum, that is, providing that before each measurement the particle is in the same state $\delta(x - x_0)$, a distribution of *different* results is obtained. The momentum indeterminacy, Δp_x , is proportional to the width of the distribution. As the position function encodes all possible momentum values (in this case a continuous spectrum) with equal weights (probabilities) $\Delta p_x = \Delta E = \infty$. Conversely, if $\Delta p_x = \Delta E = 0$, then $\Delta x = \infty$, *i.e.*, the position is undefined. In general:

$$\Delta x \Delta p_x \geq \hbar \quad (\text{Heisenberg's indeterminacy relation})$$

This relation means not what is measurable but what is knowable. Position and momentum, for example, are not known simultaneously *before* a measurement on a single particle, *i.e.*, the position or the momentum, or both, are just undefined.

Although Δx and Δp_x are estimated from very many repeated measurements, the indeterminacy principle must not be interpreted supposing that the position

and momentum of a single particle are defined simultaneously before a measurement, and that the principle expresses the uncertainties of statistical errors due to observation disturbances and instrumental incompatibilities.

Such errors are generally present, but one can, at least conceptually, eliminate them. Even so, an ideal errorless measurement of the position on a single particle in any state $|\Psi\rangle$ would generate, non-deterministically, an eigenstate $\delta(x - x_0)$ which is Fourier composed by an infinite number of momentum eigenstates. If this is followed by an errorless measurement of the momentum it generates, non-deterministically, an eigenstate $\delta(p_x - p_0)$ with sharp momentum, p_0 , which is Fourier composed by an infinite number of position eigenstates, and so forth. The same scenario results for other properties.

In the context of Fourier analysis, the indeterminacy is intrinsic, not a question of statistical errors. The reality of physical properties, that is, the existence of effective values for them, depends on the measurements. Yet, there is an *empirical reality* which not being independent of measurements *leads to the same predictions for all observers*.

Associating a monochromatic harmonic wave to a material particle with sharp momentum has, however, a physical inconsistency. In fact, the wave phase velocity, v_{pha} , and the particle velocity, v_{par} , are related by $v_{\text{pha}} = c^2/v_{\text{par}}$, where c is the light velocity. Therefore, the wave will precede the particle since $v_{\text{par}} \ll c$. But one can suppose that to the particle is associated not a monochromatic wave but a wave packet:

$$\Psi(x, t) = \int_{-\infty}^{+\infty} f(x) \exp[i(kx - \omega t)] dk$$

with k within a narrow interval $k_0 \pm \Delta k$. Then, the group velocity is:

$$v_g = \left(\frac{\partial \omega(k)}{\partial k} \right)_{k_0} = v_{\text{par}}$$

and

$$p = mv_g = \hbar k_0; \quad E = \hbar \omega_0$$

Apparently, this resolves the problem. Besides, if a Dirac delta function is ascribed to a particle with sharp position, the momentum and the energy are

totally undefined. The wave packet also circumvents this point. Then, a classical image comes out: a particle *more or less* localized moving in space-time, and encoding de Broglie's relation and Heisenberg's indeterminacy principle.

Another physical inconsistency, however, turns out: material wave-packets disperse rapidly so any image of a trajectory is nonsense. But, what about the apparent trajectories of particles observed in cloud chambers? This question motivated Heisenberg to set out his indeterminacy relations [1, 2, 4].

Obviously, there are some uncomfortable physical details in the above analysis and assumptions, at least against common sense. Yet, one thing is absolutely certain: the orthodox quantum mechanics gives results in an excellent agreement with experiment. A philosophical standpoint is then inescapable.

5.3 Philosophy and mathematics

Harald Høffding was Bohr's teacher of philosophy and a close family's friend. He is reported as having had a considerable influence on Bohr's philosophical standpoints. Høffding defended that in our endeavour to get knowledge there exists an irreducible irrational residue impossible to overpass whichever our efforts are. It appears that Bohr agreed on this view by saying that "such a residue is, in quantum mechanics, mathematically expressed in a lucid form". He also asserted: "There is no quantum world. There is only an abstract physical description. It is wrong to think that the task of physics is to find out how nature is. Physics concerns what we can say about nature" [4, 6].

This way of thinking follows, in some ways, the philosophical position of *positivism*. It claims that for a scientific statement being meaningful it has just to be a formally logical and verifiable statement. The objective reality (a reality flowing "out there" independent of the observer-instruments) is, for positivism, a metaphysical concept since it is not possible to know of a universe without observing it. If one has two theories *formally* logical and experimentally verifiable, then both theories are valid in principle. The choice between them is generally a matter of convenience or simplicity, independently of their assumptions might be *physically* contradictory or unrealistic. The matrix and wave

formulations of Heisenberg and Schrödinger are typical examples. In a strict sense, one can think of abstract concepts (physical properties) to describe the systems but for positivism they only become real upon observation or measurement. Such physical properties are a kind of “dummy variables”, undefined entities, until one can attribute to them a quality or a quantity by observation or measurement. Otherwise, they are abstract objects not existing in reality.

The point of view of *realism*, defended by Einstein, is different (in part only, we think) of the one of positivism. For a realist, logic and measurement are certainly essential ingredients of science. But, according to Einstein, for a physical property to exist in reality it suffices that: “if, without in any way disturbing a system, we can predict with certainty (*i.e.*, with a probability equal to unity) the value of a physical quantity, then there exists an element of physical reality corresponding to this physical quantity” [7]. For a theory to be considered complete there must be a one-to-one correspondence between the elements of physical reality and the elements of the theory (its physical concepts). Otherwise, the theory is incomplete. Einstein asserted: “Physics is an attempt to capture the reality as it is thought to be, independently of being observed or not” [6].

The mathematics underlying the orthodox theory is, ultimately, Fourier analysis (just one of the possible mathematical techniques to represent functions) that is endowed with a full physical meaning as an ontological principle.

In the orthodox view, quantum mechanics is a complete theory for it is formally logical and vindicated by experiment. As such, it is frequently considered as the “end of the road” of our possible knowledge. It is suggested, however, that Bohr himself was not a radical positivist but to some extent a *pragmatic*. Quoting Jim Baggott: “The pragmatist doctrine admits a more practical (or, indeed, pragmatic) approach to the reality of entities — such as electrons — whose properties and behaviour are described by theories and which produce secondary observable effects but which themselves cannot be seen. According to the pragmatist, what we can know is limited not by we can see but by we can *do*. It seems logical that the father of the modern atomic theory would want to accept the reality of atoms. But Bohr placed limits on what a theory of the internal

structure of the atom could say. He argued that we live in a classical world, and our experiments are classical experiments. Go beyond these concepts, and you cross the threshold between what you can know and what you cannot. Positivist or pragmatist, the most important feature of Bohr's philosophy is that he was anti-realist. It denied that quantum theory has anything meaningful to say about an underlying physical reality that exists independently of our measuring devices. It denied the possibility that further development of the theory could take us closer to some yet unrevealed truth" [4].

We do not believe in "end-roads" in science. Nevertheless, we do acknowledge that once a consistent set of axioms and rules is established it has always an "end-road". Also, it is not always possible, within such a set, to decide if some mathematical propositions are true or false, as Kurt Gödel demonstrated. Yet, this does not mean that other structures extending the roads of science are precluded.

John von Neumann's formulation of the quantum theory is an unassailable mathematical structure, based on a consistent set of postulates and rules. However, von Neumann asserted: "In spite of the fact that quantum mechanics agrees well with experiment, and that it has opened up for us a qualitatively new side of the world, one can never say of the theory that it has been proved by experience, but only that it is the best known summarization of experience" [6, 8]. It is noteworthy that von Neumann (who never was a fellow of the Copenhagen school) did not adhere to all Bohr's views. For example, his interpretation on the nature of measuring devices was different from the one of Bohr [4].

Whatever the discussion is, it seems to us that, after all, most of the scientists, if not all, adhere to positivist-pragmatist methodologies, though with realist outlooks. Indeed, who are the researchers that (nowadays, at least!) submit a project stating that the objects of their proposed investigations *only become real upon measurement?*

5.4 Orthodox theory

In 1932, John von Neumann established the rigorous mathematical found-

ation of the orthodox theory in the context of Hilbert's vector space [8], also explored by Dirac [9]. It is commonly expressed by a set of postulates the most important of which, for the present discussion, are:

- a) To each physical state of an individual system, at time t , corresponds a normalized vector of Hilbert's space, $|\Psi\rangle$, which describes, *completely*, the system.
- b) To a physical observable, A , corresponds in Hilbert's space a linear Hermitian operator, $\hat{\mathbf{A}}$, which has a complete and orthonormal set of eigenvectors (a *basis*), $|\alpha_i\rangle$, and corresponding eigenvalues, A_i , such that:

$$\hat{\mathbf{A}}|\alpha_i\rangle = A_i|\alpha_i\rangle \quad (i = 1, 2, \dots)$$

were the A_i 's are the only possible values obtainable from any measurement of A .

- c) If A is measured on a general state $|\Psi\rangle$, the strongest predictive statement that can be made is that the probability of obtaining the value A_k is: $|\langle\alpha_k|\Psi\rangle|^2$.
- d) A measurement generally changes non-deterministically the state vector. Regardless of the state before the measurement, immediately after it the new state will coincide with the eigenvector corresponding to the obtained eigenvalue (this is the so-called *reduction* or *collapse* of the state vector).

From the postulates, it is straightforward to prove the *expansion theorem*, *i.e.*, a state vector $|\Psi\rangle$ can be expanded into the vectors of any basis:

$$|\Psi\rangle = \sum_i \langle\alpha_i|\Psi\rangle |\alpha_i\rangle$$

The Fourier composition of Dirac's delta function, seen above for a particle with sharp position, is just a particular case of the expansion theorem.

The postulates clearly mean that the direct link between cause and effect is severed. This is the big clash with classical mechanics. Indeed, it is asserted that measurements on *exactly* the same state can give different results, *i.e.*, an initial state does not uniquely determine future outcomes. Only if the state

vector coincides with an eigenvector of an operator $\hat{\mathbf{A}}$, for example $|\alpha_k\rangle$ can one be certain that repeated measurements of the observable A give always the same result, A_k . However, in such state, repeated measurements of another observable B , whose operator, $\hat{\mathbf{B}}$, does not commute with $\hat{\mathbf{A}}$, can give different results. Moreover, a measurement in the context of the postulates, which capture the Copenhagen interpretation, remains an unexplained process, since there is nothing in the mathematics that specifies how and when the wave function collapses.

From the postulates, it is also straightforward to prove the *compatibility theorem*:

“Given two observables A and B with corresponding operators, $\hat{\mathbf{A}}$ and $\hat{\mathbf{B}}$, any one of the following conditions implies the other two: (i) A and B are compatible observables; (ii) $\hat{\mathbf{A}}$ and $\hat{\mathbf{B}}$ have a common eigenbasis; (iii) $\hat{\mathbf{A}}$ and $\hat{\mathbf{B}}$ commute”.

In text books, it is not often noted that the theorem does not assert the impossibility of two non-commuting operators having *some* eigenvectors in common, but just the impossibility of *all* the eigenvectors of a basis being common. For example, the x and z operators of the angular momentum do not commute but have *some* eigenvectors in common [10].

Bohr and Einstein discussed this matter privately. Quoting Ballentine:

“... quantum mechanics, properly understood, does not prohibit or restrict simultaneous measurement of non-commuting observables, but rather it does not deal with such measurements at all” [11].

In fact, according to Bohr, a unique instrument for simultaneously measuring incompatible observables is not conceivable. Two different devices are needed to measure such observables of the system in a given state, being the respective results always limited by the indeterminacy relations.

5.5 Time-dependence. Many-worlds formulations

According to the orthodox theory the state vector $|\Psi\rangle$ or/and the operators

can evolve in time through two distinct processes: (i) perturbing the system by measurements, leading to non-deterministic results; or (ii) letting the system unperturbed.

In the last case, the evolution is deterministic, obeying to motion equations. These depend on the particular formulation one adopts. By 1930, three different, but equivalent, pictures were definitely settled down by Heisenberg (matrix mechanics), Schrödinger (wave mechanics) and Dirac (interaction picture) [9,12], each with its own importance to further developments. Here, the non-relativistic Schrödinger's equation is adopted:

$$\hat{\mathbf{H}}|\Psi\rangle = i\hbar \frac{\partial |\Psi\rangle}{\partial t}$$

where $\hat{\mathbf{H}}$ is the Hamiltonian operator.

Schrödinger established the equation from the concept of wave packets for free-particles and assumed its validity for all cases [12]. Thus, it commonly constitutes a further postulate of the theory.

Schrödinger was a realist believing that the wave functions exist in reality as amplitudes of a “material field scalar”. He interpreted the wave-particle duality in pure undulatory terms assuming that the transitions between standing waves, that describe the stationary quantum states, are smooth and continuous. In this way he hoped to explain the apparent non-classical atomic properties with essentially classical concepts, restoring the determinism and causality that the theory appeared to abandon. He viewed an electron as a superposition of wave disturbances (wave packet) resulting in its particle-like properties.

Schrödinger's interpretation clashed with Heisenberg's matrix mechanics. Initially, Heisenberg considered the electron essentially as a corpuscle-like entity, supposedly with defined positions and momentum, and subjected to discontinuous jumps between stationary states. Matrix mechanics was, to him, no more than an operational algorithm and the uncertainty principle expressed instrumental disturbances and incompatibilities, turning the simultaneous specification of the position and momentum impossible. The heated rivalry between the two young men was tempered by Bohr and Pauli. Heisenberg soon did adhere

to Bohr's interpretation based on the complementary principle. Schrödinger never did [2–4, 6, 13, 14].

Hendrik Lorentz pointed out to Schrödinger the rapid spreading of the material wave packets dispersing into wider amplitude distributions [4]. Besides, the wave functions derived from the equation are generally complex and multi-dimensional which does not seem compatible with the realist interpretation that Schrödinger pretended. Also, any function $|\Psi\rangle \exp(i\phi)$, where ϕ is an arbitrary phase factor not experimentally accessible, is a valid solution to the equation.

These issues were conveyed, in 1926, by the humouristic ditty [6]:

Erwin with his "psi" can do Calculations quite a few.

But one thing has not been seen:

Just what does "psi" really mean?

The difficulties were circumvented, also in 1926, by Max Born's interpretation [1]: the wave function is an abstract non-local entity, just giving the probability density, $|\Psi|^2$. However, this raises another question: how can *abstract* entities explain the diffraction and interference observed in the two-slit experiment?

Furthermore, the collapse of the wave function, considered by some authors [15] as a "recipe" rather than an axiom, gave rise to an intricate and puzzling question. In fact, according to the orthodox view, the measuring device is not independent of the observed system, constituting with it an isolated super-system. If one includes this super-system in the deterministic Schrödinger's equation, a succession of entangled states is always obtained along the time, with no collapse of the total wave function in order to select one of the possible eigenstates. If another observer of the super-system is introduced, the argument repeats with no way out. This is the heart of the famous "Schrödinger's cat paradox" [4, 6].

For cosmology, at least, a question is inescapable: how was the universe created? According to the above, the collapse of the universe super-wave function is not possible, unless we postulate it. Therefore, only a virtual bunch of simultaneous possibilities could exist. The *many-worlds interpretation*, put forward

in 1957 by Hugh Everett III, assumes the deterministic side of the orthodox theory, but dismisses the postulate of the wave function collapse. It asserts the real existence of all possibilities (*worlds*) with a crucial detail: we, ourselves, are only conscious of just one of such worlds. This interesting interpretation has suffered alterations and refinements (for instance, the *many alternative histories of the universe*) that are taken seriously by many researchers, particularly cosmologists. Indeed, *quantum cosmology* can not resort to repeated measurements of the universe like the common ones in physics and chemistry laboratories. Furthermore, other approaches have been proposed either avoiding the collapse of the wave functions or introducing additional terms to Schrödinger equation to cause the collapse [4, 15–17].

5.6 Einstein, Podolsky and Rosen thought experiment (EPR)

The debate between Einstein and Bohr culminated at the 5th and 6th Solvay Conferences, held in Brussels in 1927 and 1930. Einstein asserted the incompleteness and inconsistency of the orthodox quantum theory through a series of thought experiments suggesting, on the one hand, that the theory implied a weird instantaneous action at a distance and, on the other hand, that the position-momentum and energy-time uncertainty relations could be violated. Bohr was able to rebut Einstein's arguments. Ironically, the famous “photon box experiment” was brilliantly dismantled by means of Einstein's general relativity theory.

The debate recommenced in 1935, when Einstein, Podolsky and Rosen (EPR) published a paper, entitled “Can quantum-mechanical description of physical reality be considered complete?” [7]. In the words of Léon Rosenfeld, who was at that time in Copenhagen: “... this onslaught came down upon us as a bolt from the blue” [6].

The EPR arguments can be outlined as follows. Consider two particles, A and B, initially interacting and moving apart. Suppose they reach a relative distance of years-light where they should be separate entities with independent reality, *i.e.*, there is no longer any interaction between them (*the separability*

assumption). Additionally, EPR adopted a criterion for reality: “if, without in any way disturbing a system, we can predict with certainty (*i.e.*, with a probability equal to unity) the value of a physical quantity, then there exists an element of physical reality corresponding to this physical quantity”.

They also accepted that position (q) and momentum (p) of each individual particle cannot be known simultaneously according to Heisenberg’s indeterminacy principle. Yet, both $q_A - q_B$ and $q_A + q_B$ can be sharply defined since the respective operators commute.

Now, if one measures q_A , then q_B is predicted (from $q_A - q_B$) without perturbing B. Therefore, the position of B must have a definite value, according to the above criterion, even if A is not measured (in this case, of course, we would not know what it was, but this not affect the argument). In other words, a measurement of A only affects *our knowledge* of the properties of B which were already defined before the measurement.

If one measures p_A , instead of q_A , then p_B is exactly predicted (from $p_A + p_B$) without perturbing B. So, its momentum is also an element of reality. Thus, the position and momentum of B must be, simultaneously, elements of physical reality, *i.e.*, well-defined independently of any measurement, in contradiction with the orthodox theory. Otherwise, the reality of q_B or p_B would depend upon the choice of the measurement on A, whose disturbance would be instantaneously felt by B, years-light apart from A. This would imply a “spooky” action at a distance, violating *locality* and against special relativity. EPR claimed: “No reasonable definition of reality could be expected to permit this”.

The paper ends with the statement: “While we have thus shown that the wave function does not provide a complete description of the physical reality, we left open the question of whether or not such a description exists. We believe, however, that such a theory is possible.”

It should be noted that EPR did not intend, contrary to other Einstein’s thought experiments, to challenge Heisenberg’s indeterminacy relations. It was not designed to simultaneously measure the position and momentum of a particle but just to demonstrate the *observer-independent* reality of both. The

“onslaught” was against the inseparability and non locality implicit in the orthodox theory.

Bohr’s answer [18] disagreed on the EPR criterion for physical reality, though conceding that there was no “mechanical” disturbance of particle B due to a measurement on particle A. The role of the measuring device was emphasized in the sense that any quantum object and the measuring device constitute an indivisible whole (the “phenomenon”), there being no room for a physical disturbance due to an observation.

Bohr’s wording was not much clear, as he later admitted, but its essence seems to be the following. The wave functions of the two-particle system are *inseparable*, *i.e.*, they are global instances of the same entity. The particles behave as they were just one at all distances. Once they have interacted, they are entangled for ever. The wave functions are Fourier composed by the same basic elements: monochromatic harmonic waves extending through all space and time, affected by the proper coefficients.

If one measures q_A , then q_B is predicted from $q_A - q_B$ but, according to the indeterminacy relation, p_A is unknown and so is p_B , even knowing $p_A + p_B$, as also admitted by EPR. The position or the momentum of any particle only can be attributed by means of observations, requiring two distinct and incompatible devices (two different “phenomena”) that preclude the simultaneous definition of the position and momentum. Thus, due to the inseparability of the entwined particles and the measuring device subjecting A to a position observation (one “phenomenon”), for example, is practically the same as observing B conferring to it a well-defined position. But the sharp definition of the momentum of B is a different “phenomenon”.

Although Bohr agreed that there was no “mechanical” disturbance of B due to an observation of A, he maintained that a measurement of particle A somehow instantaneously “influences” particle B. He did not explain this “influence on the very conditions which define the possible types of predictions regarding the further behaviour of the system”, and concludes that since “these conditions constitute an inherent element of the description of any phenomenon to

which the term ‘physical reality’ can be properly attached, we see that the argumentation of the mentioned authors does not justify their conclusion that quantum-mechanical description is essentially incomplete”.

Will the so-called “spooky” action at a distance (where something that happens to a particle at a location can instantaneously be reflected in other particle at a huge distance) violate the limit of light velocity? In a strict orthodox interpretation it seems that the relativity theory is not at stake. As said above, the two particles, though very far apart, continue to belong to the same physical entity. *Only* observing one of them its attributes become defined, which *correlates* to what would be observed in the other particle. But no information or signal is transmitted, at least in conventional terms, and there is no traditional relation of cause-effect. Actually, it is shown that quantum entanglement cannot be used to instantaneously send conventional and useful information. Quoting Brian Green: “the special relativity theory survives by a *hair’s breadth*” [19].

It appears that, within the mathematical framework of the non-local Fourier analysis, which is the basis of the orthodox theory, Bohr’s answer to EPR is right, suggesting that the limit of what can be known has been reached. However, it lays against the heart of Einstein’s realist belief in physical separability and locality which, once assumed, certainly support the EPR conclusions. This is the very realm of the debate. Apparently, Einstein did not question the linearity and Fourier analysis underlying the orthodox theory. Nonetheless, the EPR thought experiment paved the way to other theories, interpretations and real experiments that challenge the orthodox “end of the road”.

5.7 Hidden-variable theories

The randomness implicit in the orthodox postulates means that repeated measurements under exactly the same initial conditions can give different results. The initial wave functions only allow probabilistic predictions concerning the outcome of future measurements.

The main objective of hidden-variable theories is to remove such randomness, assuming that initial states, apparently identical, are really different and dis-

tinguishable by variables not specified (“hidden” variables). Therefore, the states defined in the orthodox theory by the wave functions would not correspond to precise values of these variables, but to averages over them. If it is possible to set up other states specifying the precise values of such variables, then the classical causality will be restored with no need of appealing to the unexplained wave function collapse. Quoting David Bohm: “lawlessness of individual behaviour in the context of a given statistical law is, in general, consistent with the notion of more detailed individual laws applying in a broader context” [20]. This presupposes the existence of a deeper quantum-mechanical level that explains the statistical realm of the orthodox theory, similar to Brownian motion theory and statistical mechanics.

The idea was lurking since Einstein’s work on spontaneous and stimulated emission of radiation by molecules (1916-1917). By that time he manifested to Max Born his discomfort about the fact that quantum theory could not predict the time and direction of the photons emission, letting the details to chance and renouncing complete causality. By 1927, he even attempted a kind of hidden variables formulation, introducing a “guiding field” to real particles, and submitted a paper that he soon withdrew for having dismissed the idea. Nonetheless, it seems to have influenced, in some way, Born’s interpretation and de Broglie’s “double-solution” based on the “pilot wave” suggestion [4].

In 1932 von Neumann stated the “impossibility theorem” [4, 8], apparently proving that “no hidden-variables theory can reproduce and explain all the results of the orthodox theory”, which certainly discouraged the pursuit of hidden-variables for the next twenty years. In fact, David Bohm revived it by 1952, impressed by the EPR experiment, and based on the older proposal of de Broglie’s “pilot wave” according to which the wave function is a guide to the motion of the particle that likely follows the path where the wave intensity is larger [4, 6, 21, 22].

Briefly, in the so-called de Broglie-Bohm hidden-variables theory, a system, at each instant, is described by a wave function (solution of Schrödinger’s equation) and by the positions and momenta of all the particles. A “quantum force” is calculated from the wave function and added to other forces (coulombic, van der

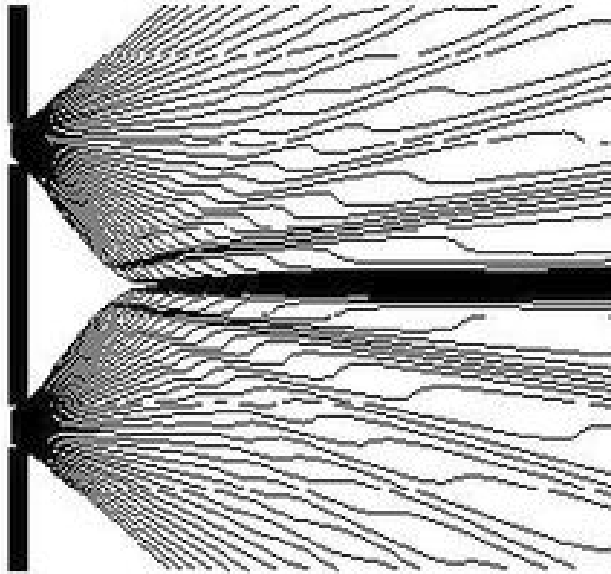


Figure 5.1. Two-slit results from de Broglie-Bohm hidden variables theory; adapted from [23].

Waals, etc.). The trajectories of the particles are then calculated by integrating Newton's motion equations. Figure 5.1 shows the theoretical results for the two-slit experiment. Apart the *sui generis* trajectories, the main conclusions are: (i) agreement with the orthodox theory; (ii) exact particle paths; and (iii) the “quantum force” operates instantaneously over arbitrarily large distances accounting for diffraction and interference effects.

The last conclusion clearly implies the violation of locality, one of Einstein's sacred beliefs. Nonetheless, the results contradict von Neumann's impossibility theorem. As matter of fact, von Neumann's proof is mathematically impeccable, but one of the primary assumptions, concerned with certain observable averages, is physically restrictive, turning the theorem incorrect as conjectured by de Broglie and Bohm, and proved by John Bell [24, 25]. Besides, inspired by Bohm and EPR, Bell derived a mathematical inequality for correlated properties (spins, for example) of two interacting particles (photons or electrons) assuming: (i) an objective reality; and (ii) the preservation of locality, according to the

EPR claims. Bell's inequality, $-2 < C(A, B) < +2$, where $C(A, B)$ are correlation coefficients, can be tested by real experiments. If the inequality is verified then the conclusions of EPR are experimentally confirmed and *local* hidden-variables theories justified.

During the 1970's and 1980's a series of experiments were carried out by the teams of John Clauser and Alain Aspect [4, 6, 16]. The majority of the results pointed to the violation of the inequality. However they did not appear conclusive on whether both Bell's assumptions should be dropped or just that of locality, *i.e.*, the experiments opened the possibility of a non-local objective reality. More recently, analyses about "loopholes" and bias on Bell's inequality tests have been reported [26–28].

In 2006, the Austrian-Polish group led by Markus Aspelmeyer and Anton Zeilinger tested a new inequality derived by Anthony Leggett [29] who altered Bell's inequality by assuming instantaneous influences through entangled particles and pitting non-local hidden variable theories against the orthodox quantum mechanics. The experimental results [30] point to the violation of Leggett's inequality according to the predictions of quantum mechanics. Soon after, Branciard *et al.* [31] claimed that the falsification of the inequality was flawed and proposed new inequalities to test Leggett's model, though the results also point to the agreement with the orthodox theory. Yet, Alain Aspect asserted that the violation of Leggett's inequality implies only that realism and a certain type of non-locality are incompatible, that is, it does not rule out *all* possible non-local models [6]. So, the matter is not settled down at all.

It is worth mentioning that Einstein became very interested in Bohm's ideas but soon disliked hidden-variable theories considering them "too cheap". To him, no amendments to the orthodox theory should be made. He accepted quantum mechanics as a correct statistical theory, though the wave function only described the behaviour of an ensemble of systems, not an individual system. Thus, he sought, without success, a new deeper *unified field theory* from which the orthodox statistical realm could come out naturally and meaningfully.

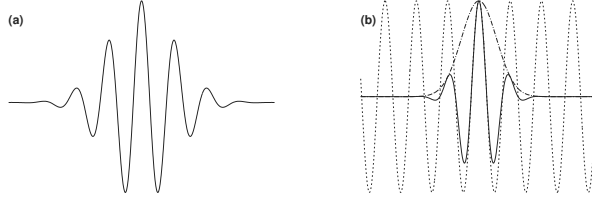


Figure 5.2. (a) Morlet's wavelet; (b) Gaussian modulation of a monochromatic harmonic wave.

5.8 A local-causal and non-linear approach

Recently a new approach to quantum physics has been put forward by José Croca and collaborators [32,33]. It should be said at the outset that the approach does not intend, in any way, to amend the orthodox theory. On the contrary, it radically changes the ontology by adopting local wavelets instead of non-local Fourier analysis. The fundamental assumptions are:

- (i) The existence of an objective reality, causal, local and non-linear. Particles have defined positions and momenta even in the absence of measurements.
- (ii) Local wavelet analysis instead of non-local Fourier analysis.

Wavelets are, essentially, wave entities localized in time and frequency, contrasting to monochromatic harmonic waves that are localized in frequency but extend infinitely in time and space [34]. The main argument is: real wave signals are always localized in space-time, generally with well-defined frequencies, whereas the infinite monochromatic harmonic waves (underlying Fourier compositions and the orthodox quantum mechanics) are ideal entities devoid of physical reality.

For example, the basic Morlet's wavelet:

$$\Psi(x, t) = \exp \left[-\frac{(x - vt)^2}{2\sigma^2} + i(kx - \omega t) \right]$$

is just a monochromatic harmonic wave modulated by a Gaussian function of width σ , *i.e.*, a localized entity (see Figure 5.2) that encodes a well-defined frequency. Note that when $\sigma \rightarrow \infty$ the harmonic wave is recovered. Taking wavelets as the building blocks for composing functions it is pos-

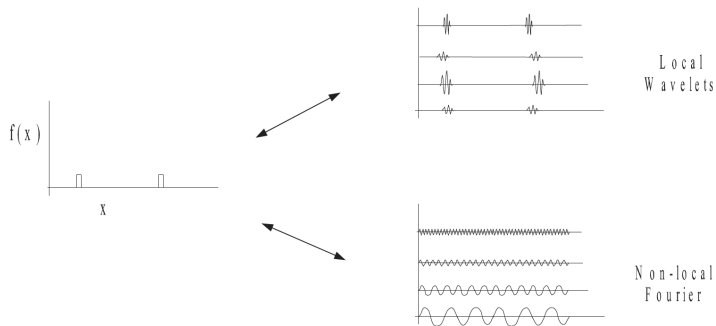


Figure 5.3. Local wavelet versus non-local Fourier analyses [32].

sible to carry out a local analysis of a given function, instead of a non-local Fourier composition for which the building blocks are monochromatic harmonics completely delocalized in space-time. The physical meaning of this can be grasped from Figure 5.3.

Suppose that $f(x)$ represents, at a given instant, the positions of two particles in a relative motion. If the position of one peak moves, it is only necessary to handle the respective group of wavelets to recompose it, *independently* of the position of the other peak that is composed by another group of wavelets. Yet, Fourier analysis takes $f(x)$ as a whole, composed by monochromatic harmonic waves extending through all space-time. Thus, the motion of one peak implies the global reconstruction of $f(x)$ by the *same* harmonic waves altering, of course, the respective coefficients. The last analysis clearly implies the entanglement of the particles as asserted by the orthodox theory, even if they are years-light apart. Both mathematical analyses are unassailable though leading to distinct physical pictures: locality versus non-locality.

- (iii) A basic natural chaotic sub-quantum medium where all physical processes occur. Particles are complex entities, stable organizations of the sub-quantum medium, composed by a guiding wave (θ), responsible for the interferometric properties, enclosing a very narrow localized structure (dubbed as “singularity” or “acron”, ξ), related to the particle size and re-

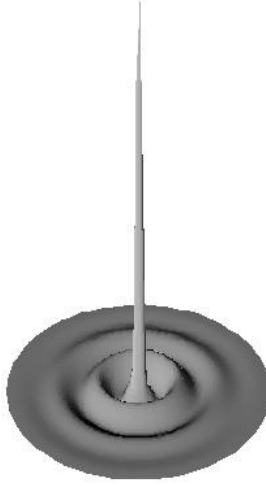


Figure 5.4. Sketch of a quantum particle [32].

responsible for the usual quadratic detection. This is sketched in Figure 5.4. The acron carries most of the energy. The theta wave, with practically no energy, guides the acron by a non-linear interacting process preferentially to regions where the intensity is higher. The non-linear process implies that the two components of the entity beat always in phase. The orthodox *indeterminacies* should now be interpreted as the ever-present statistical *uncertainties* in the measurement processes. This is, essentially, a revival of de Broglie's "pilot wave" suggestion.

- (iv) A non-linear, non-relativistic and time-dependent master equation, that combines the corpuscular and wave sides of classical physics, established from the Hamilton-Jacobi and fluid continuity equations:

$$-\frac{\hbar^2}{2m}\nabla^2\Psi + \frac{\hbar^2}{2m}\frac{\nabla^2(\Psi\Psi^*)^{1/2}}{(\Psi\Psi^*)^{1/2}} + V\Psi = i\hbar\frac{\partial\Psi}{\partial t}$$

For the special cases of potential $V = 0$ and stationary solutions, the master equation is formally identical to Schrödinger's equation. On the other hand, when the corpuscular and undulatory properties are taken as independent realities, the master equation leads to the fundamental classical equations. Thus, it is claimed that the approach unifies quantum and classical physics.

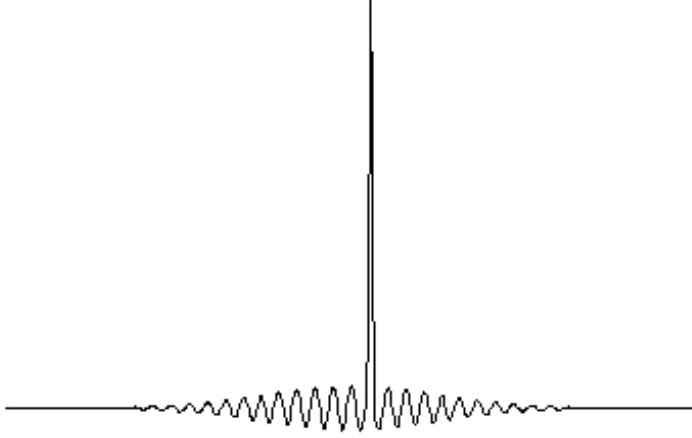


Figure 5.5. Free particle model [32].

The model analytical solution of the master equation for a free particle, for example, is:

$$\phi = \xi + \theta = \sqrt{\frac{E}{\pi^{1/2}\sigma_0}} \left\{ \exp \left[-\frac{1}{\hbar^2} \frac{(xp_x - 2Et - \varepsilon_0)^2}{2\sigma_0^2} \right] + \alpha \exp \left[-\frac{1}{\hbar^2} \frac{(xp_x - 2Et - \varepsilon)^2}{2\sigma^2} \right] \right\} \exp \left[\frac{i}{\hbar} (xp_x - 2Et) \right]$$

where σ_0 and σ are, respectively, the widths of the acron (very narrow) and the θ wave; ε_0 and ε are translation parameters for the acron and θ wave, so that the acron is always inside the guiding wave, and $0 < \alpha \lll 1$; $E = \hbar\omega$ and $p = \hbar k$. The real part of the function is represented in Figure 5.5, which is captured by the sketch of Figure 5.4.

According to this approach, the quantum particle is interpreted as a wave pulse, with defined energy and frequencies, described by the non-linear equation and moving without dispersion. This resembles the soliton phenomena [35] that also obey to a non-linear equation from which it is possible to derive a kind of non-linear Schrödinger equation.

5.8.1 The two-slit experiment

Richard Feynman once said that all the “mystery” of quantum mechanics is conveyed by the one-particle two-slit experiment (see Figure 5.6). Indeed, it

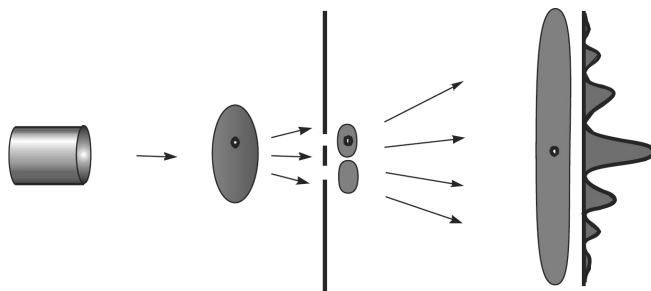


Figure 5.6. The two-slit experiment [32].

apparently shows, according to the orthodox interpretation, distinct behaviours *depending* on the observation apparatus. Thus, if two detectors are placed just after the slits, the conclusion is that the particle passes through one slit *or* the other. If a screen is placed sufficiently far away from the slits, then the conclusion is that the particle passes through one slit *and* the other accounting for the interference. The collapse of the wave function is invoked and reality appears to be created by the observation process, since two distinct processes are required to show up particle-like *or* wave-like properties. Never both simultaneously once the measuring processes are incompatible. Ultimately, the mystery is: how can an *indivisible* particle go simultaneously through both slits?

For the local-causal interpretation there is neither mystery nor collapses of the wave functions, and the reality, composed of waves *and* particles, is independent of the observer. The indivisible acron passes through one slit *or* the other, and the “pilot wave” through *both* slits. If the acron is detected right after one of the slits, then the theta wave from the other slit will follow its own way and should be possible to detect it. If not, both waves will interfere and the particle will be detected at the screen, where the intensity of the resulting wave is higher. In any case the wave-particle properties are always present, that is, they are not created by the observation process.

The last interpretation is identical to de Broglie’s view, expounded during the 5th Solvay Conference in 1927, on the “pilot wave” idea that was taken as the basis of his *double-solution theory* and de Broglie-Bohm’s hidden-variable for-

mulation. Croca's approach is also, in particular aspects, inspired by de Broglie's work. Curiously, it is reported that, by 1928, de Broglie became converted to the orthodox view, presumably influenced by fellows (particularly Pauli) of the Copenhagen school. Later, however, he was interested in Bohm's work even writing, in 1957, the forward of Bohm's book *Causality and Chance in Modern Physics* [1, 4, 6].

5.8.2 Beyond Heisenberg's uncertainty relations

Heisenberg derived the uncertainty relations in 1927, based on Born's interpretation and transformation theory. His early interpretation considered the electrons essentially as corpuscle-like entities, and the relations as an instrumental impossibility of simultaneously specifying non-commuting observables. The uncertainty principle was, to him, the very basis of quantum theory. Bohr strongly disagreed on Heisenberg's viewpoint. Arguing that the indeterminacy relations can be exclusively derived from a pure Fourier analysis of wave packets (and that Heisenberg's analysis of the γ -ray microscope experiment was flawed) he defended that the true heart of the theory was the wave-particle duality, accordingly to his complementary principle. All the rest would come out from it [1, 4, 13]. As already referred to, Heisenberg soon adhered to Bohr's interpretation.

In the context of local wavelet analysis, however, more general uncertainty relations have been derived [32]. For position-momentum:

$$\Delta x^2 = \frac{b^2}{\Delta p_x^2 + b^2/\sigma_0^2}$$

and for time-energy:

$$\Delta t^2 = \frac{b^2}{\Delta E^2 + b^2/\sigma_0^2},$$

where σ_0 is the average width of the basic (or "mother") wavelet. If $\sigma_0 \rightarrow \infty$, then the wavelet tends to a monochromatic harmonic wave (Fourier analysis) and Heisenberg's relations are obtained.

The generalized relations allow for a wider spanning of the measurement spaces than Heisenberg's relations (see Figure 5.7). Consider the measurement

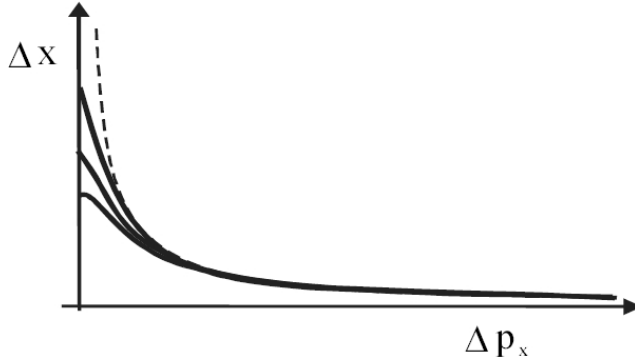


Figure 5.7. Spanning of position-momentum space: (solid lines) generalized relations for different values of the basic wavelet; (dashed line) Heisenberg's relation [32].

of the position and momentum of a particle by a common and by a tunnelling super-resolution microscope. The maximum momentum uncertainty for both is:

$$\Delta p_x = 2 \frac{b}{\lambda}$$

For the common microscope, the maximum theoretical resolution is:

$$\Delta x = \frac{\lambda}{2},$$

therefore

$$\Delta x \Delta p_x = b,$$

that is Heisenberg's relation.

As for the super-resolution microscope, the resolution is at least,

$$\Delta x = \frac{\lambda}{50},$$

whence

$$\Delta x \Delta p_x = \frac{1}{25} b$$

which is in discrepancy with Heisenberg's relation but not with Croca's one.

5.9 Some issues

Like in any new theory, multifarious questions naturally turn out, particularly to us who never worked on the present approach. For example:

(i) If $\Psi_1, \Psi_2, \Psi_3, \dots, \Psi_n$ are solutions of Schrödinger's equation so is:

$$\Psi = \Psi_1 + \Psi_2 + \Psi_3 + \dots + \Psi_n \quad (\text{superposition principle})$$

The same is not true for the master non-linear equation. Then, how to compose the solutions? $\Psi = \Psi(\Psi_1, \Psi_2, \Psi_3, \dots, \Psi_n)$ is not known in general.

- (ii) How to incorporate spin and symmetry aspects?
- (iii) The non-linear resolutions of the harmonic oscillator and the hydrogen atom are under progress, showing solutions other than the usual ones [36]. What is their meaning? Do they add new informations?
- (iv) Experiments have been proposed to detect the θ waves. At least one of them has been performed though, apparently, not conclusive [32]. What is the expectable progress?
- (v) Apart the new picture, the appealing interpretations and the more general uncertainty relations, will the heavy burden of solving non-linear equations, in complex chemical and physical problems, be rewarded for new and unexpected results not reachable by the orthodox linear theory?
- (vi) The approach suggests the possibility of understanding gravitational phenomena [32]. Is it a route to unify quantum and general relativity theories?

5.10 Linearity versus non-linearity

The linearity of the orthodox theory has been questioned by various authors. Here, we only cite Steven Weinberg: "Quantum mechanics has had phenomenal successes in explaining the properties of particles and atoms and molecules, so we know that it is a very good approximation to the truth. The question then is whether there is some other logically possible theory whose predictions are very close but not quite the same as those of quantum mechanics ... It is striking that it has so far not been possible to find a logically consistent theory that is close to quantum mechanics, other than quantum mechanics itself ...

In inventing an alternative to quantum mechanics I fastened on the one

general feature of quantum mechanics that has always seemed somewhat more arbitrary than others, its linearity ...

This theoretical failure to find a plausible alternative to quantum mechanics, even more than the precise experimental verification of linearity, suggests to me that quantum mechanics is the way it is because *any small change in quantum mechanics would lead to logical absurdities*. If this is true, quantum mechanics may be a permanent part of physics. Indeed, quantum mechanics may survive not merely as an approximation to a deeper truth, in the way that Newton's theory of gravitation survives as an approximation to Einstein's general theory of relativity, but as a precisely valid feature of the final theory" [37].

The reason of the reported failure seems to be, in fact, that *any small change in quantum mechanics would lead to logical absurdities*. Indeed, the orthodox theory is based on a rigorous mathematical structure through a consistent set of postulates intrinsically based on linearity. In this strict context, it appears a complete statistical theory, though physically and philosophically anti-realist in many aspects. Therefore, amendments can lead to absurdities since the self-consistency of the theory structure might be broken. Thus, it seems that only an approach that changes the fundamental structure of the theory may fully avoid logical and physical contradictions.

5.11 Language, thought and perception

The spoken and pictorial languages are intimately related to the thought and perception processes. Quoting Lee Whorf: "We are thus introduced to a new principle of relativity, which holds that all observers are not led by the same physical evidence to the same picture of the universe, unless their linguistic backgrounds are similar, or can in some way be calibrated" [38].

For example, the language of the American Hopi Indians contains no reference to *time* either explicitly or implicitly. Yet, it is capable of accounting for all observable phenomena of the universe. Time is not one of the measurement observables that the Hopi Indians employ. They use other means to speak of the universe. Their language expresses their perception, and it does not include

time.

On the other hand, time is not an observable in quantum mechanics, since there is no *time operator* in its structure. Curiously, for Kurt Gödel, “time does not really exist in any objective sense. It’s not really out there in the world at all; it’s our special mode, our own particular way of perceiving the world” [39].

Mathematics is also a language, simultaneously analytic and geometric (pictorial), more universal and suitable for a calibration (in Lee Whorf’s sense). But will it be essentially primitive and intrinsically connected to our processes of thought and perception? Or a language that only attempts to express facts perceived *a priori*, even in the most abstract developments? Incidentally, what would be the representations of Schrödinger and non-linear master equations in the Hopi language?

These questions appear of the utmost importance, especially in the context of quantum mechanics since its language and interpretation problems fall right into the processes of perceiving and conveying the nature of physics.

5.12 Concluding remarks

In this digression we have addressed some approaches and interpretations of quantum theory. After all, there were more questions than answers but quoting J. Joubert: “it is better to debate a question without settling it than to settle a question without debating it” [1].

Some issues on the theory interpretation and unifications will certainly continue at stake, challenging researchers and philosophers, and stimulating new steps forward.

However, one point seems inescapable: *contraria sunt complementa*, as Bohr inscribed at the top of the *yin-yang* symbol in his Cote-of-Arms, when he was knighted (Order of the Elephant) in 1947.

The eventual spiritual anguish due to the implicit contradictions might, hopefully, be relieved by:

Do I contradict myself?

Well then, I contradict myself.

I am large, I contain multitudes.

(Walt Whitman)

Acknowledgments

The author thanks Professor Simões Redinha, Universidade de Coimbra, for the kind and friendly invitation; Professor José Croca, Universidade de Lisboa, for the invaluable discussions on the non-linear quantum physics, and permission to reproduce some of his figures; Academia das Ciências de Lisboa for hosting the Colloquium and the kind reception.

References

- [1] M. Jammer, *The Philosophy of Quantum Mechanics* (Wiley, New York, 1974).
- [2] W. Heisenberg, *The Physical Principles of the Quantum Theory* (Dover, New York, 1949).
- [3] W. Heisenberg, *Physics and Philosophy* (Penguin Books, London, 1989).
- [4] J. Baggott, *Beyond Measure: Modern Physics, Philosophy and the Meaning of Quantum Theory* (Oxford University Press, Oxford, 2004).
- [5] R. Gomatam, *Phil. of Sci.* **74**, 736 (2007).
- [6] M. Kumar, *Quantum: Einstein, Bohr and the Great Debate About the Nature of Reality* (Icon Books, London, 2009).
- [7] A. Einstein, *Phys. Rev.* **47**, 777 (1935).
- [8] J. von Neumann, *Mathematical Foundations of Quantum Mechanics* (Princeton University Press, New Jersey, 1955).
- [9] P. A. M. Dirac, *The Principles of Quantum Mechanics* (Clarendon Press, Oxford, 1991).
- [10] I. N. Levine, *Quantum Chemistry* (Prentice Hall, New Jersey, 1991).
- [11] L. E. Ballentine, *Am. J. Phys.* **40**, 1763 (1972).
- [12] E. Merzbacher, *Quantum Mechanics* (Wiley, New York, 1970).
- [13] N. Bohr, *Nature* **121**, 580 (1928).
- [14] K. Popper, *Quantum Theory and the Schism in Physics* (Hutchinson, London, 1982).

- [15] *Quantum Theory Without Reduction*, edited by M. Cini and J.-M. Lévy-Leblond (Adam Hilger, New York, 1990).
- [16] E. Squires, *The Mystery of the Quantum World* (Institute of Physics Publishing, London, 1994).
- [17] M. Gell-Mann, *The Quark and the Jaguar. Adventures in the Simple and the Complex* (Freeman, New York, 1995).
- [18] N. Bohr, Phys. Rev. **48**, 696 (1935).
- [19] W. Isaacson, *Einstein: His Life and Universe* (Simon & Schuster, New York, 2007).
- [20] D. Bohm, *Wholeness and the Implicate Order* (Ark Paperbacks, London, 1985).
- [21] D. Bohm, *Quantum Theory* (Prentice-Hall, New York, 1951).
- [22] D. Bohm, Phys. Rev. **85**, 166 (1952).
- [23] C. Philippidis and C. Dewdney, Nuovo Cimento **52B**, 15 (1979).
- [24] J. S. Bell, Physics **1**, 195 (1964).
- [25] J. S. Bell, Rev. Modern Phys. **38**, 447 (1966).
- [26] C. Thompson, *arXiv:quant-ph/0508024v1* (August 2005).
- [27] C. Thompson, *arXiv:quant-ph/0210150v3* (November 2005).
- [28] C. Thompson, *arXiv:quant-ph/0512141v1* (December 2005).
- [29] A. Legget, J. Phys.: Cond. Matt. **14**, R415 (2002).
- [30] S. Gröblacher, T. Paterek, R. Kaltnbaek, C. Brukner, M. Zukowski, M. Aspelmeyer, and A. Zeilinger, Nature **446**, 871 (2007).
- [31] C. Branciard, A. Ling, N. Gisin, C. Kurtsiefer, A. Lamas-Linares, and V. Scarani, Phys. Rev. Lett. **99**, 210407 (2007).
- [32] J. R. Croca, *Towards a Nonlinear Quantum Physics* (World Scientific, New Jersey, 2003).
- [33] J. R. Croca and A. Garuccio, Adv. Sci. Lett. **3**, 1 (2010).
- [34] B. B. Hubbard, *The World According to Wavelets* (A. K. Peters, Massachusetts, 1998).
- [35] P. S. Lomdahl, Los Alamos Science **10**, 27 (1984).
- [36] J. R. Croca (private communication, 2009)

- [37] S. Weinberg, *Dreams of a Final Theory* (Vintage Books, New York, 1993).
- [38] B. LeeWhorf, *Language, Thought and Reality* (The MIT Press, Massachusetts, 1995).
- [39] E. Regis, *Who Got Einstein's Office* (Penguin Books, London, 1988).

(Página deixada propositadamente em branco)

6. ADIABATIC APPROXIMATION AND RELATED ISSUES INCLUDING TOPOLOGICAL IMPLICATIONS

A. J. C. Varandas*

Departamento de Química, Universidade de Coimbra
3004-535 Coimbra, Portugal

We provide a perspective on several issues of the adiabatic approximation to the fundamental equation of quantum chemistry as suggested by Born and Oppenheimer: separation of the electronic and nuclear motions, coupled-channel treatment, scaling properties, validity, and diabatic states. The need for its generalization such as to account for the topological implications that arise from the separation of the electronic (fast) and nuclear (slow) degrees of freedom is also described in some detail by focusing on Jahn-Teller systems. Although considerable work has been reported on the energetics and dynamics of two-fold degeneracies of the conical type, the list of references on higher electronic degeneracies is meager due to enhanced theoretical difficulty. For high degeneracies, it may therefore be convenient to avoid the dynamics altogether by making use instead of symmetry invariants. This short review will cover both types of approaches to the electron-nuclei coupling problem, but focusing on work carried out at the author's group.

6.1 Introduction

It is well established [1] that no problem in physics or chemistry can ever be solved exactly. Approximations are unavoidable, with the adiabatic approximation due to Born and Oppenheimer [2] (BO), often called a theorem [3], being most fundamental as it is instrumental for ascribing a shape to a molecule. Without it, the solution (albeit approximate) of the fundamental equation of quantum mechanics - the Schrödinger equation (SE) - cannot be obtained except for simple model systems. In fact, the SE can be solved exactly for the hydrogen atom but no exact solution exists for any multi-electron system. Strictly speak-

*Email address: varandas@qtvs1.qui.uc.pt

ing, the SE is itself an approximation as it does not account for relativistic effects, and in nature there is no such a thing as a non-relativistic Schrödinger atom or molecule. Similarly, Dirac's equation is exactly solvable for the hydrogen atom and accounts for relativity, but cannot account for the size and structure of the atomic nuclei (thus, for the atomic interaction with the electromagnetic field). In turn, quantum electrodynamics allows to achieve higher accuracy (by describing, say, the Lamb shift of levels), but this too only allows the calculation of properties at some order of approximation to the relativistic effects. The above cannot be viewed [4] as a pitiful temporary drawback but something that goes on forever reflecting the approach of physics to nature: physics is nothing but a hierarchy of approximations.

By allowing an accurate treatment of the electronic structure without concerning the nuclei, the BO approximation underpins the way most chemists think about molecules. In fact, such a dividing to conquer idea which may even predate the publication of the BO key paper [5], leads to the concept of potential energy surface (PES). Because this governs the nuclear motion, the BO approximation lies at the heart of both molecular spectroscopy and chemical kinetics. Manifestations of the breakdown of the BO approximation in systems that are expected to behave adiabatically are ubiquitous in the sense of being rather small, but they may be non-negligible if accuracy is on demand. In fact, since electrons are expected to follow imperfectly the nuclei in their vibrational and rotational motions, nonadiabatic effects are expected to be required whenever there is a need to take into account that the vibrational and rotational motions of the nuclei induce interactions with other electronic states. The BO approximation should therefore be most valuable if electronic properties are considered, although it becomes somewhat more problematic when vibrational-rotational properties are envisaged. For example, to obtain a dissociation energy of a diatomic in an adiabatic calculation one calculates first the potential energy curve and then subtracts the zero-point energy for vibration. Instead, a nonadiabatic calculation will give directly the observable dissociation energy of a molecule rather than the well depth of the PES. Yet, it is well established that, even for the

most unfavorable case of the hydrogen molecule (where the electron/nucleus ratio is 1/1836), the calculated dissociation energy lies surprisingly close [6] to the experimental value. Of course, the BO approximation can manifest itself also on systems beyond electrons and nuclei, and we have recently suggested that such an effect may explain the undissociated equator-to-pole motion of an helium atom when moving around a much heavier fullerene molecule [7–9].

The adiabatic BO approximation lies therefore on the assumption that the electronic states are well separated with the motion of the nuclei being governed by just one electronic state. Yet, it is now well established that intersections may occur between PESs of the same spatial and spin symmetry. In $2D$ Hilbert space, the necessary and sufficient condition for such an intersection (known as a conical or diabolical intersection) to occur can be satisfied if the molecule has three atoms or more. Similarly, threefold degeneracies are possible for tetratomic and larger molecules, fourfold for five atoms or more, fivefold for at least seven atoms, and so on. Such topological features bear key implications on the validity of the BO approximation, a subject that will be discussed in the present work.

A special class of systems where conical intersections occur due to symmetry reasons is known under the names of Jahn and Teller [10–13] (JT) who established the following Theorem: *all molecules (other than linear ones) distort from a symmetric configuration \mathbf{Q}_0 if, by so doing, any electronic degeneracy can be lifted*. In the vicinity of \mathbf{Q}_0 , the PES assumes the form $E_{\pm} = E_0 \pm c\rho$, where ρ is the radial polar coordinate in the subspace (v -space) that contains all JT distorted configurations¹. If the PES does not satisfy such a requirement (by having an extremum at \mathbf{Q}_0 , say), it is called non-JT: it may even touch tangentially the next non-JT excited state leading then to a pseudo-JT type instability [11, 13]. Generically, N -fold electronic degeneracies have associated the unitary and rotation groups in N dimensions [11].

The study of conical intersections in $2D$ Hilbert space [15–19] has been pi-

¹The only exception to such instabilities on linear systems are twofold spin degeneracies of Kramer's type [14]. These are of no concern as only orbital degeneracy is here envisaged. If quadratic coupling is included, the linear molecules will also not be an exception due to the so-called Renner-Teller (RT) effect, also out of the scope of the present work.

oneered by Herzberg and Longuet-Higgins [20]. In 1975, Longuet-Higgins [21] (LH) established the following two key theorems: *I. On going once around any closed path on the surface that contains the conical intersection the electronic wave function changes sign; II. If a real adiabatic electronic wavefunction changes sign when a polyatomic traverses a 1D closed loop on a 2D surface in the $(3N-6)$ -D nuclear configuration space, then the corresponding electronic state must become discontinuous and degenerate with another one at an odd number of points lying on that surface and within that loop.* There is therefore a phase factor (geometrical phase or GP) experienced by an eigenfunction of the parameter-dependent Hamiltonian when transported adiabatically such as to complete a path closing to itself around the conical intersection. In fact, such an intersection can be demonstrated by verifying [22,23] the LH theorem I, by evaluating the line integral of the derivative couplings along a closed loop [17, 24], or by using [23] the Pancharatnam [25] connection. Varandas, Tennyson and Murrell [22] have in turn demonstrated that a conical intersection needs not be forced by symmetry reasons.

Although the GP effect has been known for decades [20,21], interest on it has largely been motivated by Mead and Truhlar [26] derivation of a general phase factor formula in the context of the molecular BO problem followed by its rederivation and recasting in a more general context by Berry [24]. It became then also known as the Berry phase. Because the involved differential equations are similar to those of a charged particle moving in the presence of a magnetic solenoid, it is further often called as the molecular Aharonov-Bohm effect. Note that the GP appears whenever the BO approximation is utilized to separate the fast motion of the electrons from the slow vibrational degrees of freedom (parameters) in studying the coupled vibrational-electronic (vibronic) system. [Parenthetically, it should be noted that mathematical tools such as fibre bundles and gauge theories have specialized to describe (an)holonomies like GP; an account of this can be found in Ref. 27] Since the total BO wave function is a product of the electronic and nuclear ones, with the former changing sign when transported adiabatically along a loop that encircles a conical intersection [20,

21,24], a sign change of opposite effect must occur in the nuclear wave function such that their product becomes single-valued. This has important consequences on the quantized nuclear motion, particularly in determining the symmetry of the ground-state vibronic energy levels [13,28]. Indeed, its signature on reaction dynamics has been a theme of much debate over the years [29–33].

Compared with the vast amount of research on twofold degeneracies [17,24,26,34–42] (the list is by no means exhaustive), the number of studies on the GP effect at higher electronic degeneracies is meager [19,28,43–45]. Cullerne and O’Brien [46] have been the first to use both numerical and analytical methods to map the lowest adiabatic PESs of icosahedral molecular systems such as fullerenes with a view to understand the rich structure of their degenerate electronic and vibrational modes as well as the role of GP. They have remarked [46] “To discuss the complete structure of degeneracies and Berry phases over the full nine-dimensional ($9D$) space of $G \otimes (g \oplus b)^2$ would be a mammoth task. Indeed, it is a task that we did not even complete in the $4D$ and $5D$ phase spaces of the subsystems $G \otimes g$ and $G \otimes b$.” In 1998, Manini and De los Rios [28] and, more recently, Lijnen and Ceulemans [47] investigated the GP effect on the manifold of JT potential minima (JTM) of such species. Other developments are due to Manolopoulos and Child [43] who have utilized a model Hamiltonian to investigate the possible sign changes that can occur when N real quantum states are transported adiabatically around a N -fold electronic degeneracy. and to Baer [44] that focused on the topological features and existence of pure diabatic states. In a recent series of papers, we have instead advocated [19,45,48] the use of Lie group symmetries to study such N -fold degeneracies in JT systems. Two major questions have been addressed: (*i*) how many of the electronically degenerate states are subject to GP? (*ii*) can the GP effect be treated in a way similar to what is commonly done for the $2D$ Hilbert-space case? The basic idea is then to provide relevant answers of chemical physics interest without having to perform a diagonalization of the JT matrix and follow up the GP change in

²Although the notation is rather variable in the literature, we use the notation E for doublets, T for triplets, G for quartets and H for quintets.

configuration space, but rather make use of symmetry invariants that are inherent to each system. Interestingly, such a work has also suggested [48] that the LH theorem can provide a rationale for any arbitrary N -fold, JT type, electronic degeneracy.

The structure of this Chapter is as follows. After a presentation of the SE in section 6.2, the BO approximation follows in section 6.3 and its subsections, where the following issues are discussed: separation of the electronic and nuclear motions, coupled-channel treatment, scaling properties, BO validity, and diabatic states. A generalized BO formulation will then be discussed in section 6.4 for the $2D$ Hilbert space case, thus accounting for the topological implications due to conical intersections. After a brief presentation of function space in section 6.5, attention is driven to the treatment of higher-dimensionality JT manifolds in section 6.6, and to the generalization of the LH theorem in section 6.7. Section 6.8 explores the possibility of using the novel formalism also for solving the dynamics of the nuclear motion. The work presented is tentative and is currently being explored in our Group. Because specialized books and reviews have recently covered some of the topics discussed in the present report, this will focus primarily on the author's own work. The Chapter concludes with section 6.9.

6.2 The electronuclear Schrödinger equation

The SE describing the complete time-dependent many-body problem assumes the form

$$i\hbar \frac{\partial}{\partial t} \tilde{\Omega}(\mathbf{r}_e, \mathbf{r}_n, t) = \hat{H}(\mathbf{r}_n, \mathbf{r}_e) \tilde{\Omega}(\mathbf{r}_e, \mathbf{r}_n, t) \quad (6.1)$$

where t represents the time, $\mathbf{r}_e = \{x_i\}$ ($i = 1, \dots, 3N$) denotes the collective positions of the N electrons, $\mathbf{r}_n = \{X_I\}$ ($I = 1, \dots, 3M$) those of the M nuclei, the molecular Hamiltonian assumes the form

$$\hat{H}(\mathbf{r}_e, \mathbf{r}_n) = -\frac{\hbar^2}{2m_n} \Delta_n - \frac{\hbar^2}{2m_e} \Delta_e + V(\mathbf{r}_e, \mathbf{r}_n) \quad (6.2)$$

where m_e is the mass of the electron and, for simplicity, all nuclei have been assumed to have the same mass m_n ; $\Delta_e = \sum_{i=1}^N \nabla_i^2$ and $\Delta_n = \sum_{I=1}^M \nabla_I^2$ are the

corresponding Laplacians, with $\nabla_i = \nabla_{i,x}\hat{i} + \nabla_{i,y}\hat{j} + \nabla_{i,z}\hat{k}$ and $\nabla_I = \nabla_{I,x}\hat{i} + \nabla_{I,y}\hat{j} + \nabla_{I,z}\hat{k}$. Note that the potential energy $V(\mathbf{r}_e, \mathbf{r}_n)$ is assumed to be a real function³. Although $\Omega(\mathbf{r}_e, \mathbf{r}_n, t)$ is in general a function of the coordinates and time and cannot be expressed as a function only of time multiplied by another function only of coordinates, it turns out that we can express any solution of the SE as the sum of a series of separable ones. Substitution of the simple product $\tilde{\Omega}(\mathbf{r}_e, \mathbf{r}_n, t) = \Omega(\mathbf{r}_e, \mathbf{r}_n)\phi(t)$ into SE (6.1) and dividing both sides of the resulting equation by $\Omega(\mathbf{r}_e, \mathbf{r}_n)$ then yields:

$$\frac{i\hbar}{\phi(t)} \frac{d\phi(t)}{dt} = \frac{1}{\Omega(\mathbf{r}_e, \mathbf{r}_n)} \hat{H}(\mathbf{r}_e, \mathbf{r}_n) \Omega(\mathbf{r}_e, \mathbf{r}_n) \quad (6.3)$$

Note that \hat{H} has been chosen to be a function only of the spatial coordinates, and not of t , such as to make the first expression in this equation a function only of t , and the second a function only of \mathbf{r}_e and \mathbf{r}_n . It can then be concluded that both expressions are equal to a third that can be neither a function of spatial coordinates nor of time. If this is designated by a constant E , two differential equations can be extracted:

$$\frac{1}{\phi(t)} \frac{d\phi(t)}{dt} = -\frac{iE}{\hbar} \quad (6.4)$$

and

$$\hat{H}(\mathbf{r}_n, \mathbf{r}_e) \Omega(\mathbf{r}_e, \mathbf{r}_n) = E \Omega(\mathbf{r}_e, \mathbf{r}_n) \quad (6.5)$$

The former can be solved to yield $\phi(t) = \exp(-iEt/\hbar)$. Because the Hamiltonian is a Hermitian operator, its eigenvalues (and hence E) must be real, with the solutions $\phi(t)$ being purely oscillatory. Thus, if

$$\tilde{\Omega}(\mathbf{r}_e, \mathbf{r}_n, t) = \Omega(\mathbf{r}_e, \mathbf{r}_n) \exp(-iEt/\hbar), \quad (6.6)$$

the total wave function $\tilde{\Omega}(\mathbf{r}_e, \mathbf{r}_n, t)$ differs from $\Omega(\mathbf{r}_e, \mathbf{r}_n)$ only by a phase factor of constant magnitude. Of course, Eq. (6.6) is a particular solution of Eq. (6.1). A general solution will therefore be given by a linear combination of such particular solutions:

$$\tilde{\Omega}(\mathbf{r}_e, \mathbf{r}_n, t) = \sum_i c_i \Omega_i(\mathbf{r}_e, \mathbf{r}_n) \exp(-iE_i t/\hbar) \quad (6.7)$$

³A complex potential acts as a source or sink of probability [49].

Finding solutions of the time-independent SE will then generate the components that are necessary for building the time dependent solutions. It is on the time-independent SE that the discussion will be focused hereinafter.

6.3 The BO approximation

Assuming the atomic system of units where $\hbar = m_e = 1$ and defining the mass ratio $\epsilon^4 = m_e/m_n$, Eq. (6.2) assumes the form

$$\hat{H}(\mathbf{r}_e, \mathbf{r}_n) = -\frac{\epsilon^4}{2}\Delta_n + \hat{H}_e(\mathbf{r}_e; \mathbf{r}_n) \quad (6.8)$$

where

$$\hat{H}_e(\mathbf{r}_e; \mathbf{r}_n) = -\frac{1}{2}\Delta_e + V(\mathbf{r}_e; \mathbf{r}_n) \quad (6.9)$$

is the electronic Hamiltonian that depends parametrically on \mathbf{r}_n through $V(\mathbf{r}_e; \mathbf{r}_n)$. Clearly, in the limit of infinitely massive nuclei, these will not move from their positions and the electrons will feel only the Hamiltonian \hat{H}_e for the frozen nuclei positions. This provides the motivation for decoupling the electronic and nuclear motions, since the latter are at least 1836 times as heavy as an electron. Because the nuclei move slowly, it is then a good approximation to assume that the electrons move subject to a Hamiltonian that depends on the position of the nuclei at a given instant.

An alternative derivation of the electronic SE is by assuming that the nuclei can be treated classically. The nuclei will then be described by trajectories $\mathbf{r}_n(t)$, with \hat{H}_e being thought to depend on \mathbf{r}_n or time. If such an assumption is made, the nuclei will move infinitely slowly as we have an Hamiltonian $\hat{H}_e(t)$ that changes very slowly with time. If the electrons begin in an eigenstate of $\hat{H}_e(0)$, they will then adiabatically follow this eigenstate along such a trajectory ending up in an eigenstate of $\hat{H}_e(t)$. Note, however, that the BO approximation does not treat the nuclei classically and that, for slowly moving nuclei, the electronic SE follows naturally.

6.3.1 The electronic Schrödinger equation

The time-independent electronic structure problem is defined by the eigenvalue equation

$$\hat{H}_e(\mathbf{r}_e; \mathbf{r}_n) |\Psi_i(\mathbf{r}_e; \mathbf{r}_n)\rangle = E_i(\mathbf{r}_n) |\Psi_i(\mathbf{r}_e; \mathbf{r}_n)\rangle \quad (6.10)$$

where $|\Psi_i(\mathbf{r}_e; \mathbf{r}_n)\rangle \in \mathcal{H}_f \equiv S_a L^2(\mathbb{R}^{3N})$: it belongs to the Hilbert space for the “fast” electronic degrees of freedom. Because the electrons are fermions, S_a will then project onto the antisymmetric wave functions. In addition to bound states, $\hat{H}_e(\mathbf{r}_e; \mathbf{r}_n)$ has in general a continuous spectrum, with the eigenvectors of Eq. (6.10) being normalized: $\langle \Psi_i(\mathbf{r}_e; \mathbf{r}_n) | \Psi_j(\mathbf{r}_e; \mathbf{r}_n) \rangle = \delta_{ij}$, with the eigenvalues labeled as $E_1(\mathbf{r}_n) \leq E_2(\mathbf{r}_n) \leq \dots$ including multiplicity. The graph of $E_i(\mathbf{r}_n)$ will be called the i -th BO PES. As a rule, such a PES will display a complicated topology with crossings and avoided crossings. For the wave functions of the slow coordinates one has $\mathcal{H}_s \equiv L^2(\mathbb{R}^{3M})$, recalling that to impose the physically correct statistics for the nuclei requires extra considerations [26].

6.3.2 The nuclear Schrödinger equation

Once the electronic SE is solved, one can write down the effective Hamiltonian for the nuclei by simply adding back in the terms that were left out of \hat{H}_e :

$$\hat{H}_n = -\frac{\epsilon^4}{2} \Delta_n + E_i(\mathbf{r}_n) \quad (6.11)$$

Thus, the nuclei move on an effective PES that is defined by the electronic energy, with the wave functions for the nuclei alone being eigenfunctions of this Hamiltonian

$$\left[-\frac{\epsilon^4}{2} \Delta_n + E_i(\mathbf{r}_n) \right] |\Phi_{II}(\mathbf{r}_n)\rangle = E_{II} |\Phi_{II}(\mathbf{r}_n)\rangle \quad (6.12)$$

Note that Eqs. (6.10) to (6.12) do not treat the electrons and nuclei as independent particles: the parametric dependence of the electronic eigenstates, expressed as usual by the semicolon⁴, introduces as we shall see a non-trivial coupling

⁴The obvious dependence of $\Psi_i(\mathbf{r}_e; \mathbf{r}_n)$ and $\hat{H}_e(\mathbf{r}_e; \mathbf{r}_n)$ in the electronic coordinates will be omitted for brevity after Eq. (6.13).

between the two that reflects on topological implications. Thus, the electronic-nuclei decoupling needs not be complete for the BO approximation to be valid. In summary, if the electrons are in an electronic state i and the nuclei in the I -th state of the i -th electronic state, the total electronuclear wave function can be specified as

$$|\Omega(\mathbf{r}_e, \mathbf{r}_n)\rangle = \Phi_{II}(\mathbf{r}_n)|\Psi_i(\mathbf{r}_e; \mathbf{r}_n)\rangle \quad (6.13)$$

where we have used a mixed representation: the nuclei will be described using wave mechanics notation while the electrons employ the popular (bracket) Dirac's notation.

6.3.3 The Born-Huang ansatz and coupled-channel treatment

The BO approximation is extremely accurate by itself, as explained by its widespread use through chemistry. Even when it fails, the result may be explained by assuming that the system is adiabatic almost all time, with only a few isolated regions where corrections need to be accounted for. Thus, it is convenient to consider the exact SE expressed in the basis defined by the BO approximation.

Since the electronic eigenstates for any fixed choice of \mathbf{r}_n form a complete basis that satisfies Eq. (6.10) and, correspondingly, the nuclear eigenstates form a complete basis that satisfies Eq. (6.12) for any i -state, one may conclude that the set of products $\{\Phi_{II}(\mathbf{r}_n)|\Psi_i(\mathbf{r}_n)\rangle\}$ forms a complete basis for expanding any wave function that describes the electrons and nuclei. The total electronuclear wave function can therefore be exactly expressed (C_{Jj} are expansion coefficients) in terms of the so-called Born-Huang ansatz as:

$$|\Omega(\mathbf{r}_e, \mathbf{r}_n)\rangle = \sum_{Jj} C_{Jj} \Phi_{Jj}(\mathbf{r}_n) |\Psi_j(\mathbf{r}_n)\rangle \quad (6.14)$$

By representing now the Hamiltonian as a matrix in the Born-Huang ansatz, one gets

$$\begin{aligned} \mathbf{H}_{j'j''} &= \int \Phi_{j'j'}^*(\mathbf{r}_n) \left[-\frac{\epsilon^4}{2} \Delta_n + E_j(\mathbf{r}_n) \right] \Phi_{j''j''} \delta_{j'j''} d\mathbf{r}_n \\ &\quad - \epsilon^4 \sum_I \int \Phi_{j'j'}^*(\mathbf{r}_n) \nabla_I \Phi_{j''j''}(\mathbf{r}_n) \cdot \mathbf{F}_{j'j''}^I(\mathbf{r}_n) d\mathbf{r}_n \end{aligned}$$

$$-\frac{\epsilon^4}{2} \int \Phi_{j'j'}^*(\mathbf{r}_n) \Phi_{jj}(\mathbf{r}_n) \mathbf{G}_{j'j}^I(\mathbf{r}_n) d\mathbf{r}_n \quad (6.15)$$

where the non-adiabatic coupling matrix elements $\mathbf{F}_{j'j}^I(\mathbf{r}_n) = \langle \Psi_{j'}(\mathbf{r}_n) | \nabla_I \Psi_j(\mathbf{r}_n) \rangle$ and $\mathbf{G}_{j'j}^I(\mathbf{r}_n) = \langle \Psi_{j'}(\mathbf{r}_n) | \Delta_n \Psi_j(\mathbf{r}_n) \rangle$ are the so-called first- and second-derivative non-adiabatic coupling terms (NACTs), respectively. Clearly, the first term in Eq. (6.15) is the BO approximation, while the second and third are corrections to the latter that arise due to the parametric dependence of the electronic wave function on the nuclear coordinates. The magnitude of such corrections will depend on the rate of change (gradient) of the electronic wave function as we change the nuclear configuration. Note that $\mathbf{F}_{j'j}^I(\mathbf{r}_n)$ is a matrix where each of its elements is a vector that originates from the gradient of the electronic wave function with respect to the I -th nuclear coordinates. The direction of this gradient indicates the direction in which the electronic wave function is changing fastest, while its magnitude indicates how large the change is in absolute sense. One then takes the overlap of this gradient with the electronic function $\Psi_{j'}$. This shows, as we vary \mathbf{r}_n , how much the change in Ψ_j looks like a change from the current electronic state Ψ_j to another $\Psi_{j'}$. Indeed, the NACT represents the overlap of wave functions with differentiated functions. Because numerical differentiation of a function involves its calculation at distinct points, the determination of $\mathbf{F}_{j'j}^I(\mathbf{r}_n)$ involves “delayed” overlaps in the sense that the overlapping functions are calculated at separated nearby points. This leads one to expect that NACTs should manifest an overlap dependence which, for realistic Slater type orbitals, is expressed as an inverse exponential of the interatomic distance [50]. Another property of NACTs refers to their sign change. Indeed, because the BO eigenfunctions are determined only up to a sign, it is easy to conclude that the sign of the NACTs cannot be assigned uniquely. Criteria to fix it have been suggested [51, 52] but none is unique. Thus, there is a wealth of information in the $\mathbf{F}_{j'j}^I(\mathbf{r}_n)$ NACT: tells (via its magnitude) how likely non-adiabatic events are, what physical motions it can be associated with (through its direction), and which electronic states are involved (via overlap of the gradient of Ψ_j with $\Psi_{j'}$). If the electronic state changes rapidly over a small distance, the term involving

$\mathbf{F}'_{jj}(\mathbf{r}_n)$ is likely to be large. Conversely, the third term, so-called diagonal BO correction (DBOC), is small and often neglected. The above is known as the coupled channel representation: each electronic state is a distinct channel with the Hamiltonian governing their coupling.

Let us examine briefly two subtleties of the NACTs before concluding this section. The first refers to their dependence on the choice of origin of the coordinate system [50, 53–60], as illustrated for various diatomic species, most recently [50] for LiF. In fact, this origin-dependence of NACTs can be problematic in the case of polyatomic species since the use of different coordinate systems is known to be convenient. Unfortunately, no such a study has, to our knowledge, been reported. A second subtlety, also raised by the origin dependence of NACTs, refers to the fact that the latter may not vanish asymptotically, and then present a problem in imposing the usual scattering boundary conditions. This emerges from the fact that the difference between NACTs calculated with respect to two different origins is proportional to the dipole transition matrix [56, 57, 60]. For example, in LiF the ground state curve dissociates to $\text{Li}(^2S)+\text{F}(^2P)$ while the next state of the same symmetry yields $\text{Li}^+(^1S)+\text{F}^-(^1S)$, and hence such a difference vanishes at $R \rightarrow \infty$ as the connection between 1S and 2P states by the electric dipole operator is spin forbidden [50]. Remedies to the asymptotic problem involve either the use of electron translation factors or appropriate reaction coordinates [54–57].

We are now in position to write the full SE by replacing Eq. (6.14) in Eq. (6.5) and multiplying on the left by $\langle \Psi_j(\mathbf{r}_n) |$. This leads to an infinite set of coupled equations, which may be written in matrix form as⁵

$$\left\{ -\frac{\epsilon^4}{2} [\mathbf{I}\Delta_n + 2\mathbf{F}(\mathbf{r}_n) \cdot \nabla + \mathbf{G}(\mathbf{r}_n)] + \mathbf{V}(\mathbf{r}_n) - E\mathbf{I} \right\} \Phi(\mathbf{r}_n) = \mathbf{0} \quad (6.16)$$

where \mathbf{I} is the identity matrix, $\Phi(\mathbf{r}_n)$ is a column vector whose components are the nuclear wave functions, and $\mathbf{V}(\mathbf{r}_n)$ is now utilized as usual to represent the column vector of electronic PESs $\{E_j(\mathbf{r}_n)\}$.

⁵When unlabeled (often indicated as $\nabla_{\mathbf{R}}$), the operator nabla refers to the nuclear coordinates.

6.3.4 Scaling properties

Born and Oppenheimer argued that the two terms on the right-hand-side of Eq. (6.15) can be neglected as ϵ^4 is a very small number. Indeed, if a typical nuclear mass is taken as $m_n = 10^4 m_e$, then $\epsilon^4 = 10^{-4}$. Consider then a diatomic vibrating close to its equilibrium geometry X_e , and express the nuclear separation as $X = X_e + \epsilon u$, where the reduced distance u can be argued to be of the same order as X_e . Thus, $m_n \propto \epsilon^{-4}$, and $\partial/\partial X \propto \epsilon^{-1}$. This leads to the following typical scaling relationships [61]:

Typical vibrational energy	$\propto 1/\sqrt{m_n} \propto \epsilon^2$
Typical rotational energy	$\propto 1/(m_n X_e^2) \propto \epsilon^4$
First derivative coupling	$\propto \epsilon^4 \partial/\partial X \propto \epsilon^3$
Second derivative coupling	$\propto \epsilon^4$

6.3.5 When is the BO approximation expected to fail?

Although one is tempted to suggest that the BO approximation fails when the nuclei are light, this turns out not to be the major problem. To see this, consider a perturbative view where the first term (BO result) is treated as the zeroth-order Hamiltonian and the second is the perturbation (DBOC is ignored). Since an operator is uniquely determined by its matrix elements, the zeroth-order operator may assume the following form:

$$\hat{H}^0 = \sum_{\alpha\beta} |\Psi_\alpha\rangle \mathbf{H}_{\alpha\beta}^0 \langle\Psi_\beta| \quad (6.17)$$

where $\mathbf{H}_{\alpha\beta}^0 = \langle\Psi_\alpha|\hat{H}^0|\Psi_\beta\rangle$, and α and β are compound indexes belonging to the set of BO states that specify a particular choice of Jj . In fact, if it is assumed that

$$\hat{H}^0 = \sum_k |\Psi_k(\mathbf{r}_n)\rangle \left[-\frac{\epsilon^4}{2} \Delta_n + V_j(\mathbf{r}_n) \right] \langle\Psi_k(\mathbf{r}_n)|, \quad (6.18)$$

then $\mathbf{H}_{j'j}^0$ is identical to the set of matrix elements given by the Born-Oppenheimer term (first-term) of Eq. (6.15). Similarly, the perturbation operator assumes the form

$$\hat{U} = -\epsilon^4 \sum_{j'j} \int |\Psi_{j'}(\mathbf{r}_n)\rangle \sum_I \nabla_I \cdot \mathbf{F}_{j'j}^I(\mathbf{r}_n) \langle\Psi_j(\mathbf{r}_n)|, \quad (6.19)$$

since its matrix elements yield the perturbation correction (second term) in Eq. (6.15). Note that the perturbation operator \hat{U} depends on the momenta of the nuclei. The probability of a non-adiabatic event will then depend on how fast the nuclei are moving. Such a probability, and hence non-adiabatic effects, are then expected to be the larger the faster the nuclei are moving. Since the BO states are eigenstates of \hat{H}^0 , they will cease to be a good approximation to those of \hat{H} when \hat{U} is large. However, imposing that the dynamics evolves on a single PES may have also topological implications. How these can be overcome will be analyzed in section 6.3.7.

6.3.6 Diabatic states

We have seen that in the BO representation the Hamiltonian can be approximated by the sum of Eqs. (6.18) and (6.19). However, the first- and second-order NACTs are difficult to deal with since by using the Hellmann-Feynman theorem it may be shown to behave hyperbolically near the crossing seam where $V_i = V_j$. One may then write [62]

$$\mathbf{F}_{j'j}^I(\mathbf{r}_n) = \frac{\langle \Psi_{j'}^a(\mathbf{r}_n; \mathbf{r}_e) | \nabla^I H_e | \Psi_j^a(\mathbf{r}_n; \mathbf{r}_e) \rangle}{V_{j'}^a(\mathbf{r}_n) - V_j^a(\mathbf{r}_n)} \quad (j' \neq j) \quad (6.20)$$

which shows that the NACTs cannot be neglected especially at regions where $V_{j'}$ approaches V_j . In fact, such a behavior is responsible for severe numerical computational difficulties in the adiabatic approximation. On the other hand, the potential matrix assumes its simplest form by being diagonal in the BO (adiabatic) approximation, $V_{j'j} = V_j \delta_{j'j}$. Clearly, one would then like to avoid the calculation of NACTs. Because they arise due to the fact that the electronic wave function depends parametrically on the nuclear coordinates, one may think of choosing a \mathbf{r}_n -independent basis set, say by defining a complete electronic basis set for a selected geometry of the nuclei. Of course, there are many ways for doing it, and any such basis will be referred to as a diabatic basis [63–66].

Consider now the following (adiabatic-to-diabatic) ATD unitary transforma-

tion:

$$|\Omega(\mathbf{r}_n, \mathbf{r}_e)\rangle = \sum_{j'l'} C_{jl'} \Phi_{jl'}^a(\mathbf{r}_n) |\Psi_j^a(\mathbf{r}_n; \mathbf{r}_e)\rangle = \mathbf{C} \Psi^{a\dagger} \mathbf{U} \mathbf{U}^\dagger \Phi^a \equiv \mathbf{C} \Psi^{a\dagger}(\mathbf{r}; \mathbf{R}) \Phi^d(\mathbf{R}) \quad (6.21)$$

where the explicit dependence of the operators and wave functions is often ignored hereinafter for simplicity, and the superscript $a(d)$ has been added to indicate ‘adiabatic’ (diabatic). By replacing $\Phi^a = \mathbf{U} \Phi^d$ in Eq. (6.16), where \mathbf{U} is an orthogonal matrix, one obtains the following result [67]:

$$\left\{ -\frac{\epsilon^4}{2} \mathbf{U} \Delta_n - \frac{\epsilon^4}{2} [\Delta_n \mathbf{U} + 2\mathbf{F}(\nabla \mathbf{U}) + \mathbf{G} \mathbf{U}] - \epsilon^4 (\nabla \mathbf{U} + \mathbf{F} \mathbf{U}) \nabla + (\mathbf{V}^a - E \mathbf{I}) \mathbf{U} \right\} \Phi^d = \mathbf{0} \quad (6.22)$$

Assuming now that \mathbf{U} can ideally be chosen to solve

$$\nabla \mathbf{U} + \mathbf{F} \mathbf{U} = \mathbf{0}, \quad (6.23)$$

it can be shown that Eq. (6.22) will then reduce to

$$\left(-\frac{\epsilon^4}{2} \mathbf{I} \Delta_n + \mathbf{V}^d - E \mathbf{I} \right) \Phi^d = \mathbf{0} \quad (6.24)$$

where

$$\mathbf{V}^d = \mathbf{U}^\dagger \mathbf{V}^a \mathbf{U} \quad (6.25)$$

Note that $|\Psi_j^d\rangle$ does not vary with \mathbf{r}_n , and hence $\mathbf{F}_{jj'}^d = 0$ in the diabatic basis. Conversely, the diabatic states will not diagonalize the electronic Hamiltonian, which becomes instead more complicated. This shows that the substitution of the adiabatic ansatz by the diabatic one does lead to a system of coupled differential equations similar to Eq. (6.16) but with some notable differences. First, the potential matrix becomes nondiagonal in the diabatic basis. In fact, the adiabatic potential matrix is diagonal, while in the diabatic basis it becomes a source of transitions between the surfaces. Second, the matrix elements of the nuclear kinetic energy operator disappear, but off-diagonal terms arise instead in the diabatic potential matrix. Of course, if a complete basis set is assumed, the unitary transformation in Eq. (6.25) warrants that the eigenvalues of the diabatic

potential matrix coincide with the adiabatic potentials in Eq. (6.16). In practice, the diabatic basis is most useful very near a crossing or avoided crossing. Unfortunately, it is not possible to find strictly diabatic electronic states for which $\mathbf{F}_{j,j'}^I(\mathbf{r}_n)$ vanishes everywhere. Indeed, even if the adiabatic and diabatic results would coincide in the limit of an infinite basis, such diabatic states would not be very useful in practice due to the large number of them that would be required to describe the electronic structure. Often a linear combination of a small set of N_{ad} adiabatic states is instead chosen to be maximally diabatic:

$$|\tilde{\Psi}_k^d\rangle = \sum_{ki}^{N_{ad}} c_{ki}(\mathbf{r}_n) |\Psi_i^{ad}(\mathbf{r}_n)\rangle \quad (6.26)$$

If there is only one degree of freedom, we can even do this by choosing our maximal diabatic states [68] so that $\mathbf{d}_{jj'}^I(\mathbf{r}_n)$ is diagonal:

$$\left\langle \tilde{\Psi}_j^d(\mathbf{r}_n) \left| \frac{\partial}{\partial \mathbf{r}_n} \right| \tilde{\Psi}_{j'}^d(\mathbf{r}_n) \right\rangle \propto \delta_{jj'} \quad (6.27)$$

In this case, the diabatic states become the set of electronic states that diagonalize the nuclear kinetic energy operator, whereas the adiabatic states diagonalize $\hat{H}_e(\mathbf{r}_n)$. The point to emphasize is that the PES is no longer single-sheeted, but (nonadiabatic) multi-sheeted by assuming the form of a potential matrix. Suffice it too add that there is considerable interest in methods that yield a diabatic potential matrix from an adiabatic one as this can facilitate drastically the nonadiabatic dynamics calculations.

A wide variety of methods for producing diabatic potentials has been reported in the literature [50, 69–86], as well as (diabatic) multi-sheeted PESs [70, 71, 73, 74, 80, 82, 84, 85, 87–96] (the list is by no means comprehensive). Such methods can be divided in two categories [85] according to whether they merge into the proper adiabatic states at the asymptotes or not. The direct diabatization approach gathers methods that yield directly the diabatic states [70, 71, 73–78, 80–84, 97], either from *ab initio* energies or diabatic electronic wave functions, thus without any intermediary. The second class includes three subclasses. One includes approaches that model the various diabats from regions of the adiabatic potentials where they are supposed to play the dominant

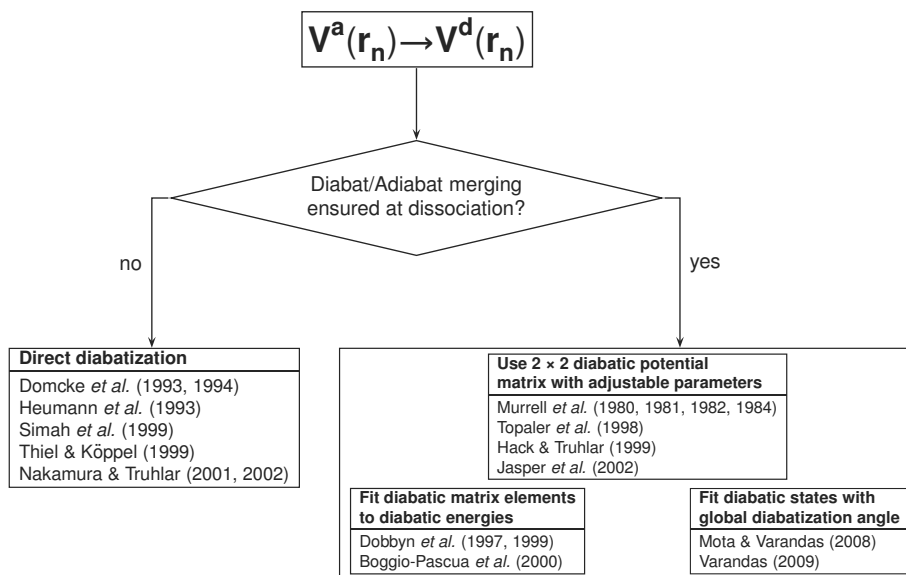


Figure 6.1. Schemes for adiabatic-to-diabatic transformation of PESs (see text).

role, thus warranting the desired asymptotic behavior by built-in construction. In another subclass the diabatic states are built with the help of molecular properties [69, 72, 79] that behave akin to the potential energy, in particular dipole or transition moments. In the third subclass, the various diabatic potentials are calculated and then assembled via a global diabatization angle. Figure 6.1 summarizes the various types of diabatization methods, with the reader being referred to Ref. 85 and the original papers for further details.

A final comment to readdress the issue of dependence on the origin of the NACTs in adiabatic theory (section 6.3.3). Although one may be tempted to think this to be a definite advantage for doing the scattering within the diabatic picture (derivative couplings are replaced by potential couplings; Ref. 98, and references therein), this is not quite so as the NACTs are still required to get the diabatic potential matrix.

6.3.7 Topological implications of the BO approximation

As noted above, the nuclei can be treated classically in the BO approximation. They may then be described by trajectories $\mathbf{r}_n(t)$, with \hat{H}_e thought to depend on

\mathbf{r}_n or time. If such an assumption is made, the nuclei will move infinitely slow as the Hamiltonian $\hat{H}_e(t)$ changes slowly with time. Consider then an arbitrary path $\mathbf{r}_n(t)$. The non-stationary time-dependent electronic SE along such a path assumes then the form

$$\hat{H}_e(\mathbf{r}_n(t)) \Psi(\mathbf{r}_n(t)) = i\hbar \frac{\partial \Psi(\mathbf{r}_n(t))}{\partial t} \quad (6.28)$$

where the obvious dependence of \hat{H}_e and Ψ on \mathbf{r}_e has been omitted for simplicity. Using the electronic basis set $\{\Psi_i(\mathbf{r}_n(t))\}$, the wave function may now be expanded as

$$\Psi(\mathbf{r}_n(t)) = \sum_j c_j(t) \Psi_j(\mathbf{r}_n(t)) \exp \left[-\frac{i}{\hbar} \int^t E_j(t') dt' \right] \quad (6.29)$$

where the term in the exponential is the dynamical phase. Eqs. (6.28,6.29) then yield

$$i\hbar \frac{dc_k}{dt} = \sum_j c_j \left\{ H_{ij} - E_j \delta_{ij} - i\hbar \langle \Psi_k(\mathbf{r}_n(t)) \left| \frac{\partial \Psi_j(\mathbf{r}_n(t))}{\partial t} \right\rangle \exp \left[-\frac{i}{\hbar} \int^t (E_j - E_k) dt' \right] \right\} \quad (6.30)$$

If the NACTs for $j \neq k$ are now neglected, and noting that $H_{kj} = S_{kj} = 0$ for the adiabatic basis set, it follows that

$$\frac{dc_k}{dt} = - \left\langle \Psi_k(\mathbf{r}_n(t)) \left| \frac{\partial \Psi_k(\mathbf{r}_n(t))}{\partial t} \right\rangle c_k \quad (6.31)$$

and hence

$$c_k = \exp \left[- \int^t \left\langle \Psi_k(\mathbf{r}_n(t')) \left| \frac{\partial \Psi_k(\mathbf{r}_n(t'))}{\partial t'} \right\rangle dt' \right] = \exp [{}^{\iota}A_k(t)] \quad (6.32)$$

where $A_k(t) = \int^t \langle \Psi_k(\mathbf{r}_n(t')) | \partial \Psi_k(\mathbf{r}_n(t')) / \partial t' \rangle dt'$ is the GP. Thus, retaining only one term in the wave function expansion, one has

$$\Psi(\mathbf{R}(t)) = \Psi_i(\mathbf{r}_n(t)) \exp \left[-\frac{i}{\hbar} \int^t E_i(t') dt' \right] \exp [{}^{\iota}A_i(t)] \quad (6.33)$$

which has the form of a generalized Born-Huang ansatz. Besides the dynamical phase factor of time evolution (first factor), a GP must be included. If the

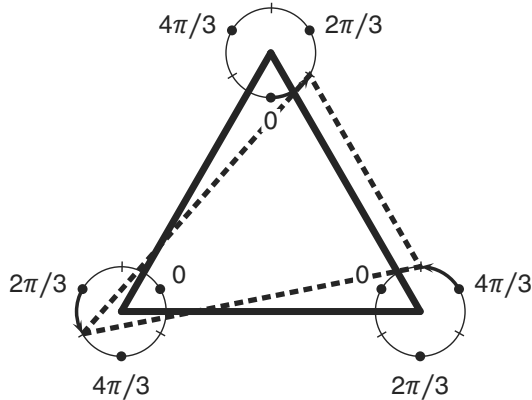


Figure 6.2. Distortions of a triatomic leading to appearance of GP in the $E \otimes e$ problem.

molecule performs a motion such that after some time $t = \tau$ it returns to its original position at time $t = 0$ [$\mathbf{R}(\tau) = \mathbf{R}(0)$], then the wave function may not only have acquired a dynamical phase as described by $\exp[-(i/\hbar) \int^t E_i(t') dt']$. Indeed, two possibilities exist: first, that the remaining part of the wave function has returned to its original value; second, that it has changed sign which simply requires that $A_i(\tau) = A_i(0) + \pi$. Recall that the sign of a wave function cannot be fixed, since it is its square that leads to an interpretation as a probability.

One may then ask when to expect the geometrical phase effect. The simplest case is that of H_3^+ , a symmetric triatomic molecular ion which has the shape of an equilateral triangle [99]. Further examples are clusters built from hydrogen or alkali (lithium, sodium, potassium, etc) atoms. Such molecules may perform a motion, called pseudo-rotation, in which each of the three nuclei moves on a circle around its equilibrium position. If at the same time the molecule is in a degenerate electronic state, pseudo-rotational motion as illustrated in Figure 6.2 will build up a GP.

6.4 Generalized Born-Oppenheimer approximation

As noted above, the BO approximation breaks down at conical intersections since a real electronic wave function changes sign [20, 21, 100] whenever traversing a nuclear path that encircles the locus of degeneracy. Because the

total electronuclear wave function must be continuous and single-valued, the nuclear wave function must change sign too such as to compensate the sign-change of the electronic counterpart. Although $\Psi_j(\mathbf{r}_n)$ and $\Phi_j(\mathbf{r}_n)$ may not be single-valued if real, there is no impediment to take them as complex in the Born-Huang [101] ansatz. For example, one may write

$$\Omega(\mathbf{r}_e, \mathbf{r}_n) = \sum_{Jj} \Phi_{Jj}(\mathbf{r}_n) \exp[iA_j(\mathbf{r}_n)] \Psi_j(\mathbf{r}_n) = \sum_{Jj} \Phi_{Jj}(\mathbf{r}_n) \tilde{\Psi}_j(\mathbf{r}_n) \quad (6.34)$$

where $A_j(\mathbf{r}_n)$ is the GP chosen to make the complex electronic wave function $\tilde{\Psi}_j(\mathbf{r}_n)$ [and hence $\Omega(\mathbf{r}_e, \mathbf{r}_n)$] be single-valued. Eq. (6.34) may alternatively be written as

$$\Omega(\mathbf{r}_e, \mathbf{r}_n) = \sum_J \tilde{\Phi}_{Jj}(\mathbf{r}_n) \Psi_j(\mathbf{r}_n) \quad (6.35)$$

where the complex nuclear wave functions $\{\tilde{\Phi}_{Jj}(\mathbf{r}_n)\}$ are now chosen to make $\Omega(\mathbf{r}_e, \mathbf{r}_n)$ be single-valued. If the ansatz in Eq. (6.35) is used, a set of coupled equations similar to Eq. (6.16) is obtained but with the real-valued nuclear wave functions replaced by the complex ones $\tilde{\Phi}_J(\mathbf{r}_n)$. If only the diagonal matrix elements are retained, then one gets

$$\left\{ -\frac{\epsilon^4}{2} [\Delta_n + \mathbf{G}_{jj}(\mathbf{r}_n)] + V_j(\mathbf{r}_n) - E \right\} \tilde{\Phi}_j(\mathbf{r}_n) = 0 \quad (6.36)$$

Alternatively, if real nuclear wave functions as in Eq. (6.34) are employed, one has

$$\left\{ -\frac{\epsilon^4}{2} [\nabla + \iota \nabla A_j(\mathbf{r}_n)]^2 + \tilde{V}_j(\mathbf{r}_n) - E \right\} \Phi_j(\mathbf{r}_n) = 0 \quad (6.37)$$

where

$$\tilde{V}_j(\mathbf{r}_n) = V_j(\mathbf{r}_n) - \frac{\epsilon^4}{2} \tilde{G}_{jj}(\mathbf{r}_n) \quad (6.38)$$

with $\tilde{G}_{jj}(\mathbf{r}_n)$ assuming the form given above but with the electronic wave functions tilded. Note that $\tilde{\mathbf{F}}_{jj}(\mathbf{r}_n) = \iota \nabla A_j(\mathbf{r}_n) + \mathbf{F}_{jj}(\mathbf{r}_n) = \iota \nabla A_j(\mathbf{r}_n)$ since, for real-valued electronic wave functions [102], $\mathbf{F}_{jj}(\mathbf{r}_n) = \langle \Psi_j(\mathbf{r}_n) | \nabla \Psi_j(\mathbf{r}_n) \rangle = 0$. Eq. (6.36) and Eq. (6.37) represent then a single-surface approach usually known as generalized BO approximation [40, 103]. Note that the ansatz in Eq. (6.34) leads to the appearance of a vector potential in the nuclear SE [26, 104, 105].

Note further that the \mathbf{r}_n -dependence of A_j must reflect the presence of any conical intersection in accordance with the GP [21, 24] condition, and hence can generally be constructed only once the conical intersections have been located. Although a general approach for determining $A_j(\mathbf{r}_n)$ has been suggested by Kendrick and Mead [103], it remains a nontrivial task. An alternative is to use Eq. (6.35), where the complex phase factor has been absorbed in the nuclear wave functions [106–108]. Such an approach is especially convenient for X_3 -type systems when using hyperspherical coordinates [36, 109], although it can be generalized [40, 110, 111] to asymmetric cases. Of course, in the absence of a conical intersection, both Eq. (6.36) and Eq. (6.37) lead to the standard adiabatic nuclear SE

$$\left[-\frac{\epsilon^4}{2} \Delta_n + \bar{V}_j(\mathbf{r}_n) - E \right] \Phi_j(\mathbf{r}_n) = 0 \quad (6.39)$$

since $\tilde{D}_{ij}^J(\mathbf{r}_n) = D_{ij}^J(\mathbf{r}_n)$, and one may choose $A_j(\mathbf{r}_n) = 0$.

Consider now a 2×2 potential matrix \mathbf{W} that is invariant and restricted to E space:

$$\mathbf{W} = W_{A_1} \begin{pmatrix} 1 & 0 \\ 0 & 1 \end{pmatrix} + W_{E_x} \begin{pmatrix} -1 & 0 \\ 0 & 1 \end{pmatrix} + W_{E_y} \begin{pmatrix} 0 & 1 \\ 1 & 0 \end{pmatrix} \quad (6.40)$$

where W_{A_1} , W_{E_x} , W_{E_y} are functions of the nuclear coordinates transforming under⁶ the C_{3v} symmetry group; as usual in polar coordinates, $x = \rho \cos \varphi$, and $y = \rho \sin \varphi$. The eigenvalues of \mathbf{W} , which reduce to the degenerate pair at the conical configuration, will then assume the form

$$W_{\pm} = W_{A_1} \pm W_{\rho} \quad (6.41)$$

where $W_{\rho} = \left(W_{E_x}^2 + W_{E_y}^2 \right)^{1/2}$. To all orders, they assume the form [112]

$$W_{A_1} = f_1 [z; \rho^2, \rho^3 \cos(3\varphi)] \quad (6.42)$$

$$W_{E_x} = \rho \cos \varphi f_3 [z; \rho^2, \rho^3 \cos(3\varphi)] + \rho^2 \cos(2\varphi) f_4 [z; \rho^2, \rho^3 \cos(3\varphi)] \quad (6.43)$$

$$W_{E_y} = \rho \sin \varphi f_3 [z; \rho^2, \rho^3 \cos(3\varphi)] - \rho^2 \sin(2\varphi) f_4 [z; \rho^2, \rho^3 \cos(3\varphi)] \quad (6.44)$$

⁶We may consider only this subgroup of D_{3h} since no out-of-plane bending is possible for a triatomic system. The component W_{A_2} must vanish, since \mathbf{W} must be Hermitian, and in our case can be real.

where f_i ($i=1-4$) are functions formally representable as a double power series in their arguments other than z , with the coefficients being constant or functions of z . From Eq. (6.41) to Eq. (6.44), it follows:

$$W_{A_1} = W_{A_1}(z; \rho^2, \rho^3 \cos 3\varphi) \quad (6.45)$$

$$W_R = r(f^2 + \rho^2 g^2 + 2\rho f g \cos 3\varphi)^{1/2} \quad (6.46)$$

$$\rightarrow \rho w(z; \rho^2, \rho \cos 3\varphi) \quad (\rho \rightarrow 0) \quad (6.47)$$

where $f=f(z; \rho^2, \rho^3 \cos 3\varphi)$, $g=g(z; \rho^2, \rho^3 \cos 3\varphi)$, and w are analytic functions. Eqs. (6.42)-(6.44) define the correct behavior of the PES in the vicinity of the conical intersection, and hence may be valuable in delineating fitting forms [112, 113]; for recent work on fitting and interpolation methods, the reader is referred to Refs. 114 and 115.

Let now $\tilde{\gamma}$ be an angle, itself a function of the nuclear coordinates, such that

$$W_{E_x} = W_\rho \cos \tilde{\gamma}, \quad W_{E_y} = W_\rho \sin \tilde{\gamma} \quad (6.48)$$

In terms of the degenerate pair of wave functions (ψ_x, ψ_y) , we may write the two adiabatic ones (Ψ_+, Ψ_-) corresponding to the eigenvalues of Eq. (6.41) as

$$\Psi_+ = \psi_x \sin(\tilde{\gamma}/2) + \psi_y \cos(\tilde{\gamma}/2), \quad (6.49)$$

$$\Psi_- = \psi_x \cos(\tilde{\gamma}/2) - \psi_y \sin(\tilde{\gamma}/2) \quad (6.50)$$

which cannot be single-valued due to the appearance of $\tilde{\gamma}/2$ (note that both Ψ_+ and Ψ_- change sign when $\tilde{\gamma}$ increases by 2π). Thus, $\tilde{\gamma}/2$ is the mixing angle that yields the adiabatic states from the diabatic ones (*i.e.*, diagonalizes the diabatic potential matrix). Single-valuedness is warranted by defining [26, 104] the GP as $A_+(\mathbf{R})=A_-(\mathbf{R})=3\varphi/2$, although other possibilities exist [40, 41] (see also Ref. 42). Since $\langle \Psi_+ | \Psi_- \rangle = \delta_\pm$, one gets

$$\tilde{\mathbf{d}} = \mathbf{d} = \langle \tilde{\Psi}_- | \nabla \tilde{\Psi}_+ \rangle = -\langle \tilde{\Psi}_+ | \nabla \tilde{\Psi}_- \rangle \quad (6.51)$$

Using now Eq. (6.49) to Eq. (6.51), one obtains

$$\mathbf{d} = \mathbf{d}^{\text{lon}} + \mathbf{d}^{\text{tra}} \quad (6.52)$$

where the curl-free longitudinal and divergence-free transverse (solenoidal) parts of the derivative coupling are given by [112]

$$\mathbf{d}^{\text{lon}} = \frac{1}{2} \nabla \tilde{\gamma} \quad (6.53)$$

$$\mathbf{d}^{\text{tra}} = \langle \psi_x | \nabla \psi_y \rangle \quad (6.54)$$

a result which is a consequence of the general Helmholtz decomposition theorem.

The longitudinal part of \mathbf{d} shows a singularity at the conical intersection but this singularity can be removed by a coordinate-dependent unitary transformation [116]. Moreover, from Eq. (6.43), Eq. (6.44) and Eq. (6.48), one may write [112]

$$\tan \tilde{\gamma} = \frac{f \sin \varphi - \rho g \sin(2\varphi)}{f \cos \varphi + \rho g \cos(2\varphi)} \quad (6.55)$$

and defining ϵ such that $\tilde{\gamma} = \varphi + \epsilon$, one has

$$\tan \epsilon = -\frac{\rho g \sin(3\varphi)}{f + \rho g \cos(3\varphi)} \quad (6.56)$$

Thus,

$$\mathbf{d}^{\text{lon}} = \frac{1}{2} \nabla_{\mathbf{r}_n} \left\{ \varphi - \tan^{-1} \left[\frac{\rho g \sin(3\varphi)}{f + \rho g \cos(3\varphi)} \right] \right\} \quad (6.57)$$

which defines the correct analytic properties of the nonadiabatic coupling near the seam of a potential energy surface exhibiting a C_{3v} conical intersection [112, 113, 117, 118].

Eq. (6.53) can be solved by integration along paths in the nuclear configuration space [119, 120]. The result will depend on the initial and final points of integration but not on the path chosen. Due to the LH theorem [20, 21, 100], if the integration is carried out along a closed loop \mathcal{C} , $\tilde{\gamma}/2$ should change by [24, 120, 121]

$$\xi_{\tilde{\gamma}} = \oint_{\mathcal{C}} \mathbf{d}^{\text{lon}}(\mathbf{r}_n) d\mathbf{r}_n = p\pi \quad (6.58)$$

where $p=0$ if \mathcal{C} does not enclose any conical intersection, but is 1 if it does enclose one.

The transverse part remains finite at the seam, and cannot generally be transformed away to zero for a polyatomic system [116, 119]. However, one may

think of defining an (adiabatic-diabatic transformation, ATD) angle [66, 76, 119] $\alpha(\mathbf{r}_n)$ such that

$$\mathbf{d} = \nabla\alpha(\mathbf{r}_n) \quad (6.59)$$

which would be [up to a constant, *cf.* Eq. (6.53)] identical to the angle capable of transforming the adiabatic basis to a diabatic one or vice-versa. Similarly, a topological phase [122] can be defined as

$$\xi_\alpha = \oint_C \mathbf{d}(\mathbf{r}_n) d\mathbf{r}_n \quad (6.60)$$

Since \mathbf{d} does not generally satisfy Eq. (6.53), the result of such an integration will be path-dependent [116]. However, since the transverse part is finite (and possibly negligible upon optimal adiabaticization [118]), one may expect to have $\xi_{\tilde{\gamma}} = \xi_\alpha$. As noted above, the mixing angle $\gamma(\mathbf{r}_n) = \tilde{\gamma}/2$ that diagonalizes the potential matrix is (up to a constant) identical to $\alpha(\mathbf{r}_n)$ [41], and also to the GP $A_j(\mathbf{r}_n)$ [40].

6.5 Configuration vs function space, and conservation laws

The configuration space forms the natural frame where to represent an adiabatic PES. For the purpose of studying the JT effect, only the subspace defined by the coordinates that are JT active is required since it contains all distorted configurations that may be reached by such vibrational modes. Their complete set subtends a real Cartesian space of dimension $\tau = [\Gamma^2] - 1$ known as [123] the *configuration space* v or simply *configuration space*. Figure 6.3 illustrates such a space the case of a triatomic belonging to the symmetry group C_{3v} , where the symmetric product leads to $[E_1^2] = A_1 \oplus E_1$. The v -space will then be defined by the e -type vibrations that span the $2D$ space $\{Q_{E_x}, Q_{E_y}\}$, which can be expressed in terms of the three bond distances (R_1, R_2, R_3) either as linear symmetrized combinations of bond distances

$$\begin{pmatrix} Q_1 \\ Q_2 \\ Q_3 \end{pmatrix} = \begin{pmatrix} 1/\sqrt{3} & 1/\sqrt{3} & 1/\sqrt{3} \\ 0 & 1/\sqrt{2} & -1/\sqrt{2} \\ 2/\sqrt{6} & -1/\sqrt{6} & -1/\sqrt{6} \end{pmatrix} \begin{pmatrix} R_1 \\ R_2 \\ R_3 \end{pmatrix} \quad (6.61)$$

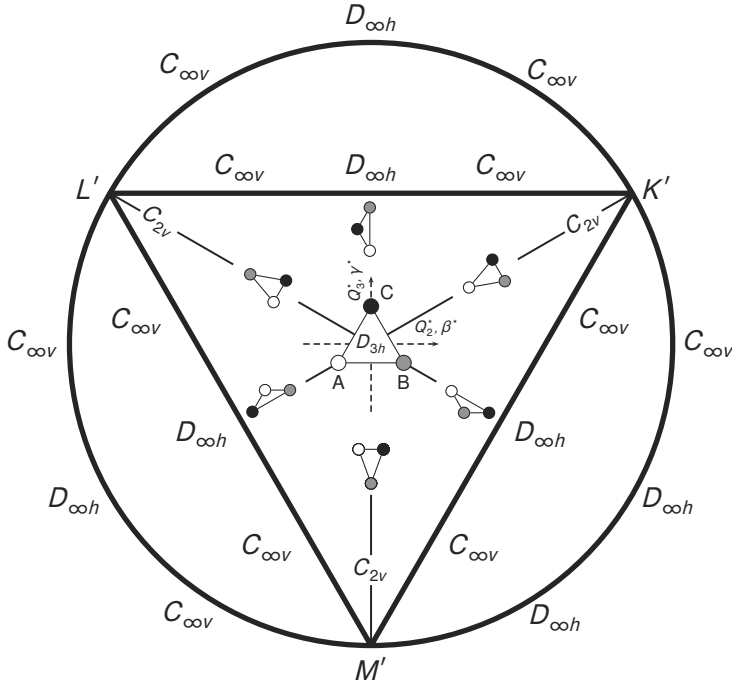


Figure 6.3. Locus of symmetry point groups assuming that the group operations are applied to three identical nuclei A, B, and C (denoted by the colored dots). The C_2 symmetry is intrinsic to the entire physical circle based on the coordinates in Eq. (6.62) [corresponding considerations apply to the physical triangle when using Eq. (6.61)]. Molecular conformations obtained by following a closed path around the origin are also shown. K' , L' , and M' indicate the points where the ‘physical triangle’ and ‘physical circle’ centered at the origin of the coordinate system touch each other and the circumscribing equilateral triangle employed for the relaxed triangular plot [124]. Completion of a circular motion of the three atoms in panel (a) originates a circular path around the origin in Figure 6.2. Q_2 and Q_3 correspond to Q_{E_x} and Q_{E_y} , respectively. See the text.

or of their squares,

$$\begin{pmatrix} Q \\ \beta \\ \gamma \end{pmatrix} = \begin{pmatrix} 1 & 1 & 1 \\ 0 & \sqrt{3} & -\sqrt{3} \\ 2 & -1 & -1 \end{pmatrix} \begin{pmatrix} R_1^2 \\ R_2^2 \\ R_3^2 \end{pmatrix} \quad (6.62)$$

Note that Q_1 and Q transform as A_1 , while $\{Q_2, Q_3\}$ and (β, γ) transform as the degenerate pair of E -symmetry $\{Q_{E_x}, Q_{E_y}\}$. Note further that the locus of degeneracy is in this case a $0D$ manifold embedded in that space, a point that coincides with the JT origin ($Q_2=0, Q_3=0$). In the vicinity of the crossing point, the PES will appear in the (β, γ) representation as a double cone, as it could be

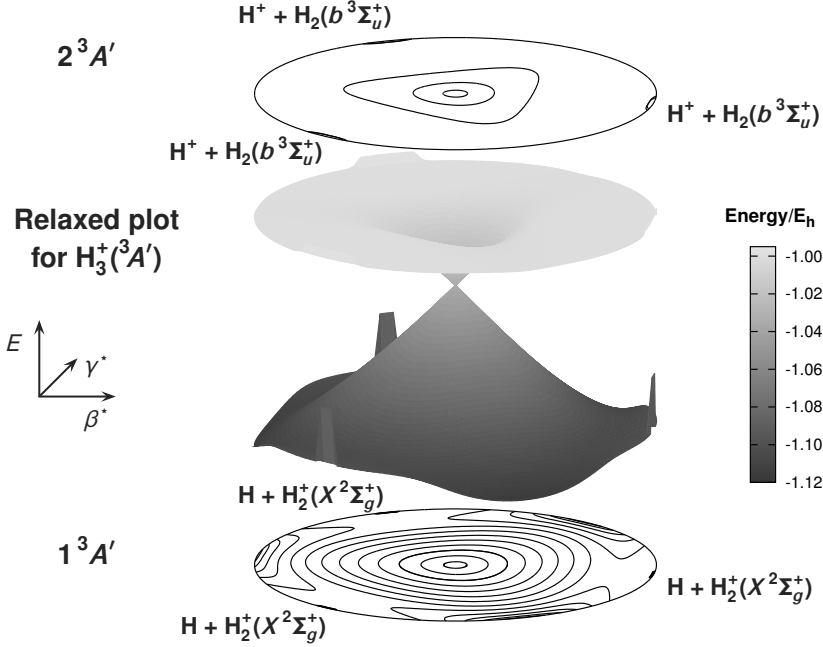


Figure 6.4. Perspective view [124] and contour plots of the adiabatic DMBE PESs of [125] $\text{H}_3^+({}^3A')$ using hyperspherical coordinates. Also indicated are the asymptotic channels. Contours generated from $E_n/E_h = -1.116 + 0.000447n^2$, where n is the contour number.

anticipated from Eq. (6.48). A realistic example is illustrated in Figure 6.4 for the $\text{H}_3^+({}^3A')$ ion, where we have utilized the symmetrized coordinates in Eq. (6.62) suitably relaxed [124] ($\beta^* = \beta/Q$, $\gamma^* = \gamma/Q$) such that Q corresponds at each point to the structure of lowest energy for that symmetry. They can be related to the hyperspherical coordinates [36] (ρ, θ, φ) through the relations

$$R_1^2 = \frac{1}{2} d_1^2 \rho^2 \left[1 + \sin \frac{\theta}{2} \cos(\varphi + \chi_3) \right] \quad (6.63)$$

$$R_2^2 = \frac{1}{2} d_2^2 \rho^2 \left(1 + \sin \frac{\theta}{2} \cos \varphi \right) \quad (6.64)$$

$$R_3^2 = \frac{1}{2} d_3^2 \rho^2 \left[1 + \sin \frac{\theta}{2} \cos(\varphi - \chi_1) \right] \quad (6.65)$$

where $d_i^2 = m_i/\mu (1 - m_i/M)$, $\chi_i = 2 \tan^{-1} (m_{i+2}/\mu)$, $\mu = (m_1 m_2 m_3/M)^{1/2}$, and $M = \sum_i m_i$. Thus, the plot in Figure 6.4 corresponds to a stereographic projection of the surface of an upper half sphere. The β^* coordinate corresponds to $\sin(\theta/2) \cos \varphi$, while γ^* denotes $\sin(\theta/2) \sin \varphi$. The hyperangle θ runs from

zero at the north pole (center of plot) to $\pi/2$ at the equator. In turn, the hyperangle φ is measured from the positive β^* axis and grows on going counterclockwise. Note the three equivalent weak minima separated from each other by a tiny barrier that along the trough for pseudorotation.

A second example refers to threefold electronic degeneracies that are inherent to cubic groups T , T_d , O , O_h , and icosahedral groups I and I_h [11]. In the absence of inversion centers, $[T_1^2] = [T_2^2] = A_1 \oplus E \oplus T_2$, while in the presence of inversion, the result is $[T_{1g}^2] = [T_{1u}^2] = [T_{2g}^2] = [T_{2u}^2] = A_{1g} \oplus E_g \oplus T_{2g}$. Thus, the JT active vibrations for a threefold degenerate electronic term (T_1 or T_2) are of e or t_2 symmetry: $T \otimes (e \oplus t_2)$ problem. If the coupling of the two t modes can be neglected, the analysis of the JT effect will be restricted to $5D$ space [126] defined by the normal coordinates $\{Q_{E_x}, Q_{E_y}\}$ for the e representation (tetragonal-type coordinates), and $\{Q_{T_x}, Q_{T_y}, Q_{T_z}\}$ for the t_2 representation (trigonal-type coordinates). Of course, such a space cannot be fully visualized. A possible way for reducing the dimensionality consists of assuming that the vibronic interaction with one of the two types of vibrations can be neglected. For other degenerate electronic terms interacting with degenerate vibrations, see Ref. 13.

Due to H invariance under time-reversal, the space of the electronic BO wave vectors can also be represented by a $(N - 1)$ -sphere in ND real space as the BO dynamics is known [123] to realize an adiabatic mapping of the ν -space into such a *projective function space* (f -space). An arbitrary adiabatic electronic state assumes then the form

$$|\Gamma\gamma\rangle = \sum_{i=1,|\Gamma|} c_i |\Gamma\gamma_i\rangle \quad (6.66)$$

with norm preserving requirement $\sum_i c_i^* c_i = 1$. The allowed transformations in f -space will then involve rotations or reflections of the points on the unit sphere. Its full symmetry group is $O(|\Gamma|)$, and the elements orthogonal matrices describing the transformation of the directional cosines c_i . Symmetry elements of the finite group G will then induce orthogonal matrix transformations, with the Γ matrix representation of G being a subgroup of $O(|\Gamma|)$. Of course, an advantage of the f -space is the lower number of parameters required to characterize an

arbitrary state: $(N - 1)$ vs τ for the f vs v spaces, respectively. The latter has been suggested by Ceulemans [123] to represent the PES itself, although we will utilize [48] it to characterize the GP effect by examining the outcome of matrix applications on an arbitrary electronic eigenvector.

Conservation laws and symmetries play a key role both in physics and mathematics as they allow to specify the dynamics of the system in terms of the first integrals of the motion. Noether's theorem plays in this context a prominent role by stating that the action admits an r -parameter Lie group as variational symmetries if there are r proper conservation laws. Thus, the vibronic Hamiltonian in the $E \otimes e$ system has the symmetry of the one-parameter axial group $O(2)$ because there is just one conserved quantity. In fact, diagonalization of the vibronic JT matrix shows that the component L_z of the angular momentum is the only constant of the motion, with the mixing (pseudo-rotation) angle that characterizes the unitary matrix being α_z . Similarly, the symmetry of the Hamiltonian of the $T \otimes (e \oplus t_2)$ system is [11] $SO(3)$, a 3-parameter Lie group. In this case, the 3×3 rotation matrix that diagonalizes the vibronic JT matrix assumes the form of a product of 3 planar rotations in configuration space, with a pseudo-rotation angle associated to every conserved component of the total angular momentum. Similar considerations hold for systems associated to other Lie groups; the symmetry invariances of the relevant linear JT Hamiltonian operators are discussed in the literature [11] (see also Table 2.3 of Ref. 19). It turns out that the group G has a dimension that does not generally coincide with the number of mixing angles required to describe an adiabatic electronic state in its associated function space. For example, only 2 mixing angles are necessary to describe the $T \otimes (e \oplus t_2)$ problem while 3 suffice for the $G \otimes (g \oplus h)$ one, respectively of dimensions 3 and 6. The former may be rationalized from the fact that only two combinations of its 3 invariants (the components of the angular momentum operator J_x, J_y and J_z), say J^2 and J_z , are known to commute. As a result, only 2 quantum numbers (or, equivalently, mixing angles) suffice to specify unambiguously an adiabatic electronic wave vector of the $T \otimes (e \oplus t_2)$ system. Similarly, although the orbital angular momentum in a $4D$ Cartesian space is described by 6 orbital angular mo-

mentum operators, only 4 commuting combinations arise, one corresponding to an operator that vanishes identically [127]. This indicates that 3 mixing angles only suffice to describe an adiabatic electronic wave vector for the $G \otimes (g \oplus b)$ problem. In fact, and more generally, although a set $N(N-1)/2$ components of the generalized orbital angular momentum can be defined for the N -fold problem, only $(N-1)$ commuting generalized orbital angular momentum operators are known to commute. Thus, they possess simultaneous eigenfunctions that depend on $(N-1)$ angular variables [128]. As above, this may explain why only $(N-1)$ angles are required to characterize unambiguously the corresponding adiabatic electronic wave vector [19, 45, 48].

The mapping in the electronic sphere is, however, two-valued since antipodal pairs of eigenvectors ($|\Gamma\gamma\rangle$ and $-|\Gamma\gamma\rangle$) refer to the same point in ν -space: a physical state may be described by any wave vector in a ray [129]. This has implications on the GP analysis, since two classes of paths (closed loops) in ν -space can be recognized [28]: paths that are continuously contractable to a point (class Π_1) and hence manifest no GP, and paths (Π_2) that manifest GP by showing a sign-change of the electronic state when going from a point A to its antipodal A' . Additionally, there are paths that connect a point to its antipodal without manifestation of GP, thus sign change. This is possible [28] provided that a point \mathbf{Q}_d exists on the path where the mapping is degenerate by linking not just a pair of opposite points but a whole circle of linear combinations $\cos\theta|\psi_1(\mathbf{Q}_d)\rangle + \sin\theta|\psi_2(\mathbf{Q}_d)\rangle$ of two degenerate electronic states (path Δ in Figure 6.5).

6.6 Case studies of Jahn-Teller vibronic coupling

6.6.1 $e \otimes E$

The title JT problem has been much studied, and hence will serve here the purpose of comparing the two different formalisms discussed in the previous sections. Let the BO electronic wave vectors be $\{\psi_1, \psi_2\} = \{|E_x\rangle, |E_y\rangle\}$ [19, 45]. The two adiabatic wave vectors can then be unambiguously expressed in f -space

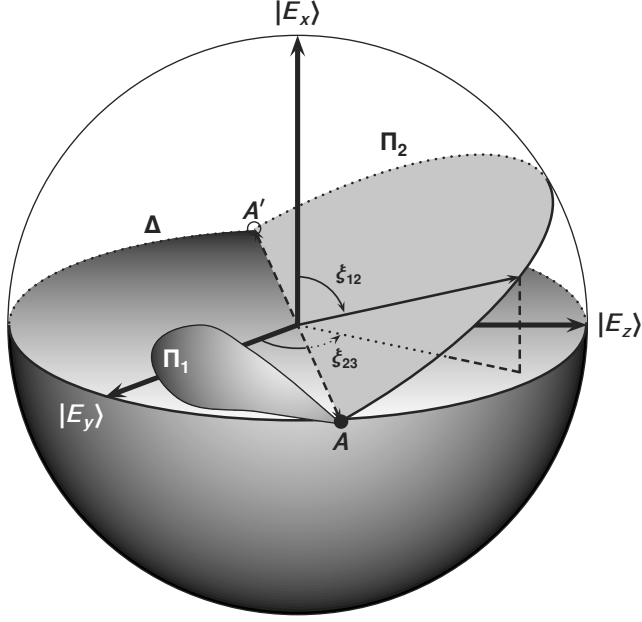


Figure 6.5. Paths in function space for $N=3$ (S^2 electronic sphere) that map onto closed loops in configuration space. Π_2 paths (from A to A' , indicated by the solid and open circles, respectively) that involve a sign change and hence GP effect. With $\xi_{12}=0$ one gets: $|\Psi_1\rangle=|E_x\rangle$, $|\Psi_2\rangle=\cos \xi_{23}|E_y\rangle + \sin \xi_{23}|E_z\rangle$, and $|\Psi_3\rangle=-\sin \xi_{23}|E_y\rangle + \cos \xi_{23}|E_z\rangle$. In turn, for $\xi_{12}=\pi$: $|\Psi_1\rangle=-|E_x\rangle$, $|\Psi_2\rangle=-\cos \xi_{23}|E_y\rangle - \sin \xi_{23}|E_z\rangle$, and $|\Psi_3\rangle=-\sin \xi_{23}|E_y\rangle + \cos \xi_{23}|E_z\rangle$. For $\xi_{12}=0$ and π , all $|\Psi_i\rangle$ change sign upon the transformation $\xi_{23} \rightarrow \xi_{23}+\pi$, but $|\Psi_2\rangle$ does so by evolving from A to A' when $\xi_{12}=0$ and returning to A when $\xi_{12}=\pi$. Thus, $|\Psi_2\rangle$ leads to a Δ -type path (simply connected) under \hat{i}_3 by not manifesting GP. Also shown is a simply connected path of type Π_1 .

as

$$\begin{pmatrix} \Psi_1(\mathbf{r}_n; \xi_z) \\ \Psi_2(\mathbf{r}_n; \xi_z) \end{pmatrix} = \begin{bmatrix} \cos \xi_z(\mathbf{r}_n) & \sin \xi_z(\mathbf{r}_n) \\ -\sin \xi_z(\mathbf{r}_n) & \cos \xi_z(\mathbf{r}_n) \end{bmatrix} \begin{pmatrix} \psi_1 \\ \psi_2 \end{pmatrix} \quad (6.67)$$

where $\xi_z = \alpha_z/2$ is the mixing angle. Thus, $\langle \Psi_1 | \nabla \Psi_2 \rangle = -\langle \Psi_2 | \nabla \Psi_1 \rangle = \nabla \xi_z$. Defining [40]

$$\tilde{\Psi} = \frac{1}{\sqrt{2}}(\Psi_1 + \iota \Psi_2) \quad (6.68)$$

it is now easy to show that $\langle \tilde{\Psi} | \nabla \tilde{\Psi} \rangle = \iota \langle \Psi_1 | \nabla \Psi_2 \rangle$. Similarly, it follows that $\langle \tilde{\Psi} | \nabla \tilde{\Psi} \rangle = \iota \nabla A(\mathbf{r}_n)$. It then follows that $\nabla A(\mathbf{r}_n) = \nabla \xi_z(\mathbf{r}_n)$, a result corroborating the statement already made that the GP is (up to a constant term that has no physical implications) identical to the mixing angle and which will be of use again at a later stage.

Consider now the equations of nuclear motion for the title $2D$ coupled problem⁷:

$$\left[-\frac{\hbar^2}{2\mu} (\nabla^2 + \langle \Psi_1 | \nabla^2 \Psi_1 \rangle) + V_1 - E \right] \Phi_1 = \frac{\hbar^2}{2\mu} [\langle \Psi_1 | \nabla^2 \Psi_2 \rangle + 2\langle \Psi_1 | \nabla \Psi_2 \rangle \cdot \nabla] \Phi_2 \quad (6.69)$$

$$\left[-\frac{\hbar^2}{2\mu} (\nabla^2 + \langle \Psi_2 | \nabla^2 \Psi_2 \rangle) + V_2 - E \right] \Phi_2 = \frac{\hbar^2}{2\mu} [\langle \Psi_2 | \nabla^2 \Psi_1 \rangle + 2\langle \Psi_2 | \nabla \Psi_1 \rangle \cdot \nabla] \Phi_1 \quad (6.70)$$

By writing [100] the complex nuclear wave function

$$\tilde{\Phi} = \frac{1}{\sqrt{2}}(\Phi_1 + \iota\Phi_2) \quad (6.71)$$

and using the NACTs given above as well as $\langle \nabla \Psi_i | \nabla \Psi_i \rangle = [\nabla \xi_z(\mathbf{r}_n)]^2$, $\langle \nabla \Psi_i | \nabla \Psi_j \rangle = 0$, $\langle \Psi_i | \nabla^2 \Psi_j \rangle = \nabla^2 \xi_z(\mathbf{r}_n)$, and $\langle \Psi_j | \nabla^2 \Psi_i \rangle = -\nabla^2 \xi_z(\mathbf{r}_n)$, yields

$$\left\{ -\frac{\hbar^2}{2\mu} [\nabla^2 - (\nabla \xi_z)^2] + E_i - E \right\} \tilde{\Phi} + \frac{\iota}{\sqrt{2}} (V_j - V_i) \Phi_j = -\iota \frac{\hbar^2}{2\mu} (\nabla^2 \xi_z + 2\nabla \xi_z \cdot \nabla) \tilde{\Phi} \quad i, j = 1, 2 \quad (6.72)$$

Near the crossing seam, the term $(V_j - V_i)$ should be negligibly small, reducing to [40]

$$\left\{ -\frac{\hbar^2}{2\mu} [\nabla^2 - (\nabla \xi_z)^2] + V - E \right\} \tilde{\Phi} = -\iota \frac{\hbar^2}{2\mu} (\nabla^2 \xi_z + 2\nabla \xi_z \cdot \nabla) \tilde{\Phi} \quad (6.73)$$

a single (uncoupled) equation that should be accurate there both for $V = V_1$ and V_2 . Note that the above differs from the Baer-Englman [37, 130] treatment in that Eq. (6.73) is valid for both sheets. Furthermore, unlike the latter, it uses the mixing angle $\xi_z(\mathbf{R})$ and no assumption is made that the upper sheet is closed to the dynamics. Of course, the BO approximation is recovered for derivative coupling constant or zero.

The implications of the GP in the dynamics can now be found by comparing the results obtained by solving the dynamics of nuclear motion in Eq. (6.73) with inclusion of GP and without it. Such studies have been carried out for a wealth of systems [18, 39, 110, 111, 115, 131–135], with the reader being referred

⁷For clarity, we return to the explicit use of \hbar , and reduced mass.

to the original papers for details. Suffice it to say that the nuclear SE including GP may be written as $\hat{H}\tilde{\Phi} = E\tilde{\Phi}$, where $\hat{H} = \hat{H}_0 + \iota\hat{H}_1$. Explicitly, it assumes in hyperspherical coordinates [36] the form

$$\begin{aligned}\hat{H}_0 = & -\frac{\hbar^2}{2\mu} \left\{ \frac{\partial^2}{\partial\rho^2} + \frac{16}{\rho^2} \left[\frac{1}{\sin\theta} \frac{\partial}{\partial\theta} \sin\theta \frac{\partial}{\partial\theta} + \frac{1}{4\sin^2(\theta/2)} \frac{\partial^2}{\partial\phi^2} \right] \right\} \\ & + \frac{\hat{j}^2 - \hat{j}_z^2}{\mu\rho^2 \cos^2(\theta/2)} + \frac{\hat{j}_z^2 + 4i\hbar\hat{j}_z \cos(\theta/2)(\partial/\partial\phi)}{2\mu\rho^2 \sin^2(\theta/2)} + \frac{15\hbar^2}{8\mu\rho^2} \\ & + \frac{\sin(\theta/2)}{\mu\rho^2 \cos^2(\theta/2)} \frac{1}{2} [\hat{j}_+^2 + \hat{j}_-^2] + V(\rho, \theta, \phi) + \frac{\hbar^2}{2\mu} [\nabla\xi_z(\rho, \theta, \phi)]^2 \\ \hat{H}_1 = & -\frac{\hbar^2}{2\mu} [\nabla^2\xi_z(\rho, \theta, \phi) + 2\nabla\xi_z(\rho, \theta, \phi) \cdot \nabla]\end{aligned}$$

with all symbols having their usual meaning. Note that singularities may arise at $\rho=0$ and $\theta=0$, which requires special care. Note especially that the generalized BO approximation requires the gradient of GP rather than the GP itself. Early applications of the theory are reviewed in Ref. 18, to where the reader is addressed for details.

Consider now Eq. (6.67) written in matrix form as

$$\Psi(\mathbf{r}_n; \xi_z) = \mathbf{R}_2(\xi_z)\psi \quad (6.74)$$

which shows that a vector state will define in function space a point on the circle of unit radius centered at its origin. A rotation $\xi_z \rightarrow \xi_z + \pi$ characterized by the operator \hat{R}_2 will then lead to $\mathbf{R}_2(\xi_z + \pi) = -\mathbf{R}_2(\xi_z)$. Since both adiabatic electronic wave vectors Ψ_1 and Ψ_2 change sign upon acting with \hat{R}_2 , the result mimics the one obtained for a closed loop in v -space ($\alpha_z \rightarrow \alpha_z + 2\pi$) or the topological impossibility of unpinning the electronic circle from an enclosed point of degeneracy. As seen from Figure 6.6 (cf Figure 6.5 for a realistic system), the JTM forms a 1D trough in the lower sheet of the $E \otimes e$ problem [11, 13], so-called the ‘Mexican hat’, with the motion along the distortion coordinate α_z being equivalent to the concerted motion of each atom around a circle [*i.e.*, pseudo-rotation in Figure 6.2]. The GP effect for systems with an orbital doublet degeneracy may then be stated as [19, 45, 48]: *an electronically adiabatic state that experiences the GP effect will change sign after completing a loop around the*

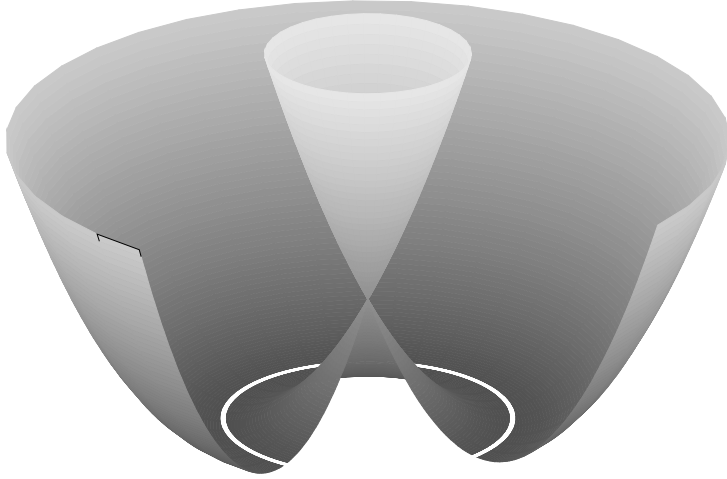


Figure 6.6. The “Mexican hat”. Besides the diagonal kinetic energy matrix, the linear JT Hamiltonian is characterized in the $\{Q_{E_x}, Q_{E_y}\}$ phase space by the potential matrix $\frac{1}{2}\omega_E^2 (Q_{E_x}^2 + Q_{E_y}^2) \sigma_0 + V_E (Q_{E_x} \sigma_x + Q_{E_y} \sigma_y)$, where $\sigma_0 = \begin{bmatrix} 1 & 0 \\ 0 & 1 \end{bmatrix}$, $\sigma_x = \begin{bmatrix} 1 & 0 \\ 0 & -1 \end{bmatrix}$, and $\sigma_y = \begin{bmatrix} 0 & i \\ -i & 0 \end{bmatrix}$ are Pauli matrices. In turn, ω_E characterizes the two harmonic oscillators and V_E the strength of the linear JT interaction. [10–12] Shown by the white line is the JTM, which corresponds to a circle of radius $\rho = (Q_{E_x}^2 + Q_{E_y}^2)^{1/2}$ centered at the vertex of the diabolo, $\rho=0$, with an energy of $-V_E^2/2\omega^2$.

conical intersection in v -space or, equivalently, upon use of the rotation operator \hat{R}_2 in f -space. Although this may appear a trivial result since a path connecting a point to its antipodal must lead to a sign change of $|\Psi_1\rangle$ and $|\Psi_2\rangle$, it is not so when $N \geq 3$.

6.6.2 $T \otimes (e \oplus t_2)$

Consider now the threefold electronic degeneracy in $T \otimes (e \oplus t_2)$. The JT Hamiltonian including linear vibronic coupling has now Lie group symmetry $SO(3)$ [11], which implies dimension 3 and hence 3 Lie group parameters. Since a norm-preserving adiabatic electronic wave vector on the electronic sphere S^2 can be unambiguously characterized in terms of two angles, there is freedom of choice for selecting the latter out of the three coordinates in $SO(3)$. The remaining one can, however, be sampled by considering all three two-angle sets. By assigning a 3×3 unitary planar rotation matrix to each of the chosen

coordinates (ξ_{12} and ξ_{23}), the full rotation matrix assumes the form

$$\mathbf{R}_3 = \rho_{12}(\xi_{12})\rho_{23}(\xi_{23}) \quad (6.75)$$

where $[\rho_{nm}]_{nm} = [\rho_{nm}]_{mm} = \cos \xi_{nm}$, and $[\rho_{nm}]_{nm} = -[\rho_{nm}]_{mn} = \sin \xi_{nm}$; all other entries satisfy $[\rho_{nm}]_{ij} = \delta_{ij}$. As in the $E \otimes e$ problem, the electronic adiabatic wave vectors will now be given by the rows of the following \mathbf{R}_3 matrix:

$$\begin{pmatrix} \Psi_1(\mathbf{r}_n; \xi_{23}, \xi_{12}) \\ \Psi_2(\mathbf{r}_n; \xi_{23}, \xi_{12}) \\ \Psi_3(\mathbf{r}_n; \xi_{23}, \xi_{12}) \end{pmatrix} = \begin{bmatrix} \cos \xi_{12} & \sin \xi_{12} \cos \xi_{23} & \sin \xi_{12} \sin \xi_{23} \\ -\sin \xi_{12} & \cos \xi_{12} \cos \xi_{23} & \cos \xi_{12} \sin \xi_{23} \\ 0 & -\sin \xi_{23} & \cos \xi_{23} \end{bmatrix} \begin{pmatrix} \psi_1 \\ \psi_2 \\ \psi_3 \end{pmatrix} \quad (6.76)$$

where $\xi_{12}(\mathbf{r}_n)$ is the first mixing angle (describes the mixing of ψ_1 and ψ_2 to form an intermediate adiabatic state Ψ_{12}), and $\xi_{23}(\mathbf{r}_n)$ is the second mixing angle (describes the mixing of Ψ_{12} and ψ_3). Upon use of the matrix \mathbf{R}_3 associated to the double-rotation in f -space defined by $\xi_{12} \rightarrow \pi - \xi_{12}$ and $\xi_{23} \rightarrow \xi_{23} + \pi$, Ψ_1 and Ψ_3 are seen to be the only eigenstates that change sign. Note that the two angles define normwise the degeneracy locus of an adiabatic state, being equivalent to the pseudo-rotational angles in v -space.

Figure 6.5 shows that a path connecting a point to its antipodal in f -space leads to a manifestation of the GP effect for Ψ_1 and Ψ_3 but not Ψ_2 . Following Ref 48, this can be understood as follows. Consider the angle ξ_{12} fixed at $\xi_{12}=0$ such that the point A and its antipodal A' lie on the equator of the electronic sphere, with the path Π_2 passing on its north pole. Thus, $\Psi_1 = \psi_1$, $\Psi_2 = \cos \xi_{23}\psi_2 + \sin \xi_{23}\psi_3$, and $\Psi_3 = -\sin \xi_{23}\psi_2 + \cos \xi_{23}\psi_3$. For ξ_{12} fixed at 0, Ψ_2 and Ψ_3 will change sign upon the transformation $\xi_{23} \rightarrow \xi_{23} + \pi$. By considering now $\xi_{12} = \pi$, one obtains $\Psi_1 \rightarrow -\Psi_1$ and $\Psi_2 = -\cos \xi_{23}\psi_2 - \sin \xi_{23}\psi_3 = \cos(\xi_{23} + \pi)\psi_2 + \sin(\xi_{23} + \pi)\psi_3$ while Ψ_3 shows the same dependence on ξ_{23} as for $\xi_{12}=0$. Thus, upon the transformation $\xi_{23} \rightarrow \xi_{23} + \pi$, Ψ_2 evolves from A to A' (changes sign) when $\xi_{12} = 0$, but closes the loop (*i.e.*, changes sign again) by returning to A when $\xi_{12} = \pi$. The notable feature is then the cancelation of signs that occurs when both ξ_{12} and ξ_{23} vary simultaneously. Equivalently, Ψ_2 keeps its sign unchanged upon acting with the matrix \mathbf{R}_3 . The same conclusions can be extracted irrespectively of the initial and final values of ξ_{12} provided that they

differ by π . The important observation is the cancelation of signs in Ψ_2 owing to the fact that the path from A to A' becomes a closed one (*i.e.*, Δ -type). Similar results are obtained irrespective of the chosen angles, provided that the matrices in Eq. (6.75) form an ordered sequence yielding physical solutions: *under the action of \hat{R}_3 , an arbitrary wave vector must either change sign or remain sign unchanged.* State labeling in Eq. (6.76) is also arbitrary showing that only one pair of adiabatic electronic states changes sign.

The above results indicate that the three branches of the three-valued PES and the electronic S^2 -sphere show a different connectedness. While the latter is simply connected (any closed path or loop can be smoothly contracted to a point), the former may well have 'holes' in their topologies and hence be multiply connected. Thus, besides trivial paths of class Π_1 , there may be nontrivial ones of Π_2 type. In fact, these two classes of paths seem to be topologically distinct in states Ψ_1 and Ψ_3 (*i.e.*, loops belonging to class Π_2 can never evolve smoothly to Π_1 -type ones), thence explaining their multiple-connectedness property. Thus, our predictions agree with previous findings [28, 35] that show the multiple-connectedness property of the JTM in the linear $T \otimes b$ problem. Instead, for state Ψ_2 , the Π_2 path evolves to one of class Π_1 by becoming of the Δ -type, and hence smoothly contractable to a point: no GP effect is observed. In other words, there is a point \mathbf{Q}_d in configuration space where the mapping is degenerate: it links \mathbf{Q}_d not just to a pair of opposite points $\pm\Psi_2(\mathbf{Q}_d)$ on the electronic sphere but to the whole circle of linear combinations $\cos \xi_{23}(\mathbf{Q}_d)\psi_2 + \sin \xi_{23}(\mathbf{Q}_d)\psi_3$.

Similarly to the $E \otimes e$ system, $\theta = 2\xi_{12}$ and $\phi = 2\xi_{23}$ define pseudo-rotational angles with the lowest adiabatic PES displaying a continuum of equipotential minima points that form a $2D$ trough on the $5D$ surface. In terms of ξ_{12} and ξ_{13} distortion angles, the motion along the bottom of the JTM can then be viewed as an internal free rotation of quadrupole distortions of a sphere where the direction of the distortion gradually changes along the (ξ_{12}, ξ_{13}) directions [12, 13]; Figure 6.7. The presence/absence of GP effect manifests then as a property inherent to sign change of the adiabatic electronic wave vectors upon action of \hat{R}_3 in f -space, thus corroborating the observation [35] that GP in the $T \otimes (e \oplus t_2)$

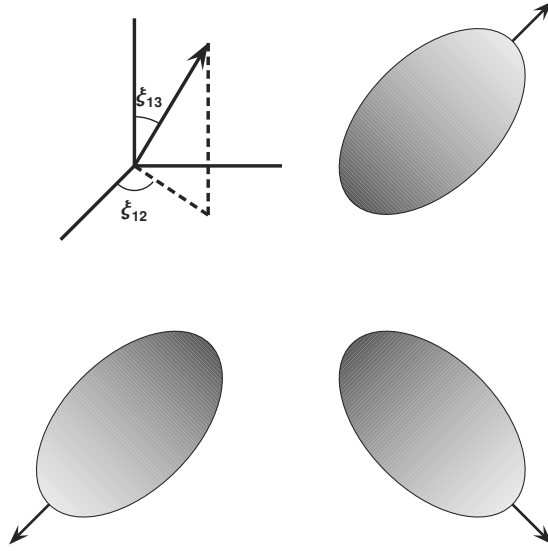


Figure 6.7. Internal free rotation of quadrupole distortions of a sphere where the direction of the distortion gradually changes along the (ξ_{12}, ξ_{13}) directions.

system is tied to the occurrence of a ground-state triplet (see Ref. 136).

6.6.3 High electronic orbital degeneracies

Fourfold and fivefold orbital degenerate electronic terms arise in icosahedral systems, with typical problems being [12] $G \otimes (g \oplus b)$ and $H \otimes (g \oplus 2b)$, respectively. These will be briefly surveyed in this section. A parametrization of the \hat{R}_N ($N=4, 5$) operator is then required, with two convenient and independent ways being available to parametrize N dimensions with angular coordinates [137]. The one followed here, which is most frequently encountered in physical applications, is the polar parametrization [19, 45, 46, 128, 137]. Such N -dimensional polar (also known as hyperspherical polar) coordinates were used by Louck [128] in pioneering work on the generalized orbital angular momentum for the N -fold degenerate harmonic oscillator, although a parametrization with biharmonic coordinates has also been used [46]. The rotation matrix in $O(N)$ assumes then the form:

$$\mathbf{R}_N = \rho_{12}(\xi_{12})\rho_{23}(\xi_{23})\rho_{34}(\xi_{34}) \cdots \rho_{N-1,N}(\xi_{N-1,N}) \quad (6.77)$$

thence showing a dependence on $(N - 1)$ mixing angles.

Consider now the the $G \otimes (g \oplus b)$ problem whose Lie symmetry of the linear JT Hamiltonian is [11] $SO(4)$, thus having six Lie-group parameters. A norm-preserving adiabatic electronic vector for this problem will then be defined by three mixing angles with the rotation matrix \mathbf{R}_4 given by the product of three 4×4 independent unitary planar rotation matrices ρ_{ij} . Any 3 mixing angles [chosen from the 6 available parameters in $SO(4)$] will then be suitable to specify an adiabatic wave vector, provided that under \hat{R}_4 it either changes sign or remains sign unchanged. Thus,

$$\mathbf{R}_4 = \begin{bmatrix} c_{12} & s_{12}c_{23} & s_{12}s_{23}c_{34} & s_{12}s_{23}s_{34} \\ -s_{12} & c_{12}c_{23} & c_{12}s_{23}c_{34} & c_{12}s_{23}s_{34} \\ 0 & -s_{23} & c_{23}c_{34} & c_{23}s_{34} \\ 0 & 0 & -s_{34} & c_{34} \end{bmatrix} \quad (6.78)$$

where $c_{ij} = \cos \xi_{ij}$, $s_{ij} = \sin \xi_{ij}$, and the angles are interpreted in a way similar to previous cases. being associated to pseudo-rotational angular coordinates in v -space. The action of \hat{R}_4 in f -space will then consist of the following rotations: $\xi_{12} \rightarrow \pi - \xi_{12}$, $\xi_{23} \rightarrow \pi - \xi_{23}$, and $\xi_{34} \rightarrow \xi_{34} + \pi$. Upon acting with \hat{R}_4 , Ψ_1 and Ψ_4 are seen to change sign while Ψ_2 and Ψ_3 remain sign-unchanged. Following Ref. 48, this may be rationalized by fixing ξ_{12} and ξ_{34} at specific values. If one considers $\xi_{12} = 0 \rightarrow \pi$ at $\xi_{34} = \pi/2$, one gets for the Ψ_2 components: $(0, c_{23}, 0, s_{23}) \rightarrow (0, -c_{23}, 0, -s_{23})$. The situation is then analogous to that of the $N = 3$ problem: both before and after the transformation $\xi_{12} \rightarrow \pi - \xi_{12}$, Ψ_2 is found to change sign but through complementary paths that close the loop and hence lead to sign cancelation as the final result (topologically, one has a path of Δ type). A similar observation applies to Ψ_3 when $\xi_{23} = 0 \rightarrow \pi$: $(0, 0, c_{34}, s_{34}) \rightarrow (0, 0, -c_{34}, -s_{34})$. The above explains why Ψ_2 and Ψ_3 keep their signs unchanged under \hat{R}_4 in f -space.

A situation where only two states change sign out of four belongs to case (2, 2); the first digit stands for the number of sign changes, the other for that of no sign changes (also referred to as [44] JT and RT cases, respectively), where also the cases (4, 0) and (0, 4) are observed. However, it finds no correspondence in the model Hamiltonian work of Ref. 43 where only cases (4, 0) and (0, 4) are found. If $2\xi_{12}$, $2\xi_{23}$ and $2\xi_{34}$ are viewed as pseudo-rotation angles in the

9D space of the g and b vibrations ($[G^2] = A+G+H$, with an equal coupling assumed for the G and H modes), one obtains [46, 138] a 3D JTM extending over the 9D coordinate space, a situation analogous to the one in 5D for the cubic quadruplet terms [$\Gamma_8 \otimes (e \oplus t_2)$ problem] [11]. Of course, it cannot be anticipated whether a warping of the adiabatic PESs occurs as this depends on the JT matrix. In fact, when the dimension of the normal-mode space is smaller than that of the function space, the PES is usually characterized by some amount of corrugation [13]. Our theory can then predict how many states manifest GP but not its presence/absence in JTM.

We now turn to fivefold electronic degeneracies, the highest known in molecular symmetry groups (except for axial ones, not interesting in JT theory), which arise in fullerenes like C_{60} via the icosahedral $H \otimes (g \oplus 2b)$ system [12]. Belonging to the symmetry group [11] $SO(5)$, the analysis for the coupling of a fivefold degenerate electronic state of H symmetry and a 9D space of nuclear distortions ($g + b$) leads to the prediction of a 4D JTM trough in the 9D PES. This is due to the fact that a norm-preserving eigenvector will show rotational invariance to changes in its direction related to an equipotential displacement on the bottom of the trough. Depending on a single-mode splitting parameter, two coupling regimes favoring either pentagonal or trigonal minima may be observed. For a nonzero splitting, the surface of the trough becomes warped with the appearance of minima of D_{3d} and D_{5d} symmetries (Refs. 12, 47, and therein).

In line with the other JT problems, use will then be made of the rotation matrix

$$\mathbf{R}_5 = \begin{bmatrix} c_{12} & s_{12}c_{23} & s_{12}s_{23}c_{34} & s_{12}s_{23}s_{34}c_{45} & s_{12}s_{23}s_{34}s_{45} \\ -s_{12} & c_{12}c_{23} & c_{12}s_{23}c_{34} & c_{12}s_{23}s_{34}c_{45} & c_{12}s_{23}s_{34}s_{45} \\ 0 & -s_{23} & c_{23}c_{34} & c_{23}s_{34}c_{45} & c_{23}s_{34}s_{45} \\ 0 & 0 & -s_{34} & c_{34}c_{45} & c_{34}s_{45} \\ 0 & 0 & 0 & -s_{45} & c_{45} \end{bmatrix} \quad (6.79)$$

where the angles ξ_{ij} are defined as above. In this case too, only two adiabatic sheets of the fivefold manifold are predicted to manifest GP: case (2, 3). Such a result seem at first to contradict existing evidence on the nature of the dynamic ground state adiabatic PES, which has been examined in detail [47, 139, 140].

In fact, the JT effect of the icosahedral quintuplet term in the trigonal regime shows an intriguing crossover of dynamic states from a degenerate to a singlet state, with coupling strength showing an apparent correlation with the phase of the tunneling paths through such minima. At stronger coupling the dominant tunneling process is believed to consist of closed loops spanning cycles of five wells, with a vanishing GP associated with these loops. Moate *et al.* [139] and Manini and De Los Rios [140] studied the $H \otimes b$ problem and have given distinct topological explanations for the absence of GP in such loops by considering their projection in a plane formed by normals to a pentagonal symmetry axis which permutes the five wells in a cyclic fashion. A connection between such topological explanations has been given by Lijnen and Ceulemans [47], who have scanned the topology of the full coordinate space using a net of triangular cross sections between the ten D_{3d} minima. By expressing the GP of every loop on the PES in terms of such 2D triangular cross sections, they have found [47] that the absence of GP for the cycles containing five trigonal wells originates from two seams of conical intersections going through these cycles. Suffice it to note that the absence of GP effect on the adiabatic ground state PES does not invalidate our prediction that only two sheets of the fivefold electronic manifold manifest GP. Of course, one may argue that, if both a conical and a tangential contact occur, one expects the former to lie lower in energy due to its nonzero slope. Yet, one can contest that the energy-ordering criterion is applicable only to adiabatic states, which need not necessarily be invoked here. In other words, a given diabatic state may be the dominant contribution to the adiabatic ground or to an adiabatic excited state depending on the region of configuration space under analysis. The above considerations seem therefore to rule out a prediction [43,44] of sign change in all states of the fivefold manifold, case (5, 0). As Table 6.1 shows the Baer [44] theory predicts cases (3, 2) and (1, 4), but not (0, 5), with similar results holding for the theory of Manolopoulos and Child [43]. Thus, none of the existing theories (including our own [48]) predicts the case (0, 5). Clearly, this is an issue that requires further analysis.

Table 6.1. Allowed adiabatic sign-changes at a N -fold electronic orbital degeneracy.

N	MC ^{a)}	B ^{b)}	this work
2	--	--	--
3	+++ -+-	+++ -+-	n.o. ^{c)} -+-
4	++++ ---- n.o.	++++ ---- -++-	n.o. n.o. -++-
5	----- n.o. ---++ -++++	----- n.o. ---++ -++++	n.o. -++++ n.o. n.o.
6	----- n.o. n.o. ++----	----- -++++- -----++ +++++	n.o. -++++- n.o. n.o.

^{a)} D.E. Manolopoulos & M.S. Child, *Phys. Rev. Lett.*, **82**, 2223 (1999).

^{b)} M. Baer, *Chem. Phys. Lett.*, **322**, 520 (2000).

^{c)} Not observed.

6.7 Is Longuet-Higgins theorem valid for any Jahn-Teller degeneracy?

It is apparent from section 6.3 that the adiabatic propagation of an electronic wave vector around a N -fold degeneracy in ν -space can be associated to a $(N-1)$ -angle pseudo-rotation or to a multiple-rotation in the f -space with the same dimensionality. In many cases, the rotation operator \hat{R}_{N-1} yields a Π_2 path in f -space. For the twofold and threefold linear JT problems, our predictions are found to agree with those obtained from the traditional loop analysis in ν -space [20, 21, 35, 136]. Not unexpectedly, perhaps, our predictions [48] do not always coincide with the ones obtained from other treatments [43, 44], nor do the latter agree amongst themselves. This may be attributed to the specific symmetry requirements involved, thus eliminating occurrences that might otherwise happen in their absence. In fact, a $(2, N-2)$ sign-change is predicted irrespective of N : only two electronic wave vectors change sign. With $N=4$, the

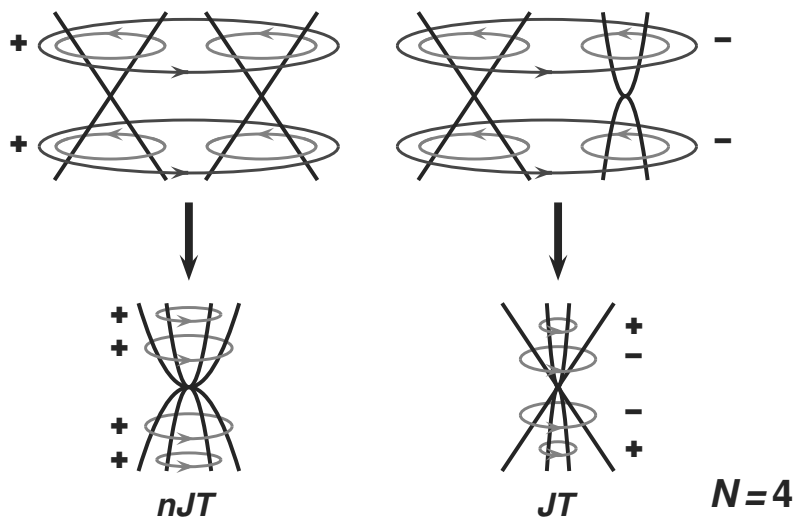


Figure 6.8. Schematic coalescence of two twofold electronic degeneracies to yield a fourfold one. For clarity, a pair of states where the sign change is not observed upon completion of a loop in v -space is indicated by two paraboloids, one up and one down, that touch tangentially (the point of contact is not necessarily an extremum). Conversely, those that change sign are indicated by a diabolo. If the two degeneracies were both of the conical type, the first LH theorem would imply that none of the four states could change sign upon adiabatic transportation of the wave function over a closed loop that encircles the two coalescing degeneracy points as this would imply an even number of conical intersections. Stated differently, only if one of the $N=2$ coalescing degeneracies is conical can yield a single pair of sign changing states.

results from our theory then agree with one of the reported Baer's [44] solutions, but disagree with his results and the ones of Manolopoulos and Child [43] in not finding the $(4, 0)$ and $(0, 4)$ cases.

An attempt to rationalize the above discrepancies is made in Figure 6.8, where a (high- N) fold degeneracy is viewed as the coalescence of two (low- N) fold ones, specialized to $N = 4$. The approach [48] stands therefore on the assumption that both the low- and (high- N)-fold degeneracies can occur along the same locus, which should generally be valid on symmetry grounds. The argument is then akin to that of viewing, *e.g.*, an $e \oplus t_2$ problem as a fivefold degenerate vibration for identical coupling parameters. Note that a pair of states where a sign change is not observed upon completion of a loop in v -space

(a Δ -path) is indicated by two paraboloids, one up and one down, touching tangentially (not necessarily an extremum, and hence should not be confused with a pseudo-JT situation [11, 13]). Conversely, the ones that change sign (Π_2 -type) are indicated by a diaboloid. Clearly, the LH theorem imposes that only one of the $N=2$ coalescing degeneracies may be conical leading to a single pair of sign changing states.

The question then arises: since an odd number of two-state conical intersections is involved in a sixfold degeneracy, does the argumentation of the previous paragraph imply the existence of the $(0, 6)$ case? As sketched in Figure 6.9, the answer will be negative. In fact, the $N=6$ case may also be viewed as a coalescence of $N=4$ and $N=2$ degeneracies. Because the LH theorem has been shown to apply to $N=4$, only one of those coalescing degeneracies can be of the conical type, leading again to just one pair of states subject to the GP effect. Since there is no reason of principle for one of the above two schemes to prevail over the other, the maximum number of sign-changing states common to both interpretations is two, *i.e.*, the $(2, 4)$ case. As Table 6.1 shows Baer's theory [44] additionally predicts the cases $(6, 0)$, $(4, 2)$ and $(0, 6)$, while the only predictions from the Manolopoulos-Child [43] theory are $(4, 2)$ and $(0, 6)$. By an extension of the above argument, one is led to conclude that only one pair of sign changing states is observable for any arbitrary N -fold degeneracy [19, 45, 48]. Note that the odd- N state cases pose no problem, since only a single sign-unchanging state needs to be added to the closest even- N state problem. Thus, the intriguing question urges of whether the LH theorem applies to arbitrary N -fold degeneracies.

To get additional physical insight into the above question, consider a JT problem where more than a pair of adiabatic states is assumed to change sign upon parallel transportation along a closed path around the locus of degeneracy. For example, assume that the case $(4, 0)$ behaves that way, with Ψ_i ($i=1-4$) denoting such states. Since they are degenerate in the vicinity of the seam, a solution of the SE would also be $\Psi = \sum_{i=1}^N C_i \Psi_i$. Recalling now that opposing wave vectors in a ray represent a unique physical state [129], all Ψ_i must change

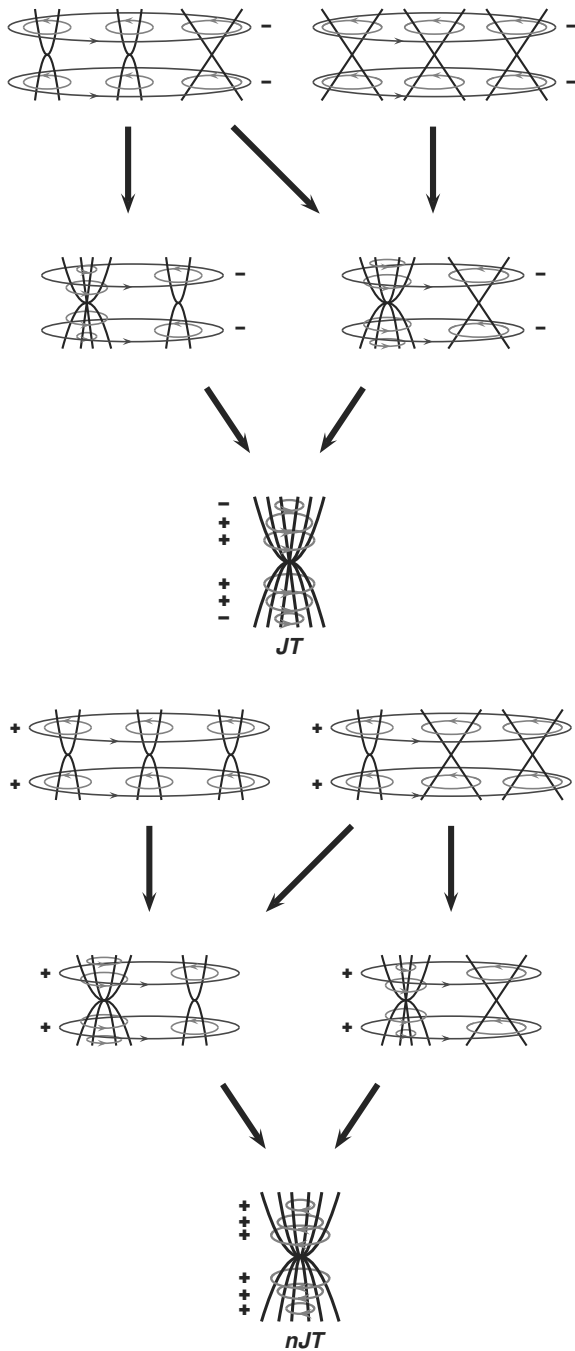


Figure 6.9. Schematic coalescence of low-order degeneracies in the configuration space of the JT system to form a sixfold electronic degeneracy.

sign simultaneously during the parallel transportation of Ψ along the loop. Since this must be further warranted for any loop, only by accident could it happen unless all pairs are identical. Stated differently, only one pair of adiabatic states can change sign. The above can be summarized in the following [48] (extended Longuet-Higgins) Theorem: *No N -fold linear JT degeneracy can have more than one pair of adiabatic electronic states that change sign upon being parallel transported in v -space along a loop that encircles the degeneracy point.* The method of *reductio ad absurdum* will be employed for the demonstration. Assume then that M such pairs show a sign change. Clearly, M cannot be even an even number as this would imply a loop encircling an even number of twofold degeneracies (conical intersections), thence violating the first LH theorem. If M is odd, then let us isolate arbitrarily one pair of states that shows such a sign change. The remaining $M-1$ pairs would then form a manifold with an even number of twofold conical intersections. This cannot be allowed since, as noted above, it would violate the first LH theorem. Thus, none of the $2M-2$ states can change sign upon completing a loop around the crossing point: only one pair (the isolated one) can show such a sign change. *QED*

6.8 Does a general relation between the geometrical phase and mixing angles exist?

For the $2D$ Hilbert space, we have shown that by writing a single complex wave function in terms of the two real ones, Eq. (6.68), a relation can be obtained between the geometrical phase and the mixing angle. Specifically, the angle $\gamma(\mathbf{r}_n) = \tilde{\gamma}/2$ that diagonalizes the potential matrix (mixing angle) has been shown to be identical to ATD angle, $\alpha(\mathbf{r}_n)$ [41], and GP, $A(\mathbf{r}_n)$ [40], at least up to a constant term that has no physical significance. The process of building the single-valued complex function for the above $O(2)$ case suggests therefore the following generalized expression for the $O(N)$ case:

$$\tilde{\Psi} = \frac{1}{\sqrt{N}} \sum_{n=1}^N \exp \left[\frac{2(n-1)\pi i}{N} \right] \Psi_n \quad (6.80)$$

Recalling now that

$$\tilde{\Psi} = \exp[\iota A(\mathbf{r}_n)]\Psi \quad (6.81)$$

one obtains upon use of Eq. (6.77) and evaluation of $\langle \tilde{\Psi} | \nabla \tilde{\Psi} \rangle$,

$$\nabla A(\mathbf{r}_n) = -\frac{1}{\sqrt{N}} \left[\nabla \xi_{12} + \sum_{n=1}^{N-2} c_{n,n+1} \nabla \xi_{n+1,n+2} - \prod_{n=1}^{N-2} s_{n,n+1} \nabla \xi_{N-1,N} \right] \quad (6.82)$$

Specializing for the $N=3$ case, one gets

$$\nabla A(\mathbf{R}) = -\frac{1}{\sqrt{3}} \left[\nabla \xi_{12} + (\cos \xi_{12} - \sin \xi_{12}) \nabla \xi_{23} \right] \quad (6.83)$$

which provides an explicit relation between the GP angle and the mixing angles $\xi_{12}(\mathbf{r}_n)$ and $\xi_{23}(\mathbf{r}_n)$. Corresponding expressions can be obtained for other Lie groups, in all cases involving $\nabla A(\mathbf{R})$ and the gradient of each of the $N - 1$ mixing angles. The problem lies therefore on the capability to reduce the Hamiltonian to a single SE as done on section 6.6.1 for the $e \otimes E$ problem. This would not only simplify considerably the generalized BO formulation recently suggested [141, 142] for the three-state problem but provide a generalization to higher-degeneracies. In this regard, the most convenient formulation appears to be the one of Eq. (6.37), where the nuclear wave functions are treated as real and a vector potential appears in the Hamiltonian. In this case, $\nabla A(\mathbf{R})$ can be replaced there to solve the dynamics problem in terms of the mixing angles. Alternatively, one may think of following the argumentation above and treat a N -fold degeneracy as a succession of $\binom{N}{2}$ twofold degeneracies solved step-by-step as done by Longuet-Higgins [*i.e.*, via repeated use of hybrid wave functions in Eq. (6.68)]. In this case the answer to the above question should be also affirmative. Research along these lines is currently in progress in our Group.

6.9 Concluding remarks

We have given a perspective on the BO approximation and several related issues: separation of the electronic and nuclear motions, coupled-channel treatment, scaling properties, validity, and diabatic states. Furthermore, considerable

emphasis has been put on the need for its generalization such as to account for the topological implications in systems with degeneracies of the conical type, due to the separation of the electronic (fast) and nuclear (slow) degrees of freedom. Without hoping for convenience at a balanced coverage of the topic, the analysis has been carried by specializing on the work developed in recent years by the author and his collaborators while providing references to other published material. Beyond well known studies on two-fold degeneracies, recent developments on the theme of high electronic degeneracies occurring for Jahn-Teller systems have been also surveyed. In particular, a theory recently proposed by the author [19, 45, 48] that avoids altogether the solution of the dynamics problem by making instead use of symmetry invariants has been reviewed in some detail. How to bring it into the realm of quantum dynamics by generalizing the procedure utilized to decouple the two-state problem into two one-state ones with the help of GP is a promising issue that warrants a future reanalysis of this topic.

Note added in proof

After completing this work, Generalized Born-Oppenheimer equations including the geometrical phase effect have been derived for three- and four-fold electronic manifolds in Jahn-Teller systems near the degeneracy seam [143]. The theory shows unprecedented simplicity while being readily extendable to N -fold systems of arbitrary dimension. In addition, an application to a model threefold system has been reported [143], and the results compared with Born-Oppenheimer (geometrical phase ignored), extended Born-Oppenheimer [141], and coupled three-state calculations [144].

Acknowledgments

I thank my coworkers for their valuable contributions. This work has the financial support of Fundação para a Ciência e a Tecnologia, Portugal, under projects PTDC/QUI-QUI/099744/2008 and PTDC/AAC-AMB/099737/2008. It has also benefited from the support of European Space Agency under ESTEC Con-

References

- [1] A. B. Migdal, *Qualitative Methods in Quantum Theory* (Addison-Wesley, New York, 1989).
- [2] M. Born and J. R. Oppenheimer, *Ann. Phys.* **84**, 457 (1927).
- [3] G. Del Re, *Ann. N.Y. Acad. Sci.*, **988**, 133 (2003).
- [4] V. N. Ostrovsky, *Int. J. Phil. Chem.* **11**, 101 (2005).
- [5] B. T. Sutcliffe, *Lect. Notes Chem.: Potential Energy Surfaces* edited by A. F. Sax (Springer, Berlin, 1999), "The idea of a potential energy surface", pp. 61.
- [6] W. Kołos and L. Wolniewicz, *J. Chem. Phys.* **43**, 2429 (1965).
- [7] A. J. C. Varandas, *Chem. Phys. Lett.* **463**, 225 (2008).
- [8] A. J. C. Varandas, *J. Comp. Chem.* **30**, 379 (2009).
- [9] A. J. C. Varandas, *Int. J. Quantum Chem.* **111**, 416 (2011).
- [10] R. Englman, *The Jahn-Teller Effect* (Wiley, New York, 1973).
- [11] I. B. Bersuker and V. Z. Polinger, *Vibronic Interactions in Molecules and Crystals* (Springer, Berlin, 1989).
- [12] C. C. Chancey and M. C. M. O'Brien, *The Jahn-Teller Effect in C₆₀ and other Icosahedral Complexes* (Princeton University Press, New Jersey, 1997).
- [13] I. B. Bersuker, *Chem. Rev.* **101**, 1067 (2001).
- [14] M. J. Klein, *Am. J. Phys.* **20**, 65 (1952).
- [15] C. A. Mead, *Rev. Mod. Phys.* **64**, 51 (1992).
- [16] A. Kupperman, in *Dynamics of Molecules and Chemical Reactions*, edited by R. E. Wyatt and J. Z. H. Zhang (Marcel Dekker, New York, 1996), pp. 411.
- [17] D. R. Yarkony, *Rev. Mod. Phys.* **68**, 985 (1996).
- [18] A. J. C. Varandas and Z. R. Xu, in *Adv. Chem. Phys.: The Role Of Degenerate States In Chemistry*, edited by M. Baer and G. D. Billing (Wiley, New York, 2002), "Permutational symmetry and the role of nuclear spin in the vibrational spectra of molecules in doubly degenerate electronic states:

- The trimers of S_2 atoms” vol. 124, pp. 659.
- [19] A. J. C. Varandas, in *Fundamental World of Quantum Chemistry: A Tribute Volume to the Memory of Per-Olov Löwdin*, edited by E. J. Brändas and E. S. Kryachko (Kluwer, Dordrecht, 2003), “On the geometric phase effect in Jahn-Teller systems”, vol. 2, chap. 2, pp. 33.
- [20] G. Herzberg and H. C. Longuet-Higgins, *Discuss. Faraday Soc.* **35**, 77 (1963).
- [21] H. C. Longuet-Higgins, *Proc. R. Soc. Ser. A* **344**, 147 (1975).
- [22] A. J. C. Varandas, J. Tennyson, and J. N. Murrell, *Chem. Phys. Lett.* **61**, 431 (1979).
- [23] Y. Fukumoto, H. Koizumi, and K. Makoshi, *Chem. Phys. Lett.* **313**, 283 (1999).
- [24] M. V. Berry, *Proc. R. Soc. London, Ser. A* **392**, 45 (1984).
- [25] S. Pancharatnam, *Ind. Acad. Sci. A* **44**, 247 (1956).
- [26] C. A. Mead and D. G. Truhlar, *J. Chem. Phys.* **70**, 2284 (1979).
- [27] R. W. Batterman, *Studies in History and Philosophy of Modern Physics* **34**, 527 (2003).
- [28] N. Manini and P. de los Rios, *J. Phys.: Condens. Matt.* **10**, 8485 (1998).
- [29] A. Kuppermann and Y.-S. M. Wu, *Chem. Phys. Lett.* **241**, 229 (1995).
- [30] B. K. Kendrick and R. T Pack, *J. Chem. Phys.* **104**, 7475 (1996).
- [31] S. Mahapatra, H. Köppel, and L. S. Cederbaum, *J. Phys. Chem. A* **105**, 2321 (2001).
- [32] B. K. Kendrick, *J. Chem. Phys.* **107**, 6739 (2003).
- [33] J. C. Juanes-Marcos, A. J. C. Varandas, and S. C. Althorpe, *J. Chem. Phys.* **128**, 211101 (2008).
- [34] F. S. Ham, *Phys. Rev. Lett.* **58**, 725 (1987).
- [35] C. C. Chancey and M. C. M. O’Brien, *J. Phys. A: Math. Gen.* **21**, 3347 (1988).
- [36] A. J. C. Varandas and H. G. Yu, *J. Chem. Soc. Faraday Trans.* **93**, 819 (1997).
- [37] M. Baer and R. Englman, *Chem. Phys. Lett.* **265**, 105 (1997).

- [38] B. K. Kendrick, C. A. Mead, and D. G. Truhlar, *J. Chem. Phys.* **110**, 7594 (1999).
- [39] A. J. C. Varandas and Z. R. Xu, *Chem. Phys. Lett.* **316**, 248 (2000).
- [40] A. J. C. Varandas and Z. R. Xu, *J. Chem. Phys.* **112**, 2121 (2000).
- [41] Z. R. Xu, M. Baer, and A. J. C. Varandas, *J. Chem. Phys.* **112**, 2746 (2000).
- [42] B. Kendrick, C. A. Mead, and D. G. Truhlar, *Chem. Phys. Lett.* **277**, 31 (2002).
- [43] D. E. Manolopoulos and M. S. Child, *Phys. Rev. Lett.* **82**, 2223 (1999).
- [44] M. Baer, *Chem. Phys. Lett.* **322**, 520 (2000).
- [45] A. J. C. Varandas and Z. R. Xu, *Int. J. Quant. Chem.* **99**, 385 (2004).
- [46] J. P. Cullerne and M. C. O'Brien, *J. Phys.: Condens. Matt.* **6**, 9017 (1994).
- [47] E. Lijnen and A. Ceulemans, *Phys. Rev. B* **71**, 014305 (2005).
- [48] A. J. C. Varandas, *Chem. Phys. Lett.* **487**, 139 (2010).
- [49] *Subatomic Physics*, edited by E. M. Henley and A. Garcia (World Scientific, New Jersey, 2007).
- [50] A. J. C. Varandas, *J. Chem. Phys.* **131**, 124128 (2009).
- [51] A. Vibók, G. J. Halász, S. Suhai, and M. Baer, *J. Chem. Phys.* **122**, 134109 (2005).
- [52] C. Hu, H. Harai, and O. Sugino, *J. Chem. Phys.* **127**, 064103 (2007).
- [53] T. G. Heil, S. E. Butler, and A. Dalgarno, *Phys. Rev. A* **23**, 1100 (1981).
- [54] J. B. Delos, *Rev. Mod. Phys.* **53**, 287 (1981).
- [55] A. Macias and A. Riera, *Phys. Rev.* **90**, 299 (1982).
- [56] B. C. Garrett, D. G. Truhlar, and C. F. Melius, *Energy Storage and Redistribution in Molecules* (Plenum Press, New York, 1983).
- [57] R. McCarroll and D. S. F. Crothers, *Adv. Atom., Mol., Opt. Phys.* **32**, 253 (1994).
- [58] R. J. Buenker and Y. Li, *J. Chem. Phys.* **112**, 8318 (2000).
- [59] H. Nakamura and D. G. Truhlar, *J. Chem. Phys.* **117**, 5576 (2002).
- [60] A. K. Belyaev, A. Dalgarno, and R. McCarroll, *J. Chem. Phys.* **116**, 5395 (2002).
- [61] J. C. Tully, *Theor. Chem. Acc.* **103**, 173 (2000).

- [62] *Adv. Series Phys. Chem.: Conical Intersections: Electronic Structure, Spectroscopy and Dynamics*, edited by W. Domcke, D. R. Yarkony, and H. Köp-
pel (World Scientific Publishing, Singapore, 2004).
- [63] W. Lichten, *Phys. Rev.* **164**, 131 (1967).
- [64] F. T. Smith, *Phys. Rev.* **179**, 111 (1969).
- [65] T. F. O'Malley *Adv. At. Mol. Phys.* **7**, 223 (1971).
- [66] M. Baer, *Mol. Phys.* **40**, 1011 (1980).
- [67] *State Selected and State-to-State Ion-Molecule Reaction Dynamics. Part 2. Theory*, edited by C. Y. Ng and M. Baer (John Wiley & Sons, New York, 1992), vol. 82.
- [68] H. Köppel, *Faraday Discuss.* **127**, 35 (2004).
- [69] A. Macías and A. Riera, *J. Phys. B: Atom. Molec. Phys* **11**, 489 (1978).
- [70] S. Carter and J. N. Murrell, *Mol. Phys.* **41**, 567 (1980).
- [71] J. N. Murrell, S. Carter, I. M. Mills, and M. F. Guest, *Mol. Phys.* **42**, 605 (1981).
- [72] H. J. Werner and W. Meyer, *J. Chem. Phys.* **74**, 5802 (1981).
- [73] P. G. Hay, R. Pack, R. B. Walker, and E. J. Heller, *J. Phys. Chem.* **86**, 862 (1982).
- [74] S. Carter, I. Mills, J. N. Murrell, and A. J. C. Varandas, *Mol. Phys.* **45**, 1053 (1982).
- [75] W. Domcke and C. Woywod, *Chem. Phys. Lett.* **216**, 362 (1993).
- [76] T. Pacher, L. S. Cederbaum, and H. Köppel, *Adv. Chem. Phys.* **84**, 293 (1993).
- [77] W. Domcke, C. Woywod, and M. Stengle, *Chem. Phys. Lett.* **226**, 257 (1994).
- [78] G. J. Atchity and K. Ruedenberg, *Theor. Chem. Acc.* **97**, 47 (1997).
- [79] A. J. Dobbyn and P. J. Knowles, *Mol. Phys.* **91**, 1107 (1997).
- [80] M. S. Topaler, D. G. Truhlar, P. P. X. Y. Chang, and J. C. Polanyi, *J. Chem. Phys.* **108**, 5349 (1998).
- [81] A. Thiel and H. Köppel, *J. Chem. Phys.* **110**, 9371 (1999).
- [82] M. D. Hack and D. G. Truhlar, *J. Chem. Phys.* **110**, 4315 (1999).

- [83] H. Nakamura and D. G. Truhlar, *J. Chem. Phys.* **115**, 10353 (2001).
- [84] A. W. Jasper, M. D. Hack, D. G. Truhlar, and P. Piecuch, *J. Chem. Phys.* **116**, 8353 (2002).
- [85] V. C. Mota and A. J. C. Varandas, *J. Phys. Chem. A* **112**, 3768 (2008).
- [86] A. J. C. Varandas, *Chem. Phys. Lett.* **471**, 315 (2009).
- [87] B. Heumann, K. Weide, R. Duren, and R. Schinke, *J. Chem. Phys.* **98**, 5508 (1993).
- [88] C. Leforestier, F. Lequere, K. Yamashita, and K. Morokuma, *J. Chem. Phys.* **101**, 3806 (1994).
- [89] C. Woywod, M. Stengle, W. Domcke, H. Flöthmann, and R. Schinke, *J. Chem. Phys.* **107**, 7282 (1997).
- [90] D. Simah, B. Hartke, and H. J. Werner, *J. Chem. Phys.* **111**, 4523 (1999).
- [91] A. J. Dobbyn, J. N. L. Connor, N. A. Besley, P. J. Knowles, and G. C. Schatz, *Phys. Chem. Chem. Phys.* **1**, 957 (1999).
- [92] M. Boggio-Pasqua, A. I. Voronin, P. Halvick, J. C. Rayez, and A. J. C. Varandas, *Mol. Phys.* **98**, 1925 (2000).
- [93] V. Kurkal, P. Fleurat-Lessard, and R. Schinke, *J. Chem. Phys.* **119**, 1489 (2003).
- [94] J. Brandão and C. A. Rio, *J. Chem. Phys.* **119**, 3148 (2003).
- [95] Z.-W. Qu, H. Zhu, S. Y. Grebenshchikov, and R. Schinke, *J. Chem. Phys.* **123**, 074305 (2005).
- [96] S. Y. Grebenshchikov, R. Schinke, Z. Qu, and H. Zhu, *J. Chem. Phys.* **124**, 204313 (2006).
- [97] J. N. Murrell and A. J. C. Varandas, *Mol. Phys.* **57**, 415 (1986).
- [98] R. F. Lu, T. S. Chu, Y. Zhang, K. Han, A. J. C. Varandas, and J. Z. H. Zhang, *J. Chem. Phys.* **125**, 133108 (2006).
- [99] A. Alijah and A. J. C. Varandas, *Phys. Rev. Lett.* **93**, 243003 (2004).
- [100] H. C. Longuet-Higgins, *Adv. Spectrosc.* **2**, 429 (1961).
- [101] M. Born and K. Huang, *Dynamical Theory of Crystal Lattices* (Clarendon Press, Oxford, 1954).
- [102] R. Jackiw, *Comments At. Mol. Phys.* **21**, 71 (1988).

- [103] B. K. Kendrick and C. A. Mead, *J. Chem. Phys.* **102**, 4160 (1995).
- [104] C. A. Mead, *Chem. Phys.* **49**, 23 (1980).
- [105] C. A. Mead, *J. Chem. Phys.* **72**, 3839 (1980).
- [106] Y.-S. M. Wu, A. Kuppermann, and B. Lepetit, *Chem. Phys. Lett.* **186**, 319 (1991).
- [107] Y.-S. M. Wu and A. Kuppermann, *Chem. Phys. Lett.* **201**, 178 (1993).
- [108] A. Kuppermann and Y.-S. M. Wu, *Chem. Phys. Lett.* **213**, 636 (1993).
- [109] G. D. Billing and N. Markovic, *J. Chem. Phys.* **99**, 2674 (1993).
- [110] Z. R. Xu and A. J. C. Varandas, *Int. J. Quantum Chem.* **80**, 454 (2000).
- [111] Z. R. Xu and A. J. C. Varandas, *J. Phys. Chem. A* **105**, 2246 (2001).
- [112] T. C. Thompson and C. A. Mead, *J. Chem. Phys.* **82**, 2408 (1985).
- [113] A. J. C. Varandas, F. B. Brown, C. A. Mead, D. G. Truhlar, and N. C. Blais, *J. Chem. Phys.* **86**, 6258 (1987).
- [114] A. J. C. Varandas, *Advanced Series in Physical Chemistry: Conical Intersections*, edited by W. Domcke, D. R. Yarkony, and H. Köppel (World Scientific Publishing, Singapore, 2004), vol. 15, chap. 5, p. 91.
- [115] L. P. Viegas, A. Alijah, and A. J. C. Varandas, *J. Chem. Phys.* **126**, 074309 (2007).
- [116] C. A. Mead and D. G. Truhlar, *J. Chem. Phys.* **77**, 6090 (1982).
- [117] R. Abrol, A. Shaw, A. Kuppermann, and D. R. Yarkony, *J. Chem. Phys.* **115**, 4640 (2001).
- [118] R. Abrol and A. Kuppermann, *J. Chem. Phys.* **116**, 1035 (2002).
- [119] M. Baer, *Chem. Phys. Lett.* **35**, 112 (1975).
- [120] D. R. Yarkony, *J. Chem. Phys.* **105**, 10456 (1996).
- [121] D. R. Yarkony, *J. Phys. Chem. A* **101**, 4263 (1997).
- [122] R. Englman and M. Baer, *J. Phys.: Condens. Matter* **11**, 1059 (1999).
- [123] A. Ceulemans, *J. Chem. Phys.* **87**, 5374 (1987).
- [124] A. J. C. Varandas, *Chem. Phys. Lett.* **138**, 455 (1987).
- [125] A. J. C. Varandas, A. Alijah, and M. Cernei, *Chem. Phys.* **308**, 285 (2005).
- [126] A. Ceulemans, D. Beyens, and L. G. Vanquickenborne, *J. Am. Chem. Soc.* **106**, 5824 (1984).

- [127] J. D. Louck, *Am. J. Phys.* **5**, 378 (1963).
- [128] J. D. Louck, *J. Mol. Spectrosc.* **4**, 298 (1960).
- [129] M. Hammermesh, *Group Theory and its Application to Physical Problems* (Dover, New York, 1989).
- [130] M. Baer, *J. Chem. Phys.* **107**, 2694 (1997).
- [131] O. Friedrich, A. Alijah, Z. R. Xu, and A. J. C. Varandas, *Phys. Rev. Lett.* **86**, 1183 (2001).
- [132] Z. R. Xu and A. J. C. Varandas, *Int. J. Quantum Chem.* **83**, 279 (2001).
- [133] A. J. C. Varandas and L. P. Viegas, *Chem. Phys. Lett.* **367**, 625 (2003).
- [134] L. P. Viegas, A. Alijah, and A. J. C. Varandas, *J. Phys. Chem. A* **109**, 3307 (2005).
- [135] L. P. Viegas and A. J. C. Varandas, *Phys. Rev. A* **77**, 032505 (2008).
- [136] M. C. O'Brien, *J. Phys. Rev. B* **53**, 3775 (1996).
- [137] L. C. Biedenharn, *J. Math. Phys.* **3**, 433 (1961).
- [138] A. Ceulemans and P. W. Fowler, *Phys. Rev.* **39**, 481 (1989).
- [139] C. P. Moate, M. C. M. O'Brien, J. L. Dunn, C. A. Bates, Y. M. Liu, and V. Z. Polinger, *Phys. Rev. Lett.* **77**, 4362 (1996).
- [140] N. Manini and P. De Los Rios, *Phys. Rev. B* **62**, 29 (2000).
- B. Sar
- [141] kar and S. Adhikari, *J. Chem. Phys.* **124**, 074101 (2006).
- [142] B. Sarkar and S. Adhikari, *Int. J. Quantum Chem.* **60**, 650 (2009).
- [143] A. J. C. Varandas and B. Sarkar, *Phys. Chem. Chem. Phys.* (in press).
- [144] S. Adhikari, G. D. Billing, A. Alijah, S. H. Lin, and M. Baer, *Phys. Rev. A* **62**, 032507 (2000).

(Página deixada propositadamente em branco)

7. THE QUANTUM ASPECTS OF PROTEINS AND THEIR BIOLOGICAL FUNCTION

H. G. Bohr*

Quantum Protein (QuP) Center, Technical University of Denmark (DTU),
Department of Physics, DK-2800 Kgs. Lyngby, Denmark

Peptides, proteins, and especially enzymes, are studied with respect to their quantum behavior which includes electronic states, vibronic states involving the coupling of nuclear and electron motions, excited electronic state dynamics, electron and nuclear tunneling phenomena, bio-Auger processes, charge-density fluctuations and general charge transfer. All these issues are elucidated by quantum electronic calculation of vibrational spectra for small peptides in water solutions, for nucleic acids and finally for protein illustrated by the particular cases of the gene repair processes involving the peptides and then the proteins: Photolyase and Peridinin/ chlorophyll which, respectively, repair UV-radiation damages on genes and harvest light. In the latter two cases the quantum phenomena, such as bio-Auger, are playing a big role.

7.1 Introduction

Vibrational spectroscopies, *e.g.*, vibrational absorption (VA), vibrational circular dichroism (VCD), Raman scattering, and Raman optical activity (ROA), have many virtues, including many of the following: being easily accessible (FT IR/VA and FT Raman instruments are now common in most biospectroscopy laboratories, along with the chiral analogues FT VCD and FT ROA), being non-invasive techniques, being able to be measured on a solution and hence one is able to treat solvent effects and observe the biomolecules in their native or near-native environment, and finally with the addition of colloidal particles, as in SERS, it can detect nano-molar quantities which virtually are single molecules or singular

*Email address: hgbohr@gmail.com

molecular complexes or singular molecular machines in dilute solutions [1–3].

However, the difficulty has been to derive theoretical vibrational spectra from quantum electronic calculations in the case of large molecules with more than 10 atoms in their native or near-native environments. This is due to all the couplings between the involved bonds between the atoms. The vibrations basically all couple to each other and this creates a complex picture of superposition of vibrational modes that are hard to interpret and especially if one has to take into account the harmonic and anharmonic couplings with the solvent.

Another problem is that of the large number of conformational states or conformers (as one calls the stable conformations) which appear during the molecular dynamics simulations of peptides (the time scale during with the experiments are being made). These problems, however, open great opportunities in time-resolved spectroscopy since conformational changes can be monitored in time-resolved fluorescence and VA spectroscopy down to the time-scale of nano seconds.

7.2 Quantum analysis of small peptides

We shall firstly present how to use the quantum mechanical calculations of the electronic structures and properties of biomolecules and biomolecular complexes, especially peptides in their native environments, to interpret and understand vibrational spectra and changes in the vibrational spectra either as a reaction proceeds, or in response to a perturbation. From calculated structures and selected molecular properties, the vibrational absorption (VA) and vibrational circular dichroism (VCD) can be simulated from *first principles* within the mechanical harmonic approximation for the vibrational frequencies and normal modes, the electronic harmonic approximation for the electric dipole moments and their derivatives with respect to the nuclear displacements (the atomic polar tensors, APT), and beyond the Born-Oppenheimer approximation for the magnetic dipole transition moments and their derivatives with respect to the nuclear velocities (the atomic axial tensors, AAT). For amino acids, peptides and polypeptides solvent and environmental effects have been shown to affect even

the stability of the conformational states and species present. In addition, the changes which occur as one perturbs a system can be monitored and followed in time with time resolved vibrational spectroscopy. But to do so requires one to be able to reliably take into account the effects of the aqueous environment. These effects have been shown to stabilize both species (the zwitterionic form of amino acids) and conformers, the P_{II} conformational state of the L-alanine dipeptide (N-acetyl L-alanine N'-methylamide, NALANMA), which are not stable in the isolated state (as single molecular species) in the gas phase or in non-polar solvents. Hence it is fundamental to include explicit water molecules and any other species which are in the first solvation shell (hydration) layer and are responsible for stabilizing the biomolecular complex, the species of interest, and not the so-called isolated biomolecule. Hence not single molecule, but biomolecular complex, or better biomolecular machine or catalyst. Next we present two illustrative cases of our methodology applied to large biomolecules.

The 3 molecules we chose in which to illustrate the types of problems that can arise and how one can overcome/solve there problems are 1. L-alanine (LA); 2. the di-peptide, L-alanyl L-alanine (LALA); and 3. the L-alanine dipeptide, N-acetyl L-alanine N'-methylamide (NALANMA).

In the following sections we present a brief discussion of each molecule and why it is important. This is followed by the most commonly used methodology for simulating vibrational spectra using density functional theory (DFT). The methodology of how one actually can simulate the VA and VCD spectra is presented, followed by a summary of our work which documents and shows the usefulness of our methodology to solve real life structural and functional problems in molecular biophysics and molecular biology.

7.2.1 L-alanine

L-alanine (LA) is the simplest chiral amino acid with the methyl group replacing one of the two achiral hydrogens in glycine. All other amino acids are more complicated. The chiral nature of 19 of the 20 naturally occurring amino acids gives the preference for right handed α helices over the left hand variant

in peptides and proteins. In addition, the preference of the so-called C_7^{eq} conformer over the so-called C_7^{ax} conformer for small peptides is due to the bulky C_β group of the 19 chiral amino acids. Here we focus initially on the various possible species of the L-alanine in aqueous solution, its native environment, at neutral pH. In the isolated single molecular state in either the gas phase or in non-polar solvents like carbon tetrachloride or carbon disulfide, the species of L-alanine present is the non-ionic neutral species, $\text{NH}_2 - \text{CH}(\text{CH}_3) - \text{COOH}$, while in aqueous solution the species present is the ionic neutral species, the so-called zwitterionic species, $\text{NH}_3^+ - \text{CH}(\text{CH}_3) - \text{COO}^-$. We and others have shown that to correctly simulate and interpret the VA, VCD, Raman and ROA spectra of the zwitterionic form of LA in aqueous solution, one must include explicit water molecules [4–9]. Hence the molecule or molecular complex of interest is not the individual single molecule, but the hydrated zwitterionic species. Which and how many of the water molecules are not only important, but an integral part of the species of interest is the more relevant question.

7.2.2 L-alanyl L-alanine

On peptide formation, two amino acids interact chemically to form a peptide bond. The species present in aqueous solution at neutral pH is again the ionic neutral zwitterionic species, and not the nonionic species present as a isolated single molecule either in the gas phase or in nonpolar solvents. Here, once again, the species of interest is stabilized by the presence of a finite number of strongly interacting water molecules of the aqueous environment. The isolated single molecular state in either the gas phase or in non polar solvents is the non-ionic neutral species, $\text{NH}_2 - \text{CH}(\text{CH}_3) - \text{CO} - \text{NH} - \text{CH}(\text{CH}_3) - \text{COOH}$.

To simulate the aqueous environment, we initially added a small number of explicit water molecules to stabilize the zwitterionic species of the L-alanyl L-alanine (LALAZ) [4], but subsequently used classical molecular dynamics simulations of LALAZ in a box of water molecules to determine the number and positions of the water molecules in the so-called first solvation shell of water molecule encapsulating and stabilizing the LALAZ. We initially kept only those

water molecules which were directly interacting with the polar and ionic groups of the LALAZ via hydrogen bonding and subsequently performed geometry optimizations [10]. For one of these optimized structures, we performed a Hessian calculation and subsequently APT and AAT which allowed us to simulate both the VA and VCD spectra. Finally we also used Gaussian and CADPAC to calculate the tensors necessary for us to simulate the Raman and ROA spectra, that is the various polarizability derivatives, all at the restricted Hartree-Fock (RHF) level of theory [11].

In this work we extend that work by increasing the number of water molecules interacting with the LALAZ and, in addition, use DFT polarizability derivatives, which have been shown to be in general more accurate than those calculated at the RHF level of theory. For the di-peptide zwitterion, LALAZ, we have simulated the VA and VCD spectra in aqueous solution. The LALAZ molecular complex has 23 atoms in addition to the 14, 17 and 40 water molecules which we have used to solvate the LALAZ. This case represents a quite formidable task for a complete quantum mechanical calculations of the VA, VCD, Raman and ROA spectra in a native aqueous environment.

For simple energy only calculations, the LALAZ may be a relatively small molecule, but for calculation of the dynamical nature of the solvent shell of water molecules and the molecular properties for the LALAZ, one requires a larger basis set and more sophisticated methods than one normally uses for the former case. For the case of individual single isolated state molecules, one can normally use the PM6 and SCC-DFTB or SCC-DFTB+Disp semi-empirical based wave function and density functional theory methods. But these methods do not allow one to calculate the tensors required for VCD, the AAT, and the ROA, electric dipole-magnetic dipole polarizability derivatives (EDMDPD) and the electric dipole-electric quadrupole polarizability derivatives (EDEQPD), in addition to the APT and the electric dipole-electric dipole polarizability derivatives (EDEDPD) which are required for the VA and Raman spectral simulations.

7.2.3 N-acetyl L-alanine N'-methylamide

When one forms a tri-peptide, one for the first time introduces the so-called ϕ and ψ angles, which determine uniquely the backbone structure for peptides, polypeptides and proteins. Rather than deal with these two backbone angles and additionally, the zwitterionic species, we and many others have decided to cap the ammonium group with the N-acetyl group to form a peptide group at the N-terminal and cap the carboxylate group with the N'-methylamide group to form a second peptide group at the C-terminal: N-acetyl AA N'-methylamide dipeptide.

The most recent works where we have given a very thorough review of the existing literature on NALANMA and the problem which we addressed, that is, what structural changes in NALANMA are responsible for the large changes seen in the VA, VCD, Raman and ROA spectra when one changes form either an inert gas matrix or nonpolar solvent, to aqueous solution [4, 9, 12–15]. Here we and others have found that the conformer present in aqueous solution, the P_{II} conformer, is not stable in the nonpolar solvents or at low temperature in inert gas matrices [4, 9, 12–14, 16, 17]. In addition, it has recently been found that some of the positions of the bound waters of biomolecules actually are stable on the time scale of the VA and VCD spectra and actually have been shown to possess a chiral character [18], further documenting and supporting our paradigm that explicit water molecules are an inherent part of the structure, and in many cases of function, of biomolecules in their native environment.

7.2.4 Materials and methods

At the various optimized geometries various zwitterionic species stabilized by varying numbers of water molecules form biological complexes which have been embedded within the Onsager, PCM, CPCM and COSMO continuum models. Hessian and atomic polar tensor (APT) (Amos 1984) [19] and atomic axial tensor (AAT) calculations with Gaussian 94, 98 and 03. Restricted Hartree-Fock (RHF) atomic axial tensor (AAT) (Stephens 1985, 1987 [20, 21]; Buckingham *et al.* 1987 [22]; Amos *et al.* 1987 [23]) calculations have also been performed util-

izing the Cambridge Analytical Derivatives Package (CADPAC) Issue 5.2, 6.0 - 6.3. These calculations were performed utilizing the distributed origin gauge (Stephens 1987 [21]; Amos *et al.* 1988 [24]) and restricted Hartree-Fock (RHF) wave functions. Coupled Hartree-Fock theory has been utilized for the Hessian, APT and AAT calculations [25]. The AAT tensors have also been implemented in Gaussian 98 by Cheeseman *et al.* 1996 [26]. The AAT have also been derived such that they can be calculated by a sum over states methodology [27] and have been implemented in the SYSYM suite of programs by Lazzaretti and Zanasi [28]. The AAT tensors have also been implemented at the MCSCF level by Bak *et al.* 1993 [29,30]. The EDEDPD have been implemented at the RHF and DFT level [31–34]. These are the tensors which are needed to predict the Raman intensities. In addition to these tensors, one requires the EDEQPD and the EDMDP. The EDEQP and EDMDP have been implemented at the RHF level and more recently the EDMDP have also been implemented at the DFT level [35–38]. The DFT EDMDP have also been recently used to calculate the optical rotation for a number of molecules [39]. Recently much work has appeared at the DFT and other correlated levels to calculate the static and frequency dependent polarizabilities and hyperpolarizabilities [40–47].

VA calculations

The Hessian and APT calculations were performed using the 6-31G* basis set with Gaussian 94, 98 and 03. The vibrational absorption spectra is related to molecular dipole strength via

$$\epsilon(\bar{\nu}) = \frac{8\pi^3 N_A}{3000bc(2.303)} \sum_i \bar{\nu} D_i f_i(\bar{\nu}_i, \bar{\nu}), \quad (7.1)$$

where ϵ is the molar extinction coefficient, D_i is the dipole strength of the i -th transition of wavenumbers $\bar{\nu}_i$ in cm^{-1} , $f(\bar{\nu}_i, \bar{\nu})$ is a normalised line-shape function, and N_A is Avogadro's number.

For a fundamental (0→1) transition involving the i -th normal mode within

the harmonic approximation

$$D_i = \left(\frac{\hbar}{2\omega_i} \right) \sum_{\beta} \left(\sum_{\lambda\alpha} S_{\lambda\alpha,i} \mu_{\beta}^{\lambda\alpha} \right) \left(\sum_{\lambda'\alpha'} S_{\lambda'\alpha',i} \mu_{\beta}^{\lambda'\alpha'} \right), \quad (7.2)$$

where $\hbar\omega_i$ is the energy of the i -th normal mode, the $S_{\lambda\alpha,i}$ matrix interrelates normal coordinates Q_i to Cartesian displacement coordinates $X_{\lambda\alpha}$, where λ specifies a nucleus and $\alpha = x, y$ or z :

$$X_{\lambda\alpha} = \sum_i S_{\lambda\alpha,i} Q_i. \quad (7.3)$$

$\mu_{\beta}^{\lambda\alpha}$ ($\alpha, \beta = x, y, z$) are the APT of nucleus λ . $\mu_{\beta}^{\lambda\alpha}$ are defined by

$$\mu_{\beta}^{\lambda\alpha} = \left(\frac{\partial}{\partial X_{\lambda\alpha}} \left\langle \psi_G(\tilde{R}) | (\mu_{el})_{\beta} | \psi_G(\tilde{R}) \right\rangle \right)_{\tilde{R}_0} \quad (7.4)$$

$$\mu_{\beta}^{\lambda\alpha} = 2 \left\langle \left(\frac{\partial \psi_G(\tilde{R})}{\partial X_{\lambda\alpha}} \right)_{\tilde{R}_0} \mid (\mu_{el}^e)_{\beta} \mid \psi_G(\tilde{R}_0) \right\rangle + Z_{\lambda} e \delta_{\alpha\beta}, \quad (7.5)$$

where $\psi_G(\tilde{R})$ is the electronic wavefunction of the ground state G, \tilde{R} specifies nuclear coordinates, \tilde{R}_0 specifies the equilibrium geometry, $\tilde{\mu}_{el}$ is the electric dipole moment operator, $\tilde{\mu}_{el}^e = -e \sum_i \tilde{r}_i$ is the electronic contribution to $\tilde{\mu}_{el}$ and $Z_{\lambda} e$ is the charge on nucleus λ .

VCD calculations

The vibrational circular dichroism spectra is related to the molecular rotational strengths via

$$\Delta\epsilon(\bar{\nu}) = \frac{32\pi^3 N}{3000bc(2.303)} \sum_i \bar{\nu} R_i f_i(\bar{\nu}_i, \bar{\nu}), \quad (7.6)$$

where $\Delta\epsilon = \epsilon_L - \epsilon_R$ is differential extinction coefficient, R_i is the rotational strength of the i -th transition of wavenumbers $\bar{\nu}_i$ in cm^{-1} , $f(\bar{\nu}_i, \bar{\nu})$ is a normalised line-shape function, and N_A is Avogadro's number.

$$R_i = \hbar^2 \text{Im} \sum_{\beta} \left(\sum_{\lambda\alpha} S_{\lambda\alpha,i} \mu_{\beta}^{\lambda\alpha} \right) \left(\sum_{\lambda'\alpha'} S_{\lambda'\alpha',i} m_{\beta}^{\lambda'\alpha'} \right), \quad (7.7)$$

where $\hbar\omega_i$ and the $S_{\lambda\alpha,i}$ matrix are as previously defined. $\mu_{\beta}^{\lambda\alpha}$ and $m_{\beta}^{\lambda\alpha}$ ($\alpha, \beta = x, y, z$) are the APT and AAT of nucleus λ .

$\mu_\beta^{\lambda\alpha}$ is as previously defined and $m_\beta^{\lambda\alpha}$ is given by

$$m_\beta^{\lambda\alpha} = I_\beta^{\lambda\alpha} + \frac{i}{4\hbar c} \sum_\gamma \epsilon_{\alpha\beta\gamma} R_{\lambda\gamma}^0(Z_\lambda e) \quad (7.8)$$

$$I_\beta^{\lambda\alpha} = \left\langle \left(\frac{\partial \psi_G(\tilde{R})}{\partial X_{\lambda\alpha}} \right)_{\tilde{R}_e} \left| \left(\frac{\partial \psi_G(\tilde{R}_e, B_\beta)}{\partial B_\beta} \right)_{B_\beta=0} \right. \right\rangle, \quad (7.9)$$

where $\psi_G(\tilde{R}_0, B_\beta)$ is the ground state electronic wavefunction in the equilibrium structure \tilde{R}_e in the presence of the perturbation $-(\mu_{mag}^e)_\beta B_\beta$, where $\tilde{\mu}_{mag}^e$ is the electronic contribution to the magnetic dipole moment operator [20, 22]. $m_\beta^{\lambda\alpha}$ is origin dependent. Its origin dependence is given by

$$(m_\beta^{\lambda\alpha})^0 = (m_\beta^{\lambda\alpha})^{0'} + \frac{i}{4\hbar c} \sum_{\gamma\delta} \epsilon_{\beta\gamma\delta} Y_\gamma^\lambda \mu_\alpha^{\lambda\delta}, \quad (7.10)$$

where \tilde{Y}^λ is the vector from O to O' for the tensor of nucleus λ [21, 24, 48]. Equation (10) permits alternative gauges in the calculation of the set of $(m_\beta^{\lambda\alpha})^0$ tensors. If $\tilde{Y}^\lambda = 0$, and hence O = O', for all λ the gauge is termed the Common Origin (CO) gauge. If $\tilde{Y}^\lambda = \tilde{R}_\lambda^o$, so that in the calculation of $(m_\beta^{\lambda\alpha})^0$ O' is placed at the equilibrium position of nucleus λ , the gauge is termed the DO gauge (Stephens 1987 [21]; Jalkanen 1988 [48]; Amos *et al.* 1988 [24]). Density functional theory atomic axial tensors have also been implemented in Gaussian 94 (Cheeseman *et al.* 1996) [26]. We have utilized Gaussian 98, 03 to calculate the AAT used in this work.

QM methods

The B3LYP hybrid exchange-correlation functional method is a hybrid DFT method where the exchange-correlational (XC) functional has been parameterized to reproduce experimental data. The parameter values were specified by Becke by fitting to atomization energies, ionization potentials, proton affinities and first-row atomic energies in the G1 molecule set [49–54]. Recently, Frish and coworkers showed that the B3LYP/6-31G* method accurately reproduce gas phase and nonpolar solution geometries, vibrational frequencies and absorption, and vibrational circular dichroism (VCD) intensities [13]. This level of theory has been documented to model structures and VA spectra of NALANMA, LA and

LALA in aqueous solution by adding explicit waters to take into account the first solvation shell which strongly interact with the peptide as well as the Onsager continuum model added to take into account the interaction of the peptide with bulk water [5, 10, 11, 14]. At this level of theory, we are confident in that many properties of interest for small peptides, i.e., structural parameters, vibrational frequencies, and relative VA intensities can be accurately modelled.

7.2.5 Results and discussion about the peptide calculation

Structures of LA, LALA and NALANMA

The zwitterionic forms of both LA and LALA were only found by including explicit water molecules. The use of the Onsager, PCM and CPCM continuum models were all shown to be inappropriate for taking into account the first solvation shell of water molecules responsible for stabilizing not only the zwitterionic species, but the most stable conformer for each. In the case of the alanine dipeptide, the importance of explicit water molecules was again shown to be fundamental, as the conformer seen in aqueous solution and evidenced by the VA, VCD, Raman, ROA and NMR spectra was that of the conformer which IS NOT STABLE on either the gas phase isolated state potential energy surface or that obtained with one of the three continuum models, be it Onsager, PCM or CPCM. Hence the use of these continuum solvent models for the treatment of first solvation shell water molecules should be DISCONTINUED, and these models should only be used to treat bulk water effects.

VA, VCD, Raman and ROA spectra of LA, LALA and NALANMA

The VA, VCD, Raman and ROA spectra, both experimental and theoretical have been presented in a number of publications now so there is no need to reproduce that data here. The summary is that the VA and VCD or the Raman and ROA spectra alone are not sufficient to answer all structural and functional problems, so that the set of all four spectra should not only be measured, but also simulated. In addition, it also pays to measure the NMR spectra and if possible, also, the inelastic incoherent neutron scattering (IINS) spectra, as the

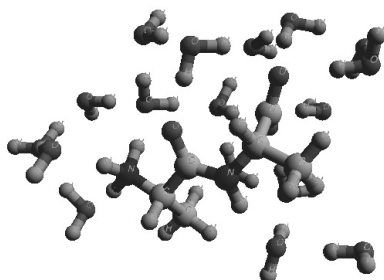


Figure 7.1. L-alanine L-alanine zwitterion plus 17 waters

selection rules for IINS vibrational spectroscopy are fundamentally different than those for VA and VCD or Raman and ROA. A model or paradigm which is not able to reproduce all of the available experimental data is not of much general use. Hence we also advocate measuring not only the conventional VA/IR and Raman, but also the chiral analogues, VCD and ROA, and the IINS vibrational spectra. Recent work by Kearley and coworkers at ANSTO in Australia and Holderna-Natkaniec and coworkers in Poland have shown that this additional data is complementary to that gained from the other spectroscopies [55, 56]. Hudson has also shown that the IINS can be used interpreted using ab initio calculations [57].

In Figure 7.1 we show an ab-initio optimized structure of LALA with 17 water cluster/droplet embedded within the cavity created with the polarized continuum model (PCM) using the B3LYP hybrid exchange correlation functional (DFT) with the 6-31G* basis set. In Figs. 7.2, 7.3 and 7.4 we show the simulated vibrational absorption (VA), vibrational circular dichroism (VCD) and Raman spectra for the LALA zwitterion in a droplet of 17 water molecules embedded with the PCM cavity.

7.2.6 Summary and conclusions of the alanine peptides studies

By analyzing not only the VA, VCD, Raman and ROA spectra of LA, LALA and NALANMA, but also the spectra of the various isotopomers, we have been

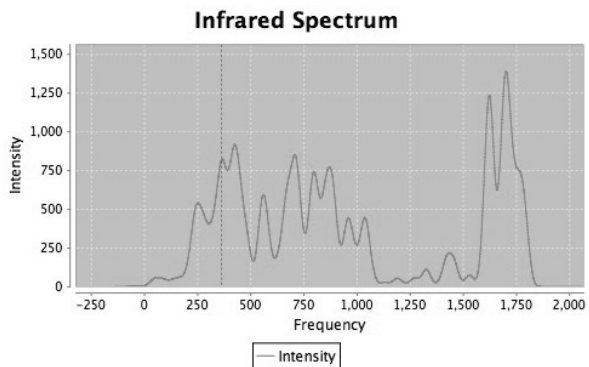


Figure 7.2. Vibrational absorption of L-alanine L-alanine zwitterion plus 17 waters

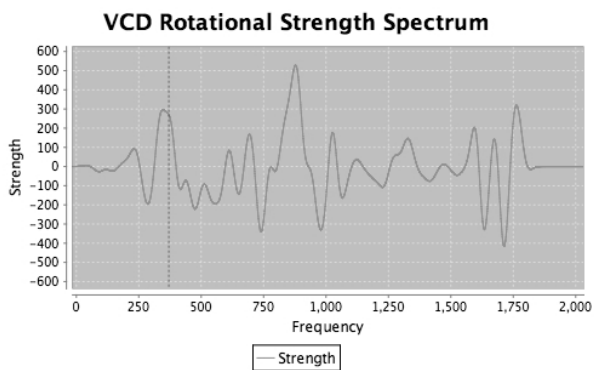


Figure 7.3. Vibrational circular dichroism of L-alanine L-alanine zwitterion plus 17 waters

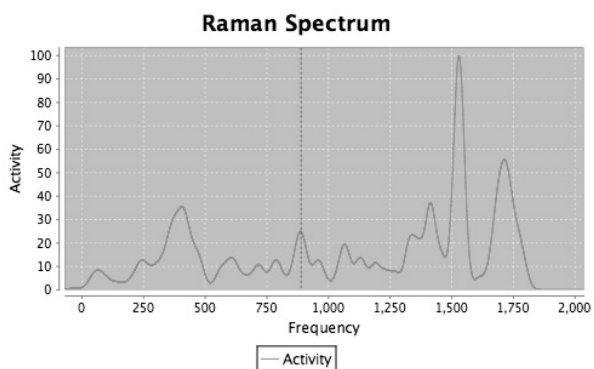


Figure 7.4. Raman spectra of L-alanine L-alanine zwitterion plus 17 waters

able to address the issue raised by Freedman [58, 59] on the previous Raman and ROA simulations for LALA [60]. This work shows that analysis of the isotopic data both experimentally and theoretically is very valuable in verifying the accuracy of both the force field and the various tensor quantities necessary to simulate the VA, VCD, Raman and ROA spectra. The issue of having the correct structure, species and conformer (or conformers) are also important. Our previous works [4–7, 13, 14] have shown that it is very important to take into account the first solvent shell water molecules which are interacting strongly with the solute via H-bonding explicitly. The continuum model can be used to treat the effect due to the bulk water molecules.

To be able to simulate L-alanine in aqueous solution it has been important and fundamental to add explicit water molecules to not only stabilize the zwitterionic species, but to also get the the conformer of the zwitterionic species found in aqueous solution. The simple continuum models and even simple Hartree-Fock theory are in some cases able to get a stable zwitterionic species, but not the variety of conformers stabilized and populated in aqueous solution. Our most recent work shows that to completely solvate the zwitterionic species requires 20 water molecules. The initial placement of the water molecules has been obtained from Born-Oppenheimer DFT molecular dynamics simulations. This is due the problem with classical molecular dynamics models for water failing to reproduce the first hydration layers around biomolecules correctly.

To be able to simulate the alanine dipeptide in aqueous solution has also required one to include the first solvation shell water molecules which actually stabilize a conformer which is not stable in the gas phase. Hence without the explicit water molecules, like in the case of the L-alanine zwitterion, one cannot get the variety of conformers stabilized and populated in aqueous solution. Our new paradigm has solved the problem of what is the stable conformer of the alanine dipeptide in aqueous solution, and WHY. NMR studies have conformed our work and provided even more evidence for the importance of including explicit water molecules not only for simulating the vibrational spectra, but also the NMR spectra, and also function.

Finally to take into account temperature effects, one could consider the use of QM/MM methodology as an alternative to our hybrid model and we are pursuing this methodology also and look forward to presenting our comparison of these two methods in the near future. Here one would run molecular dynamics simulations using high level *ab initio* methods (beyond simple Hartree-Fock) or DFT methods like those being developed in the Bartlett group in Gainesville, Florida, the so-called *ab initio* DFT [61]. Here one uses the accumulated knowledge from wave functional quantum mechanics to develop local exchange and correlation functionals based on the optimized effective potential (OEP) method. Preliminary works by the Bartlett group and many others have shown that this methodology provides a way to systematically improve both exchange and correlation functions. So the so-called Holy Grail of DFT may be found in the not so-distant future, providing a methodology which will allow us to perform ground electronic state Born-Oppenheimer molecular dynamics simulations. This will in theory allow us to do the correct averaging over time to get the conformational fluctuations and even chemical reactions. This will allow us to do quantum nanobiology. Of course the methods will need to be benchmarked, like our work on LA, LALA and NALANMA. Finally the extension to do excited electronic state molecular dynamics simulations will be the next obvious extension. Many groups and researchers are currently working in that field, which is beyond the scope of our work, but we would like to make the readers of this work aware of the extension of this work to that field.

7.3 Examples on quantum electronic calculations on protein complexes

In the following we shall give 2 interesting examples of quantum electronic calculations for proteins in the gene repair processes and for the photosynthesis processes.

7.3.1 Case I: Electronic processes of photolyase protein in gene repair

This work presents a study on the ground and excited state properties of thymine, thymine dimers and thymine duplex as the work relates to the damage

of nucleic acids and the repair system by DNA photolyase. We especially present our contribution to this problem based on our theoretical simulations. It is also interesting to study the species which are results of the absorption of radiation, the free radicals. In some cases the resulting species is a neutral radical and in other cases a radical cation. We also analyze the mechanisms of DNA damage and radiation mediated DNA repair both from an evolutionary and genetic engineering point of view. The main result of the study is that excited electronic state is a necessary ingredient of the repair process due to the energy balance since it gives means for overcoming the reaction barrier.

7.3.2 Introduction to Gene Repair

The damage of DNA by UV-radiation is a well-known problem which has been studied for some time [68,69]. It appears that the repair mechanism is present in many plants and animals exposed to the damaging radiation. One repair mechanism, which is the focus of this paper, is making use of external blue light for the reactivation but there are other repairs which directly replace the erroneous DNA patch.

Here we would like to study the influence of the wavelength of the radiation on the various chemical and photochemical processes that both lead to the damage, but also that lead and contribute to the repair. Both of these processes seem to have mechanisms (processes) that appear to be photo-activated. The influence of the environment plays an important role in these processes. The mechanism(s) will probably very much depend on what the system is and the environment. Here by system we refer to the object which is interacting with the electromagnetic radiation. The DNA photolyase repair process is here seen as a prime example of a process that only can proceed provided electronic excited states are included in the reaction path.

Normally one must treat this part or entity quantum mechanically. If one uses either visible or ultraviolet radiation as the exciting radiation, one excites an electron in the system to a higher energy level which is not populated in the ground state. Hence we can call the state to which the electron is excited

an excited state. One also has the question as to what is the best or even an adequate level of theory to represent these excited states. Density functional theory as originally formulated is a theory to represent or find the energy for the ground state potential energy surface. Hence we can use it with confidence to follow conformational changes which do not involve the making and breaking of chemical bonds. It can also be used to model chemical reactions, but if the barrier and/or mechanism involves states which can not be represented by a single Slater determinant of either the Hartree-Fock or Kohn-Sham orbitals, then one must be careful in trusting or having confidence in the results. Also the questions of how large a basis set to use, whether one required diffuse and/or polarization orbitals, and how to treat both electron correlations and electron exchange must be dealt with. In the section of this paper which follows, we shall give our overall strategy for approach and the preliminary results we have to date.

In this study we will focus on the damaged thymine molecule and its repaired state. It is the calculation of this molecule that gives results that can lead to new insight into the repair mechanism. The phosphodiester backbone of the DNA molecule and the co-inzyme, flavin, molecule are included as background for the dithymine molecule as well as the photolyase protein.

Let us briefly review what is up to now believed to be the photo-reactivation repair process with photolyase seen from a bio-molecular physics viewpoint. Ultra-violet radiation, particular in the range of 200-300 nm wavelength, irradiated on 2 thymine nucleotides in DNA, creates a dimerization attaching them together, thereby creating a lesion on DNA in the form of a disruption on the helical axis. This lesion perturbs the structure of DNA and leads to an error in the code and causing problems for the transcription [70]. Under photoreactivation in the visible and near UV region (basically just blue light) the defect is repaired, breaking the the new bonds constituting the lesion, and restoring the thymines back to the original state of two separate thymine nucleotides. The photolyase protein and its cofactor, riboflavin FADH, are thought to catalyze the repair process by absorbing light and transferring electrons to the destroyed

DNA patch of dithymine. In the following study we shall be analyzing the repair mechanism and perform electronic quantum calculations on the reaction complex. Firstly, we give an overview of the methodology and of the strategy in the calculations and next we shall, in the subsequent chapter, be giving results of the computer calculations and analyze the data. Finally, we conclude the study.

7.3.3 A model for the repair process

Ultra violet radiation, particularly in the range of 200-300 nm wavelength, irradiated on thymine in DNA, creates a dimerization attaching two of them, thereby creating a kink in the helical axis of DNA. This lesion perturbs the structure of DNA and leads to an error in the code and causing problems for the transcription [71, 72]. Under photo-reactivation in the visible and near UV region the defect is repaired, breaking the lesion and restoring the thymines back to the original state [73].

The whole process is a fascinating one from the energy balance as well as a regenerative repair viewpoint. A mutation caused by electromagnetic (EM) radiation of higher energy is restored to its original structure by exposing the mutant to photons having lower energy. This requires careful development of a theory which addresses the question of the energy conservation in the whole process (see Ref. 70). There have been many investigations studying separately the mechanisms of the absorption of UV radiation and the repair process, but there has, so far, been no report examining both processes taken together. For example, Reuther et al. [74] have done an extensive study on the UV absorption process involved in the aqueous solution of thymine but do not relate the role of these physical properties to the repair mechanism. Similarly, much effort have gone into the study of repair mechanisms, particularly the role of photolyase and DNA [75–77] but no attempt has been made to address the question of imbalance of energy occurring between the mutation and the repair mechanism. In this note, we attempt to analyze the energy and charge balance question and investigate both the mutation and repair processes in a common, quantum physical framework discussed in the next section. The formation of a

meta-stable electronically excited state by absorbing the incident UV radiation via inter-system crossing and its eventual de-excitation by radiationless Auger transition, provide two mechanisms that are compatible with the energy balance in the process. The restoring mechanism of Auger transition, usually being a radiationless phenomenon, cannot cause further radiation damage.

The important question now is to investigate whether an electronic excitation causing a structural change can result into the formation of a dimer. Clearly, 4 to 6 eV energy is insufficient to ionize a thymine, which requires an energy of about 12 eV. The energy associated in splitting a covalent bond between two C, or H – O, or H – C etc. is between 0.59 to 0.8 eV, which is equivalent to 3.67 to 5.00 eV [69]. Certainly, 200 to 300 nm UV radiation is in the position to break many of the covalent bonds that bind to form a thymine. However, the breaking of one or more of these bonds is likely to cause a major disruption to its structure. This would be difficult to reverse by illuminating it with optical radiation which does not simply have enough energy to restore these bonds. For example, optical radiation of 400 and 580 nm has energies of 3.09 and 2.13 eV, respectively, which are significantly below the energy necessary to form these bonds. The problem of the energy imbalance persists in case one of the covalent bonds of a member molecule of a thymine is detached and then attached covalently to another molecule of a different thymine to form a dimer, because the energy difference to these processes is far less than 4 to 6 eV incident energy dumped by UV radiation. This amount of energy cannot simply be argued to be lost in dissipation, because in the process of restoration of a dimer to two detached thymines, the difference of energy between UV and optical radiation must be put back from somewhere causing a change in entropy to be negative, which is against the laws of physics as known. There could of course be extra solvent effects but that will imply a much more complex machinery to restore the dimer in its original state.

The electronic transition from the ground state configuration of thymine to an excited electronic state remains as an alternative. To gain further insight in that possibility, we consider a few diatomic pyrimidine ring components (PRC),

e.g., CH, CO and NH. The ionization potential of these PCR are, respectively, 10.64, 14.01, and 14.1 eV see Ref. 10 making ionization of these PCR energetically impossible. On the other hand, there are many electronic excited states in the energy range of 4 to 6.5 eV in these PCR [70].

7.3.4 Overview of strategy

Ab initio methods

The building blocks of DNA are the four base pairs, adenine, thymine, guanine, and cytosine. In RNA uracil replaces thymine. In addition to the four bases, there is also present the five membered deoxyribose (ribose in RNA) carbohydrate and the phosphate moiety. There has been much work on the individual bases and the nucleotides. These results have been at the restricted and unrestricted Hartree-Fock, 2nd order Møller Plesset and DFT levels of theory. For the ground state one can also utilize approximate DFT methods. To be able to understand the photo activated DNA repair via DNA photolyase, then we must also consider the whole mechanism. Recently Sancar has written a 50 year review on enzymatic photo-reactivation [81]. Here he states that his field started in 1949 with the discovery of photo-reactivation by Alfred Kelner [82,83]. Shortly after the seminal work by Kelner, Dulbecco reported the reactivation of ultraviolet exposed bacteriophage, but only when the phage and E. coli were together during exposure to the photo-reactivating light [84].

The main focus of our study of the photolyase system is to try to calculate the electronic structure and see if such structure corresponds to the experimental data observed. We have hence made quantum mechanical calculations using the Density Functional Theory (DFT), to obtain electronic structures of part of the protein-DNA-cofactor complex. A big issue have been to extract knowledge about the electronic excited states even though the standard programs are only available at the ground state level.

In the following section we will discuss the *ab initio* and semi-empirical DFT based methods as applied to calculating the ground state properties.

Methods for ground state calculations

Basically the following methods are used for the electronic calculation:

- The Hartree-Fock methods
- The 2nd order Møller Plesset methods
- The density functional method
- The local density approximation
- The generalized gradient approximation in DFT
- The hybrid DFT approximation

We would like to introduce our work on the development of a relatively new semi-empirical method based on an approximation to density functional theory, the so called self consistent charge tight binding method (SCC-DFTB) [85–87]. It had been previously been used in solid state physics, but had not been parameterized for modeling biomolecules. We have previously benchmarked this theory for use in modeling small peptides [15] and small ring systems [88].

Methods for excited state calculations

To treat the excited states one faces additional problems, which do not have to be dealt with when modeling the ground state. One problem involves the optimization of the electronic states. Ordinarily the optimization will relax the electronic state. One can, however, within the standard quantum mechanics “Gaussian” program get a hint about the excited state by looking at the lowest unoccupied electronic orbital (LUMO) and the highest occupied electronic orbital (HOMO) in a quantum mechanical calculation of the electronic system. This is what automatically comes out of the calculation. The only extra thing one will have to do with respect to the excited states, is to carry an electron from the HOMO state to the LUMO state, since this state has no electrons, and take into account that extra energy.

We therefore calculate the HOMO/LUMO state gap for the various ground state structures of the thymine molecules. The energy and occupancy of these states are given for the different structures in Table 1 and 2 of Ref. 78.

A serious objection to just use the LUMO state as an excited state is that it is empty by definition. That is even though the notion of the HOMO/LUMO gap gives us an understanding of the level splitting in energy. This splitting in energy serves the understanding of the basic question of this paper, which is that of energy conservation: "How can a damage caused by UV light be repaired by a process requiring much less energy of blue light. The answer is that by making use of the excited electronic states, the repair processes can circumvent overcoming the large barrier between the ground state of dithymine and bonded duplex of thymine, the latter being the damaged state caused by UV radiation. When calculating the HOMO/LUMO gap and using that as a measure of a relevant energy difference we just have to make sure that the extra energy for an electron present in the LUMO state is negligible compared to the bare HOMO/LUMO gap.

Therefore we should do the calculation again with an electron taken from the HOMO state and put it into the LUMO state. Such calculation can be performed again in the standard DFT calculation programme and the results are presented in reference [78].

7.3.5 Empirical computational methods: Molecular mechanics and molecular dynamics for DNA and proteins

For nucleic acids and proteins molecular mechanics and molecular dynamics methods have been the methods of choice. This is due to the computational cost. These methods are much faster than *ab initio* and even semi-empirical methods. But one must normally have a force field. Here one must choose a functional form and then determine empirical parameters [89]. There has been a whole evolution of force fields and here we will not go into detail into that, since it would require a complete work in itself. But we will describe the history, development and current status as it relates to the work on amino acids and small and intermediate sized peptides. The most commonly used force fields are the Amber force fields [90,91], the MM4 force fields [92], the Groningen MOlecular Simulation (GROMOS) program package force fields [93,94], the optimized po-

tentials for liquid simulations (OPLS) force fields [95], the Sybyl/TINKER force fields [96, 97], the Charmm force fields [98, 99], the Discover force field [89, 100] and the empirical conformational energy program for peptides (ECEPP) force fields [101]. Each of these force fields has also undergone an evolutionary process, with all starting with simple harmonic terms for the bond and valence angles, Fourier series for the torsions and simple point charge electrostatic and van der Waals 6-12 (or 9) non-bonded terms. This simple functional form was used at the early stages both for its simplicity and also due to the problem of determining the parameters. As one adds complexity to the functional form, one also adds complexity to the parameterization scheme. Using a nonlinear least squares parameterization requires that one have data to use to determine the parameters. Originally only experimental data was used, but in the second and third generation force fields, *ab initio* data has been used in the parameterization, first RHF/6-31G* data and subsequently MP2/6-31G* and now Becke3LYP/6-31G* data. As computers have gotten faster, the use of higher level theory has been used. Here one must be careful when one fits to *ab initio* data, in that the level of theory whose data one is using, actually accurately can determine the parameters one is trying to fit. A good example is using RHF and DFT data to determine the van der Waals parameters. This is not a good idea, since the dispersion energy is not accurately determined at either level of theory. Hence Hagler and coworkers have utilized experimental crystal data to determine these parameters. But then one has a problem in how to put the various parameters together, since some are determined by fitting to various levels of *ab initio* data and others are determined by fitting to various experimental data. Solvent reaction field models have also been implemented at the RHF and DFT levels of theory [102]. There has also been some debate on the recently derived polarizable force fields parameterized from *ab initio* calculations [103, 104].

7.3.6 Conformational States

The duplex consists of two chemically linked thymine nucleotides while the dimer consists of two thymine nucleotides linked by nonbonded forces, the so

called stacked dispersion interactions, which are not well treated by currently implementations of DFT, that is, pure GGA and the simple B3LYP hybrid. Note that Goddard has recently developed a new hybrid which treats dispersion as an exchange term correction, though many believe this to be purely a correlation effect. Note that in DFT the clear distinction between exchange and correlation is not always clear. With the use of the exact nonlocal Hartree exchange operator, this becomes clear. This is very important for the treatment of excited states, in addition to the treatment of dispersion. The one last term, the charge transfer effect, is also poorly treated in general by DFT. Hence the most accurate simulations for the benzene dimer which gets the attractive potential for the stacking dispersion interactions, as a CCSDTQ, which is clearly not feasible for the system we are treating in this work. The other alternative is to add a correction term to DFT as we have done in our work on LeuE (SCC-DFTB+Disp).

There are two distinct conformational states in the damaged DNA duplex which dominate. Hence it is important to have a spectroscopic probe which can distinguish between the two. Without this probe, one does not have a way to know how the DNA is damaged. Note that there are two distinct proteins for repair. Photolyase complex is involved with cyclobutane damaged duplex and which repairs the oxetane damaged duplex.

7.3.7 Vibrational spectroscopy from *ab initio* wave function and density functional theory (DFT) calculations

Finally we would like to use vibrational spectroscopy as one of our main tools in both benchmarking and testing our various methods, but also in parameterizing and developing our methods. This has been done in the past, as vibrational frequencies have been used in determining vibrational force fields, that is, force fields used to predict the vibrational frequencies of molecules. Here the frequencies of small symmetrical molecules have been used to determine harmonic force constants which have then been transferred to larger molecules. But recently people in the molecular mechanics and molecular dynamics field have begun to interact with those in the vibrational force field field.

It was very early recognized that the vibrational frequencies predicted by the molecular mechanics force fields were of much lower accuracy than those predicted by vibrational force fields. One of the reasons was the methodology, functional form and data used by each group. On the basis of our DFT calculations of the dimer and duplex of thymine we have simulated the VA and Raman spectra as seen in [62]. This is in order to investigate the changes in electronic structure that UV radiation causes reflected in the changes in bonding as seen in these spectra. We can in a visual simulation see the characteristic modes and which internal coordinates these modes. In many cases the mode is a collective motion, that is, the excitation is clearly not localized.

7.3.8 *Ab initio* computational methods for nucleotides

The computational methods which we have used are restricted Hartree-Fock, second order Møller Plesset theory (MP2) and density functional theory (DFT). In most of work we have utilized the 6-31G* basis set. We also compare to results utilizing the AM1 and PM3 semi-empirical methods [63–65].

Ultra violet radiation, particularly in the range of 200 – 300 nm wavelength, irradiated on thymine in DNA, creates a dimerization attaching two of them, thereby creating a kink in the helical axis of DNA. This lesion perturbs the structure of DNA and leads to an error in the code and causing problems for the transcription [71, 72]. Under photo-reactivation in the visible and near UV region the defect is repaired, breaking the lesion and restoring the thymines back to the original state [73].

Density Functional Theory (DFT) calculations have been performed on several structures of thymine configurations. This was done in order to obtain optimized electronic structures of the atomic configurations of the important molecules participating in the UV damaging and subsequent repair processes. The central molecule to calculate is the one that is being damaged and then repaired. Therefore we chose first to calculate the various thymine configurations in the presence of the cofactor, riboflavin, and the phosphor-sugar DNA-backbone. Since the main question of the paper was the energy balance we would calcu-

late the energy of the thymine molecule in the various electronic states, *i.e.*, the ground state and the first excited state. Thus the basic task here was to calculate the electronic orbitals of the two different thymine systems, *i.e.*, the 2 thymine molecules separated and the duplex thymine molecule where the 2 pyrimidine rings are attached to each other. After calculating the configurations in the ground state we want to determine their energies in the ground state and first excited state. By filling up the electronic orbitals with electrons one can get an estimate of the energy of the highest occupied molecular orbital (HOMO) and the lowest unoccupied molecular orbital (LUMO) and then obtain the difference of those two energies, the HOMO-LUMO gap. Our hypothesis of the paper requires that this gap is sufficient to overcome for blue light and furthermore is much smaller than the energy barrier between the two di-thymine states. This was indeed what we found:

1. The energy of the HOMO-LUMO gap for separate di-thymine is 4.458 eV.
2. The energy of the HOMO-LUMO gap for attached di-thymine is 3.967 eV.
3. The energy barrier height between the ground state of the two di-thymine is 8.672 eV.

The last number was obtained from the estimate of the formation of the relevant attaching bonds. All energies were translated from Hartree to electron Volt energies. The results mentioned above suggest that the repair process when utilizing blue visible light will have to employ the excited state where the barriers are smaller than that of the ground state being around twice of what blue light can overcome in energy. The optimization in the DFT calculation was carried out with the 3BLYP methodology and within the DO gauge. The Gaussian 98 and 03 computer software packages were used for the calculation.

Nucleic acids (bases) in gas phase and isolated state

Data in the gas phase or isolated state are rather limited for biological methods. But recently people have tried to perform more gas phase experiments on the nucleic acid bases, with the hopes of trying to understand the mechanism(s) of radiation damage [66, 67].

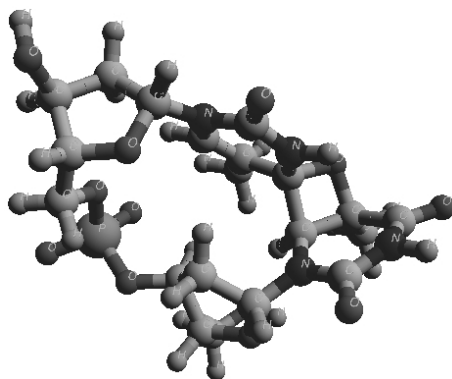


Figure 7.5. First dithymine dimer structure with oxetane damaged 4-membered ring

7.3.9 Nucleic acids in aqueous solution

The spectra of the nucleic acids in the aqueous phase must be carefully measured. This is due to the possible concerning uncontrolled pH, ionic strength, counter-ions, etc. In the following we discuss the energy and structure of the various oligomers of nucleic acids.

Relative energies, structures

The most important feature of proteins is their flexibility, as exemplified by the phi and psi backbone angles, which determine the secondary structure of proteins. As mentioned above, there are two main secondary structural elements prevailing in proteins, helices and beta sheets. But for small peptides there are many conformations which are possible. The relative energies of these various structures have been used exclusively as data for parameterization and also for testing.

In Figs. 7.5 and 7.6 we see the model for the dithymine dimer damaged by UV radiation. Finally to model the separate thymine molecules we have optimized the structure of two thymine molecules such that they can interact via base stacking as shown in Figure 7.7. This is also the case when one adds the phosphate backbone and ribose sugars. The reason that the damaged DNA structures be modelled at this level of theory is that the two thymine rings are connected via the chemical bonds within the oxetane and cyclobutane 4-membered ring

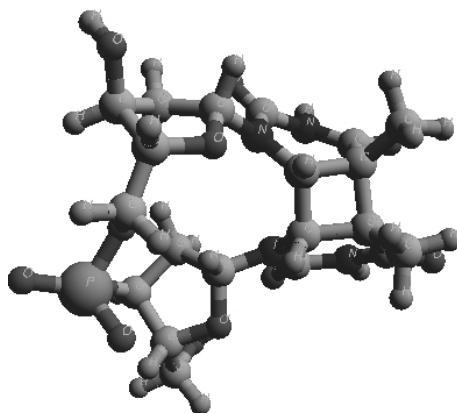


Figure 7.6. Second dithymine dimer structure with cyclobutane damaged 4-membered ring

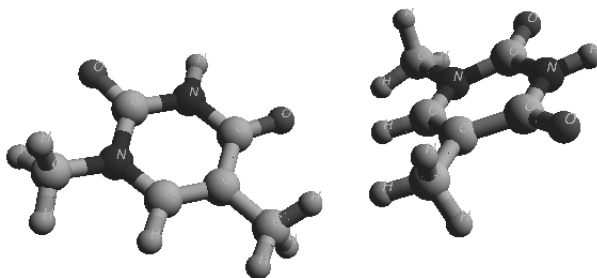


Figure 7.7. Third dithymine dimer structure, here without the phosphate backbone and ribose sugars

systems. As one can see the B3LYP hybrid exchange correlation functional is not optimal for these types of interactions. The Truhlar group has developed the MO5 and MO6 meta hybrid exchange correlation functionals to deal with such cases.

7.3.10 Case II: Electronic studies of processes in photosynthesis

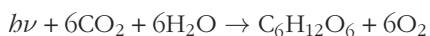
A study of electronic processes in the chlorophyll and carotenoid molecules of the photo-reaction center II is presented with the focus on the electronic excitations and charge transfer in the photosynthetic process. Several novel ideas are mentioned especially concerning the electron replenishment and nuclear vibrational excitations. For detailed information there are excellent reviews on

the matter both in proceedings [105–108] and in books or periodicals [105, 109, 110].

7.3.11 Introduction

The sun is the primary source of energy for almost all life on the earth and it supplies this energy in the full electromagnetic spectrum besides other radiation. The energy from the sunlight is supplied to the biosphere through the photosynthetic process, either directly (by incident photons) or indirectly (by climate changes, evaporation etc..) Needless to say, all organisms require energy for the chemical reactions of their life processes where chemical reactions are involved with reproduction, growth and maintenance.

Photosynthesis is the essential source of energy for plants that use solar energy to produce carbohydrates (glucose) to be stored in bonds for later needs of energy to the cell [108]. For animals the energy is supplied mostly by the reverse process of photosynthesis, respiration, although photo-radiation is important also as a secondary means. Below we give the fundamental chemical formulas for 1) photosynthesis and 2) respiration where water and carbondioxide (and light) in the former case is supplied while oxygen and glucose is the product opposite to the latter case where oxygen and glucose is supplied and where the products are water and carbondioxide. In a simple way, we can write the overall chemical reaction as:



Subsequently, we shall discuss these reactions in terms of the electronic structure of the atoms and molecules involved. Basically the will be a transfer of electrons along with a dissociation of water.

Plants receive light at daytime when the photosynthetic process is active but at night the metabolic processes basically become active, as an overall tendency [108].

The photosynthetic process is one of the most effective and sophisticated en-

ergy harvesting processes known in nature with a quantum efficiency of around 95% [111, 112] in getting photo-energy converted into electrical energy. Besides, there is the remarkable property of the molecules in photosynthesis that they are able to collect and transfer more than 99% of the collected solar energy to their reaction center [113, 114].

7.3.12 Bio-organisms using photosynthesis

There are three types of organisms that use photosynthesis: Archaea, Bacteria, and Eucarya of which the last one is considered to be a higher level organisms. They all convert light into chemical free energy. The more primitive Archaea includes the halobacteria that also convert light into chemical energy but without oxidation/reduction chemistry and hence no use is made of CO_2 as a carbon source, *cf.* [108].

The higher photosynthetic organisms can be divided into oxygenic, photosynthetic organisms such as plants and algae and an-oxygenic photosynthetic organisms being certain types of bacteria. The former class has organisms that reduce CO_2 into carbohydrate by extraction of electrons from H_2O yielding O_2 and H^+ while the latter class, believed to be more ancient, involves extraction of electrons from molecules other than water and without oxygen [109].

The process of photosynthesis in plants and algae is centered around certain organelles, the chloroplasts, which consists of a “light” reaction part involving transfer of electrons and protons and a “dark” reaction part that involves the biosynthesis of carbohydrates from CO_2 [108] also called carbon fixation.

We shall in this article mostly be concerned with the “light” reaction which occurs in a membrane system comprising proteins, electron carriers embedded in lipid molecules building up a membrane that divides the space into inner and outer domains and through which molecules or ions can pass. The protein complex, the light harvesting complex, gives a scaffold for the organic compounds, the chlorophylls and peridinin. The electron carriers are aromatic groups and metallic ion complexes. The protein complex controls the electron pathway entering the complex via an antenna molecule, peridinin or carotenoid, that ab-

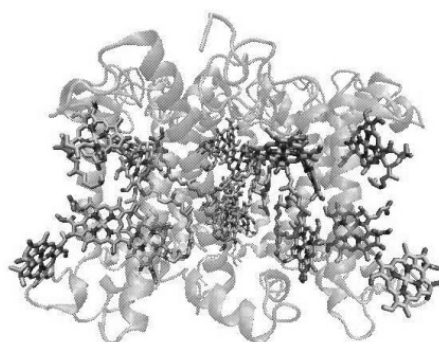
sorbs the photons and thereby causes the excitation of electrons. The electrons, or actually the charge displacements caused by the excitations, are then being transferred from one carrier to another.

7.3.13 The basic molecules of photosynthesis

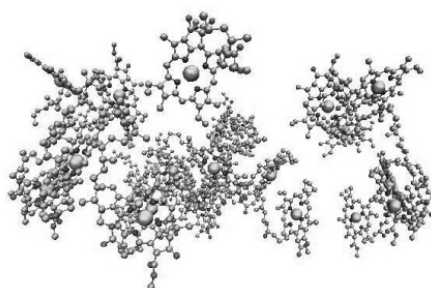
There are today crystallographic X-ray diffraction structures of the photosynthetic reaction center in the protein databases, *e.g.*, from the organism *Rhodospirillum rubrum* [117]. In Figure 7.8 the molecular system is illustrated. The center of the protein with ligands is anchored in the membrane and which, in the case of plants, are the chloroplasts anchored in the thylakoid membrane (the membrane containing light harvesting complex, electron transport chain and the ATP synthase). The small plackets in Figure 7.8 are the chlorophyll molecules that are the focus of the present study.

In Figure 7.8(b) the chlorophyll molecules from the light harvesting complex are arranged in a ring around the structure [118] where they receive incoming photons from peridinin or carotenoid [119]. We shall propose an overall picture of the processes involving photosynthesis that concerns chlorophyll and we shall present electronic pathways in support of that.

Basically, an incoming photon excites the antenna molecule and creates an exciton moving to the chlorophyll ring which acts as a storage ring consisting of 16 chlorophyll molecules arranged in asymmetric pairs of almost parallel plackets. Such a storage ring consisting of smaller rings can accumulate up to 8 electrons and reject bunches of 4 electrons that are carried away by certain proteins to another similar reaction center. This storage ring, or rather sink, is dependent on the nature of the excited states of the chlorophyll and carotenoid molecules and that, in turn, is very dependent on the excitation gap energy derived from the HOMO-LUMO value calculated in an energy-density functional theory. The ionization energy of the relevant quantum states can also be derived from this calculation as discussed later.



(a) Light Harvesting Complex



(b) Chlorophylls

Figure 7.8. (a) shows the pea light-harvesting complex at 2.5 Å resolution (PDB ID: 2BHW) [115]. The protein is represented as NewCartoon and the chlorophyll a/b using licorice. (b) shows the chlorophyll molecules from the crystal structure represented in licorice. The chlorophylls are organized in two ring structures, one upper and one lower. The figures were generated using the VMD program developed in the group of Professor Klaus Schulten at UIUC [116].

7.3.14 Efficiency Dichotomy in electronic transfer mechanisms

A much studied process is that of the photo-absorption of the antenna molecules, peridinin or carotenoid [120, 121]. They can, upon the absorption of a photon, shuffell excitons between conjugated π -bonds. alternating double and single carbon bonds thereby creating excitons that can propagate down to the attached chlorophyll packet molecule. The direction of the propagation of the exciton is dependent on the dipole orientation of the peridinin or carotenoid molecule that points towards the chlorophyll molecule, it is attached to.

The transfer along the antenna and from the antenna to a chlorophyll packet and from one packet to another in the chlorophyll ring system is usually con-

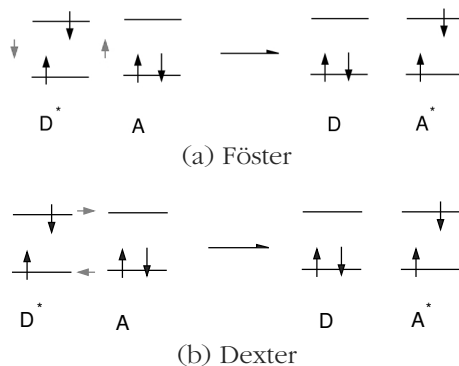


Figure 7.9. (a) illustrates the Förster mechanism where the excited electron is transferred due to dipole coupling. (b) illustrates the Dexter mechanism where an excited electron is transferred.

sidered to involve a Coulomb multipole-multipole interaction that de-excites an initially excited electron at a donor molecule and pass on this energy to directly excite an electron on the acceptor molecule and is usually called Förster mechanism [122]. Another way to de-excite the molecule is to transfer the energy to an adjacent molecule, known as the Dexter mechanism [123] and illustrated in Figure 7.9 and where an excited electron is exchanged for a ground state electron or a hole going oppositely (See Figure 7.9 for schematic illustration). In the latter case of transfer between different molecules we find it improbable that electrons are running between molecules like fixed entities. We shall instead propose that energy and excitation is transferred through electromagnetic interaction which is discussed in the next chapter. The purpose of this paper is to propose an interaction involved in causing both Förster and Dexter mechanism. That, namely a mechanism other than radiative transition is involved, is evident from the analysis of the efficiency factor. As mentioned, the proposed mechanism is responsible for a donor chromophore with electrons in excited states to be able to transfer energy by a long-range, non-radiative dipole-dipole interaction to another acceptor chromophore within a distance of about 10 nm. This remarkable mechanism is typically being used for resonance fluorescence phenomena [124] (or FRET, Fluorescence Resonance Energy Transfer) but in our case the focus is on chlorophyll molecules. The efficiency, E , of the mechanism

is often expressed in terms of the quantum yield of the energy transfer as

$$E = \frac{k_{\text{ET}}}{k_f + k_{\text{ET}} + \sum_i k_i} \quad (7.11)$$

where k_{ET} is the rate of energy transfer, k_f is the radiative decay rate and k_i is the rate constant for other de-excitation processes. In terms of the donor-acceptor separation distance a one can also write the efficiency E depending on the inverse 6th power law of a :

$$E = \frac{1}{1 + (a/a_0)^6} \quad (7.12)$$

where a_0 is a normalization factor (separation of the donor-acceptor at which the resonance transfer is 50%) and is called the Förster distance. Even more interesting is that this distance, a_0 is related to the overlap integral between the donor emission spectrum and the acceptor absorption spectrum along with the mutual molecular orientation. The overlap integral is expressed as

$$L = \int \epsilon_d(\nu)\alpha_a(\nu)\nu d\nu \quad (7.13)$$

where ϵ_d and the α_a are respectively the emission spectrum of the donor and the absorption spectrum (molar extinction coefficient) of the acceptor. This leads to a relation between the Förster distance and the overlap integral:

$$a_0^6 = 8.8 \times 10^{-28} \kappa^2 n^{-4} F_l L \quad (7.14)$$

κ is the dipole orientation factor often set to $\kappa^2 = 2/3$ [122]. F_l is the fluorescence quantum yield of the donor in the absence of the acceptor and n is the refractive index of the medium.

Similar to the Förster mechanism of electron transfer (displacement) is the Dexter mechanism, which as described above involves both transfer of electron and hole and hence works predominantly on shorter distances. The formula for the efficiency of the Dexter mechanism is similar to the Förster that, however, has an $1/a^6$ behavior rather than an exponential e^{-a} as in Dexter mechanism [123].

One can compare the radial behavior of the two mechanisms and at what distances they dominate. Basically Dexter dominates at distances $a < 10 \text{ \AA}$ and

Förster mechanism at distances $20 < a < 100 \text{ \AA}$ [125]. The Förster and the Dexter mechanisms help adding to (but not fully explain) the strong efficiency of the photosynthesis process with a total quantum efficiency of around 99%. The efficiency of the two mechanisms can also be expressed in terms of fluorescence lifetime of the donor molecule:

$$E = (1 - \tau_D^{ua}/\tau_D^a) \quad (7.15)$$

where τ_D^a and τ_D^{ua} are the fluorescence lifetimes of the donor state with and without the presence of an acceptor state. Such number is expected to be very low since the usual quantum yield or the fluorescence efficiency is given by the number n_{pe} of photons emitted divided by the number n_{pa} of photons absorbed, *i.e.*,

$$Q = \frac{n_{pe}}{n_{pa}} \quad (7.16)$$

which is a number close to 1. In the case of chlorophyll we expect the Förster and Dexter mechanisms to contribute much less than 100% [126] to the total quantum efficiency and thus, in order to explain this 99% quantum efficiency mentioned above we need another component which we shall explain in the next chapter.

7.3.15 The energy transfer mechanism in photosynthesis

We shall now try to formulate the entire photosynthesis process from a more abstract physical side. In such formulation the chloroplast is considered a whole molecular entity with chemical bonds and metal ions. In short our proposed process is as follows: *Basically, charges are being transferred around in the chloroplast system by the Coulomb interaction which can be expanded in multi-poles, the dipole part of which is responsible for Förster mechanism [122, 127]. However, we believe that there also appears to be electromagnetic interaction as a means of charge transfer and, most importantly, as a result of electron excitation that gives rise to nuclear vibration, which is in the far infrared region and to some extend verified in references [113, 114].*

As we argue, light being incident on a leaf with chlorophyll exhibits typical

resonant absorption peaks, particularly around 400 and 680 nm, see Refs. 113. The corresponding energy may be calculated using:

$$E = h\nu = 1.237 \times 10^3 \text{ eV}/\lambda(\text{nm}) \quad (7.17)$$

which leads, respectively, to 3.093 and 1.767 eV.

These energies could induce electronic excitations in many ligands chl(A, B, ..., Z) that are constituents of chlorophylls. Thus, symbolically one has



where Chl(A, B, C, ..., Z) stands for the electrons A, B, ...in the chlorophyll molecule, Chl, and A* stands for excitation of electron A.

The electronic excitation could be Frank-Condon type or excimer type since electronic clouds of neighboring atoms overlap. In either case, the electronically excited state of one of the molecules can pass the electron to another one in excited state forming a kind of dipole. Before doing so, it could de-excite along the vibronic states emitting infrared radiation. Thus,



The electronically excited negative ion (C*)⁻ could de-excite to lower states leading ultimately to an isomeric state *i*, (C_{*i*})⁻. At this stage one has a dipole A⁺, ..., C_{*i*}⁻). The distance between two nuclei at this stage is affected and oscillates about their previous mean position, effectively creating **oscillating – dipoles**. This is supported by the experiments of Refs. 113, 114. In effect one has now a series of oscillating dipoles of dipole length *l* of about 2 to 3 Å or (0.2 to 0.3 nm). The components of electric field emitted by such an oscillating dipole in classical electrodynamics are [128] (z-axis is the axis of the dipole, θ is with respect to that), for $\lambda \gg l$:

$$E_r = \frac{I_0 l}{4\pi} 2\eta \cos \theta \left[\frac{1}{r^2} - \frac{i}{kr^3} \right] \exp(-ikr) \quad (7.20)$$

$$E_\theta = \frac{I_0 l}{4\pi} 2\eta \cos \theta \left[\frac{ik}{r} + \frac{1}{kr^2} - \frac{i}{kr^3} \right] \exp(-ikr) \quad (7.21)$$

where $\eta = \sqrt{\mu/\epsilon}$ (μ is permeability in Henry/m and ϵ is permittivity in Farad/m) which is the intrinsic impedance of the medium, k , the wave number = $2\pi/\lambda$, λ being the wavelength radiated and I_0 is the current.

Assuming that the current is uniform and q is the charge at the endpoints, in the frequency domain ω , one can write $I_0 = i\omega q$ and use $\eta/k = (\omega\epsilon)^{-1}$.

Then for the emitted radiation, with $\lambda/2\pi \gg r$ we have:

$$E \cong \frac{ql}{4\pi\epsilon r^3} [2 \cos(\theta)\hat{e}_r + \sin(\theta)\hat{e}_\theta] \quad (7.22)$$

and in the same approximation:

$$H = \frac{I_0 l}{4\pi r^2} \sin(\theta)\hat{e}_\theta \quad (7.23)$$

The average Poynting vector, $\langle S \rangle$, is defined as $\frac{1}{2}$ times the real part of the Poynting vector $\mathbf{S} = (\mathbf{E} \times \mathbf{H})^*$, so therefore, in terms of w/m^2 :

$$\langle S \rangle = \frac{1}{8} \eta \sin^2 \theta \left(\frac{I_0 l}{\lambda r} \right) \hat{a}_r \quad (7.24)$$

and the total radiated power (in Watts), P , is thus:

$$P = 40\pi^2 I_0^2 \left(\frac{l}{\lambda} \right)^2 \quad (7.25)$$

In the case $l \cong \lambda/1000$; $P \cong (40\pi^2) I_0^2 \times 10^{-6}$ (I_0 in Amps) then $I_0 \approx q\nu$ where ν is the frequency of vibration of 2 nuclei which can be estimated from vibrational spectra of one of the ligands. One can get this number from the vibrational spectra of aromatic molecules. The electric charge, q , is about 1.602×10^{-19} C for a single dipole. In the case of 10^{20} dipoles per cm^3 , this is a substantial energy.

Apart of the usual electron transfer mechanisms we have propose another electron transfer mechanism, the Bio-Auger process, that can replace or at least supplement the usually mentioned processes. In the figure below we have sketched the very interesting possibility of electrons being pumped to higher electronic energy states. This is because the electron that takes the place of the hole left from electron excitation by light absorption will deliver the extra energy gained from the hole replacement to the excited electron that has a higher

angular momentum state and thus cannot go back to the previous ground state position.

This boost or pumping of electrons are needed in order to cross from the carotenoid antenna molecule to the chlorophyll molecule that is at a much higher energy state. However the pumping of the excited electron can cause the crossing of the barrier between carotenoid and chlorophyll. the boosting is involving about 2 – 3 eV extra [129].

As mentioned earlier, the electronic transition caused by resonant absorption sets into motion a vibronic excitation due to the change of inter-nucleonic motion. This is in infrared frequencies. They are playing an important role contributing to the breaking up of water in the process where the manganese atoms in the center of the chloroplast play an important role of oxidation. The electromagnetic radiation is directed towards the center causing electron transports and oxidation as described above. The chlorophyll molecules are fixed in pairs (in a so-called C_2 pseudo symmetry where each partner being rotated 180 degrees compared to the other). These pairs are then arranged almost in parallel around a ring (altogether 8 pairs) and will have electrons excited and de-excited arranged as a series of positive and negative charges working as a series of dipoles which effectively acts as capacitors adding up to the picture of chlorophyll molecules arranged as a storage ring of electrons. The issue here, from a theoretical solid-state point of view, is really how localized these kind of transfer mechanisms are in this “electron storage ring”. We expect that, after the electrons have been transferred to the chlorophyll ring they become de-localized and eventually be “spilled out” in portions of $4e^-$ to the docking quinone-cytochrome molecule-complex to be carried away.

7.3.16 The structure and organization of chlorophyll

The chlorophyll molecule is composed of a ring system with four nitrogens coordinating a magnesium ion and is part of the light harvesting complex. A single chlorophyll molecule, which is pictured in Figure 7.10, has a ring structure with 5 pyrine rings arranged inside the ring around a magnesium atom that

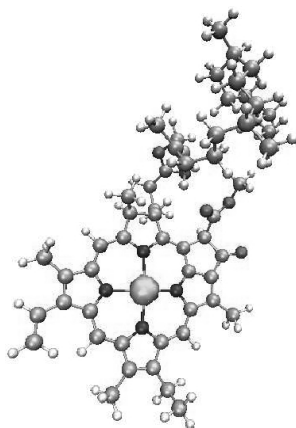


Figure 7.10. It shows the chlorophyll molecule where the green sphere is the Mg^{2+} coordinated by four nitrogen atoms (blue spheres). Carbon atoms are colored cyan, hydrogen white, and oxygens are colored red. Figure was generated using VMD.

coordinates to the neighboring nitrogens [117]. The tail of the molecule anchors to the protein complex.

The chlorophylls are arranged in two layers within the thylakoid membrane where each layer is located near either side of the membrane pointing toward the stromal or luminal surface. In each layer neighboring chlorophylls are located 11.26 \AA away from each other measured from the Mg^{2+} ion. These chlorophyll molecules are slightly asymmetric and are positioned in pairs of mirror images and arranged around a ring of 8 mirror image pairs. The molecules are located with a pseudo C_2 -symmetry between each pair of chlorophylls [118].

Computation of chlorophyll analog

We start by performing calculation of a single chlorophyll analog molecule where the tail of molecule has been removed resulting in 82 atoms. The main function of the tail is anchoring of the head group so for transfer properties it can be neglected. Tentatively we could calculate a HOMO-LUMO gap to be $3 - 4 \text{ eV}$. Such a HOMO (Highest Occupied Molecular Orbital) - LUMO (Lowest Un-occupied Molecular Orbital) is somewhat artificial in standard DFT formalism unless time-dependent methods are being used.

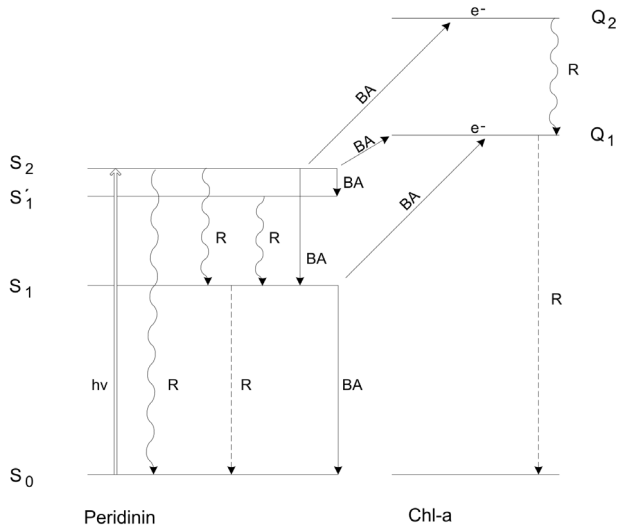


Figure 7.11. Schematic level scheme of peridinin-Chl-a complex. Thick arrow refers to the absorption of pigment from the ground state of peridinin, S_0 , to the allowed state, S_2 , the $S_0 \rightarrow S_1$ being symmetry forbidden. Solid, broken and wavy lines refer, respectively, to Bio-Auger, fluorescence and allowed (dipole) radiative transitions. The case of the state Q_1 is lower than S_1 and S_2 .

7.3.17 ESR experiments on the chloroplast system

To verify experimentally the assumptions made in the presented model, we arranged a preliminary experiment on chloroplast systems from plants in an ESR (Electron Spin Resonance) apparatus operated at low temperature. Thus we should, for example, be able to see if there was a difference in the signal from the unpaired electrons from day time with incident light and night time of no incident light. The most clear signal of electronic spin is expected to come from the manganese atoms. We have made recordings during specific periods (5 min. each) with incident full-spectral light and with no light at the sample cell situated in the magnet. One can observe a clear difference in the recording of the two types of periods.

In Figures 7.11 and 7.12 we have sketched examples of the Bio-Auger process. It shows schematically the transfer of electrons from peridinin to chlorophyll in the peridinin-chl-a complex. On the next figure the boosting of the

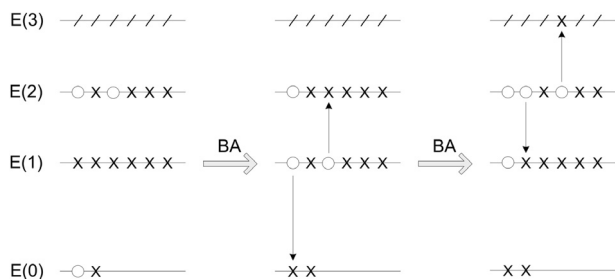


Figure 7.12. Schematic diagram exhibiting the upward boosting of an electron from a lower to higher energy states.

electron energy is illustrated by electron-hole examples.

7.4 Conclusions

A theory of the electronic pathways in the photosynthesis involving carotenoid and chlorophyll molecules has been proposed here. Upon exposure to incident light, the photo-excited carotenoid charge transfer electrons to carotenoid effectively creating an oscillating dipole. The chlorophyll molecules, arranged in a “storage” ring around a manganese atom, will transfer excitations of electrons alternating between π and π^* states exchanging quanta by a Förster-like mechanism that can account for 80-90% of the energy output. The rest is explained by EM radiation originating from nuclear vibrations.

Acknowledgments

HGB would like to thank the Danish National Research Foundation for financial support and acknowledge the Danish Research Council for the funding of the Quantum Protein Centre in the Department of Physics at the Technical University of Denmark, 2800 Kgs. Lyngby, Denmark for the years 2001 to 2009. HGB would like to thank Karl James Jalkanen, FRSC, for many years of collaboration in the field of molecular biophysics and biospectroscopy, a long lasting friendship and for help in preparing this manuscript and finally Vladislav Vasilyev for developing the jamberoo program and making it available to the

computational molecular biophysics, quantum chemistry, computational physics and chemistry communities. The jamberoo program can be obtained at <http://sf.anu.edu.au/~vvv900/cct/appl/jmoleditor> and the citation for the program is <http://dx.doi.org/10.1007/s00214-009-0636-7> "Towards interactive 3D graphics in chemistry publications" *Theor. Chem. Acc.* **125**, 173-176 (2010).

References

- [1] G. J. Thomas, Jr., *Ann. Rev. Bioph. Biom.* **28**, 1 (1999).
- [2] T. A. Keiderling, *Spectroscopic Methods For Determining Protein Structure in Solution* (VCH Publishers, Weinheim, 1996), "Protein Structural Studies Using Vibrational Circular Dichroism Spectroscopy", chap. 8, pp. 163.
- [3] G. J. Thomas, Jr., *Vibrational Spectra and Structure* (Elsevier, Amsterdam, 1975), "Raman Spectroscopy of Biopolymers", vol. 3, pp. 239.
- [4] K. J. Jalkanen, H. G. Bohr, and S. Suhai in *Proceedings of the International Symposium on Theoretical and Computational Genome Research*, edited by S. Suhai (Plenum, New York, 1997), pp. 255.
- [5] E. Tajkhorshid, K. J. Jalkanen, and S. Suhai, *J. Phys. Chem. B* **102**, 5899 (1998).
- [6] K. Frimand, K. J. Jalkanen, H. G. Bohr, and S. Suhai, *Chem. Phys.* **255**, 165 (2000).
- [7] K. J. Jalkanen, R. M. Nieminen, K. Frimand, J. Bohr, H. Bohr, R. C. Wade, E. Tajkhorshid, and S. Suhai, *Chem. Phys.* **265**, 125 (2001).
- [8] S. Abdali, K. J. Jalkanen, H. Bohr, S. Suhai, and R. N. Nieminen, *Chem. Phys.* **282**, 219 (2002).
- [9] K. J. Jalkanen, I. M. Degtyarenko, R. M. Nieminen, X. Cao, L. A. Nafie, F. Zhu, and L. D. Barron, *Theor. Chem. Acc.* **119**, 191 (2008).
- [10] M. Knapp-Mohammady, K. J. Jalkanen, F. Nardi, R. C. Wade, and S. Suhai, *Chem. Phys.* **240**, 63 (1999).
- [11] K. J. Jalkanen, R. M. Nieminen, M. Knapp-Mohammady, and S. Suhai, *Int. J. Quantum Chem.* **92**, 239 (2003).
- [12] Z. Deng, P. L. Polavarapu, S. J. Ford, L. Hecht, L. D. Barron, C. S. Ewig,

- and K. J. Jalkanen, *J. Phys. Chem.* **100**, 2025 (1996).
- [13] K. J. Jalkanen and S. Suhai, *Chem. Phys.* **208**, 81 (1996).
- [14] W.-G. Han, K. J. Jalkanen, M. Elstner, and S. Suhai, *J. Phys. Chem. B* **102**, 2587 (1998).
- [15] H. G. Bohr, K. J. Jalkanen, K. Frimand, M. Elstner, and S. Suhai, *Chem. Phys.* **246**, 13 (1999).
- [16] C.-D. Poon, E. T. Samulski, C. F. Weise, and J. C. Weisshaar, *J. Am. Chem. Soc.* **122**, 5642 (2000).
- [17] C. F. Weise and J. C. Weisshaar, *J. Phys. Chem. A* **107**, 3265 (2003).
- [18] M. Losada and Y. Xu, *Phys. Chem. Chem. Phys.* **9**, 3127 (2007).
- [19] R. D. Amos, *Chem. Phys. Lett.* **108**, 185 (1984).
- [20] P. J. Stephens, *J. Phys. Chem.* **89**, 748 (1985).
- [21] P. J. Stephens, *J. Phys. Chem.* **91**, 1712 (1987).
- [22] A. D. Buckingham, P. W. Fowler, and P. A. Galwas, *Chem. Phys.* **112**, 1 (1987).
- [23] R. D. Amos *Adv. Chem. Phys.: Ab Initio Methods in Quantum Chemistry*, edited by K. P. Lawley (Wiley, Chichester, 1987), "Molecular property derivatives", chap. 2, vol. 67, pp. 99.
- [24] R. D. Amos, K. J. Jalkanen, and P. J. Stephens, *J. Phys. Chem.* **92**, 5571 (1988).
- [25] R. M. Stevens, R. M. Pitzer, and W. N. Lipscom, *J. Chem. Phys.* **38**, 550 (1962).
- [26] J. R. Cheesman, M. J. Frisch, F. J. Devlin, and P. J. Stephens, *Chem. Phys. Lett.* **252**, 211 (1996).
- [27] D. P. Craig and T. Thirunamachandran, *Mol. Phys.* **35**, 825 (1978).
- [28] P. J. Stephens, K. J. Jalkanen, R. D. Amos, P. Lazzeretti, and R. Zanasi, *J. Phys. Chem.* **94**, 1811 (1990).
- [29] K. L. Bak, P. Jørgensen, T. Helgaker, K. Ruud, and H. J. Aa. Jensen, *J. Chem. Phys.* **98**, 8873 (1993).
- [30] K. L. Bak, P. Jørgensen, T. Helgaker, K. Ruud, and H. J. Aa. Jensen, *J. Chem. Phys.* **100**, 6621 (1994).

- [31] A. Komornicki and J. W. McIver, *J. Chem. Phys.* **70**, 2014 (1979).
- [32] R. D. Amos, *Chem. Phys. Lett.* **124**, 376 (1986).
- [33] M. J. Frish, Y. Yamaguchi, J. F. Gaw, H. F. Schaefer III, and J. S. Binkley, *J. Chem. Phys.* **84**, 531 (1986).
- [34] B. G. Johnson and J. Florian, *Chem. Phys. Lett.* **247**, 120 (1995).
- [35] R. D. Amos, *Chem. Phys. Lett.* **87**, 23 (1982).
- [36] T. Helgaker, K. Ruud, K. L. Bak, P. Jørgensen, and J. Olsen, *Faraday Discuss.* **99**, 165 (1994).
- [37] J. R. Cheeseman, M. J. Frisch, F. J. Devlin, and P. J. Stephens, *J. Phys. Chem. A.* **104**, 1039 (2000).
- [38] P. J. Stephens, F. J. Devlin, J. R. Cheeseman, and M. J. Frisch, *J. Phys. Chem. A.* **105**, 5356 (2001).
- [39] P. J. Stephens, F. J. Devlin, J. R. Cheeseman, M. J. Frisch, B. Mennucci, and J. Tomasi *Tetrahedron: Asymmetr.* **11**, 2443 (2000).
- [40] J. E. Rice and N. C. Handy, *J. Chem. Phys.* **94**, 4959 (1991).
- [41] S. M. Colwell, C. W. Murray, N. C. Handy, and R. D. Amos, *Chem. Phys. Lett.* **210**, 261 (1993).
- [42] A. M. Lee and S. M. Colwell, *J. Chem. Phys.* **101**, 9704 (1994).
- [43] S. J. A. van Gisbergen, J. G. Snijders, and E. J. Baerends, *J. Chem. Phys.* **103**, 9347 (1995).
- [44] S. J. A. van Gisbergen, J. G. Snijders, and E. J. Baerends, *Chem. Phys. Lett.* **259**, 599 (1996).
- [45] S. J. A. van Gisbergen, K. Kootstra, P. R. T. Schipper, O. V. Gritsenko, J. G. Snijders, and E. J. Baerends, *Phys. Rev. A* **57**, 2556 (1998).
- [46] S. J. A. van Gisbergen, J. G. Snijders, and E. J. Baerends, *J. Chem. Phys.* **109**, 10644 (1998).
- [47] S. J. A. van Gisbergen, J. G. Snijders, and E. J. Baerends, *J. Chem. Phys.* **109**, 10657 (1998).
- [48] K. J. Jalkanen, P. J. Stephens, R. D. Amos, and N. C. Handy, *J. Phys. Chem.* **92**, 1781 (1988).
- [49] A. D. Becke, *J. Chem. Phys.* **98**, 5648 (1993).

- [50] A. D. Becke, J. Chem. Phys. **96**, 2155 (1992).
- [51] A. D. Becke, J. Chem. Phys. **97**, 9173 (1992).
- [52] A. D. Becke, J. Chem. Phys. **88**, 1053 (1988).
- [53] C. Lee, W. Yang, and R. G. Parr, Phys. Rev. B **37**, 785 (1988).
- [54] S. H. Vosko, L. Wilk, and M. Nusair, Can. J. Phys. **58**, 1200 (1980).
- [55] K. Holderna-Natkaniec, K. Jurga, I. Natkaniec, D. Nowak, and A. Szyzewski, Chem. Phys. **317**, 178 (2005).
- [56] M. R. Johnson, M. Prager, H. Grimm, M. A. Neumann, G. J. Kearley, and C. C. Wilson, Chem. Phys. **244**, 49 (1999).
- [57] B. S. Hudson, J. Phys. Chem. A, **105**, 3949 (2001).
- [58] T. B. Freedman, Faraday Discuss. **199**, 210 (1994).
- [59] P. L. Polavarapu, Faraday Discuss. **199**, 210 (1994).
- [60] P. L. Polavarapu and Z. Deng, Faraday Discuss. **99**, 151 (1994).
- [61] R. J. Bartlett, I. V. Schweigert, and V. F. Lotrich, J. Mol. Struct.: THEOCHEM, **771**, 1 (2006).
- [62] K. J. Jalkanen, Jürgensen, V.W., A. Claussen, A. Rahim, G. M. Jensen, R. C. Wade, F. Nardi, C. Jung, I. M. Degtyarenko, R. M. Nieminen, F. Herrmann, M. Knapp-Mohammady, T. A. Niehaus, K. Frimand and S. Suhai, Int. J. Quantum Chem., **106**, 1160 (2006).
- [63] J. S. Dewar, Zebisch, E., E. F. Healy, and J. J. P. Stewart, J. Am. Chem. Soc. **107**, 3902 (1985).
- [64] J. J. P. Stewart, J. Comp. Chem., **10**, 209 (1989).
- [65] J. J. P. Stewart, J. Comp. Chem. **10**, 221 (1989).
- [66] S. Gohlke and E. Illenberger, Europhysics News **33**, 207 (2002).
- [67] S. D. Wetmore, R. Boyd, and L. A. Erikson, Chem. Phys. Lett., **322**, 129 (2000).
- [68] R. Kakkar, and R. Garg, J. Mol. Struct.: THEOCHEM **620**, 139 (2003).
- [69] M. S. Cheung, I. Daizadeh, A. A. Stuchebrukhov, and P. F. Heelis, Biophys. J. **76**, 1241 (1999).
- [70] D. Ramaiah, Y. Kan, T. Koch, H. Ø rum, and G. B. Schusgter, P. Natl. Acad. Sci. USA **95**, 12902 (1998).

- [71] W. Harm, *Biological Effects of Ultraviolet Radiation* (Cambridge University Press, Cambridge, 1980).
- [72] I. Husain, J. Griffith and A. Sancar, P. Natl. Acad. Sci. USA **85**, 2558 (1988).
- [73] A. Sancar and C. S. Rupert, Gene **4**, 295 (1978).
- [74] R. P. Sinha and D.-P. Hüder, Photochem. Photobiol. Sci. **1**, 225 (2002).
- [75] A. Sancar, Chem. Rev. **103**, 2203 (2003).
- [76] A. Reuther, D. N. Nikogosyan and A. Laubereau, J. Phys. Chem. **100**, 5570 (1996).
- [77] A. Sancar, Biochemistry **33**, 2 (1994).
- [78] H. Bohr, J. K. Jalkanen and J. B. Malik, Mod. Phys. Lett. B **19**, 473 (2005).
- [79] P. F. Heelis, J. Photoch. Photobiol. B **38**, 31 (1997).
- [80] T. Carell, L. T. Burgdorf, L. M. Kundu, and M. Cichon, Curr. Opin. Chem. Biol. **5**, 491 (2001).
- [81] G. B. Sancar, Mutat. Res. **451**, 25 (2000).
- [82] A. Kelner, P. Natl. Acad. Sci. USA **35**, 73 (1949).
- [83] A. Kelner, J. Bacteriol. **58**, 511 (1949).
- [84] R. Dulbecco, Nature **163**, 949 (1949).
- [85] M. Elstner, *Weiterentwicklung quantenmechanischer Rechenverfahren fuer organische Molekuele und Polymere*. PhD thesis (Universitaet-Gesamthochschule Paderborn, Deutschland, 1998).
- [86] M. Elstner, D. Porezag, G. Jungnickel, J. Elsner, M. Haugk, Th. Frauenheim, S. Suhai, and G. Seifert, Phys. Rev. B **58**, 7260 (1998).
- [87] T. Heine, *Die Berechnung von Structur, Energetik und kernmagnetischen Abschirmungen von Fullerenen und ihren Derivatzen*. PhD thesis (Technische Universitat Dresden, Germany, 2000).
- [88] K. Frimand and K. J. Jalkanen, Chem. Phys. **279**, 161 (2002).
- [89] J. R. Maple, M.-J. Hwang, K. J. Jalkanen, T. P. Stockfish, and A. T. Hagler J. Comp. Chem. **19**, 430 (1998).
- [90] S. J. Weiner, P. A. Kollman, Nguyen, D.T., and D. A. Case, J. Comp. Chem. **7**, 230 (1986).
- [91] S. J. Weiner, P. A. Kollman, D. A. Case, U. C. Singh, C. Ghio, G. Alagona,

- S. Profeta Jr., and P. Weiner, *J. Am. Chem. Soc.* **106**, 765 (1984).
- [92] C. H. Langley, J.-H. Lii, and N. L. Allinger, *J. Comp. Chem.* **22**, 1396 (2001).
- [93] H. Yu, T. Hanson, and W. F. van Gunsteren, *J. Chem. Phys.* **118**, 221 (2003).
- [94] W. R. P. Scott, P. H. Huenenberger, I. G. Tironi, A. E. Mark, S. R. Billeter, J. Fennen, A. E. Torda, T. Huber, P. Krueger, and W. F. van Gunsteren, *J. Phys. Chem.* **103**, 3596 (1999).
- [95] W. L. Jørgensen and J. Tirado-Rives, *J. Am. Chem. Soc.* **110**, 1657 (1988).
- [96] P. Ren and J. W. Ponder, *J. Comp. Chem.* **23**, 1497 (2002).
- [97] M. Clark, R. D. Cramer III, and N. van Opdenbosch, *J. Comp. Chem.* **10**, 982 (1989).
- [98] A. D. J MacKerell, D. Bashford, M. Bellott, J. R. L. Dunbrack, J. D. Evanseck, M. J. Field, S. Fisher, J. Gao, Guo, H., S. Ha, D. Joseph-McCarthy, L. Kuchnir, K. Kucyera, F. T. K. Lau, C. Mattos, S. Michnick, T. Ngo, D. T. Nguyen, B. Prodhom, W. E. Reiher III, B. Roux, M. Schlenkrich, J. C. Smith, R. Stote, J. Straub, M. Watanabe, J. Wiorkiewicz-Kuczera, D. Yin, and M. Karplus, *J. Phys. Chem. B.* **102**, 3586 (1998).
- [99] B. R. Brooks, R. E. Bruccoleri, B. D. Olafson, D. J. States, S. Swaminathan, and M. Karplus, *J. Comp. Chem.* **4**, 187 (1983).
- [100] D. McKay, A. T. Hagler, J. R. Maple, and C. Herd, *Discover User's Guide* (Biosym Technologies (MSI) Inc., San Diego, 1991).
- [101] M. Vasquez, G. Nemethy, and H. A. Scheraga, *Macromolecules* **16**, 1043 (1983).
- [102] L. Jensen, P. Th. van Duijnen, and J. G. Snijders, *J. Chem. Phys.* **118**, 514 (2003).
- [103] G. Tabacchi, C. J. Mundy, J. Hutter, and M. Parrinello *J. Chem. Phys.* **117**, 1416 (2002).
- [104] R. Chelli and P. Procacci *J. Chem. Phys.* **118**, 1571 (2003).
- [105] J. Ames, *Photosynthesis* (Elsevier, Amsterdam, 1987).
- [106] *The Photosystems: Structure, Function and Molecular Biology*, edited by

- J. Barber (Elsevier, Amsterdam, 1992).
- [107] *Photosynthesis and the Environment*, edited by J. Barber (Kluwer Academic, Dordrecht, 1996).
- [108] J. Whitmarsh and Govindjee, *Concepts in Photobiology: Photosynthesis and photomorphogenesis*, edited by G. S. Singhal, G. Renger, S. K. Sopory, K.-D. Irrgang and Govindjee (Narosa, New Delhi, 1999), chap. "The photosynthetic process", pp 11.
- [109] P. H. Raven and G. B. Johnson, *Biology* (William C. Brown, Dordrecht, 1996),
- [110] P. R. Chitnis, *Annu. Rev. Plant Phys.* **52**, 593 (2001).
- [111] R. J. Sension, *Nature*, **446**, 740 (2007).
- [112] G. S. Engel, T. R. Calhoun, E. L. Read, T.-K. Ahn, T. Mancal, Y.-C. Cheng, R. E. Blankenship, and G. R. Fleming, *Nature* **446**, 782 (2007).
- [113] T. Brixner, J. Stenger, M.H. Vaswani, M. Cho, R. E. Blankenship, and G. R. Fleming, *Nature* **434**, 625 (2005).
- [114] C. Day, *Phys. Today* **58**, 23 (2005).
- [115] J. Standfuss, A. C. T. van Scheltinga, M. Lamborghini, and W. Kühlbrandt, *Embo.J.* **24**, 919 (2005).
- [116] W. Humphrey, A. Dalke, and K. Schulten, *J. Mol. Graph.* **14**, 33 (1996).
- [117] J. Koepke, X. Hu, C. Muenke, K. Schulten, and H. Michel, *Structure* **4**, 581 (1996).
- [118] Z. Liu, H. Yan, K. Wang, T. Kuang, J. Zhang, L. Gui, X. An, and W. Chang, *Nature* **428**, 287 (2004).
- [119] A. Damjanovic, T. Ritz, and K. Schulten, *Phys. Rev. E*, **59**, 3293 (1999).
- [120] H. M. Vaswani, N. E. Holt, and G. R. Fleming, *Pure Appl. Chem.*, **77**, 925 (2005).
- [121] D. Zigmantas, T. Polivka, R. G. Hiller, A. Yartsev, and V. Sundström, *J. Phys. Chem. A* **105**, 10296 (2001).
- [122] Th. Förster, *Ann. Phys. (Leipzig)* **2**, 55 (1948).
- [123] D. L. Dexter *J. Chem. Phys.* **21**, 836 (1963).
- [124] J. R. Lakowicz, *Principle of Fluorescence Spectroscopy*. (Springer, Heidel-

- berg, 2006).
- [125] P. Andrew and W. L. Barnes, *Science* **306**, 1002 (2004).
- [126] V. Sundström, T. Pullerits, and R. van Grondelle, *J. Phys. Chem. B* **103**, 2327 (1999).
- [127] G. Cinque, R. Croce, A. Holzwarth, and R. Bassi, *Biophys. J.* **79**, 1706 (2000).
- [128] K. R. Demarest, *Engineering Electromagnetics* (Prentice Hall, NJ, 1998), chap. 14, p. 576.
- [129] H. Bohr and F. B. Malik, *Handbook of Molecular Biophysics* (Wiley-VCH, 2009), edited by H. Bohr, pp. 67.

8. COMPUTATIONAL PROTEOMICS – FROM METHODOLOGICAL DEVELOPMENTS TO BIOLOGICAL APPLICATIONS

Irina S. Moreira, Natércia F. Bras[†], Alexandra T. P. Carvalho[†], Nuno M. F. S. A. Cerqueira[†], Daniel F. Dourado[†], Marta A. S. Perez[†], Antonio J. M. Ribeiro[†], Sergio F. Sousa[†], Pedro A. Fernandes, and Maria J. Ramos^{*}

REQUIMTE/Departamento de Química, Faculdade de Ciências da Universidade do Porto, Rua do Campo Alegre 687, 4169-007 Porto - Portugal

Proteomics, a chimera of proteins and genomics, involves the study of the proteins expressed in a cell, organism, or tissue. Proteins are essential in all aspects of life, and so the computational study of proteomics is becoming a vital element in understanding the underlying concepts. In this review we are going to address some of the challenges and latest developments focusing in four different aspects that are thematic in our group: (a) Molecular Dynamics Simulations; (b) Drug Design; (c) Enzymatic Mechanisms; and (d) Benchmarking of DFT functionals.

8.1 Introduction

Proteomics, a chimera of **proteins** and **genomics**, was invented by Professor Mark Wilkins in the early 1990s and involves the study of the proteins expressed in a cell, organism, or tissue. This includes protein identification and quantification, protein-protein interactions, protein complexes prediction, protein modifications and protein localization in the cell. As proteins are essential for all life, proteomics is crucial in biomedical applications, and although more recent, the computational study of proteomics is becoming a key element in this biological field.

Computational proteomics involves the computational methods, algorithms, databases and methodologies used to model protein structure, dynamics and

^{*}Email address: mjramos@fc.up.pt

[†]Equal participation.

function. In this review we are going to focus on four different aspects that are thematic in our group, and range from methodological developments to their biological application: (a) Molecular Dynamics Simulations; (b) Drug Design; (c) enzymatic Mechanisms; and (d) Benchmarking of DFT functionals.

8.2 Classical Molecular Dynamics Simulations

Classical molecular dynamics (MD) simulations have become during the past two decades, a particularly important discipline within the field of computational biochemistry, allowing the computationally efficient evaluation of a variety of properties in the study of biological molecules for which atomic and molecular motion is vital.

Generically speaking, MD simulations follow the time evolution of a system through the numerical integration of the equations of motion of the corresponding particles. In particular, MD simulations are based on the application of classical mechanics, with intra and inter-molecular interactions described by a sum of different contributions described by mathematical formulations of simple physics phenomena. The corresponding mathematical formulae and the accompanying parameters, which are typically fitted to reproduce experimental data or high-level *ab initio* calculations, are normally described under the generic designation of force field. A variety of different force fields is presently available, differing in features such as scope, accuracy and cost associated.

The range of application of MD simulations is remarkably wide and encompasses the study of phenomena such as protein and/or small molecule conformational changes, molecular association and recognition, folding, ion transport, etc. Over the last few years we have employed MD simulations in the study of several biological systems of interest, often in combination with other computational methods. In this section, we highlight 5 particularly different applications of this very powerful methodology, selected from our own work on biological systems. These include our MD studies on the elusive metalloenzyme farnesyltransferase (FTase), the medically critical HIV reverse transcriptase enzyme (RT), and the economically appealing carbohydrate-binding modules (CBMs)

from family 11.

8.2.1 Farnesyltransferase

Farnesyltransferase is a Zinc metalloenzyme that catalyses the addition of farnesyl groups from farnesyl diphosphate (FPP) to protein cysteine residues present in characteristic carboxyl terminal –CAAX motifs. In this motif C represents the cysteine residue that is farnesylated, A is an aliphatic amino acid, and X represents the terminal amino acid residue [1]. Proteins substrates bearing a CAAX motif include a number of biologically relevant protein targets, most notably the Ras family of proteins known to be implicated in something like 30% of all human cancers [2].

Performing MD simulations on FTase is particularly challenging, compared with the typical enzymes that are comprised simply by standard amino acid residues, because of the presence of a covalently bound Zinc atom with a metal coordination sphere that changes during catalysis. Metal atoms, and the corresponding bonds, angles, dihedrals, charges, and van der Waals parameters are normally absent in the typical biomolecular force fields such as AMBER, CHARMM or OPLS. Their inclusion involves not only the parameterization of the metal atom itself, but also of the directly interacting amino acid residues, and naturally a subsequent process of validation against experimental data. We have parameterized the three different Zn coordination spheres that are formed during the catalytic mechanism of this enzyme using quantum calculations and experimental data and have validated the new parameters against EXAFS and X-Ray crystallographic information [3].

Following this process, we have performed comprehensive MD simulations with the AMBER software package on the several intermediate states formed during the catalytic mechanism of this enzyme, in an attempt to understand the way this enzyme works at a molecular level, and taking into consideration features such as the effect of the solvent and the dynamic effects arising from the interaction of the enzyme, solvent and the substrate/product molecules [4,5]. Starting from extensive 10 ns MD simulations on the enzyme resting state, binary

complex (FTase-FPP), ternary complex (FTase-FPP-CAAX substrate) and product complex (FTase-Product), we have performed comparative analysis of the amino acid flexibility along the FTase sequence, radial distribution functions of water molecules around catalytically relevant atoms, statistic variations on key catalytic distances, detailed analysis on the conformation and orientation adopted by the substrate and product molecules in the presence of the enzyme, and hydrogen bonding analysis on the most important molecular recognition sites.

These results provided very useful information for the subsequent modeling of the catalytic mechanism of this enzyme, guiding and supporting the choice of the models used from QM or QM/MM calculations, and of the several approximations adopted.

8.2.2 Reverse Transcriptase

Reverse transcriptase (RT) is the human immunodeficiency virus (HIV) enzyme whose function is to copy the viral RNA into double-stranded DNA suitable to be integrated in the host cell genome. Several combinations of different RT inhibitors are currently used in antiretroviral therapy. Our study focused on nucleoside reverse transcriptase inhibitors (NRTIs). These are substrate analogues that compete for binding and incorporation into the nascent DNA chain. However, because they lack a 3'OH, after they are incorporated they do not allow the addition of the next incoming nucleoside blocking DNA synthesis. It is presently known that the long-term failure in the treatment of AIDS with the currently available NRTIs is related to the development of resistance by RT at the binding or incorporation level, or subsequent to the nucleotide incorporation (excision).

We have conducted a series of MD simulations of RT with different inhibitors in explicit solvent in order to correlate the structural characteristics of the inhibitors with the stage at which RT resistance emerges. To achieve a greater insight on how RT discrimination gets established we compared incorporation of a normal substrate (dNTP) with incorporation of two very similar inhibitors for which resistance emerges by different mechanisms: phosphorylated zalcitabine,

ddCTP, which is discriminated and phosphorylated stavudine, d4TTP, which is mainly excised [6]. We found that the different resistance profiles arise from the different conformations adopted by the inhibitors at the active site. d4TTP adopts an ideal conformation for catalysis because it forms an ion-dipole intramolecular interaction with the α -phosphate oxygen of the triphosphate, as does the normal substrate. In ddCTP, the lack of this essential interaction results in a different, noncatalytic conformation [6]. To achieve a greater insight on why RT excision occurs we conducted molecular dynamics simulations of complexes of HIV-1 RT with the incorporated substrate and the antiretrovirals AZT and d4T with and without pyrophosphate. For these two inhibitors resistance emerges via the excision mechanism, however they are very different structurally: AZT was a bulky azide group at the 3' position that could impose steric hindrances to translocation and d4T only was an hydrogen at this position [7]. We found that RT preferably excises these inhibitors over the substrate as a consequence of a different pattern of hydrogen bridges they establish with the N site after incorporation. In the complexes with normal nucleotides, the fingers residues K65 and R72 establish hydrogen bonds mainly with the leaving PPI. With the inhibitors, those same residues establish hydrogen bonds primarily with the substituted nucleotides. Consequently, pyrophosphate is eliminated before the opening of the fingers domain for the inhibitors, which allows ATP binding, with subsequent excision and development of drug resistance [7]. Our main conclusion was that although the lack of the 3'OH is the determinant that makes NRTIs inhibitors, it seems that the enzyme is highly specialized in recognizing structures with this group. This seems to be the cause for resistance to NRTIs being so common.

8.3 Carbohydrate Binding-Modules (CBMs)

The conversion of plant cell wall polysaccharides into soluble sugars is one of the most important reactions in nature. This process is of high economical interest as the products obtained (such as glucose derivatives) are very useful in food and pharmaceutical industries. They also have an enormous poten-

tial for the bio-fuel industry, as ethanol can be directly obtained from glucose monomers [7,8]. An efficient degradation of cellulose chains into soluble glucose monomers can be achieved using chemical means or by certain microorganisms such as *Clostridium thermocellum* (*Ct*). The latter method has become the most attractive due to reasons of economy and efficiency [8]. These organisms possess a cluster of enzymes organized in a high-hierarchy multi-subunit complex called cellulosome [9] The enzymes are generally modular proteins that contain non-catalytic carbohydrate-binding modules (CBMs), which increase the activity of the catalytic module and are thus crucial for the efficient degradation of polysaccharides [10].

Since the X-ray structure of *Ct*CBM11 with a bound substrate is not available, we have used MD simulations with both CHARMM and AMBER force fields [11,12], integrated with the recently developed MADAMM docking protocol [13], to determine the molecular recognition of glucose polymers by CBMs from family 11. MD simulations demonstrate that the side chain conformations of some tyrosine residues near the binding pocket (Tyr22, Tyr53, Tyr129 and Tyr152) give rise to a steric obstacle, precluding the efficient binding of the ligands. To overcome this limitation, a novel docking protocol that introduces a certain degree of flexibility to these amino acids in standard docking processes was used. Our results have shown that the binding interface of the *Ct*CBM11 can bind only one single polysaccharide chain, and we have used cellobiose, cellotetraose, cellohexaose, celloctaose and cellotrideose as model substrates. We propose a general mechanism for the interaction between *Ct*CBM11 and cellulose chains, in which four main charged amino acids (Asp99, Arg126, Asp128, and Asp146) have a key role in the interaction with the cellulose chains. Another feature is that a minimum of four glucose monomers in the polymer chains are required for a strong interaction with the central binding site, with the remaining units attached equidistantly to both sides of the *Ct*CBM11 cavity. MD simulations also indicate that the strongest hydrogen interactions occur with the hydroxyl groups attached to C-2 and C-6 of central glucose units of the polymer chain, which is in agreement with STD and line broadening NMR studies [11,12,14].

Furthermore, our data have shown that the three aromatic tyrosine residues (Tyr22, Tyr53, and Tyr129) at the *Ct*CBM11 interface induce a certain distortion in the glucose rings that was found to be important for guiding, reorientation and packing of the polysaccharide chain to the charged region, providing important insights into substrate binding by this important class of proteins. We also suggest that these aromatic residues are crucial to detach the carbohydrate chain from the solvent or other polysaccharide chains, by inducing a reorientation of the hydrogen bonds [11,12].

Considering that the *Ct*CBM11 is topologically similar and structurally homologous to CBMs of families 4, 6, 15, 17, 22, 27 and 29, we suggest that similar molecular determinants drive the binding and recognition of polysaccharides to these CBMs. The knowledge of the interactions that occur at the molecular level between several polysaccharides and the CBMs can be used to improve the efficiency of the linked enzymes and/or possibly of the cellulosome itself.

8.4 Drug Design

The natural tendency of proteins to bind to each other as well as to several small-molecules (ligands), forming stable and specific complexes is essential for all biological processes. The description of the structural and functional properties behind protein–protein or protein–ligand interactions and protein-binding is very important not only to increase the scientific knowledge in basic terms, but also for applied research in biomedical science and industrial pharmaceuticals.

One of the most important fields is Medicinal chemistry, at the interface of chemistry and biology, which has created an important tool in the search for new drug candidates with a combination of good pharmacodynamic and pharmacokinetic properties. Although this study can be carried out by having only an X-ray crystallographic structure of the target, additional structural and functional insights are important for the rational design of more bioactive molecules. The drug design process includes the structural determination of target protein's, hit selection, lead optimization, development of structure-activity relationships and the design of new compounds. The process of drug development is chal-

lenging, time-consuming, labor intensive, and expensive. but has as a final goal to find, develop, and market new chemical entities (NCEs), which can be used against untreatable diseases, or which have superior properties when compared to currently available drugs.

Structure-based drug design was usually a field involving the binding of a small molecule to a biomolecular target that functioned by inhibiting its function. A typical drug-like molecule had to obey the Lipinski's rule of five: no more than five hydrogen-bond acceptors and 10 hydrogen-bond donors, a molecular weight under 500 Dalton, and a partition coefficient $\log P$, a measure of lipophilicity, under 5 [15]. Veber *et al.* added that the candidates should have 10 or fewer rotatable bonds, and polar surface area equal or less than 140 \AA^2 [16]. This ensure that it has the physicochemical and pharmacokinetic properties such as good solubility, a correct balance between lipophilicity and hydrophilicity, metabolic stability (a good absorption, distribution, metabolism, excretion ADME), and bioavailability necessary to inhibit specific interactions. It has to take into account also the toxicity, radical attack (biodegradation), good quantitative structure–property relationships (QSPR) and good quantitative structure–activity relationship (QSAR). Nowadays this concept has enlarged and includes the inhibition of protein–protein interactions (PPI). However, the discovery of molecules capable of selectively inhibiting PPI encounters many obstacles such as the large interfacial areas and the relatively flat topographies of the surface of protein–protein interfaces. Small-peptides capable of disrupting this kind of interactions, usually cyclic peptides and other modified peptides do not necessarily obey to the Lipinski's rule of five. Thus, as peptides present higher number of degrees of freedom than small molecules, we face a crucial challenge of the level of flexibility of the systems under study. So, the rational design of the inhibitors has to take into account the conformational plasticity of the protein and the interplay between different conformations. Modeling a protein–peptide complex allows the determination of the pharmacophore model (geometrical arrangements of chemical features such as hydrogen bonding and electrostatic and hydrophobic interactions) that can be used to design small

molecules capable of mimicking the peptide [17].

In this part of the review we are going to focus on some *in silico* methods used to facilitate the modeling of protein–protein interfaces and protein-binding. Among these methods, we stress the determination of the three-dimensional structures of complexes (protein-protein and protein–ligand) as well as the structural determination of the crucial amino acids residues involved in binding by sequential mutagenesis of the entire protein interface (Alanine Scanning Mutagenesis, ASM), and computational approaches used to design new drugs and/or optimize the lead.

8.4.1 Protein-Protein Studies

Protein-Protein Docking

Protein-protein binding is one of the critical events in biology. It is extremely valuable in obtaining structural information and a complete understanding of both the biochemical nature of the process for which the components come together, and to facilitating the design of compounds that might influence it. However, due to the greater difficulty in crystallizing protein-protein complexes, there is relatively little structural information available about them compared to the proteins that exist as single chains or form permanent oligomers. Hence, experimental studies are faced with remarkable technical difficulties and the number of solved complexes deposited in the Protein Data Bank (PDB; www.rcsb.org/pdb) is still orders of magnitude smaller than those of experimental information on protein interactions and of structures of individual proteins. Nevertheless the practical difficulties for a better understanding of the biological function of a protein, knowledge of its three-dimensional structure is fundamental. Thus, in the past two decades there was an emergence of a large variety of theoretical algorithms designed to predict the structures of protein–protein and protein-ligand complexes – a procedure named docking.

Computational methods, if accurate and reliable, could therefore play an important role, both to infer functional properties and to guide new experiments. The first protein–protein docking algorithm was developed by Janin and Wodak

in 1978 [18-20]. Albeit important successes, docking screens remain hampered by the prediction of false positives and negatives [21]. Because of the complexity of the problem, protein–protein docking is still largely at the theoretical stage and there is still considerable scope for the development of methodology [22,23].

The goal of predictive protein–protein docking [24] is to predict the 3D arrangement of a protein–protein complex from the coordinates of its component molecules, being an accurate prediction the one that will point out most of the residue-residue contacts involved in the target interaction. Usually, this involves an exhaustively searching of the rotational and translational space of one protein with respect to the other, resulting in a six dimensional search. Hence, there are three key ingredients in the docking: representation of the system, conformational space search, and ranking of potential solutions [21]. Although these can vary, the protein–protein docking contains certain problems common to all procedures: “searching and scoring” [25]. Therefore, “searching” is how to accurately describe the energy function of a given protein–protein complex and “scoring” is how to obtain the global minimum energy structure of the complex using the energy function [21]

Protein–protein docking studies originated a very complete review [21] and are a subject of study in your lab. We are currently trying to find new ways to rank the solutions proposed by one of the best softwares in literature (HADDOCK) and achieve a good docking structure [25-30].

Alanine Scanning Mutagenesis (ASM)

Since its initial application to human growth hormone and the growth hormone binding protein, alanine scanning mutagenesis continues to be a valuable procedure for both hot spot detection and analysis of a wide range of protein–protein interfaces. Although slow and labour-intensive, alanine-scanning mutagenesis is the most trendy method for mapping functional epitopes, as alanine substitutions remove side-chain atoms past the β -carbon without introducing additional conformational freedom. With the application of this methodological approach, it has been found that there is a highly uneven distribution of en-

energetic contributions of individual residues across each interface, and that only a few key residues do contribute significantly to the binding free energy of protein–protein complexes: the hot spots [31].

Hot spots have been defined as those sites where alanine mutations cause a significant increase in the binding free energy of at least $2.0 \text{ kcal mol}^{-1}$. To have a strong impact in protein building the binding free energy should be higher than 4 kcal mol^{-1} (3 orders of magnitude in the binding affinity constant). However, residues whose mutation results in such large differences are quite unusual, and the threshold for the hot spots had to be lowered to 2 kcal mol^{-1} in order to get enough data for statistical analysis. Systematic analysis of hot spots has shown a non-random composition: tryptophan (21.0%), arginine (13.3%) and tyrosine (12.3%) [31].

Even though it is very important to develop an accurate, predictive computational methodology for alanine scanning mutagenesis, capable of reproducing and interpreting the experimental mutagenesis values, until recently the success rates had been modest. Two of the major problems were the fact that alanine mutation of charged amino acids usually generates values in disagreement with the experimental ones, and the fact that the computational time involved is much too high to permit a systematic mutagenesis of protein-protein interfaces. Thus, having as a basis the Molecular Mechanics Poisson-Boltzman Surface Area (MM-PBSA) approach, we have focussed our attention in ways to decrease the computational time involved, as well as in techniques that enable the achievement of the chemical accuracy of roughly 1 kcal mol^{-1} [32-39].

So, we developed a fully atomistic computational methodological approach schematized in Figure 8.1 that consists in a computational Molecular Dynamics simulation protocol performed in a continuum medium using the Generalized Born Solvation Model of the wild-type system. The post-processing treatment of the wild-type allows the calculation of the free binding energy of the mutant complex and all the monomers involved. There are 20 alpha amino acids commonly found in proteins and they can be divided into basically four groups according to the structure of the side chain: non-polar and neutral (valine,

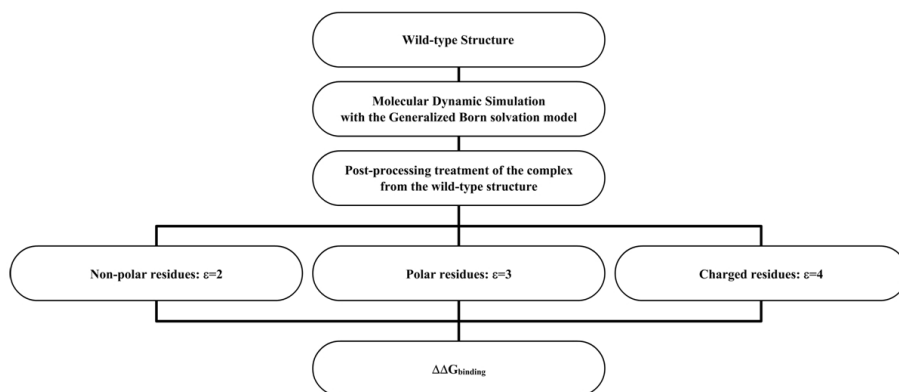


Figure 8.1. Resume of the methodological approach for computational alanine screening mutagenesis.

alanine, leucine, isoleucine, phenylalanine, proline, glycine, methionine and tryptophan), polar and neutral (asparagine, glutamine, cysteine, tyrosine, serine and threonine), acidic and charged (aspartic acid and glutamic acid), basic and charged (lysine, arginine, and histidine). As histidine can be uncharged or charged at physiological pH we have grouped this residue with lysine and arginine at the basic and charged amino acids. Recalling that we used only one trajectory for the computational energy analyses, it is important to highlight that side chain reorientation is not included explicitly in the formalism. As amino acid polarity increases, the structural effect beyond the neighbour residues also increases, and the conformational reorganization after alanine mutagenesis should be more extensive. This reorganization is not explicitly taken into account in the single trajectory protocols but its effect can be implicitly included by raising the internal dielectric constant. It is not possible to know the correct internal dielectric constant value that should be used because it depends on the mutated amino acid and the interacting residues. Nevertheless, we have noticed that by using only an internal dielectric constant set of three different values, exclusively characteristic of the mutated amino acid (2 for the non-polar amino acids, 3 for the polar residues and 4 for the charged amino acids), it was possible to obtain an excellent agreement with the experimental results for the $\Delta\Delta G_{\text{binding}}$ values. If we consider a deviation of $\pm 1.4 \text{ kcal mol}^{-1}$ from the experimental value as an

accurate result, we have an overall success rate of 82%, a 82% success rate for hot-spots [32-39].

8.4.2 Protein-Ligand Studies

Protein-Ligand Docking- MADAMM as an example

Proteins are an essential part of the organisms and participate in virtually every process within cells. A vast number of these processes require that small molecules bind to specific spots of these macromolecules. These molecules can act as switches to turn on or off a protein function, or can be the substrates of a particular chemical reaction that is catalyzed by a specific protein. Understanding the mechanism by which proteins associate and interact with small molecules, has thus become a subject of paramount importance in drug discovery. Conventional experimental techniques for obtaining detailed structural information about protein-ligand complexes are time and resource intensive. To overcome these limitations, several computational methodologies and algorithms have emerged in the last 10 years endeavoring to foresee and improve the understanding of this difficult-to-obtain structural information. These techniques are normally defined as protein-ligand docking and predict as well as rank the structure(s) arising from the association between a given ligand and a target protein of known 3D structure.

Generally speaking, as we have previously stated, all molecular docking methodologies are composed by two different algorithms: the search algorithm and the scoring function. Despite the apparent simplicity of these methodologies, they have several hidden weaknesses and present a number of problems from the computational point of view. One of the major problems arises from the tremendous complexity of the system, from which result hundreds of thousands of degrees of freedom that need to be analyzed, requiring huge computational resources. Furthermore, the combination of the energetic forces acting on the binding process is not-completely-known or/and it is difficult to calculate. Therefore, different simplifications are imposed to these methodologies to turn them fast, accurate, and attractive in different situations.

The degree and number of approximations upon which these theories are based on have thus become the major cornerstone issue in this field. Most of the simplifying assumptions are helpful in order to reduce the computation time, but they can also lead to unusable results [40]. Therefore, the correct balance between these two aspects has become the key of success in this field.

With respect to the dynamics aspects of molecular recognition, most of the molecular docking methodologies lie along a spectrum of models bound by the lock-and-key and induced-fit theories for ligand binding. In such models, the receptor is treated as a rigid body and only in the second one the translation, rotation, and torsion degrees of freedom are calculated. During the last decade, several protein-ligand docking algorithms based on these simplifications have been successfully applied in several problems [41-45]. Despite the breathtaking advances in the field and the widespread application of these methods, several downsides still exist. Particularly, protein flexibility is a major hurdle in current protein-ligand docking efforts that needs to be more efficiently accounted for.

Many programs have been developed in the last 5 years that account for protein flexibility in protein-ligand docking methodologies. All of them have their own merits and shortcomings, and reveal that accounting for protein flexibility in protein-ligand docking algorithms is still challenging. One of the latest is MADAMM, a multi staged Docking with an Automated Molecular Modeling protocol [13]. This program is a new molecular docking protocol that allows introducing a certain degree of flexibility (as much as we want/need) to the receptor and full flexibility to the ligand, without requiring an excessive time of computation in the full process. This docking software has shown excellent results in several studies, in which standard and popular docking software failed to achieve the correct result. To demonstrate the potential and capabilities of the MADAMM protocol, in Figure 8.2 we present our attempts to dock the progesterone to the active site of monoclonal antiprogestosterone antibody DB3. Looking at the active site region of the unbound and bound structures of the receptor (A—dark blue and B—light blue) we can see that Trp100 adopts two distinct conformations. In the unbound form, it is facing to the center of the active site,

whereas in the bound form it is displaced to the right hand side. This small, but crucial conformation rearrangement is sufficient to generate a faulty result when we try to dock the ligand to the active site region of the unbound structure, using standard docking software (A–black). This result is not dependent on the limitations of the search algorithm or scoring function of the docking algorithms. It simply results from the conformation adopted by Trp100, which in the active site of the unbound structure occupies the space that is required for the correct binding of the ligand (as it can be observed analyzing the conformation of Thr100 in the bound structure).

When the MADAMM protocol was applied to this case study, we were able to flexibilize several residues in the region of the active site, including Thr100. After the docking procedure, several complexes were obtained with the ligand bound in different conformations to the active site of the receptor. Each complex was subsequently subjected to a set of minimizations and small dynamics jobs that were recursively ranked and clustered in distinct groups taking into account the protein-ligand affinity. After a set of cycles, the top scored solutions were selected. The best solution is displayed in Figure 8.2 (D–Yellow). This structure almost resembles what is found in the unbound X-ray structure, showing only a small RMSD of 0.13 Å.

This case study has shown that MADAMM can efficiently accomplish a good compromise between what can be predicted and what is obtained experimentally. This means that this protocol can be viewed as a powerful tool to understand protein-ligand interactions, especially on those cases where few or no experimental structures of the complexes are available. The same study also alerts for the limitations of the standard docking software especially on those cases where the orientation of particular residues at the protein-ligand interface is neglected. The results have shown that the conformations adopted by some residues in the region of the active site can have a crucial influence on the way the ligand interacts with the receptor. Disregarding its presence can be responsible for most of the false positives results that are obtained with the available rigid-based docking software.

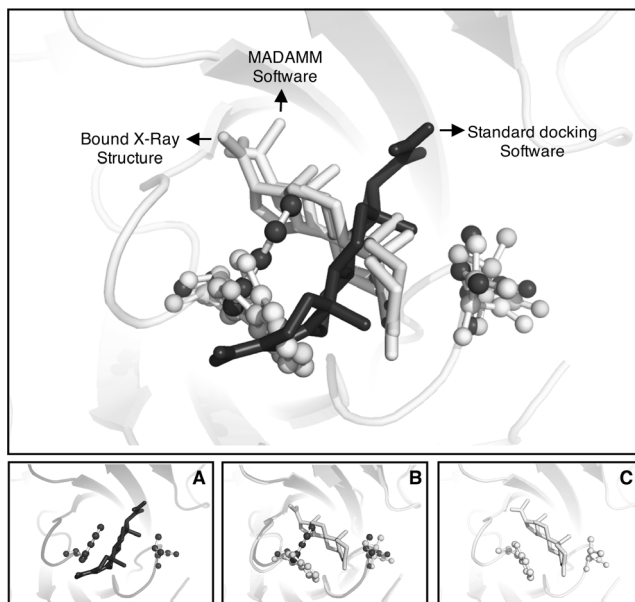


Figure 8.2. Dark blue: X-ray structure of the unbound form of the protein. Light blue: co-crystallized X-ray structure with the bound substrate. Yellow: MADAMM result. Black: standard docking result (using the GOLD software).

Design of Inhibitors and Energy Assessment

Efficient and accurate calculation of protein-ligand affinities is another focus of our group. During the past few years we have studied the ability of the enzymes, namely enzymes involved in lethal diseases, to bind preferentially to a set of ligands (substrates, inhibitors, new inhibitors, proteins). To quantify the preferential binding of a set of ligands, we have calculated values of free energy of binding, using a complex but accurate computational method, called Thermodynamic Integration (TI) [46-49], and/or the more computationally accessible MMPBSA [50] method. TI is a rigorous method for calculating free energies, but requires extremely time consuming simulations, even with a large high-performance computer cluster. The faster and simpler, but still accurate, MMPBSA method is many times used as an alternative to TI.

We have been particularly interested in protein-ligand studies with HIV-1 Protease. All treatments for HIV-1 infected persons include, at least, one Protease inhibitor. Based on Protease-ligand studies we have published a new theory for

HIV-1 Protease recognition [51] and developed new inhibitors for HIV-1 Protease using other inhibitors (Nelfinavir [52], Amprenavir) as leads. The understanding of the mechanism of Substrate recognition by HIV-1 Protease is a key step for drug design targeting the enzyme. In this section we present three new inhibitors, designed with computational tools, with greater affinity for HIV-1 Protease than Nelfinavir itself.

Nelfinavir (Viracept®) is a potent, orally bioavailable inhibitor of the enzyme HIV-1 Protease, which has been developed through structure-based drug design projects and has been approved worldwide for the treatment of HIV infected patients. However, HIV-1 develops drug-resistance and the affinity of Nelfinavir for the binding pocket of Protease is decreased. We have presented three new variants (Figure 8.3) of Nelfinavir, designed with computational tools, with greater affinity for HIV-1 Protease than Nelfinavir itself. In order to increase the inhibitory efficiency, we have introduced rational modifications in Nelfinavir, optimizing its affinity to the most conserved amino acids in Protease. The new inhibitors interact more favourably with well-conserved residues, Leu23, Ala28, Gly49, Arg87, and Asp29, which cannot mutate, as the mutants would render the Protease catalytically inactive [53]. Figure 8.3 shows a schematic representation of the binding region for Nelfinavir with which the substitutions introduced in the inhibitors are meant to interact. The dashed lines give an idea of the location of the empty pockets between the well-conserved amino acids and the inhibitors. Figure 8.3 shows also three examples for which significant increases in affinity can still be achieved without changing the overall structure, molecular mass and hydrophobicity of the inhibitors, thus preserving their very favourable ADME properties. Minimization and molecular dynamics simulations [46] have been carried out on the complexes, HIV-1 Protease with Nelfinavir and subsequently with the new inhibitors, in order to analyze the behavior of the systems. To quantify the affinity of the new inhibitors relatively to Nelfinavir, we have calculated values of free energy of binding, first using the TI approach and subsequently the less computationally demanding MMPBSA [50] methodology. The values for the binding free energy difference presented (Figure 8.3) are val-

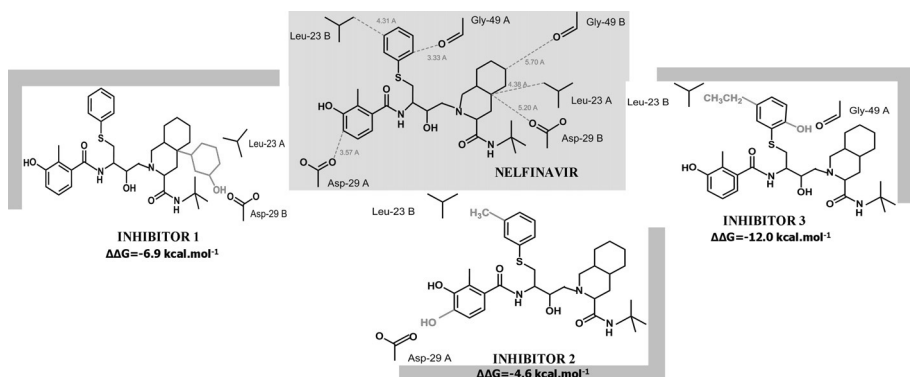


Figure 8.3. Three new inhibitors; based on Nelfinavir as lead, which have a higher affinity *in silico* for Protease than Nelfinavir (the negatives binding free energy difference $\Delta\Delta G$ reflect this).

idated by the correct reproduction of the experimental binding free energy for Nelfinavir.

This example shows how powerful the design of inhibitors can be for rational lead optimisation, avoiding handling dangerous and toxic materials and greatly reducing experimental costs. There have been dramatic successes with drug design.

8.5 Enzymatic Mechanisms

In addition to the several applications outlined in the preceding sections, a particularly strong and promising area in the field of computational proteomics is that of computational enzymology, *i.e.* the use of computational methods to study enzymatic activity, in particular catalytic pathways. In fact, computational methods allow the detailed analysis of important enzymatic reaction mechanisms, providing atomistic insight into very specific processes of highly biological significance, often very difficult to tackle by means of experimental studies alone. While a vast number of experimental techniques are normally employed in the study of reaction mechanism, from spectroscopic experiments and mutagenesis studies to kinetic evaluations, no experimental technique, by itself, can normally give a full view of an entire catalytic pathway. In addition, the interplay between different experimental methodologies is often not peaceful, with differ-

ent techniques frequently pointing to different (at least apparently) conclusions. Computational methods often offer an unbiased way to concert and validate the information obtained from different experimental methods, providing also the missing pieces. So, in a process in which something always seems to be missing computational methods often have the final word, which frequently comes in the form of a structure for the transition state intermediate and of the corresponding energy barrier, indispensable requirements to fully assess the viability of a mechanistic proposal.

During the last decade, we have studied a large number of enzymatic catalytic mechanisms. From these, we would like to highlight 5 particularly important biological systems, in which our effort helped to shape and validate the presently accepted pathway. These are the radical enzyme ribonucleotide reductase, the very important glutathione transferase, thioredoxine, glycosidase, and the Zn metalloenzyme farnesyltransferase.

8.5.1 Ribonuclease Reductase (RNR)

Nowadays, with the exception of viroids and virusoids, all modern organisms have their genetic information encoded into a DNA molecule. The exploit and maintenance of this information depends on the availability of deoxyribonucleotides. These compounds cannot be obtained by external sources and the only way by which they can be synthesized is through the reduction of ribonucleotides into deoxyribonucleotides. This reaction is strictly conserved in all living organisms and is catalyzed by a peculiar enzyme called ribonucleotide reductase (RNR). This key role makes RNR a rate limiting step in DNA replication and repair, turning it into an attractive target for antitumor, antiviral and antibacterial therapies [54,55]

RNRs are mechanistically fascinating proteins because of their free radical chemistry, unusual metallocofactors and complex regulatory mechanisms. In the past 20 years, several studies have been addressed at this enzyme, aiming to understand its peculiar mode of action. However, and despite its success as a target in many cancer therapies and HIV/bacterial treatments, the underlying

mechanisms by which this enzyme is either inhibited or reduces ribonucleotides into deoxyribonucleotides is poorly understood taking into account the information available from the experimental data. Great advances in this field were achieved when RNRs related mechanisms were studied by theoretical and computational methodologies. These methods and particularly the quantum chemical calculations have become an indispensable tool in this field, allowing to solve a puzzle of many unrelated and disconnect pieces that were found out by structural biology studies and biochemical experiments. The main advantage of the computational methods is that they can provide structural information on transition states and snapshots of molecules in the act of reaction, whose direct detection is not possible or is difficult to obtain by normal physical methods. This is particularly important in RNR since it is a radical enzyme, and these methods enable to identify and characterize unstable intermediates at an atomic detail.

During the past 10 years, our group has developed a comprehensive knowledge and thorough understanding of every process involved in the normal RNR functioning and in its inhibition mechanisms, using theoretical and computational means. In this process, we began by exploring different strategies to model the active site of this enzyme. A good balance between the size of the system and accuracy of the results is always difficult to achieve in computational chemistry. This is especially true when we aim to study biological systems where the results can be largely influenced by size of the model that is used. Therefore, we started to study RNR testing *several models of the active site that range from 20 atoms [56], 300 atoms [57] to the full R1 monomer (that contains 30000 atoms) [58]. To complete this task, hybrid methodologies, and particularly ONIOM approach*, were used with the larger models. These methodologies allow to divide the model in different layers that can be treated with different theoretical levels. The atoms directly involved in the reaction are calculated with higher theoretical levels and the remaining ones with a lower theoretical level. This approach has proven to be most successful, allowing us to tune the best approach to study this enzyme, from a computational point of view. This information

was then used to explore all relevant chemical pathways that could be involved in the catalytic mechanism [56,59] of RNR as well as in the inhibitory mechanism of several substrate analogues inhibitors that inactivate the function of the enzyme [60-67]. Some of the results obtained through computational methodologies were pioneers in the RNR field and later confirmed and acknowledged by experimental findings.

Theoretical and computational methodologies were therefore a major groundbreaker in this field allowing to unravel the unsolved mysteries around RNR. Without their value contribution it would be very difficult to understand, explain and predict most of the knowledge that is currently available. All the work developed in this area can now be used to understand, which are the most important checkpoints that must be triggered during the inhibitory mechanism in order to enhance and improve the potency of a RNR inhibitor, or develop new ones. These results have thus created a trend in which researchers can now base their studies to conduct a more rational drug design approach in the development of novel drugs against RNR.

8.5.2 Glutathione Transferase

Glutathione transferases (GSTs) have been known as fundamental enzymes of the cell detoxification system for almost fifty years now. The cell detoxification mechanism of xenobiotic and endobiotic compounds follows a series of different steps. In the first step toxic compounds are converted into strong electrophiles by the mixed-function oxidation activity of cytochrome P-450. Those electrophiles are subsequently transformed into more soluble and less toxic substrates, by conjugation with glutathione (GSH) due to the catalytic activity of GST. Finally, these resulting conjugates can be recognized by ATP-dependent transmembrane pumps, such as P-glicoproteins and MRP family proteins, and consequently expelled from the cell. On the other hand, GSTs have also an active role in byosynthesis, cell signaling pathways [68], and are related to human diseases such as Parkinson's [69,70], Alzheimer's [70-74], atherosclerosis [75-77], liver cirrhosis [78,79], aging [80] and cataract formation [81]. The reaction cata-

lyzed by GST consists in the nucleophilic addition of the sulfur thiolate of GSH to a wide range of electrophilic compounds. When GSH binds to the GST G-site active center the pKa of the thiol group drops from 9.1 to about 6.2-6.6 pH units [82], promoting its deprotonation. After GSH activation, the nucleophilic sulphur atom attacks the electrophilic toxic compound present in the H-site active center, producing a less dangerous compound.

Despite cytosolic GST's being vastly studied by the scientific community, the main aspects of the catalytic events are still to be understood. Recently, using as a model the GSTA1-1 enzyme, we proposed a GSH activation mechanism consistent with the experimental data [83,84]. Our studies have demonstrated that a water molecule is able to assist a proton transfer between GSH thiol and alpha carboxylic groups with an activation energy of $13.39 \text{ kcal mol}^{-1}$, after a first conformational rearrangement of GSH ($\Delta G_{\text{conf}} = -1.62 \text{ kcal mol}^{-1}$) that allows the water molecule to interact simultaneously with both the thiol and the glutamyl alpha carboxylate groups. This energy barrier is in agreement with the experimental kinetics for the GST catalyzed GSH-CNDB conjugation, a common electrophilic substrate ($k_{\text{cat}} = 88 \pm 3 \text{ s}^{-1}$, $\Delta G^{\ddagger} = 15.06 \text{ kcal mol}^{-1}$ [85]). Figure 8.4 resumes all the events. We also demonstrated that a catalysed direct proton transfer between the two GSH active groups is very unlikely (energy barrier = $15.88 \text{ kcal mol}^{-1}$) for the GSH conformational rearrangement, plus $19.44 \text{ kcal mol}^{-1}$ for the actual proton transfer). In order to study the free energy associated with the initial GSH conformational rearrangement we calculated its potential of mean force (PMF) using the umbrella sampling method. All the molecular dynamics simulations and subsequent analyses were carried out using the Gromacs software package conjugated with the AMBER99 force field [86-89]. To study the actual proton transfer an ONIOM model of the GSH G-site active center was built. Then we performed a scan of the water proton approach to the most suitable GSH glutamate alpha carboxylate oxygen. With the three stationary points we were able to calculate the proton transfer activation energy, ΔG .

Arg15 is a strictly conserved active site residue in class Alpha GSTs [90],

however very little is known about its role in catalysis. In order to clarify the importance of this conserved residue we analyzed the activation energy barrier and structural details associated with the GSTA1-1 mutants R15A, R15R ϵ , η -c (an Arg residue with the ϵ, η -nitrogens substituted by carbons) and R15Rneutral (a neutral Arg residue due to the addition of a hydride in the ζ -carbon) [91]. A similar mechanism to the one used in our GSH activation proposal was used. The energy barriers associated are in agreement with the experimental values available [90] and can be analyzed in Figure 8.4. The structural analyses of the enzymes allow concluding that in the wild type enzyme GSH binds to the G-site pocket in a specific arrangement not seen in the mutants. The charged Arg15 establishes a strong ion-dipole interaction and a hydrogen bond with the GSH cysteine mainchain, which dictates the arrangement of the substrate. For the R15Rneutral mutant, hydrogen bond interactions are still possible to be established between the residue 15 sidechain ϵ, η nitrogen atoms and the GSH cysteine mainchain carbonyl group. However, without the positive charge, the spatial arrangement of residue 15 changes leading to a new, not catalytically efficient, GSH conformation. In the other mutants this new GSH conformation is also observed and is supported by the experimental data available for the mutant R15A (K_M GSH is 10-fold increased relatively to wildtype enzyme [90]). The volume of Arg15 does not seem to be as catalytically relevant as the charge. The R15Rneutral mutant residue 15 has the same volume as the wildtype Arg15, however this mutant shows an energy barrier similar with the smaller R15A mutant.

8.5.3 Thioredoxins (Trx)

The enzymes of the thioredoxin (Trx) family fulfill a wide range of physiological functions. Although they are structurally similar and have a similar CXYC active site motif, with identical environment and stereochemical properties, where C stands for cysteine and XY for two variable residues, the redox potential and pKa of the cysteine pair varies widely across the family. As a consequence, each family member promotes oxidation or reduction reactions, or

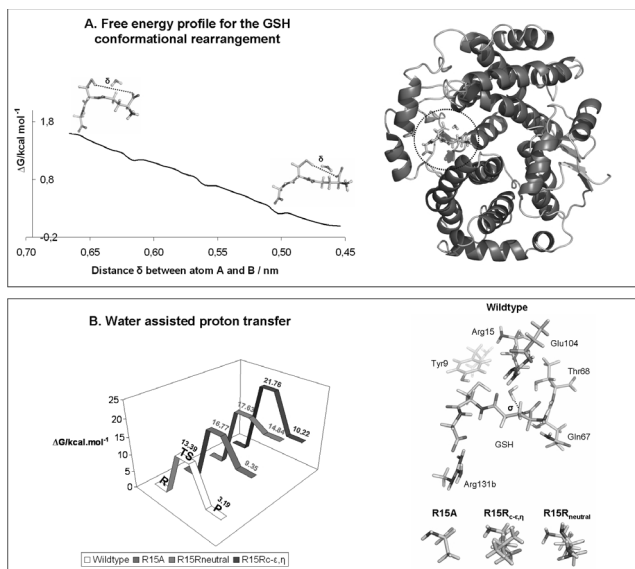


Figure 8.4. GSTA1-1 water assisted GSH activation mechanism.

A – Distance δ was steadily decreased in each PMF window. The curve represents the sum of the entire data obtained from the PMF forward and backward processes. On the right hand side a detailed view of the GSTA1-1 complex, in which GSH has been circled, is represented.

B – Wild type and mutant enzymes water assisted proton transfer Gibbs energies of the three stationary points: Reagent (R), Transition State (TS) and Product (P). Energies calculated with DFT, functional B3LYP and basis set 6-311++G(2d,2p). On the right hand side the G-site model is represented along with distance σ , decreased at each scan point.

even isomerization reactions.

We carried out a set of quantum mechanical calculations in active site models to gain more understanding on the molecular-level origin of the differentiation of the properties across the family. We theoretically explored the reaction mechanisms, both in the gas phase and in water, using density functional theory [92,93]. The mechanism of disulfide reduction involves two consecutive thiol-disulfide exchange reactions, that is, nucleophilic substitutions at sulfur (SN2@S): first, by the nucleophilic cysteine-thiolate group (Cys_{nuc}) at a sulfur atom of the disulfide substrate and, second, by the other cysteine-thiolate group (called buried cysteine, Cys_{bur}) at the sulfur atom of the Cys_{nuc}.

The obtained results, together with earlier QM/MM ONIOM calculations in which absolute and relative pKas of the nucleophilic cysteines for Trx and DsbA

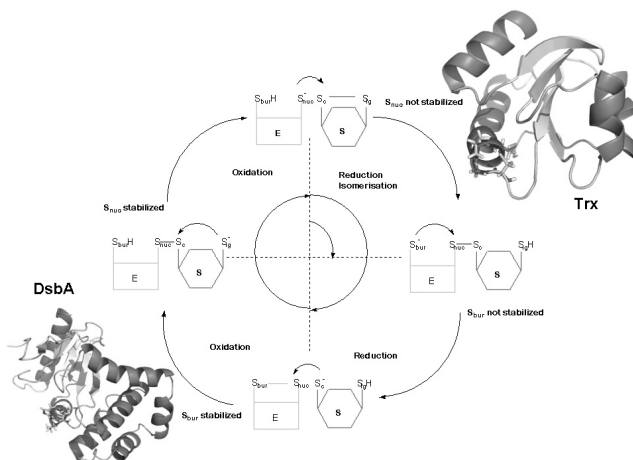


Figure 8.5. DFT calculations on small models and larger ONIOM models gave rise to a consistent line of evidence that thiol-disulfide exchange reactions regulation across the thioredoxin family are promoted by the differential stabilization of both active site cysteines.

were calculated and the possible causes for thiolate stabilization were investigated [94,95], gave rise to a consistent line of evidence, which points to the fact that both active site cysteines play an important role in the differentiation. Contrary to what was assumed, differentiation is not achieved through a different stabilization of the solvent exposed cysteine but, instead, through a fine tuning of the nucleophilicity of both active site cysteines [94,95]. The feasibility of shifting the chemical equilibrium toward oxidation, reduction, or isomerization only through subtle electrostatic effects is quite unusual, and it relies on the inherent thermoneutrality of the catalytic steps carried out by a set of chemically equivalent entities all of which are cysteine thiolates.

8.5.4 Beta-Galactosidase

Carbohydrates are involved in many cellular processes, being crucial to life. Glycosidases constitute a vast family of enzymes that catalyze the breaking and formation of glycosidic bonds. β -Galactosidase is a retaining glycosidase that catalyzes both the hydrolytic breaking of the very stable glycosidic bond of lactose, as well as a series of transglycosylation reactions [96]. It has great bi-

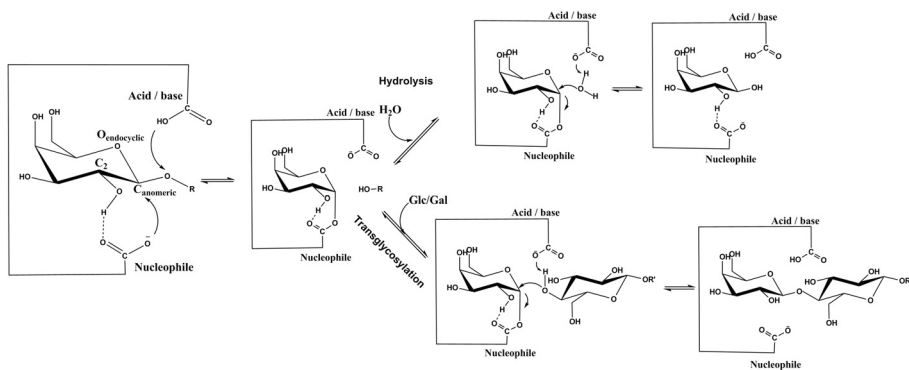


Figure 8.6. Representation of the catalytic mechanism for the hydrolysis/transglycosylation reactions, catalyzed by retaining Glycosidases.

otechnological interest for the food and pharmaceutical industries, where it is used to catalyze the large-scale production of oligosaccharides [97]. To understand the atomic-level factors that determine the outcome of the reaction (hydrolysis/transglycosylation) and the yield of each of the many transglycosylation products, an atomic level study of this catalytic mechanism was performed, using DFT and Molecular Mechanics as theoretical levels [97-100]. In order to shed some light over these topics, we have developed a model system that includes a simplified reaction center and a small substrate molecule to capture the intrinsic reactivity of the active-site motif. A very small enzyme model, containing only the two reactive carboxylic amino acids and a small substrate was used in DFT calculations [99,100]. Our results were able to confirm and provide molecular-level detail to the general mechanism proposed for this family of enzymes (Figure 8.6): a double-displacement mechanism involving a glycosylation and a deglycosylation step, in which one of these key carboxylic acids acts as a nucleophile and the other as an acid/base catalyst, with the reaction proceeding via a covalent intermediate. In the transition states (TSs), a very interesting and short hydrogen bridge is formed between the nucleophilic residue of the enzyme and the HO – C₂ of the sugar ring. Our calculations reveal that the role of this hydrogen interaction is to lower the energy of the TSs by *circa* 5 kcal mol⁻¹, contributing considerably to the stabilization of these states in both steps. A

structural rearrangement of the sugar ring is also observed; therefore, we suggest that the hydrogen bridge facilitates the change from the typical chair form to the half-chair conformation at this stage, which helps to stabilize the nascent oxocarbenium ion.

The performance of a wide variety of DFT functionals was tested in order to choose the one that better describes the thermodynamics and kinetics of our model system. The results have shown that the obtained energies indeed depend on the particular density functional employed. In our case, the correct choice of the functional was crucial as the most widely used have resulted in uncertainty in the activations energies values of over 8 kcal mol^{-1} . Comparison with the very high level calculations (MP2, MP3, MP4 and QCISD(T)) allowed for the identification of the most accurate functionals (BB1K, MPW1K and MPWB1K) for this particular reaction. Based on these conclusions, the ONIOM method (BB1K:AMBER//B3LYP:AMBER calculations) was employed to address such a large enzymatic system [98]. This enzymatic model can efficiently account for the restrained mobility of the reactive residues, as well as the long-range enzyme-substrate interactions. Figure 8.7 shows the enzymatic model studied, which includes a 15 \AA radius of the amino acids around lactose. The high-level layer (treated with quantum mechanics) is also represented. QM/MM calculations demonstrate the crucial importance of the enzyme scaffolding beyond the first-shell amino acids in the stabilization of TSs, indicating the need to include the enzyme explicitly in computational studies. Our results suggest that the role of the magnesium ion in the catalytic reaction is to lower the activation barrier by $14.9 \text{ kcal mol}^{-1}$, contributing considerably to the stabilization of the TS structure. Comparison of the energetic values for the different transglycosylation reactions ($\beta(1-3)$, $\beta(1-4)$ and $\beta(1-6)$) studied shows that these reactions are all very similar from a kinetic perspective, which seems reasonable given the similarity in the bond-breaking/bond-forming processes. However, thermodynamically, they are quite dissimilar: the formation of $\beta(1-3)$ glycosidic linkages is thermodynamically very unfavorable, whilst the formation of $\beta(1-6)$ glycosidic bonds is the most favored, in total agreement with the enantioselectivity

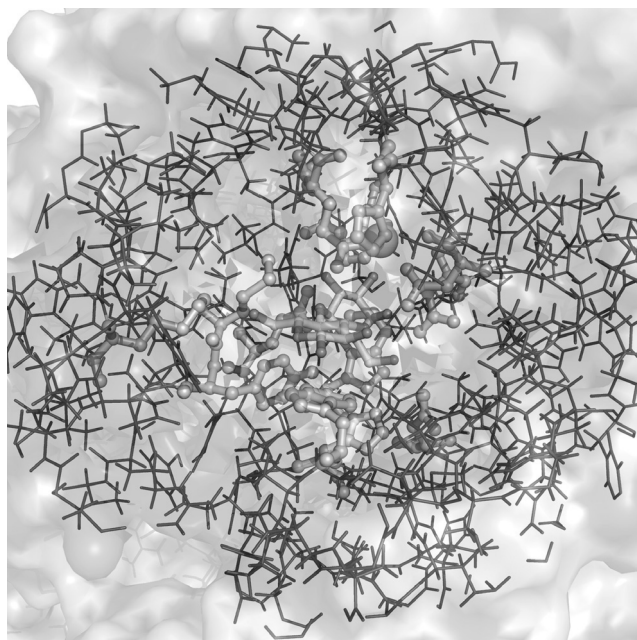


Figure 8.7. Representation of the enzymatic model (colored blue), which includes a 15 Å radius of the amino acids around lactose (shown in green and red). The magnesium ion is the yellow sphere, whereas the high-level layer (treated with quantum mechanics) is colored in orange.

observed experimentally.

As the β -Galactosidase from *E. coli* is an enzyme commonly used in molecular biology research, a complete knowledge of the different reaction pathways is crucial to the development of new chromophore substrates. Furthermore, these results help to improve the efficiency of large-scale industrial design and synthesis of new inhibitors and carbohydrates for both the pharmaceutical and food industries.

8.5.5 Farnesyltransferase

In addition to the enzymatic studies outlined above, computational methods provide particularly important insights into the study of metalloenzymes, acting as a bridge between the several spectroscopic methods normally employed to handle such systems.

In the case of the Zinc metalloenzyme FTase, for example, the large body of

experimental results available from kinetic studies on mutant FTase species and X-ray crystallography, and the information obtained from the relatively limited range of spectroscopic methods directly applicable to biological Zinc complexes, were insufficient to allow an univocal atomic-level interpretation of the catalytic mechanism followed by this enzyme [101-103]. Computational methods can be used in such cases to go beyond the traditional limitations of standard experimental studies, providing the missing pieces [104-106].

We have used first principles quantum mechanics (B3LYP) and ONIOM (B3LYP:PM3) to analyze the several possible Zn coordination modes suggested from the apparently contradicting experimental studies on the FTase resting state. Interestingly, we have found that both coordination proposals discussed in the literature – a tetracoordinated Zn sphere with a monodentate Asp ligand and water molecules versus a bidentate Asp proposal without water – were in agreement with the EXAFS structural data available and could be valid. In addition, our computational studies showed that both alternatives were at a remarkably close energetic proximity and that a conversion between the two could take place with a very small energetic barrier at room temperature. These conclusions allowed us to develop a new and unified paradigm regarding the nature of the Zn coordination sphere in FTase and the identity of the ligands present [107], considering that both alternatives exist at equilibrium, and that such process is achieved through a carboxylate-shift mechanism, where a monodentate to bidentate change (and vice-versa) by the Asp ligand helps to compensate ligand entrance (or exit) processes [108].

This main idea was later applied into the study of the several Zn sphere formed along the FTase catalytic mechanism, also with small model QM and/or QM:QM calculations [109-111], paving the way into an understanding of the more complex catalytic step, which involved a very significant conformational rearrangement of one of the substrate inside the enzyme active-site and which required significantly larger models for accurate computational modeling.

Our mechanistic studies on this enzyme culminated with the finding of the transition state intermediate of this highly concerted step [112], a structure that

could provide a blueprint for the design of more potent and specific FTase inhibitors.

8.6 Density Functional Benchmarking

According to the Hohenberg-Kohn theorems, every electronic property of a ground-state, non degenerate system, can be directly calculated by a functional where the unique variable is the electronic density [113]. Hence, opposed to wave function theories of electronic structure which treat each electron in the chemical system as a single entity, density functional theory works with the electron density as a whole. Here lies the great power of DFT, its simplicity allows its application to very large systems, with dozens or even hundredths of atoms, at much lesser computational effort than other methods where electronic correlation is also accounted for [114]. But what is the problem with DFT? In principle, DFT is exact, as the functional whom relates electron density with energy was proven to exist; in practice, the theory is only an approximation, as the functional is not fully known. For the electronic energy functional, the problematic term is the one used to calculate the exchange-correlation energy, related with the punctual interaction between electrons, either of the same spin (exchange), or opposite spin (correlation). All of the problems with DFT come from this limitation. As this term is not known, dozens of exchange-correlation functionals spawned in the field, along the years, trying to make up for this void. They are distributed among some groups, increasing in complexity: LDA (Local Density Approximation), GGA (Generalized Gradient Approximation), Meta-GGA, Hybrid-GGA and Hybrid-Meta-GGA [3,115,116]. Mostly, the functionals have empirical motivation, as well as empirical parameters, and although as a general trend more complex functionals are better, this is not an exact rule. The empirical character of the functionals make them unfit to apply outside certain chemical problems, to which they were not parameterized. Being so, there is no theoretical way of telling which functional is better for a determined system, and the only way to test it is by doing a functionals benchmarking study. Supporting this consideration one could cite a modest number of benchmarking studies,

each one aiming for certain chemical properties: geometry [117,118], kinetic barriers and thermochemistry [119], binding and dissociation energies [119], non-bonded interactions [120] There are three major concepts in a benchmarking study, each one of them with their proper considerations: *(i)* The model - The model system chosen to do the benchmarking should be representative of the subject being studied, as usually one is not interested in that system in particular but in a certain detail of it, such as hydrogen bonding or a phosphodiester bond hydrolysis. Furthermore, the model should be small enough, allowing the use of very accurate reference methods, which are, by definition, computationally costly; *(ii)* The reference value - The reference value should be as accurate as possibly for the system in question. Here, the use of composite methods can be quite resourceful. These methods take advantage of error cancellations by stating, for example, that the difference between the correlation energy at MP2 level and CCSD(T) is independent of the basis-set. Furthermore, there are various methods who emulate the use of a complete basis-set at an acceptable range of error and computer demands. By conjugating these two types of approximations one can proudly state in an abstract an energy reference value calculated at a CCSD(T)/CBS level for a system of twenty atoms; *(iii)* The functionals - Regarding the choice of the functionals, one could opt by testing them all, although that is hardly a good path as there are a huge number of them. Instead, a representative group should be created, one that includes functionals from all types (GGA, M-GGA) and preferentially the most recent ones. After that, in order to rank the functionals one should compare their results with the results from the reference methods.

At the end of the Benchmarking one should be able to say what functional is more adequate to evaluate a certain chemical property. Provided with this information, another researcher can wisely choose the functional for their study without going for the trendy functional - B3LYP -, the most typical situation, or without the need of doing a functional benchmarking study himself.

Benchmarking of DFT functionals for the hydrolysis of phosphodiester bonds

In our group we work mainly with enzymes and their catalytic mechanisms. These systems, large as they are, tend to be divided into layers, being the outer layer described either by molecular mechanics or semi-empirical methods, and the inner layer by DFT. Most of the times, we stand before the mentioned problem of not knowing the best functional to study the enzymatic reaction. Hence, we usually do a benchmarking study to fix this. In a recent work [121], we take dimethylphosphate hydrolysis as a model for phosphodiester bonds hydrolysis. These kinds of reactions are present on many enzymes involving DNA, RNA and phospholipids. Therefore, this study has great scope and could be applied to many important biological systems. In our particular case, the main motivation behind the study was the 3' end processing reaction of HIV Integrase.

In the work done, we described four reactions paths, all involving dimethylphosphate as the major reactant. We varied the nucleophile, which could be a molecule of water or a hydroxide ion, and the medium that could be either implicit water or vacuum. The potential energy surface for each one of these reactions was obtained at a CCSD(T)/CBS//B3LYP/6311++G(2*d*,2*p*) level, being CCSD(T)/CBS the reference energy. Subsequently, we tested a total of 52 functionals with the obtained structures. Furthermore, the performances of HF, MP2, MP3, MP4 and CCSD were also evaluated. When comparing with the reference energy, the results showed that MPWB1K, MPW1B95 and PBE1PBE are the most accurate functionals for calculating activation and reaction energies, with MUEs (Mean Unsigned Error) below 2 kcal mol⁻¹. Concerning only activation energies, MPWB1K, MPW1B95 and B1B95 give the best results. Furthermore, we take two other important conclusions from this work: the basis-set 6-311+G(2*d*,2*p*) is the most balanced one regarding the relationship between computational time and accuracy; and the inclusion of the triples excitations on CCSD(T) has major implications in the obtained energies.

The necessity for benchmarking studies will be present all the time, as the progress in this field occurs at fast pace and the number of functionals tend to

increase daily. We hope that with this and other works, researchers can always achieve the best outcome from their experiments without being overwhelmed by the enormous amount of DFT functionals available.

References

- [1] S. F. Sousa, P. A. Fernandes, and M. J. Ramos, *J. Biol. Inorg. Chem.* **10**, 3 (2005).
- [2] S. F. Sousa, P. A. Fernandes, and M. J. Ramos, *Curr. Med. Chem.* **15**, 1478 (2008).
- [3] S. F. Sousa, P. A. Fernandes, and M. J. Ramos, *Theor. Chem. Acc.* **117**, 171 (2007).
- [4] S. F. Sousa, P. A. Fernandes, and M. J. Ramos, *Bioorg. Med. Chem.* **17**, 3369 (2009).
- [5] S. F. Sousa, P. A. Fernandes, and M. J. Ramos, *J. Phys. Chem. B* **112**, 8681 (2008).
- [6] A. T. P. Carvalho, P. A. Fernandes, and M. J. Ramos, *J. Med. Chem.* **49**, 7675 (2006).
- [7] A. T. P. Carvalho, P. A. Fernandes, and M. J. Ramos *J. Phys. Chem. B* **111**, 12032 (2007).
- [8] A. L. Demain, M. Newcomb, and J. H. D. Wu, *Microbiol. Mol. Biol. Rev.* **69**, 124 (2005).
- [9] V. M. R. Pires, J. L. Henshaw, J. A. M. Prates, D. N. Bolam, L. M. A. Ferreira, C. Fontes, B. Henrissat, A. Planas, H. J. Gilbert, and M. Czjzek, *J. Biol. Chem.* **279**, 21560 (2004).
- [10] A. B. Boraston, D. N. Bolam, H. J. Gilbert, and G. J. Davies, *Biochem. J.* **382**, 769 (2004).
- [11] A. Viegas, N. F. Bras, N. Cerqueira, P. A. Fernandes, J. A. M. Prates, C. Fontes, M. Bruix, M. J. Romao, A. L. Carvalho, M. J. Ramos, A. L. Macedo, and E. J. Cabrita, *Febs J.* **275**, 2524 (2008).
- [12] N. F. Bras, N. Cerqueira, P. A. Fernandes, and M. J. Ramos, 3rd International Theoretical Biophysics Symposium, Cetraro, ITALY, Jun 16-20, pp 2030

- (2007).
- [13] N. Cerqueira, N. F. Bras, P. A. Fernandes, and M. J. Ramos, *Proteins: Struct. Funct. Bioinf.* **74**, 192 (2009).
- [14] A. L. Carvalho, A. Goyal, J. A. M. Prates, D. N. Bolam, H. J. Gilbert, V. M. R. Pires, L. M. A. Ferreira, A. Planas, M. J. Romao, and C. Fontes, *J. Biol. Chem.* **279**, 34785 (2004).
- [15] C. A. Lipinski, F. Lombardo, B. W. Dominy, and P. J. Feeney, *Adv. Drug Delivery Rev.* **46**, 3 (2001).
- [16] D. F. Veber, S. R. Johnson, H. Y. Cheng, B. R. Smith, K. W. Ward, and K. D. Kopple, *J. Med. Chem.* **45**, 2615 (2002).
- [17] T. S. Thorsen, K. L. Madsen, N. Rebola, M. Rathje, V. Anggono, A. Bach, I. S. Moreira, N. Stuhr-Hansen, T. Dyhring, D. Peters, T. Beuming, R. Haganir, H. Weinstein, C. Mulle, K. Stromgaard, L. C. B. Ronn, and U. Gether, *Proc. Natl. Acad. Sci. U.S.A.* **107**, 413 (2010).
- [18] S. J. Wodak and J. Janin, *J. Mol. Biol.* **124**, 323 (1978).
- [19] S. J. Wodak and J. Janin, *Arch. Int. Physiol. Biochim.* **86**, 473 (1978).
- [20] S. J. Wodak and J. Janin, *Acta Crystallogr. A* **34**, S49 (1978).
- [21] I. S. Moreira, P. A. Fernandes, and M. J. Ramos, *J. Comp. Chem.* 2010, 31(2), 317.
- [22] J. Janin, K. Henrick, J. Moulton, L. Ten Eyck, M. J. E. Sternberg, S. Vajda, I. Vasker, and S. J. Wodak, *Proteins: Struct. Funct. Bioinf.* **52**, 2 (2003).
- [23] J. Janin and S. J. Wodak, *Protein Modules and Protein-Protein Interactions* **61**, 1 (2003).
- [24] Y. Han, I. S. Moreira, E. Urizar, H. Weinstein, and J. A. Javitch *Nat. Chem. Biol.* **5**, 688 (2009).
- [25] A. M. J. J. Bonvin, *Febs J.* **274**, 67 (2007).
- [26] A. D. J. van Dijk, R. Boelens, and A. M. J. J. Bonvin, *Febs J.* **272**, 249 (2005).
- [27] S. J. De Vries, A. D. J. van Dijk, M. Krzeminski, M. van Dijk, A. Thureau, V. Hsu, T. Wassenaar, and A. M. J. J. Bonvin, *Proteins: Struct. Funct. Bioinf.* **69**, 726 (2007).

- [28] C. Dominguez, R. Boelens, and A. M. J. J. Bonvin, *J. Am. Chem. Soc.* **125**, 1731 (2003).
- [29] A. D. J. van Dijk and A. M. J. J. Bonvin, *Bioinformatics* **22**, 2340 (2006).
- [30] A. D. J. van Dijk, S. J. De Vries, C. Dominguez, H. Chen, H. X. Zhou, and A. M. J. J. Bonvin, *Proteins: Struct. Funct. Bioinf.* **60**, 232 (2005).
- [31] I. S. Moreira, P. A. Fernandes, and M. J. Ramos, *Proteins: Struct. Funct. Bioinf.* **68**, 803 (2007).
- [32] I. S. Moreira, P. A. Fernandes, and M. J. Ramos, *Proteins: Struct. Funct. Bioinf.* **63**, 811 (2006).
- [33] I. S. Moreira, P. A. Fernandes, and M. J. Ramos, *J. Phys. Chem. B* **110**, 10962 (2006).
- [34] I. S. Moreira, P. A. Fernandes, and M. J. Ramos, *Theor. Chem. Acc.* **117**, 99 (2007).
- [35] I. S. Moreira, P. A. Fernandes, and M. J. Ramos, *Int. J. Quantum Chem.* **107**, 299 (2007).
- [36] I. S. Moreira, P. A. Fernandes, and M. J. Ramos, *J. Comp. Chem.* **28**, 644 (2007).
- [37] I. S. Moreira, P. A. Fernandes, and M. J. Ramos, *J. Chem. Theory Comput.* **3**, 885 (2007).
- [38] I. S. Moreira, P. A. Fernandes, and M. J. Ramos, *J. Phys. Chem. B* **111**, 2697 (2007).
- [39] I. S. Moreira, P. A. Fernandes, and M. J. Ramos, *Theor. Chem. Acc.* **120**, 533 (2008).
- [40] D. Goodsell, G. Morris, and A. Olson *J. Mol. Recognit.* **9**, 1 (1996).
- [41] S. Gupta, L. M. Rodrigues, A. P. Esteves, A. M. F. Oliveira-Campos, M. S. J. Nascimento, N. Nazareth, H. Cidade, M. P. Neves, E. Fernandes, M. Pinto, N. M. F. S. A. Cerqueira, and N. Bras, *Eur. J. Med. Chem.* **43**, 771 (2008).
- [42] M. L. Lamb, K. W. Burdick, S. Toba, M. M. Young, K. G. Skillman, X. Q. Zou, J. R. Arnold, and I. D. Kuntz, *Proteins* **42**, 296 (2001).
- [43] C. N. Cavasotto and N. Singh, *Curr. Comput.-Aided Drug Des.* **4**, 221 (2008).

- [44] N. C. J. Strynadka, M. Eisenstein, E. KatchalskiKatzir, B. K. Shoichet, I. D. Kuntz, R. Abagyan, M. Totrov, J. Janin, J. Cherfils, F. Zimmerman, A. Olson, B. Duncan, M. Rao, R. Jackson, M. Sternberg, and M. N. G. James, *Nature Struct. Biol.* **3**, 233 (1996).
- [45] R. T. Kroemer, *Curr. Protein Pept. Sc.* **8**, 312 (2007).
- [46] D. A. Case, T. A. Darden, T. E. Cheatham III, C. L. Simmerling, J. Wang, R. E. Duke, R. Luo, H. M. Merz, B. Wang, D. A. Pearlman, M. Crowley, S. Brozell, V. Tsui, H. Gohlke, J. Mongan, V. Hornak, G. Cui, P. Beroza, C. Schafmeister, J. W. Caldwell, W. S. Ross, and P. A. Kollman, AMBER 9 (University of California, San Francisco, 2006).
- [47] M. R. Shirts, J. W. Pitera, W. C. Swope, and V. S. Pande, *J. Chem. Phys.* **119**, 5740 (2003).
- [48] J. W. Pitera and W. F. Van Gunsteren, *Mol. Simulat.* **28**, 45 (2002).
- [49] A. Blondel, *J. Comp. Chem.* **25**, 985 (2004).
- [50] P. A. Kollman, I. Massova, C. Reyes, B. Kuhn, S. H. Huo, L. Chong, M. Lee, T. Lee, Y. Duan, W. Wang, O. Donini, P. Cieplak, J. Srinivasan, D. A. Case, and T. E. Cheatham, *Accounts Chem. Res.* **33**, 889 (2000).
- [51] M. A. S. Perez, P. A. Fernandes, and M. J. Ramos, *J. Phys. Chem. B* **114**, 2525 (2010).
- [52] M. A. S. Perez, P. A. Fernandes, and M. J. Ramos, *J. Mol. Graph. Model.* **26**, 634 (2007).
- [53] W. Wang, and P. A. Kollman, *Proc. Natl. Acad. Sci. U.S.A.* **98**, 14937 (2001).
- [54] N. M. F. S. A. Cerqueira, P. A. Fernandes, and M. J. Ramos, *Recent Pat. Anti-Canc.* **2**, 11 (2007).
- [55] N. M. F. S. A. Cerqueira, S. Pereira, P. A. Fernandes, and M. J. Ramos, *Curr. Med. Chem.* **12**, 1283 (2005).
- [56] N. M. F. S. A. Cerqueira, P. A. Fernandes, L. A. Eriksson, and M. J. Ramos, *J. Mol. Struct: THEOCHEM* **709**, 53 (2004).
- [57] N. M. F. S. A. Cerqueira, P. A. Fernandes, L. A. Eriksson, and M. J. Ramos, *J. Comput. Chem.* **25**, 2031 (2004).
- [58] N. M. F. S. A. Cerqueira, P. A. Fernandes, L. A. Eriksson, and M. J. Ramos,

- Biophys. J. **90**, 2109 (2006).
- [59] P. A. Fernandes, L. A. Eriksson, and M. J. Ramos, *Theor. Chem. Acc.* **108**, 352 (2002).
- [60] S. Pereira, N. M. F. S. A. Cerqueira, P. A. Fernandes, and M. J. Ramos, *Eur. Biophys. J. Biophys.* **35**, 125 (2006).
- [61] P. A. Fernandes and M. J. Ramos, *Chem.-Eur. J.* **9**, 5916 (2003).
- [62] N. M. F. S. A. Cerqueira, P. A. Fernandes, and M. J. Ramos, *J. Phys. Chem. B* **110**, 21272 (2006).
- [63] S. Pereira, P. A. Fernandes, and M. J. Ramos, *J. Comput. Chem.* **25**, 227 (2004).
- [64] S. Pereira, P. A. Fernandes, and M. J. Ramos, *J. Comput. Chem.* **25**, 1286 (2004).
- [65] N. M. F. S. A. Cerqueira, P. A. Fernandes, and M. J. Ramos, *Chem.-Eur. J.* **13**, 8507 (2007).
- [66] S. Pereira, P. A. Fernandes, and M. J. Ramos, *J. Am. Chem. Soc.* **127**, 5174 (2005).
- [67] P. A. Fernandes and M. J. Ramos, *J. Am. Chem. Soc.* **125**, 6311 (2003).
- [68] D. F. A. R. Dourado, P. A. Fernandes, B. Mannervik, and M. J. Ramos, *Curr. Protein Pept. Sci.* **9**, 325 (2008).
- [69] A. Yoritaka, N. Hattori, K. Uchida, M. Tanaka, E. R. Stadtman, and Y. Mizuno, *Proc. Natl. Acad. Sci. U.S.A.* **93**, 2696 (1996).
- [70] Y. J. Li, S. A. Oliveira, P. Xu, E. R. Martin, J. E. Stenger, C. R. Scherzer, M. A. Hauser, W. K. Scott, G. W. Small, M. A. Nance, R. L. Watts, J. P. Hubble, W. C. Koller, R. Pahwa, M. B. Stern, B. C. Hiner, J. Jankovic, C. G. Goetz, F. Mastaglia, L. T. Middleton, A. D. Roses, A. M. Saunders, D. E. Schmechel, S. R. Gullans, J. L. Haines, J. R. Gilbert, J. M. Vance, M. A. Pericak-Vance, C. Hulette, and K. A. Welsh-Bohmer, *Hum. Mol. Genet.* **12**, 3259 (2003).
- [71] T. J. Montine, D. Y. Huang, W. M. Valentine, V. Amarnath, A. Saunders, K. H. Weisgraber, D. G. Graham, and W. J. Strittmatter, *J. Neuropath. Exp. Neur.* **55**, 202 (1996).
- [72] R. J. Mark, M. A. Lovell, W. R. Markesbery, K. Uchida, and M. P. Mattson,

- J. Neurochem. **68**, 255 (1997).
- [73] D. A. Butterfield, Free Radical Res. **36**, 1307 (2002).
- [74] H. Kolsch, M. Linnebank, D. Lutjohann, F. Jessen, U. Wullner, U. Harbrecht, K. M. Thelen, M. Kreis, F. Hentschel, A. Schulz, K. von Bergmann, W. Maier, and R. Heun, Neurology **63**, 2255 (2004).
- [75] W. Palinski, M. E. Rosenfeld, S. Yla-Herttuala, G. C. Gurtner, S. S. Socher, S. W. Butler, S. Parthasarathy, T. E. Carew, D. Steinberg, and J. L. Witztum, Proc. Natl. Acad. Sci. U.S.A. **86**, 1372 (1989).
- [76] G. Jurgens, Q. Chen, H. Esterbauer, S. Mair, G. Ledinski, and H. P. Dinges, Arterioscler. Thromb. **13**, 1689 (1993).
- [77] J. H. Brasen, T. Hakkinen, E. Malle, U. Beisiegel, and S. Yla-Herttuala, Atherosclerosis **166**, 13 (2003).
- [78] K. Tsuneyama, K. Harada, N. Kono, M. Sasaki, T. Saito, M. E. Gershwin, M. Ikemoto, H. Arai, and Y. Nakanuma, J. Hepatol. **37**, 176 (2002).
- [79] M. Parola, G. Bellomo, G. Robino, G. Barrera, and M. U. Dianzani, Antioxid. Redox Signal **1**, 255 (1999).
- [80] E. R. Stadtman, Science **257**, 1220 (1992).
- [81] N. H. Ansari, L. Wang, and S. K. Srivastava, Biochem Mol Med **58**, 25 (1996).
- [82] A. M. Caccuri, G. Antonini P. G. Board, M. W. Parker, M. Nicotra, M. Lo Bello, G. Federici, and G. Ricci, Biochem. J. **344** Pt 2, 419 (1999).
- [83] D. F. A. R. Dourado, P. A. Fernandes, B. Mannervik, and M. J. Ramos, Chem.-Eur. J. **14**, 9591 (2008).
- [84] D. F. A. R. Dourado, P. A. Fernandes, and M. J. Ramos, Theor Chem Acc, **124**, 71 (2009).
- [85] M. Widersten, R. Bjornestedt, and B. Mannervik, Biochemistry **35**, 7731 (1996).
- [86] E. Lindahl, B. Hess, and D. Van der Spoel, J. Mol. Model **7**, 306 (2001).
- [87] E. J. Sorin and V. S. Pande, Biophys. J. **88**, 2472 (2005).
- [88] W. D. Cornell, P. Cieplak, C. I. Bayly, I.R. Gould, K.M. Merz Jr., D.M. Ferguson, D. C. Spellmeyer, T. Fox, J. W. Caldwell, and P.A. Kollman, J.

- Am. Chem. Soc. **117**, 5179 (1995).
- [89] J. M. Wang , P. Cieplak, and P. A. Kollman, *J. Comput. Chem.* **21**, 1049 (2000).
- [90] R. Bjornestedt, G. Stenberg, M. Widersten, P. G. Board, I. Sinning, T. A. Jones, and B. Mannervik, *J Mol Biol* **247**, 765 (1995).
- [91] D. F. A. R. Dourado, P. A. Fernandes, B. Mannervik, and M. J. Ramos, *J. Phys. Chem. B* **114**, 1690 (2010).
- [92] A. T. P. Carvalho, P. A. Fernandes, M. Swart, J. N. P. van Stralen, F. M. Bickelhaupt, and M. J. Ramos, *J. Comp. Chem.* **30**, 710 (2009).
- [93] A. T. P. Carvalho, M. Swart, J. N. P. van Stralen, P. A. Fernandes, M. J. Ramos, and F. M. Bickelhaupt, *J. Phys. Chem. B* **112**, 2511 (2008).
- [94] A. T. P. Carvalho, P. A. Fernandes, and M. J. Ramos, *J. Comp. Chem.* **27**, 966 (2006).
- [95] A. T. P. Carvalho, P. A. Fernandes, and M. J. Ramos, *J. Phys. Chem. B* **110**, 5758 (2006).
- [96] D. H. Juers, T. D. Heightman, A. Vasella, J. D. McCarter, L. Mackenzie, S. G. Withers, and B. W. Matthews, *Biochemistry* **40**, 14781 (2001).
- [97] N. F. Bras, P. A. Fernandes, and M. J. Ramos, *Theor. Chem. Acc.* **122**, 283 (2009).
- [98] N. F. Bras, P. A. Fernandes, and M. J. Ramos, *J. Chem. Theory Comp.* **6**, 2565 (2010).
- [99] N. F. Bras, P. A. Fernandes, and M. J. Ramos, *J. Mol. Struct.: THEOCHEM* **946**, 125 (2010).
- [100] N. F. Bras, S. A. Moura-Tamames, P. A. Fernandes, and M. J. Ramos, *J. Comp. Chem.* **29**, 2565 (2008).
- [101] D. A. Tobin, J. S. Pickett, H. L. Hartman, C. A. Fierke, and J. E. Penner-Hahn, *J. Am. Chem. Soc.* **125**, 9962 (2003).
- [102] S. B. Long, P. J. Casey, and L. S. Beese, *Nature* **419**, 645 (2002).
- [103] H. W. Park, S. R. Boduluri, J. F. Moomaw, P. J. Casey, and L. S. Beese, *Science* **275**, 1800 (1997).
- [104] M. J. Ramos and P. A. Fernandes, *Accounts Chem. Res.* **41**, 689 (2008).

- [105] M. Leopoldini, T. Marino, M. D. Michelini, I. Rivalta, N. Russo, E. Sicilia, and M. Toscano, *Theor. Chem. Acc.* **117**, 765 (2007).
- [106] F. Himo, *Theor. Chem. Acc.* **116**, 232 (2006).
- [107] S. F. Sousa, P. A. Fernandes, and M. J. Ramos, *Biophys. J.* **88**, 483 (2005).
- [108] S. F. Sousa, P. A. Fernandes, and M. J. Ramos, *J. Am. Chem. Soc.* **129**, 1378 (2007).
- [109] S. F. Sousa, P. A. Fernandes, and M. J. Ramos, *J. Comp. Chem.* **28**, 1160 (2007).
- [110] S. F. Sousa, P. A. Fernandes and M. J. Ramos, *Proteins: Struct. Funct. Bioinf.* **66**, 205 (2007).
- [111] S. F. Sousa, P. A. Fernandes, and M. J. Ramos, *J. Mol. Struct.: THEOCHEM* **729**, 125 (2005).
- [112] S. F. Sousa, P. A. Fernandes, and M. J. Ramos, *Chem.-Eur. J.* **15**, 4243 (2009).
- [113] W. Kohn, A. D. Becke, and R. G. Parr, *J. Phys. Chem.* **100**, 12974 (1996).
- [114] A. Ghosh, *J. Biol. Inorg. Chem.* **11**, 671 (2006).
- [115] Y. Zhao and D. G. Truhlar, *Accounts Chem. Res.* **41**, 157 (2008).
- [116] N. E. Schultz, Y. Zhao, and D. G. Truhlar, *J. Phys. Chem. A* **109**, 11127 (2005).
- [117] S. F. Sousa, P. A. Fernandes, and M. J. Ramos, *J. Phys. Chem. B* **111**, 9146 (2007).
- [118] P. Jurecka, J. Cerny, P. Hobza, and D. R. Salahub, *J. Comput. Chem.* **28**, 555 (2007).
- [119] A. Karton, A. Tarnopolsky, J. F. Lamere, G. C. Schatz, and J. M. L. Martin, *J. Phys. Chem. A* **112**, 12868 (2008).
- [120] Y. Zhao and D. G. Truhlar, *J. Chem. Theory Comput.* **3**, 289 (2007).
- [121] A. J. M. Ribeiro, M. J. Ramos, and P. A. Fernandes (submitted).

9. COMPUTATIONAL THERMOCHEMISTRY: ACCURATE ESTIMATION AND PREDICTION OF MOLECULAR THERMOCHEMICAL PARAMETERS

Victor M. F. Morais*

Instituto de Ciências Biomédicas Abel Salazar, ICBAS, Universidade do Porto,
P-4099-003 Porto, Portugal

The problems involved in the Quantum Mechanical calculation of molecular energies are identified, with special emphasis on the problem of correctly describing the effects of the correlated electronic motions. Some of the available Quantum Mechanically based methods for the calculation of molecular energies are then briefly described and their application to some selected systems are detailed. The quality of the results so obtained illustrates the usefulness and the accuracy achieved through the use of conveniently based computational techniques and the fact that contemporary thermochemists have now the real possibility of complementing their experimental measurements with well founded very accurate calculated data or, even, of obtaining original and very accurate thermochemical data entirely from computational techniques.

9.1 Computational Methods

Since the introduction of Quantum Mechanics, in the first quarter of twentieth century, very important advances in chemistry have emerged, particularly in those fields where accurate numerical data is required, such as thermochemistry and chemical kinetics. Indeed, it is now recognized that Quantum Mechanics constitutes the ultimate, most accurate and complete description of the behaviour of matter at the atomic and molecular scale and, as such, much hope has been put in the development of efficient computational methods which can provide accurate estimates of the molecular thermochemical parameters.

*Email address: vmmorais@icbas.up.pt

Such achievements would contribute to definitely establish computational thermochemistry as a reliable complement to experimental thermochemistry, thus opening new frontiers to the study of chemical species whose instability or short lifetime has prevented experimental analysis up to now.

This talk is concerned with the difficulties found when the methods of Quantum Mechanics are to be applied to real systems and with the description of some state-of-the-art computational techniques which have been developed to provide accurate molecular thermochemical parameters. We will describe also some applications of those computational methods with particular emphasis to the analysis of the stability of selected molecular species.

The task of accurately describing the properties of molecular systems starting from the concepts of Quantum Mechanics would appear as very straightforward if it is accepted that such theory provides the most accurate and complete description of the behaviour of matter at the atomic and molecular level. According to this point of view it becomes obvious that in order to obtain reliable and accurate estimates of molecular thermochemical parameters it suffices to solve the corresponding Schrödinger equation

$$\hat{H}\Psi = E\Psi \quad (9.1)$$

which is a differential eigenvalue equation providing, as solutions, the energy, E , and the wavefunction, Ψ , of the stationary states of the molecular system. In this equation \hat{H} is the Hamiltonian operator, acting on the wavefunction Ψ , which depends explicitly on the spatial and spin coordinates of the electrons and the nuclei. Even though Schrödinger equation can be easily solved for hydrogen atom and, in general, for any system with just one electron, in which case it provides accurately the experimentally observed energies, when we proceed to more complex systems, with at least two electrons, such exact solution reveals unattainable, and some kind of approximate solution must be seek instead. The vast majority of the methods used to obtain approximate solutions to the Schrödinger equation is based on a general approximation introduced to the model of the wavefunction used to describe the system under study. This

approximation assumes that each electron in the system moves independently of the other electrons (an independent particle model is thus adopted) and the interactions among the various electrons are accounted for through the introduction of a potential energy function representing just the time average of the instantaneous interactions between each electron and the remaining ones. Thus, each electron will then be described by a particular spatial function, φ_i , which depends on its spatial coordinates. According to the Pauli antisymmetry principle each such spatial function, generically called molecular orbital, can really accommodate two electrons, as long as they have different spin coordinates, α or β . The wavefunction describing the overall electronic system can then be represented by a function with the following general form:

$$\Psi = \frac{1}{\sqrt{n!}} \det |(\varphi_1\alpha)(\varphi_1\beta)(\varphi_2\alpha)\cdots| \quad (9.2)$$

where the determinant, called Slater determinant, ensures the proper antisymmetry of the wavefunction, as is required for systems constituted by fermions. The energy of the system can then be obtained through variation of the molecular orbitals in order to minimize the expectation value of the Hamiltonian operator:

$$E = \langle \Psi | \hat{H} | \Psi \rangle \quad (9.3)$$

Such variational procedure leads to a system of coupled differential equations, called Fock equations, whose solutions are the molecular orbitals, φ_i . Thus, in the Hartree-Fock model each electron feels a potential which is the average of the instantaneous potential created by the other electrons. Such replacement of the true (instantaneous) potential by the average potential ensures that the Hartree-Fock method can easily lead to approximate solutions of the Schrödinger equation. However, those solutions will certainly reflect the nature of the adopted approximations, in the sense that they should incorporate the errors associated with the assumptions assumed for the wavefunction model. We must stress that the solutions of the Fock equations (the molecular orbitals, φ_i) are obtained in numerical form, as tables of numerical values, instead of some kind of analytical form, which would be preferable for those aiming to

analyse the properties of the electronic systems in terms of the contributions resulting from the subsystems constituting them, *e.g.*, the properties of a molecule as resulting from contributions of their individual atoms. This situation soon conducted to a proposal involving the mathematical representation of the molecular orbitals as expansions in terms of selected mathematical functions, collectively called basis set:

$$\varphi_i = \sum_{k=1}^N c_{i,k} \chi_k \quad (9.4)$$

The adoption of such representation had the very important consequence of allowing the replacement of the system of coupled differential equation, the Fock equations, by a system of algebraic equations, the so-called Hartree-Fock-Roothaan equations, involving the coefficients of the individual members of the basis set in each molecular orbital, φ_i . In this way, the required flexibility of the wavefunction which allows for the minimization of the expectation value (9.3) is thus transferred to the variation of the molecular orbital coefficients, whose values must then be optimized in order to (variationally) minimize the expectation value of the energy. The basis sets are usually chosen to consist of atomic centered functions which are often assimilated to the corresponding atomic orbitals. Since the basis sets used in practice are necessarily limited in size, their capability of description of the molecular orbitals is also limited and, as such, the resulting expectation value for the energy is affected by numerical errors. We can thus observe that, up to this point, two possible sources of errors are present in the computational procedure we are describing: on the one hand the errors resulting from the particular model (9.2) of wavefunction adopted by the Hartree-Fock scheme and on the other hand the limitations resulting from using finite sets of basis functions for the molecular orbital representation. Even if we used a complete set of basis functions to represent the molecular orbitals (so eliminating the second source of inaccuracy) the energy obtained by the Hartree-Fock method, which is then called Hartree-Fock energy, E_{HF} , would be in error when compared with the observed (non-relativistic) one, E_{exact} . Such

Table 9.1. Correlation errors for two simple molecular systems.

	E_{exact}	E_{HF}	E_{corr}	%	$E_{\text{corr}}/\text{kcal mol}^{-1}$
H ₂	-1.1749	-1.1340	-0.0409	3.48	~ -26
H ₂ O	-76.435	-76.065	-0.37	0.48	~ -232

error:

$$E_{\text{corr}} = E_{\text{exact}} - E_{\text{HF}} \quad (9.5)$$

which is always negative, since the Hartree-Fock method is variational, is called correlation energy, or correlation error, a designation reflecting its phenomenological origin related to the fact that the motions of the electrons with different spins are described as completely non-correlated by Hartree-Fock theory. Even though this error seems often very small when we consider its value relative to the total electronic energy (typically less than 1% of the total electronic energy), its contribution to the properties which are of interest to chemists, like bond energies or, more generally, reaction energies, is so large that its very existence precludes using the energies so obtained to get reliable estimates of such energetic parameters. Table 9.1 shows typical contributions of the correlation energy for small molecular systems. We can observe from that Table that the absolute errors resulting from neglecting the correlation energy are unacceptable, even for the most simple systems, when we come to consider accurate description of reaction energies. Indeed, the absolute errors shown in that Table are by far much larger than the errors chemists can accept, *i.e.*, about 1 kcal/mol.

We must, in addition, stress that real calculations for truly interesting molecules can only be conducted with severe limitations on the basis sets completeness, and, as such, the actual errors involved in the results are even much more important than the correlation error, because we don't even reach the Hartree-Fock limit in such cases. So, if quantum mechanical techniques, based on the Hartree-Fock wavefunction, are to be fruitfully used to get reliable energetic information, we must proceed by simultaneously correcting the Hartree-Fock method along two independent routes: (*i*) by improving the model (9.2) of the wavefunction and (*ii*) by using basis sets as close to completeness as possible.

A logical route to get better results than simple Hartree-Fock theory can provide follows directly from the observation that the Hartree-Fock solution (9.2) usually involves more molecular orbitals, φ_i , than those which are needed to accommodate the electrons constituting the molecule. Thus, even though only the lowest energy molecular orbitals, φ_i , are used to construct the Slater determinant (9.2), a considerably higher number of molecular orbitals is obtained in the procedure of variationally minimization of the energy. The remaining molecular orbitals are thus unoccupied in the configuration (9.2); such unoccupied orbitals are called virtual orbitals. Distribution of the electrons by the low energy molecular orbitals, as in (9.2), can thus be viewed as just one of the many possible ways of distributing the electrons by the available molecular orbitals. It has been found that the description provided by the Hartree-Fock method can be improved by adding to the single-determinant wavefunction (9.2) a number of configurations resulting from alternative distributions of the electrons by the remaining available virtual molecular orbitals. This procedure leads to an alternative description of the molecular wavefunction which can then be symbolically represented as:

$$\Psi = a_0\Psi_0 + \sum_{i,a} a_i^a\Psi_i^a + \sum_{i,a} \sum_{j,b} a_{ij}^{ab}\Psi_{ij}^{ab} + \dots \quad (9.6)$$

In this equation Ψ_0 represents the Hartree-Fock wavefunction (9.2), while Ψ_i^a a Slater determinant (also called configuration) obtained by promoting one electron from occupied molecular orbital i to virtual molecular orbital a , Ψ_{ij}^{ab} the doubly excited configuration obtained by simultaneously promoting two electrons from occupied orbitals i and j to virtual orbitals a and b , ... *etc.* This linear combination of Slater determinants is the philosophy of the so called Configuration Interaction (CI) method. Simply put, a CI wavefunction is a linear combination of Slater determinants (configurations) whose coefficients are to be determined variationally. Of course, in real calculations this linear combination must be severely truncated in order to lead to workable tasks. The simplest standard CI method which improves upon Hartree-Fock is a CI calculation which adds all singly and doubly substituted determinants (CISD). However, the CISD

wavefunction has soon fallen out of favor because truncated CI wavefunctions short of full configuration interaction are not size-extensive, meaning that their quality degrades as the size of the molecules becomes larger. This is a general result about the Configuration Interaction method: when used in a truncated way the CI series leads to results which are not size consistent. A formulation of Configuration Interaction which remains size consistent even when arbitrarily truncated, called quadratic CI (QCI), has been proposed, the simplest method to improve Hartree-Fock results being, in this case, designated by QCISD and being now preferred to the earlier implementations.

An alternative attractive formulation involves perturbation theory using the Hartree-Fock wavefunction as the zeroth-order wavefunction and the difference between the complete Hamiltonian and the Hartree-Fock Hamiltonian, *i.e.*, the correlation energy, as the perturbation. This is the Møller-Plesset formulation of perturbation theory and is based on a perturbational series for the energy, involving successively higher order corrections to the this parameter:

$$E = E_0 + E_1 + E_2 + E_3 + \dots \quad (9.7)$$

together with a corresponding series for the wavefunction. As in the case of the CI method, the complete perturbation treatment leads to the best description we can get with the used basis set. Indeed, both expansions, variational and perturbational, are conceptually very similar, to the point that when considered non-truncated they will lead exactly to the same result: the exact one. Naturally, in real calculations, only approximate treatments can be conducted, taking account of a limited number of terms in the perturbation series: the simplest way of improving the Hartree-Fock energy (which is correct to the first order, thus being just the sum of the first two terms in the perturbational series) through perturbation methods involves including just the second order contributions, leading to the so called MP2 method. Successive perturbative methods thus adopt the designations MP3, if all terms up to third order are included in the perturbational series, MP4, when all terms up to fourth order are included, and so on. One important advantage of perturbation techniques over the CI method

is that truncated (to any order) perturbation calculations always lead to size consistent results, while truncated configuration interaction calculations do not. The two methods are, otherwise, thought as equivalent in the sense that including all possible configurations in a combination which is compatible with the spin symmetry of the molecular state we are aiming to describe, leads to the so called full CI (FCI) limit, and describes the system so rigorously as including all terms in the perturbational expansion. Thus, both methods will provide naturally the best possible description we can obtain with the basis set which is being used.

There are also some other important methods, of which we will only refer the coupled cluster (CC) methods because of their growing importance as a size-consistent alternative to configuration interaction. As with the CI method, coupled cluster techniques are also usually implemented in very truncated versions, leading to different CC flavours: thus CCSD considers only single and double excitations, while CCSD(T) also includes a perturbative account of the effect of triple excitations, *etc.* We have just mentioned some procedures which are most often adopted in order to surpass the natural limitations of the Hartree-Fock formulation, *i.e.*, some useful post-Hartree-Fock techniques.

Conversely, by proceeding along the other route to better describe the system, *i.e.*, by enhancing the capability of representation of the basis set in order to get so close as possible to basis set completeness, we will obtain the better description possible, restricted to a chosen model of the wavefunction. So, it seems obvious that any systematic search for accurate calculation of molecular energetic parameters procedures must simultaneously progress along both directions, performing a kind of two-dimensional progression, in order to include the larger possible number of terms in the configurational or perturbational expansions, thus approaching the FCI limit and, additionally, to extend, as possible, the basis set in order to approach the complete basis set (CBS) limit. Such technique would naturally lead to the exact solutions, that is, to the energies observed experimentally, when we reach simultaneously both individual limits, FCI and CBS, as is schematically depicted in Figure 9.1. Of course this limit can only be attained if we are just considering very simple electronic systems, more complex

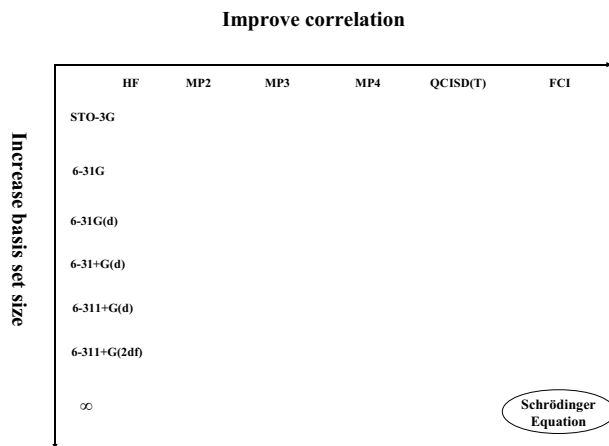


Figure 9.1. Bidimensional route to exact solution of Schrödinger equation.

systems leading to so computationally demanding tasks that the calculations are really precluded by the necessarily limited resources. In order to further proceed and provide reliable insights into the properties of more complex real systems we thus need to accept the incorporation of additional approximations to the above protocol. A large number of computational recipes have already been suggested and tested; we will limit ourselves to a very short description of some of those methods, particularly those we have selected to conduct calculations on some interesting molecules. Almost all accurate procedures for obtaining energetic data share the basic philosophy, which involves using less sophisticated, yet reliable, calculations to obtain the molecular geometry and the vibrational frequencies (both of these are generally very time consuming tasks, but are essential for forthcoming calculations) and then introduce the correlation energy estimates from a much more sophisticated level of theory and with the most extensive basis set compatible with available computational resources.

Such composite procedures would ideally be rigorously formulated and should conduct to the equivalent result of a single calculation much more sophisticated than each of the individual calculations involved. The most accurate of the methods we currently use, G3, belongs to the series of techniques named

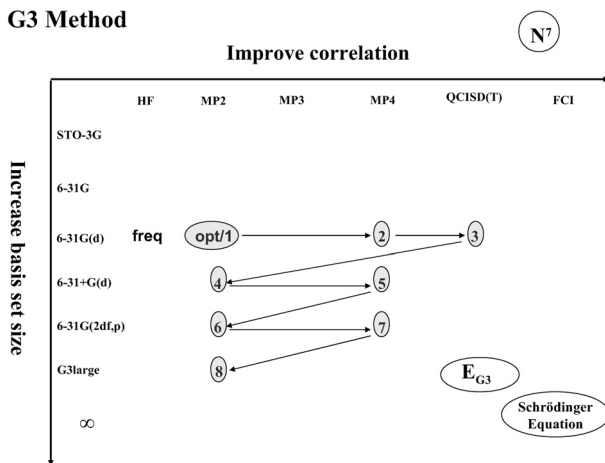


Figure 9.2. Schematics of the individual calculations involved in the G3 method.

G(aussian)- N ($N = 1, 2, 3$), originally suggested by Pople and co-workers [1]. The detailed sequence of individual computations integrating a G3 calculation are schematically depicted in Figure 9.2. The final energy at the G3 level is obtained as a MP4 energy calculated with the 6-31G(d) basis set properly corrected for several effects:

$$E_{G3} = 2 + (3 - 2) + (5 - 2) + (7 - 2) + (8 - 1) - (4 - 1) - (6 - 1) \quad (9.8)$$

The correction terms represent several effects described as follows:

$(5 - 2) \equiv \Delta E(+)$ is a correction aiming to account for the effect of using diffuse (+) functions;

$(7 - 2) \equiv \Delta E(2df, p)$ is a correction for the use of higher polarization functions on nonhydrogen atoms and p functions on hydrogen atoms;

$(3 - 2) \equiv \Delta E(QCI)$ corrects for correlation effects beyond fourth order of perturbation theory using the method of quadratic configuration interaction;

$(8 - 1) - (4 - 1) - (6 - 1) \equiv \Delta E(G3 \text{ Large})$ is a correction for larger basis set and nonadditivity effects. Thus, as we can observe from the scheme, the G3 energy is really a presumably good approximation to a QCISD(T) energy calculated with a large basis set (G3 Large), but obtained without really conducting such very expensive calculations.

This computational method has been much tested now and reveals a very accurate computational method. Its computational cost scales formally as N^7 , where N is roughly the number of atoms in the molecule, and so becomes very heavy even for moderately sized molecules. As such, other methods have been selected to proceed with the calculation of thermochemistry properties. Some less expensive variants of G3 have been suggested: G3B3 is a G3 method which involves using the B3LYP method to obtain the geometry and frequencies while G3(MP2) replaces the MP4 steps of the original procedure by calculations at the MP2 level. Among many other available methods we also adopted some of those based on a slightly different philosophy. The basis of the multi-coefficient correlation methods (MCCM) of Truhlar and coworkers [2,3] is similar to that adopted in the Gaussian- N series but, instead of simply adding the individual corrections to the reference calculations, these are introduced after being scaled, or weighted, by optimizable parameters. These parameters are then optimized so that the errors in the atomization energies (or perhaps other energetic parameter or even a combination of several parameters) of a set of representative test molecular systems are minimized. The use of adjustable parameters allows for the inclusion of lower levels of correlation and/or smaller basis sets to achieve a given level of accuracy. Thus the cost of both methods we usually use to predict thermochemical parameters, MCUT and MCQCISD, scale “simply” as N^6 , thus allowing to consider much larger molecules than the G3 method. The individual calculations involved within these methods are graphically depicted in Figures 9.3 and 9.4, respectively for MC-UT and for MC-QCISD. MC-UT method aims to reproduce MP4(SDQ) calculations with the modified Gaussian 3 semidiffuse (MG3S) basis set, by judiciously combining several individual calculations as:

$$E_{\text{MC-UT}} = 1 + c_1(2 - 1) + c_2(3 - 2) + c_3[(4 - 2) - (3 - 1)] + c_4(5 - 3) \quad (9.9)$$

while MC-QCISD aims to reproduce QCISD calculations obtained with the modified Gaussian 3 semidiffuse (MG3S) basis set, by combining several individual

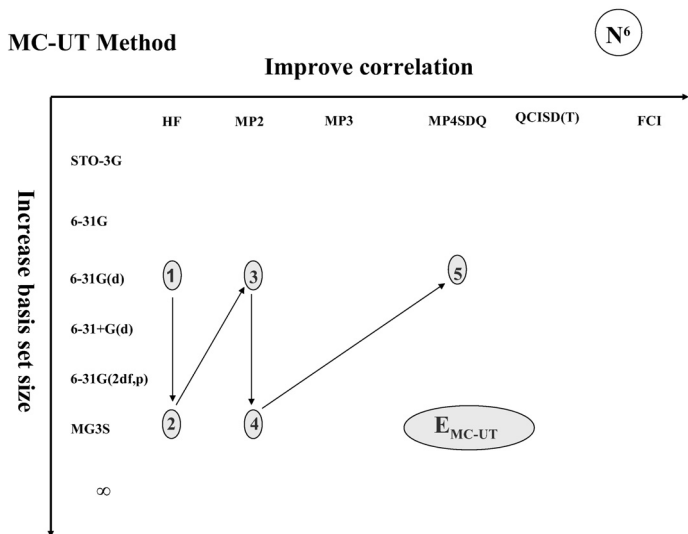


Figure 9.3. Schematics of the individual calculations involved in the MCCM/MC-UT method.

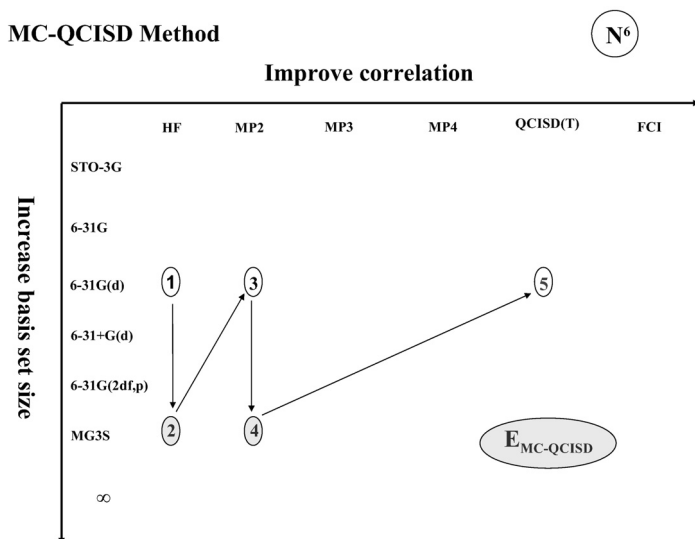


Figure 9.4. Schematics of the individual calculations involved in the MCCM/MC-QCISD method.

CBS Extrapolation

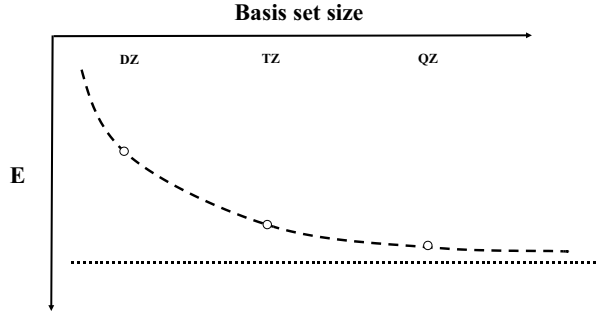


Figure 9.5. Schematic representation of CBS extrapolation technique.

calculations as:

$$E_{\text{MC-QCISD}} = 1 + c_1(2 - 1) + c_2(3 - 2) + c_3[(4 - 2) - (3 - 1)] + c_4(5 - 3) \quad (9.10)$$

In addition to the aforementioned methods other relevant techniques based on somewhat different principles have also been suggested. The CBS (complete basis set) series of methods [4] share the following individual calculations:

- (i) (U)HF/6-31G[†] geometry optimization and frequencies;
- (ii) MP2(FC)/6-31G[†] optimized geometry for subsequent calculations;
- (iii) (U)MP2/6-311+G(3d2f;2df,2p) energy and CBS extrapolation;
- (iv) MP4(SDQ)/6-311G(d(f), p) energy;
- (v) (QCISD(T)/6-31+G[†] energy.

The innovative key step is the use of an extrapolation of the results of the MP2/6-311+G(3d2f;2df,2p) calculation to the complete basis set (CBS) limit (Figure 9.5). This extrapolation is based on the asymptotic behaviour of the natural orbitals and allow the obtention of very accurate results without having to conduct the most expensive individual steps involving very high levels of electron correlation and very extensive basis sets.

Much important in the context of basis set extrapolation techniques has been the introduction [5] of classes of hierarquical basis sets specially designed to suc-

Table 9.2. Fraction of correlation energy of water molecule accounted for by several computational methods.

	HF	MP2FC	MP2FU	MP4	CCSD	CCSD(T)	CCSD(T) (Full)	G3	Exact
Energy	-76.058	-76.319	-76.332	-76.333	-76.325	-76.332	-76.346	-76.382	-76.435
%	99.51	99.85	99.87	99.87	99.86	99.87	99.88	99.93	100
$\Delta(\text{kcal mol}^{-1})$	-236	73	-65	-64	-69	-65	-55	-33	0.0

cessively cover more extensively the available electronic space. These sophisticated basis sets use acronyms which indicate clearly their degree of completeness, *e.g.*, cc-pVXZ, cc-pCVXZ, aug-cc-pVXZ, *etc.*, where X (D, T, Q, 5, 6, ...) indicates the cardinality of the basis set: $X=D$ indicates a double- ζ quality basis set, $X=T$ a triple- ζ quality, *etc.* This methodology aims thus to provide results which tend systematically and uniformly to those which will be obtained at the complete basis set limit. This way the extrapolation formulae become much more precise. Since the rate of convergence of the correlation part of the molecular energy is significantly slower than that of the Hartree-Fock component, it is usually adopted a separation of the molecular electronic energies into their components, each of which is then extrapolated independently. This route has been exploited in several works [6-8] and constitutes a much promising tool, which is believed to perform much better than the extrapolations based on classical Gaussian basis sets.

The real importance of the correlation energy and the difficulty of accounting for it in practice is well illustrated by the data in Table 9.2, which shows the fraction of the correlation energy of water molecule recovered by several computational methods (all data, except G3, obtained from calculations using the cc-pVTZ basis set on the MP2(FC)/6-31G* geometry).

We can observe that even the most sophisticated computational techniques still include errors which are exceedingly large when compared to chemically meaningful quantities. As a consequence, even if the size of the molecular species allows for the use of the most sophisticated techniques, it is nevertheless mandatory to combine the raw energetic results with judiciously chosen chemical reaction schemes in order to obtain a maximal cancellation of the errors still

affecting both sides of reaction, a result which is more likely to be achieved the more “similar” are reactants and products in the chosen reactions. In this context the reaction schemes we use must preferably be, at least, of the isodesmic type, *i.e.*, they must conserve the number and qualitative “types” of chemical bonds in passing from reactants *to products*, or even of the homodesmotic type (if, in addition, the number of atoms of each formal type in each hybridization state is also conserved), thus ensuring the desired error cancellation and a good description of the energetics by computational results. Very restrictive reaction types are however often not feasibly usable, mainly because no experimental accurate data is available for some of the involved species. In such cases we are compelled to use other types of reactions, particularly atomization reactions. Atomization reactions are very appellative since writing them involves no ambiguity, *i.e.*, they are uniquely defined; however their use is likely to lead to a description which is prone to large inaccuracies. Indeed, since, by definition, all bonds in the molecule are destroyed in such reactions, these reactions are as far from an isodesmic reaction as possible and, as a consequence, no error cancellation occurs. Thus the task of calculating accurate atomization energies becomes very difficult when using atomization reactions.

Even though some of the methods we cited above are indeed very accurate computational techniques which allow the reliable prediction of the thermochemical parameters of chemical systems, their usefulness has serious drawbacks since their computational cost rises so steeply that they become unpractical unless we restrict the studies to very small molecular systems. In the context of the study of larger systems useful alternatives are provided by the methods based on density functional theory (DFT). Since the account these methods take of the electronic correlation effects is not exact, the usual implementations involve a considerable amount of empirical parameterization thus becoming conceptually very distant from the the philosophy of *ab initio* theory. The main advantage of such methods is their much higher performance-to-cost ratio when compared to the wavefunction based methods, enabling their application to much larger molecular systems. A major drawback of DFT techniques, which has not been

surpassed yet, is that, contrary to what happens with the methods based on the treatment of the wavefunction, there is no straightforward procedure allowing the systematic convergence of the results of DFT calculations obtained with truncated basis sets to the exact ones.

Additionally to the methods used to obtain the accurate values of the energy of the molecular systems, other additional tools are required to analyse the so obtained wavefunctions and several effects which can occur. Aromaticity, being a multifaceted and elusive molecular property observed in systems containing one or more cyclic arrangements of atoms, has been traditionally considered and analysed from three starting viewpoints: structural, energetic and magnetic. In our work we are mainly concerned with the analysis of the aromatic behaviour of molecules based on the consideration of their magnetic properties. In fact, these properties are likely to show special relationships to the microscopic phenomena which is believed to be the basis of aromatic behaviour, *i.e.*, the circular delocalization of electrons. Briefly, the response of cyclic electronic systems to an external magnetic field is manifested through the creation of a ring current which, ultimately, will produce an induced magnetic field opposing the external magnetic field (aromatic behaviour) or reinforcing it (antiaromatic behaviour). In either case the net result will be observable in Nuclear Magnetic Resonance (NMR) experiments as the properties called nucleus chemical shifts. Since Quantum Mechanics can be used to calculate the molecular chemical shielding tensor, we can thus hope that this is a truly direct way of testing the emergence of the ring currents associated with the aromatic/antiaromatic behaviour, and will thus provide an objective test of the aromatic/antiaromatic behaviour itself. Using computational techniques based on Quantum Mechanics is indeed advantageous over NMR experiments since in this case we can even probe the ring current (chemical shielding) at any point within the molecule and not just at the nuclei. Thus, from the computational viewpoint, the relevant properties are the so called Nucleus Independent Chemical Shifts (NICS), as first suggested by Schleyer and co-workers [9].

Traditionally NICS are shown as the symmetric of the isotropic component of

the chemical shielding tensor evaluated at the center of the rings or, in order to properly account for the nodal properties of the π -orbitals, and to minimize the (contaminating) effects of the σ electronic framework, at some point above or below that geometric center; significantly negative values of the NICS are then associated with aromatic behaviour while positive values indicate antiaromaticity.

Additionally, NICS calculation are often combined with Natural Bond Orbitals (NBO) [10-13] analysis of the wavefunctions to get usefull insights about the detailed contribution of selected orbitals to the magnetic properties. We can then separate unequivocally the effect of π -electrons on the calculated NICS, *i.e.*, the individual effects on the observed aromaticity/antiaromaticity of the systems under analysis.

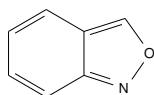
9.2 Typical Results for Selected Molecules

Unless otherwise stated, the equilibrium geometries of all studied systems have been determined from density functional theory using the Becke-3-parameter hybrid exchange [14] and the Lee_Yang_Parr [15] correlation density functional (B3LYP) together with two basis sets: 6-31G* [16] and 6-311G** [17,18]. The harmonic vibrational frequencies were obtained from the optimum B3LYP/6-31G* geometries using the same basis set and were scaled by a factor [19] of 0.9614 in order to correct for anharmonicity. More accurate energies were also obtained from single-point calculations at the most stable B3LYP/6-311G** geometries, using the triple- ζ correlation-consistent basis set, cc-pVTZ [5] together with the B3LYP functional. These optimized geometries were also used to obtain the energies at the MC-UT, MC-QCISD, while the calculations using the G3 type series of methods use their own optimized geometries. The NICS values were calculated using RHF/6-31G* wavefunctions derived from the B3LYP/6-311G** geometries. The methodology used was developed by Schleyer and co-workers [9]. Two different NICS values were calculated for each ring and each molecule: one at the geometrical centre of the ring (*i.e.*, the point whose coordinates are the nonweighted mean of the homologous coordinates of the

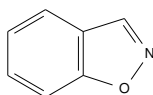
heavy atoms of the rings), denoted NICS(0), and 1.0 Å above the center of the ring, denoted NICS(1.0).

9.2.1 Anthranil Aromaticity [20]

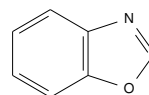
Anthranil (benzo[*c*]isoxazole, **I**) is a highly unsaturated bicyclic nitrogenous heterocycle with 10π -electrons, distributed among two rings each one with 6π -electrons, and a single, classical resonance structure. Thus, each individual ring, as well as the anthranil molecule as a whole, satisfies the Huckel $4n + 2$ rule. We ask “is it aromatic?”, for this species is π -isoelectronic/isoconjugate with its isomers 1,2-benzisoxazole (**II**) and benzoxazole (**III**), as well as with quinoline (**IV**) and isoquinoline (**V**), for which the presence of aromaticity seems unambiguous.



benzo[*c*]isoxazole
[Anthranil]
(I)

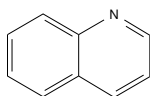


benzo[*d*]isoxazole
(II)

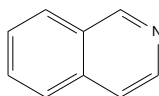


benzo[*d*]oxazole
(III)

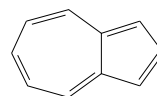
On the other hand, the carbon–carbon bond conjoining the two rings is an essentially single bond in that, like the corresponding bond in azulene (**VI**) and the Ph–Ph bond in biphenyl (**VII**), it is always a single bond in any resonance structure lacking a long bond (cf. the “Dewar” structure) or a dipolar/zwitterionic description.



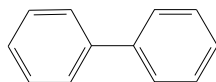
quinoline
(IV)



isoquinoline
(V)



azulene
(VI)



biphenyl
(VII)



oxazole
(VIII)



isoxazole
(IX)

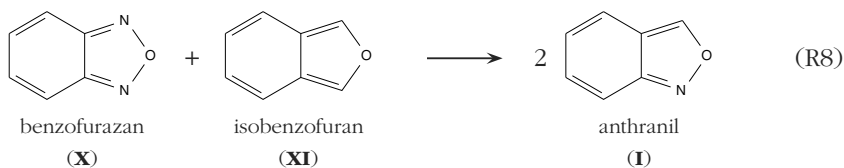
Table 9.3. Calculated and experimental reactions enthalpies at 298.15 K.

	$\Delta_r H_G^0(T = 298.15 \text{ K})/\text{kJ mol}^{-1}$					Exp.
	B3LYP			G3(MP2)	G3	
	6-31G	6-311G**	cc-pVTZ			
Reaction (R1)	-150.4	-153.5	-152.5	-157.1	-157.0	-(136.0±2.2)
Reaction (R2)	-90.9	-94.4	-93.6	-96.9	-97.1	-(94.1±0.7)
Reaction (R3)	-59.5	-59.0	-59.0	-60.2	-59.0	-(41.9±2.3)
Reaction (R4)	-13.2	-13.1	-13.0	-13.3	-13.0	—
Reaction (R5)	-46.3	-46.0	-46.0	-46.9	-46.8	—
Reaction (R6)	-122.7	-153.1	-150.9	-155.3	-155.6	-(148.0±3.0)
Reaction (R7)	-76.4	-107.2	-104.9	-108.3	-108.7	-(112±8.4)

ation of the auxiliary molecules were taken from Refs. 21,22). For the isomerization reactions R1 and R2, we obtain an experimental value for $\Delta_r H$ of $-(136.0 \pm 2.2) \text{ kJ mol}^{-1}$, for the former, and $-(94.1 \pm 0.7) \text{ kJ mol}^{-1}$, for the latter. These values are in good agreement with the results of our calculations and allow us to attribute the observed difference to a change in aromaticity of about $(41.9 \pm 2.3) \text{ kJ mol}^{-1}$. By regarding reaction R3 as the sum of reactions R1 and R2, an experimental value for $\Delta_r H$ of $-(41.9 \pm 2.3) \text{ kJ mol}^{-1}$ is obtained, which is the result of a balancing of isomerization energies and aromaticity change. So it seems that the hypothetical reaction R4 should essentially be thermoneutral, because isomerization energies plausibly cancel (1,2-benzisoxazole \rightarrow benzoxazole; oxazole \rightarrow isoxazole) and also because there is no particular difference in aromaticity between the reagents and the products. Theoretical calculations give a value of about -13 kJ mol^{-1} for this reaction, in good agreement with these assumptions. Note that the theoretical value of for reaction R3 is about -59 kJ mol^{-1} (Table 9.3), which shows a deviation of -17 kJ mol^{-1} from the experimental value. From the thermoneutrality of reaction R4 and by using the enthalpies of formation [21] of the gaseous species involved [oxazole: $-(15.5 \pm 0.5) \text{ kJ mol}^{-1}$; isoxazole: $(78.6 \pm 0.5) \text{ kJ mol}^{-1}$; benzoxazole: $(44.8 \pm 0.5) \text{ kJ mol}^{-1}$] we estimate the enthalpy of formation of 1,2-benzisoxazole to be $(138.9 \pm 5) \text{ kJ mol}^{-1}$. Similarly, for Equation R5 we estimate a value of $\Delta_r H$ of about $-(41.9 \pm 2.3) \text{ kJ mol}^{-1}$ [the theoretical results for re-

action R5 of *ca.* -46 kJ mol^{-1} corroborate this estimation] and consequently we obtain a value of $(138.9 \pm 3.1) \text{ kJ mol}^{-1}$ for the enthalpy of formation of 1,2-benzisoxazole. This value can favourably be compared with the estimates obtained from atomization energies at the G3(MP2) and G3 levels (Table 9.4)

To further corroborate this estimate, we considered the ring-opening isomerization reaction R6 for which the experimental value for $\Delta_r H$ is $-(148.0 \pm 3.0) \text{ kJ mol}^{-1}$, in good agreement with the theoretical calculation, allowing a value of about $-(106.1 \pm 3.8) \text{ kJ mol}^{-1}$ [$= -(148.0 \pm 3.0) + (41.9 \pm 2.3) \text{ kJ mol}^{-1}$] to be estimated for the enthalpy of reaction R7, which involves the ring opening of 1,2-benzisoxazole. Reaction R7 was also studied in the liquid phase (aqueous alcohol) and the value of $\Delta_r H$ is $-(112 \pm 8) \text{ kJ mol}^{-1}$ [23], not that different from the one we have considered above. This is not too strange if the isomers have similar solvation energies. From the value of $\Delta_r H(\text{R7})$ [$-(106.1 \pm 3.8) \text{ kJ mol}^{-1}$] and the enthalpy of formation of 2-cyanophenol [$(32.8 \pm 2.1) \text{ kJ mol}^{-1}$] [22], we estimate a value of $(138.9 \pm 4.3) \text{ kJ mol}^{-1}$ for the enthalpy of formation of 1,2-benzisoxazole. Another interesting comparison involves reaction R8:

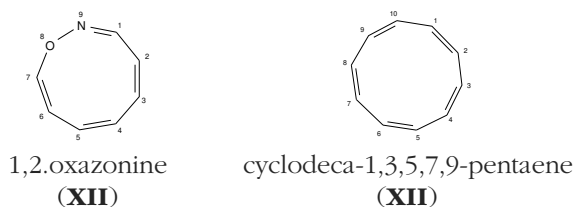


Naively, by neglecting any differential aromaticity effects in the rings and the N–O–N anomeric interaction found only in benzofurazan (X), we are tempted to suggest that this reaction should be thermoneutral. There are three measurements for the enthalpy of formation of gas-phase benzofurazan: (302.3 ± 2.1) [24], (300.7 ± 2.1) [25] and 272.7 [26] kJ mol^{-1} . We believe that the third value can safely be neglected because of “age” and a lack of consensus, and so, we take an average value of $(301 \pm 3) \text{ kJ mol}^{-1}$. No measurements have been reported for isobenzofuran (XI). Computationally, from accurate G3 atomization energies, we got an enthalpy of formation for benzofurazan of $311.1 \text{ kJ mol}^{-1}$ while, for isobenzofuran we got 77.3 kJ mol^{-1} from identical level calculations. As referred above, through an acceptable reasoning we could suggest reaction

Table 9.4. Estimated enthalpies of formation (from atomization reactions).

	G3(MP2)	G3	Exp.
Anthranil	187.4	190.7	180.8±2.1
Benzoxazole	30.3	33.7	44.8±5.0
Benzisoxazole	140.5	143.8	138.9±4.3
2-Cyanophenol	32.1	35.1	32.8±2.1
Isoxazole	85.9	85.9	78.58±0.54 82.0±0.6
Oxazole	-11.1	-11.3	-15.5±0.54

R8 would likely be approximately thermoneutral; in this case we would obtain an enthalpy of formation of about 189.2 or 194.2 kJ mol⁻¹, for anthranil, respectively by using the experimental estimate of the enthalpy of formation of benzofurazan or our G3 estimate of the same parameter. However, accurate computational techniques allows us to go further and calculate the reaction enthalpy as -7.1 kJ mol⁻¹, again from G3 energies and, again, not that different from our conjecture of thermoneutrality. In this case our estimates of the enthalpy of formation of anthranil would be 185.6 or 190.7 kJ mol⁻¹, respectively using experimental or computational data for the enthalpy of formation of benzofurazan. In either case we must recognize the quality of our calculations if we consider the close similarity between the last estimates and the experimentally measured value of the enthalpy of formation of anthranil, 180.8 ± 2.1 kJ mol⁻¹. One may regard both isomers anthranil and 1,2-benzisoxazole as derivatives of 1,2-oxazonine (*i.e.*, 1-oxa-2-aza-2,4,6,8-cyclononatetraene, XII) with an additional transannular C-C bond that transforms this monocycle into a bicyclic species with five- and six-membered rings:



In the absence of any additional information, one would assume that the above procedures would lead to bicyclic systems with very similar enthalpies

Table 9.5. Nucleus independent chemical shifts (ppm).

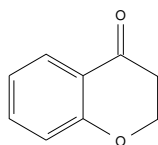
	6-membered-ring		5-membered-ring	
	NICS(0)	NICS(1.0)	NICS(0)	NICS(1.0)
Anthranil	-6.0	-8.1	-14.8	-13.0
1,2-benzisoxazole	-10.3	-11.6	-10.8	-10.1
Benzoxazole	-10.9	-11.8	-9.9	-9.4
2-cyanophenol	-9.4	-10.2	—	—
Oxazole	—	—	12.2	10.4
Isoxazole	—	—	12.6	11.0
Phenol	-9.7	-10.7	—	—
Benzene	-8.9	-11.1	—	—
Benzonitrile	-9.1	-11.0	—	—
Naphthalene	-9.3	-11.5	—	—

of formation. In fact, as enunciated above, our studies show that the difference is about 42 kJ mol^{-1} . This difference is significant, but is far less than the 140 kJ mol^{-1} by which naphthalene is more stable than its aromatic isomer azulene, both of which can be considered as resulting from cyclodeca-1,3,5,7,9-pentaene (XIII) through convenient transannular bond formation. This suggests that by thermochemical criteria, if we ascribe aromatic character to 1,2-benzisoxazole, then we should ascribe significant aromatic character to anthranil as well. Magnetic properties provide an alternative way of analysing aromaticity [9]. The NICS (nucleus-independent chemical shift) values for the molecules involved in this study have been calculated from the RHF/6-31G* wavefunctions at the most stable B3LYP/6-311G** geometries the main results being collected in Table 9.5.

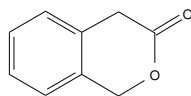
The NICS values calculated above the ring and at the center of the ring are in very good agreement with each other and both sets of values indicate that all the species have aromatic character since they have negative values. The benzenic rings of all these systems, with the exception of anthranil, shows NICS values that are consistent with the value found for benzene itself with the same basis set and wavefunctions [NICS(0) = -9.7 ppm], but they are slightly more negative. Similar comparisons apply to the NICS calculated at the centre of the five membered rings, which compare with the values found for pyrrole (-15.1 ppm) and furan

(−12.3 ppm) [9]. The NICS values for anthranil are remarkably different from those of the other compounds studied in this work; anthranil has a larger NICS value for the six-membered ring and a correspondingly lower value for the five-membered ring. This indicates a loss of aromaticity in the six-membered ring and an increase in the aromaticity of the five-membered ring, which seems to be in agreement with our calculations thus suggesting that anthranil is less benzenoid than its isomeric molecules. Benzene and 2-cyanophenol (as well as the monosubstituted phenol and benzonitrile) are not that different in terms of aromaticity. Even benzoxazole and 1,2-benzisoxazole are not that different in terms of their six-membered rings. What about anthranil? Interestingly, in that the sum of the NICS values [(0.0) or (1.0)] for the five- and six membered rings in anthranil is very nearly the same as those for its isomers 1,2-benzisoxazole and benzoxazole, it would appear that the aromaticity of these three species are very nearly the same as well.

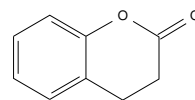
9.2.2 Stability of Chromanone and Coumarin Isomers [27,28]



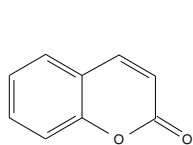
chromanone
(XIV)



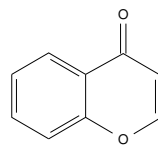
3-isochromanone
(XV)



dihydrocoumarin
(XVI)



coumarin
(XVII)

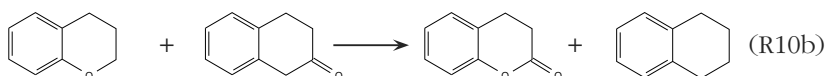
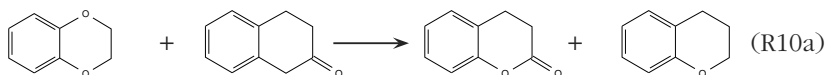
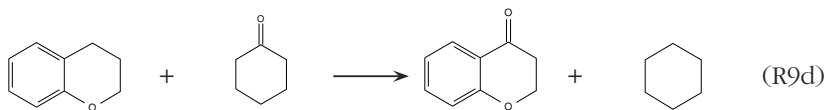
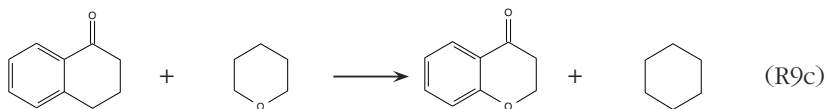
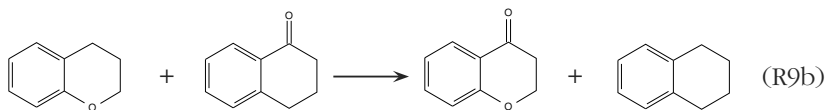
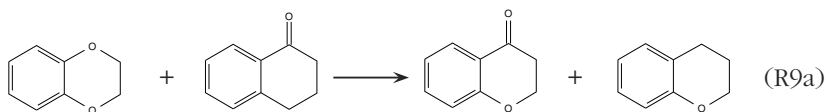


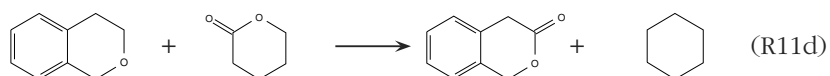
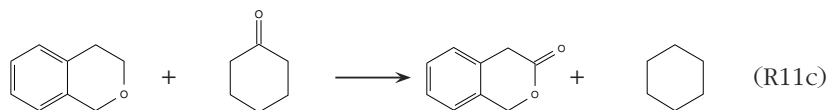
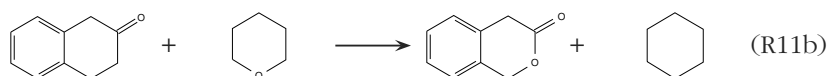
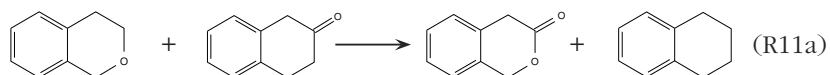
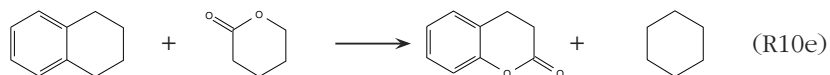
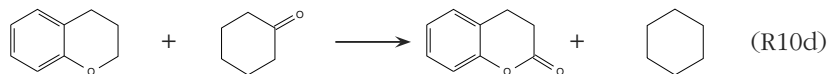
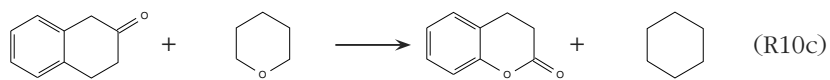
chromanone
(XVIII)

Each of the three isomeric chromanones has an optimum geometry consisting of a planar benzenic ring and a heterocyclic ring largely distorted from planarity. Planarity of the last ring is inhibited either by the angular strain within the sp^3 hybridized carbon atoms as well as the repulsion between contiguous $-CH_2-$ groups. The hydrogen atoms of these fragments are, in fact, observed to adopt almost perfectly mutually staggered conformations for the chromanone

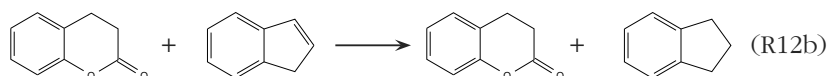
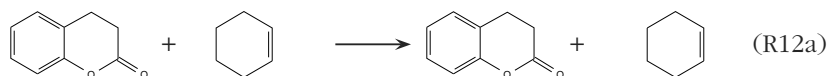
and dihydrocoumarin isomers. Contrasting with the above behaviour, both coumarin and chromone, systems mainly consisting of sp^2 -hybridized fragments, are found to adopt completely planar structures at their most stable molecular geometries. Indeed, such planar conformation favours the occurrence of stabilizing extended electronic delocalization between all those fragments, which, when involving cyclic structures, evidences the peculiar stabilizing effect we generally call aromaticity.

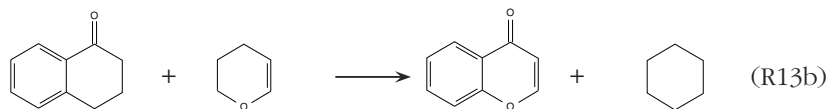
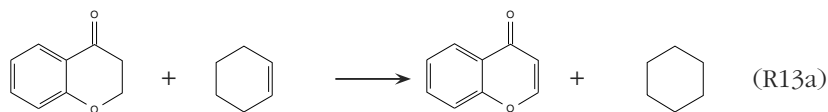
In order to estimate the enthalpies of formation of the systems from the calculated energies, we used the following set of homodesmotic reactions involving auxiliary systems whose thermochemical properties are well established experimentally [21,29-32]:





while for the other isomeric pair we used the following set of isodesmic/homo-desmotic reactions:





The resulting estimated enthalpies of formation are collected in Table 9.6. Considering first the most saturated set of molecules (chromanone, 3-isochromanone and dihydrocoumarin) we observe a good agreement between our computational estimates and the experimental data, with almost no significant difference between the DFT and the most accurate correlated MC-UT and MC-QCISD results, this being, certainly, an indication of the adequacy of the chosen homodesmotic reactions. Differences between the two sets of calculations become apparent when we consider the estimates of the enthalpies of formation obtained from atomization reactions. Even though we get acceptable results from the MC-UT and MC-QCISD energies, with deviations not exceeding 12.5 kJ mol^{-1} , the estimates obtained from the more modest B3LYP energies become clearly unacceptable, since the associated errors can exceed 50 kJ mol^{-1} for the B3LYP/ccPVTZ results and are even worse for the B3LYP/6-311G** ones. The experimentally observed stability ordering, however, is well described by all our calculations, which correctly predict dihydrocoumarin to be the most stable isomer, followed by 3-isochromanone (about 12 kJ mol^{-1} less stable) and by chromanone (about 44 kJ mol^{-1} more unstable).

Both chromone and coumarin had been experimentally studied previously [29,33,34], but the obtained enthalpies of formation differ considerably from the present measurements. Indeed, the earlier obtained enthalpies of formation of $-176.8 \pm 1.8 \text{ kJ mol}^{-1}$ for coumarin and of $-148.5 \pm 2.9 \text{ kJ mol}^{-1}$ for chromone are in disagreement with our own measurements by as much as 13.4 kJ mol^{-1} (coumarin) and 22.4 kJ mol^{-1} (chromone), both being predicted as being excessively stable as compared with the present work.

Table 9.6. Calculated and Experimental Formation Enthalpies at 298.15 K.

Compound	R	$-\Delta_f H^\circ(\text{g})/\text{kcal mol}^{-1}$					Exp.
		DFT/B3LYP		MC-UT	MC-QCISD	G3(MP2)	
		6.311G**	cc-pVTZ				
Chromanone	9a	202.9	202.3	198.8	199.2	—	204.5±2.4
	9b	202.4	202.2	201.3	201.6	—	
	9c	213.4	212.5	206.2	206.7	—	
	9d	204.4	201.5	196.0	196.5	—	
	<i>At</i>	<i>110.1</i>	<i>152.9</i>	<i>192.0</i>	<i>192.1</i>	—	
Dihydrocoumarin	10a	239.4	238.6	233.8	234.7	—	247.9±2.3
	10b	239.0	238.5	236.3	237.1	—	
	10c	250.0	248.8	241.2	242.2	—	
	10d	245.7	245.0	241.9	242.5	—	
	10e	251.4	249.5	247.2	246.9	—	
	<i>At</i>	<i>151.4</i>	<i>196.5</i>	<i>237.9</i>	<i>238.1</i>	—	
3-Isochromanone	11a	226.6	226.3	221.7	223.1	—	236.4±2.3
	11b	234.5	234.5	228.9	230.4	—	
	11c	233.4	232.8	227.3	228.5	—	
	11d	235.9	235.2	234.9	235.1	—	
	<i>At</i>	<i>135.9</i>	<i>182.2</i>	<i>225.6</i>	<i>226.2</i>	—	
Coumarin	12a	181.8	185.8	159.7	161.5	164.2	163.4±3.3 (176.8±1.8)
	12b	171.5	172.1	159.5	160.8	162.3	
	<i>At</i>	<i>80.5</i>	<i>129.2</i>	<i>140.8</i>	<i>143.6</i>	173.8	
Chromone	13a	140.3	144.5	123.6	124.4	127.5	126.1±2.5 (148.5±2.9)
	13b	133.5	133.4	119.8	121.3	124.2	
	<i>At</i>	<i>42.0</i>	<i>88.7</i>	<i>103.3</i>	<i>104.9</i>	<i>134.0</i>	

As can be seen from the results in Table 9.6, our calculations describe very accurately our own experimental data; indeed, with the exception of the results obtained from reaction (13b) and from MC-UT/3 and MC-QCISD/3 calculations, the most accurate composite methods [MC-UT/3, MC-QCISD/3, and G3(MP2)] provide estimates of the enthalpy of formation of these compounds with deviations from the experimental data which do not exceed 4 kJ mol^{-1} (*i.e.*, we achieve the standard of “*chemical accuracy*”). In addition, for the most accurate G3(MP2) calculations, even the results obtained from the atomization processes are in good agreement with what we found experimentally, with deviations not larger than 10.5 kJ mol^{-1} , a remarkably accurate result for non-isodesmic reactions. Additional corroboration of our suggested values is that we find a $38.3 \pm 4.1 \text{ kJ mol}^{-1}$ difference between the enthalpies of formation of coumarin

and chromone, as opposed to the earlier $28.3 \pm 3.4 \text{ kJ mol}^{-1}$ value, but in agreement with the *ca.* 40 kJ mol^{-1} difference found by our various calculational approaches.

Thus, our very accurate computational estimates correctly describe our experimental data and, on the other hand, crudely diverge clearly from the earlier experimental data of Sabbah and Watik, with deviations of 16 kJ mol^{-1} (coumarin) and 27.2 kJ mol^{-1} (chromone). Consequently, we feel confident to propose our new experimental data as the most reliable ultimate thermochemical data for coumarin and chromone.

Attempting to rationalize the stability order within each set of compounds, we recognize that those isomers which are more stabilized involve the $\text{O} = \text{C} - \text{O}$ fragment (lactone) and we can anticipate that their behaviour is likely to be understood from the interactions involving electron delocalization of the lone-electronic pairs of the oxygen atoms. Quantitatively, such interactions can be probed through an analysis of the wave functions in the framework of Natural Bond Orbital (NBO) theory [10-13], according to which the electronic population should be distributed over a set of localized one-centre ("lone-pair") and two-centre ("bond") orbitals. This localized description closely mimics a classical Lewis-type picture of the electronic system, while delocalization effects are evidenced by small occupancies of the set of anti-bonding orbitals. The stabilizing effect of such delocalization interactions can be quantitatively obtained as second-order perturbative estimates of the corresponding bonding–antibonding interactions. By doing so, we are thus able to identify the leading donor–acceptor interactions which are responsible for the differences in the stabilities of the chromanone isomers as being those involving the π lone-electronic pair of the ring oxygen and the anti-bonding $\pi_{\text{C}=\text{O}}^*$, which contributes with a stabilization energy of about 36 kcal mol^{-1} and 43 kcal mol^{-1} , respectively for dihydrocoumarin and for 3-isochromanone, and the π lone-electronic pair of the carbonyl oxygen and the anti-bonding $\sigma_{\text{C}-\text{O}}^*$ involving the carbon atom of the same group and the other oxygen atom, contributing with 36 kcal mol^{-1} and 34 kcal mol^{-1} , respectively for dihydrocoumarin and for 3-isochromanone. Note that neither

of the above interactions is allowed to occur in chromanone. The other important interaction justifying differences in stability involve electronic delocalization from the π lone-electronic pair of the ring oxygen to the closer anti-bonding $\pi_{\text{C}=\text{C}}^*$ of the benzenic ring. This interaction, which is absent in 3-isochromanone, contributes a stabilization of about 22 kcal mol^{-1} and 28 kcal mol^{-1} , respectively for dihydrocoumarin and chromanone. Considering now the isomeric pair coumarin/chromone, we find that both experiment and our computational results predict coumarin to be more stable than chromone (by about $37.3 \pm 4.1 \text{ kJ mol}^{-1}$), a feature which can again be ascribed to the peculiar structure of the former isomer involving the much more stable $\text{O} - \text{C} = \text{O}$ (lactone) fragment. We also recall that this ester fragment has considerable stabilization energy, identified as resonance energy and comparable to that of $\text{N} - \text{C} = \text{O}$, *i.e.*, the highly stabilized isoelectronic amide group [35,36]. Similarly to what we found above, coumarin, the unsaturated analog of the most stable dihydrocoumarin, is also the most stable isomer. Considering only the homologous pairs of both classes of compounds, we can observe that dihydrocoumarin is $43.4 \pm 3.3 \text{ kJ mol}^{-1}$ more stable than chromanone while coumarin is only $37.3 \pm 4.1 \text{ kJ mol}^{-1}$ more stable than chromone, thus evidencing an attenuation of the stabilizing capacity of the $\text{O} - \text{C} = \text{O}$ fragment by somewhat more than 6 kJ mol^{-1} . As we stressed before, the enhanced stability afforded by that fragment results from the possibility of involvement of the lone-electronic pairs of both oxygen atoms in conjugative or hyperconjugative mutual interactions, which are especially important for these isomers, since the $\text{O} - \text{C} = \text{O}$ fragment can directly interact with the contiguous aromatic ring, thus enhancing the extended electronic delocalization. Thus, fragmentation of this group results in the observed stability differences, but the destabilizing effect is less pronounced for the pair coumarin/chromone, since, in the latter system, the intercalation of a $\text{C} = \text{C}$ double bond between both oxygen atoms in the pyrone ring still tends to allow the mutual interactions involving the respective π -lone electronic pairs to occur, thus avoiding the destabilization becoming so severe for these systems. These interactions involving both π -lone electronic pairs through the $\text{C} = \text{C}$ double bond should presumably be evid-

Table 9.7. Nucleus independent chemical shifts (ppm).

	Benzene ring		Pyrone ring	
	NICS(0.0)	NICS(1.0)	NICS(0.0)	NICS(1.0)
Coumarin	-9.40	-10.69	-0.42	-3.24
Chromone	-10.27	-11.30	0.41	-3.12
Benzene	-9.7	-11.5	—	—
2-Pyrone	—	—	-1.3	-3.8
4-Pyrone	—	—	-0.2	-3.4
Naphthalene	-9.3	-11.5	-9.3	-11.5
1,2-dihydroNapht.	-7.8	-10.3	+2.6	-0.7

enced by some aromatic character in the pyrone ring of the coumarin, while no aromatic character should be evidenced by the homologous ring of dihydrocoumarin. In fact, nucleus independent chemical shifts (NICS) calculated from the corresponding B3LYP/6-311G** wave functions of both systems indicate that the NICS values at the center of the pyrone ring of chromanone and 1.0 Å above it are, respectively, +2.49 ppm and -0.16 ppm, while the corresponding values for dihydrocoumarin are +0.45 ppm and -0.73 ppm, respectively. These findings thus indicate essentially no aromatic character for both systems, even though the out of plane NICS value at the pyrone ring of dihydrocoumarin is somewhat more negative (the ring is consequently somewhat more aromatic), which is certainly a consequence of the electronic interactions involving the lone electronic pairs of both oxygen atoms integrating the fragment O - C = O. In contrast, the NICS values for chromone (and also for coumarin) reported in Table 9.7 indicate a moderate aromatic character of the pyrone ring of both systems, as is likewise shown for the monocyclic 2- and 4-pyrones as well. How aromatic are these pyrones? Enthalpy of formation data for these monocyclic pyrones, or any substituted derivative thereof, appear to be absent [37]: while the isomerization enthalpy interrelating 4-methoxy-6-methyl-2-pyrone and 2-methoxy-6-methyl-4-pyrone has been measured,[38] the presence of the exocyclic methoxy groups confounds comparison, as we have insufficient thermochemical knowledge of enol ethers and dialkoxyalkenes, as well as with pyrones of any type.

Complementing the above analysis of aromaticity based on magnetic property values we can also study the aromaticity of the studied systems on the basis of energetic criteria. We might think that both species (coumarin and chromone) should be rather aromatic, since they are π -isoelectronic or isoconjugate to the aromatic hydrocarbon, naphthalene, much as furan is related to benzene. The hydrogenation enthalpies of dihydrocoumarin and chromanone (dihydrochromone) can easily be obtained from their formation enthalpies and from the known formation enthalpy of molecular hydrogen; we thus find the enthalpies of hydrogenation to be -78.4 ± 3.5 and $-84.5 \pm 4.4 \text{ kJ mol}^{-1}$, respectively, for dihydrocoumarin and for chromanone. By contrast, the likewise derived hydrogenation enthalpy of the aromatic naphthalene to 1,2-dihydronaphthalene (using the enthalpy of formation of the former from Ref. 39 and the latter from Ref. 40) is the far smaller $-24.3 \pm 1.6 \text{ kJ mol}^{-1}$. The coumarin and chromone values are comparable to that of the 1,2-dihydronaphthalene with its nonaromatic ring to tetralin (1,2,3,4-tetrahydronaphthalene; data from Ref. 21), numerically $100.3 \pm 2.2 \text{ kJ mol}^{-1}$. Equivalently, the value for coumarin resembles that of the nonaromatic dihydronaphthalene more than that of the aromatic naphthalene, where we remind the reader that we are referring to the second “non-benzenoid” ring in the dihydrospecies. Alternatively, with precedent to the energetics of 1-ring species and the “experimental realized Dewar-Breslow model” of Ref. 41 we find, for the “aromatic” naphthalene and ring-opened *trans*-stilbene, the enthalpy of formation difference of 75.5 kJ mol^{-1} while, for the “non-aromatic” 1,2-dihydronaphthalene, the difference is 23.6 kJ mol^{-1} . The difference for coumarin and phenyl benzoate is but 20.8 kJ mol^{-1} . This again documents that coumarin lacks aromaticity other than found in its benzene ring. The above analysis cannot be applied to chromone. However, in that chromone contains the same groups as coumarin, the fact that coumarin is rather much more stable than chromone suggests that chromone likewise lacks aromatic character beyond that of its benzene ring as well.

References

- [1] A. Curtiss, K. Raghavachari, P. C. Redfern, V. Rassolov, J. A. Pople, *J. Chem. Phys.* **109**, 7764 (1998); L. A. Curtiss, K. Raghavachari, *The Encyclopedia of Computational Chemistry*, P. v. R. Schleyer (editor-in-chief), John Wiley & Sons Ltd, Athens, USA, **2**, 1104 (1998); L. A. Curtiss, P. C. Redfern, K. Raghavachari, V. Rassolov, J. A. Pople, *J. Chem. Phys.* **110**, 4703 (1999); A. G. Baboul, L. A. Curtiss, P. C. Redfern, K. Raghavachari, *J. Chem. Phys.* **110**, 7650 (1999).
- [2] P. L. Fast, J. Corchado, M. L. Sanchez, D. G. Truhlar, *J. Phys. Chem. A* **103**, 3139 (1999); J. M. Rodgers, P. L. Fast, D. G. Truhlar, *J. Chem. Phys.* **112**, 3141 (2000); B. J. Lynch, D. G. Truhlar, *J. Phys. Chem. A* **107**, 3898 (2003); B. J. Lynch, D. G. Truhlar, *J. Phys. Chem. A* **107**, 8996 (2003); B. J. Lynch, D. G. Truhlar, *J. Phys. Chem. A* **109**, 1643 (2005).
- [3] Y. Zhao, D. G. Truhlar, *J. Phys. Chem. A* **108**, 6908 (2004); Y. Zhao, B. J. Lynch, D. G. Truhlar, *J. Phys. Chem. A* **108**, 4786 (2004); Y. Zhao, B. J. Lynch, D. G. Truhlar, *Phys. Chem. Chem. Phys.* **7**, 43 (2005).
- [4] M. R. Nyden, G. A. Petersson, *J. Chem. Phys.* **75**, 1843 (1981); G. A. Petersson, M. A. Al-Laham, *J. Chem. Phys.* **94**, 6081 (1991); G. A. Petersson, T. G. Tensfeldt, J. A. Montgomery Jr., *J. Chem. Phys.* **94**, 6091 (1991); J. A. Montgomery Jr., J. W. Ochterski, G. A. Petersson, *J. Chem. Phys.* **101**, 5900 (1994); J. W. Ochterski, G. A. Petersson, J. A. Montgomery Jr., *J. Chem. Phys.* **104**, 2598 (1996); J. A. Montgomery Jr., M. J. Frisch, J. W. Ochterski, G. A. Petersson, *J. Chem. Phys.* **112**, 6532 (2000); J. A. Montgomery Jr, M. J. Frisch, J. W. Ochterski, G. A. Petersson, *J. Chem. Phys.* **110**, 2822 (1999).
- [5] T.H. Dunning Jr., *J. Chem. Phys.* **90**, 1007 (1989); R. A. Kendall, T. H. Dunning, Jr., R. J. Harrison, *J. Chem. Phys.* **96**, 6796 (1992); D.E. Woon, T.H. Dunning Jr., *J. Chem. Phys.* **98**, 1358 (1993); D.E. Woon, T.H. Dunning Jr., *J. Chem. Phys.* **100**, 2975 (1994); D. E. Woon, T. H. Dunning, Jr., *J. Chem. Phys.* **103**, 4572 (1995); A. K. Wilson, T. van Mourik, T. H. Dunning, Jr., *J. Mol. Struct. THEOCHEM* **388**, 339 (1996); A.K. Wilson, D.E. Woon, K. A. Peterson, T. H. Dunning Jr., *J. Chem. Phys.* **110**, 7667 (1999).

- [6] D. G. Truhlar, *Chem. Phys. Lett.* **294**, 45 (1998); W. Klopper, *J. Chem. Phys.* **115**, 761 (2001), F. Jensen, *Theor. Chem. Accounts*, **113**, 267 (2005); A. Karton, J. M. L. Martin, *Theor. Chem. Accounts*, **115**, 330 (2006).
- [7] A. J. C. Varandas, *J. Chem. Phys.* **113**, 8880 (2000); A. J. C. Varandas, *J. Chem. Phys.* **126**, 244105 (2007); A. J. C. Varandas, *Chem. Phys. Lett.*, **443**, 398 (2007); A. J. C. Varandas, *J. Chem. Phys.* **127**, 114316 (2007); A. J. C. Varandas, *Theor. Chem. Accounts* **119**, 511 (2008); A. J. C. Varandas, *J. Chem. Phys.* **129**, 234103 (2008); A. J. C. Varandas, *Chem. Phys. Lett.*, **471**, 315 (2009); A. J. C. Varandas, *J. Chem. Phys.* **131**, 124128 (2009).
- [8] T. Helgaker, W. Klopper, H. Koch, and J. Noga, *J. Chem. Phys.* **106**, 9639 (1997); A. Halkier, T. Helgaker, P. Jørgensen, W. Klopper, H. Koch, J. Olson, A. K. Wilson, *Chem. Phys. Lett.* **286**, 243 (1998); A. Halkier, T. Helgaker, W. Klopper, P. Jørgensen, A. G. Császár, *Chem. Phys. Lett.* **310**, 385 (1999).
- [9] P. v. R. Schleyer, C. Maerker, A. Dransfeld, H. Jiao, N. J. R. v. E Hommes, *J. Am. Chem. Soc.* **118**, 6317 (1996).
- [10] A. E. Reed, L. A. Curtiss, F. Weinhold, *Chem. Rev.* **88**, 899 (1988).
- [11] J. P. Foster, F. Weinhold, *J. Am. Chem. Soc.* **102**, 7211 (1980).
- [12] A. E. Reed, F. Weinhold, *J. Chem. Phys.* **78**, 4066 (1983).
- [13] E. D. Glendening, J. K. Badenhop, A. E. Reed, J. E. Carpenter, J. A. Bohmann, C. M. Morales, F. Weinhold, NBO 5.0, Theoretical Chemistry Institute, University of Wisconsin, Madison, **2001**.
- [14] D. Becke, *J. Chem. Phys.* **98**, 5648 (1993).
- [15] T. Lee, W. T. Yang, R. G. Parr, *Phys. Rev. B* **37**, 785 (1998).
- [16] M. M. Francl, W. J. Pietro, W. J. Hehre, J. S. Binkley, M. S. Gordon, D. J. DeFrees, J. A. Pople, *J. Chem. Phys.* **80**, 3654 (1982).
- [17] P. C. Hariharan, J. A. Pople, *Chem. Phys. Lett.* **16**, 217 (1972).
- [18] P. C. Hariharan, J. A. Pople, *Theor. Chim. Acta* **28**, 213 (1973); M. J. Frisch, J. A. Pople, J. S. Binkley, *J. Chem. Phys.* **80**, 3265 (1984).
- [19] P. A. Scott, L. Radom, *J. Chem. Phys.* **100**, 16502 (1996).
- [20] M. A. R. Matos, M. S. Miranda, V. M. F. Morais, J. F. Liebman, *Eur. J. Org. Chem.* **15**, 3340 (2004).

- [21] J. B. Pedley, *Thermochemical Data and Structures of Organic Compounds*, TRC Data Series, College Station, Texas, vol. 1, **1994**.
- [22] The standard molar enthalpy of 2-cyanophenol is from: M. A. R. Matos, M. S. Miranda, V. M. F. Morais, *Struct. Chem.* **15**, 99 (2004).
- [23] M. L. Casey, D. S. Kemp, K. G. Paul, D. D. Cox, *J. Org. Chem.* **38**, 2294 (1973).
- [24] M. L. Leitão, G. Pilcher, W. E. Acree, Jr., A. I. Zvaigzne, S. A. Tucker, M. D. M. C. Ribeiro Da Silva, *J. Chem. Thermodyn.* **22**, 923 (1990).
- [25] M. T. Arshadi, *J. Chem. Thermodyn.* **12**, 903 (1980).
- [26] C. R. Brent, PhD Thesis, Tulane University, New Orleans, **1963**.
- [27] M. A. R. Matos, C. C. S. Sousa, V. M. F. Morais, *J. Chem. Thermodyn.*, **41**, 308 (2009).
- [28] M. A. R. Matos, C. C. S. Sousa, M. S. Miranda, V. M. F. Morais, J. F. Liebman, *J. Phys. Chem. B* **113**, 11216 (2009).
- [29] S. Verevkin, *Thermochim. Acta* **310**, 229 (1998).
- [30] M. A. R. Matos, C. C. S. Sousa, V. M. F. Morais, *J. Chem. Thermodyn.* **40**, 1552 (2008).
- [31] M. A. R. Matos, C. C. S. Sousa, V. M. F. Morais, *J. Phys. Chem. A* **112**, 7961 (2008).
- [32] M. A. R. Matos, C. C. S. Sousa, V. M. F. Morais, *J. Chem. Thermodyn.* **41**, 308 (2009).
- [33] R. Sabbah, L. E. Watik, *Bull. Soc. Chim. Fr.* **4**, 626 (1988).
- [34] L. E. Watik, R. Sabbah, *Bull. Soc. Chim. Fr.* **128** 344 (1991).
- [35] J. F. Liebman, A. Greenberg, *Biophys. Chem.* **1**, 222 (1974).
- [36] A. Greenberg, Y. Chiu, J. L. Johnson, J. F. Liebman, *Struct. Chem.* **2**, 117 (1991).
- [37] L. Lorenz, H. Sternitzke, *Elektrochem. Z. Angew. Phys. Chem.* **40**, 501 (1934). While these authors assert pyrone, as found in its 2,6-diphenyl derivative, "resembles the benzene ring", no data is in fact given therein to further discuss this point.
- [38] P. Beak, *Tetrahedron* **20**, 631 (1964); P. Beak, D. S. Mueller, J. Lee, *J. Am.*

Chem. Soc. **96** 3867 (1974).

[39] M. V. Roux, M. Temprado, J. S. Chickos, Y. Nagano, *J. Phys Chem. Ref. Data* **37**, 1855 (2008).

[40] R. D. Chirico, W. V. Steele, *J. Chem. Thermodyn.* **40**, 806 (2008).

[41] R. S. Hosmane, J. F. Liebman, *Tetrahedron Lett.* **32**, 3949 (1991).

10. CREATING METAMATERIALS AT THE NANO-SCALE

J. M. Pacheco^{1,2*} and C. L. Reis¹

¹Departamento de Matemática e Aplicações, Universidade do Minho
4710 - 057 Braga, Portugal

²ATP-group, CMAF, Complexo Interdisciplinar da Universidade de Lisboa,
Av. Prof. Gama Pinto 2, 1649 - 003 Lisboa, Portugal

The fact that the founding papers of Density Functional Theory are among the most cited papers ever, testifies for the importance of Quantum Mechanics and its (often) counter intuitive features in characterizing many-particle systems at a nano and sub-nano scale. Density Functional Theory has enabled one to use the computer to predict quantitatively several of the properties of the aforementioned many-particle systems. The prediction of new materials, often exhibiting meta-stability, is one of its distinctive features. In this lecture we will discuss a new class of meta-materials which, being silicon based, exhibit properties which in no way resemble those of its main constituent. In particular, we will discuss the structural and electronic properties of new materials of the form $X@Si_{16}$ (with $X=Ti, Zr$ and Hf) which are predicted to be (meta) stable at room temperature and exhibit a remarkable potential as possible high- T_c superconductors.

10.1 Introduction

A fundamental challenge for nanotechnology is to control fabrication with atomic precision in order to assemble new materials with outstanding properties or functions. Modern theoretical and computational methods are already able to predict the properties of such materials. The importance of this has been recognized with the 1998 Nobel Prize award to Walter Kohn for his development of the Density Functional Theory [1, 2] (DFT) and to John Pople for his development of computational methods in quantum theory. Today, theoretical predictions are competitive with experimental techniques for controlling single

*Email address: jmpacheco@math.uminho.pt

molecule chemistry given that the required hardware for performing computer simulations is often orders of magnitude cheaper and may be more effective than experiments. The quantitative predictions based on DFT rely on Quantum Mechanics which itself is on the basis of the technological revolution of the XXth century.

Much of what is considered now the information technology revolution has been dependent of an ever increasing miniaturization of devices based on silicon. The number of transistors that can be placed in an integrated circuit, which is a measure of its computing power, has doubled every 20 months since 1971. However, physical limits to miniaturization of devices based on bulk silicon have already been met in the recent 45 nm generation of devices, where a high- k dielectric material like HfO_2 has replaced SiO_2 as a gate insulator [3] for the first time since the beginning of the integrated circuit. The potential “brick wall” facing Moore’s Law [4] has motivated an incredible amount of experimental and theoretical work in the search for alternative materials to bulk silicon. Silicon clusters in particular have been under focus, given that nano-structured materials are known to exhibit very different properties from their bulk counterparts. But contrary to fullerene-like carbon clusters, pure silicon clusters have been found to be chemically reactive, precluding the synthesis of cluster assembled materials [5]. Along another route, early experiments by Beck [6, 7] indicated the feasibility of using metal atoms to nucleate several silicon atoms into stable $X@Si_n$ clusters, of which $X@Si_{16}$ was found to be particularly stable. Recent experimental [5, 8–15] and theoretical [16–24] work has confirmed these results for a variety of mixed metal-silicon sandwich [8, 25] and cage [16, 17, 23, 24] clusters, and a special class of clusters with stoichiometry $X@Si_{16}$, with X a metal atom, has been identified [16] as especially stable by means of ab-initio computer simulations. In particular, the stability of $X@Si_{16}$ ($X=\text{Ti, Zr, Hf}$) nano particles has been confirmed experimentally [13], via selective formation of neutral gas phase clusters, using a dual laser vapourisation technique of pure metal and pure silicon targets in an inert helium atmosphere. An additional experimental confirmation of the synthesis of these nano-particles has been reported recently using a mag-

neutron co-sputtering technique [15].

Using first-principles computer simulations within DFT we investigate the main electronic properties of $X@Si_{16}$ ($X=Ti, Zr$ and Hf) clusters. The vibrational modes and infrared spectra are also determined. We show the feasibility of using the clusters as elementary building blocks to synthesize stable bulk materials, and find that all the $X@Si_{16}$ ($X=Ti, Zr$ and Hf) cluster-assembled materials crystallize in hexagonal closed packed structures (HCP). We further characterize the main structural and electronic properties of these materials, while illustrating their differences. We predict that these materials should be possible to stabilize in a metastable phase at room temperature and normal pressure conditions. This phase is predicted to be maintained under isotropic compression up to ~ 1 GPa. Similar to $Ti@Si_{16}$, both $Zr@Si_{16}$ and $Hf@Si_{16}$ are especially stable semiconductors with GGA (see below) band gaps of 1.6 eV, 0.3 eV larger than that previously found for bulk $Ti@Si_{16}$.

This paper is organized as follows: In section two details of the method and simulations carried out are provided. Results and discussion are left to section three, whereas the main conclusions and future prospects are postponed to section four.

10.2 Methods

All *ab-initio* calculations were performed within the generalized gradient approximation (GGA [27]) to DFT using norm-conserving pseudopotentials [26, 28] and a plane-wave basis [29, 30]. An energy cut-off of 30.0 Hartree (816 eV) was used throughout, leading to well converged forces within 0.02 eV/Bohr. This value was also used as a stopping criteria for structural optimizations. Large energy cutoffs are crucial to ensure reliable results (and good convergence of the forces). We note that if less restrictive (and consequently, less computer demanding) parameters are used in structural optimizations, the forces (gradients of the energy with respect to atomic positions) will be poorly determined. As a consequence artificial structures and cage breakup can be obtained using $X@Si_{16}$ clusters as building blocks.

10.2.1 Isolated Clusters

Structural optimization

The atomic coordinates of the isolated clusters were computed employing a super-cell hexagonal lattice with parameters $a = c = 27.0$ Bohr to avoid mirror-image interactions. To ensure proper structure determination we performed several Quantum Langevin Molecular Dynamics [31] (QLMD) simulations at different temperatures starting from arbitrary configurations of Si atoms always nucleated around the central metal atom. Subsequently we performed geometry optimizations employing a conjugated gradient algorithm starting from the lowest energy configurations obtained in the QLMD runs.

Electronic properties

We computed the total energy, the one-electron Kohn-Sham levels as well as the total valence electronic density $\rho(\mathbf{r})$ of each nano-structure at the equilibrium configuration. From the electronic density $\rho(\mathbf{r})$ we constructed the radial electronic density, $\rho(r) = \rho(|\mathbf{r}|)$ by calculating its average over the solid angle:

$$\rho(r) = \frac{1}{4\pi} \int_{\Omega} \rho(\mathbf{r}) d\Omega$$

The number of valence electrons is given by:

$$N = \int d^3r \rho(\mathbf{r}) = \int_0^{\infty} dr 4\pi r^2 \rho(r) \equiv \int_0^{\infty} dr \eta(r) \quad (10.1)$$

The quantity $\eta(r)$ defined in the last integral can be useful in quantifying the electronic density inside the nanoparticle, providing a qualitative measure of its chemical inertia.

We computed the cohesive energy *per atom* for each cluster subtracting from the total energy E_{tot} the atomic energies $E_{\text{ps}}^{\text{Si}}$ and E_{ps}^X ($X=\text{Ti, Zr, Hf}$) of the pseudopotential calculation, $E_{\text{coh}} = (E_{\text{tot}} - 16E_{\text{ps}}^{\text{Si}} - E_{\text{ps}}^X)/17$.

Vibrational modes and infrared spectrum

The vibrational modes of frequency ω are described by a periodic displacement in time of each nuclei I :

$$\mathbf{u}_I(t) = \mathbf{u}_I e^{i\omega t}$$

This leads to the following eigenvalue equation:

$$-\omega^2 M_I \mathbf{u}_I = \sum_J \frac{\partial^2 E(\mathbf{R})}{\partial \mathbf{R}_I \partial \mathbf{R}_J} \mathbf{u}_J$$

which involves second order derivatives of the ground state energy $E(\mathbf{R})$ with respect to all N nuclei positions \mathbf{R}_I ($I = 1, \dots, N$). Solving these equations leads to a set of frequencies ω^ν ($\nu = 1, \dots, 3N$) and corresponding normal modes $\mathbf{u}^\nu = \mathbf{u}_{\tau,\alpha}^\nu \mathbf{e}_\alpha$ involving the collective displacements of the nuclei ($\tau = 1, \dots, N$) along the Cartesian directions ($\alpha = x, y, z$).

The absolute infrared intensity of the mode ν is given by [32]:

$$I_\nu^{\text{IR}} = K \left| \sum_{\tau,\alpha,\beta} Z_{\tau,\alpha,\beta}^* u_{\tau,\beta}^\nu \right|^2$$

with $\tau = 1, \dots, N$ and $\alpha, \beta = x, y, z$. For intensities in $(\text{D}/\text{\AA})^2 \text{amu}^{-1}$ and Z in atomic units $K = 4.2056 \times 10^4$. The Born effective charge tensor \mathbf{Z}^* is the second derivative of the energy with respect to both the electric field \mathbf{G} and the nuclei displacement \mathbf{R}_τ :

$$Z_{\tau,\alpha,\beta}^* = \frac{\partial^2 E}{\partial G_\alpha \partial R_{\tau,\beta}}$$

The second order derivatives of the ground state energy, with respect to atomic displacements and/or homogeneous electric fields are computed using density functional perturbation-theory (DFPT) [33, 34].

10.2.2 Bulk phase

Structural optimization

In a first step, we investigate bulk forms of cluster assembled materials, using the equilibrium structures of the isolated cages. To this end, we computed the cohesive energy per cluster varying the distance between clusters in a given bulk structure, while freezing the cluster geometry and the angles between primitive lattice vectors. The cohesive energy per cage in the bulk E_{coh}^b is defined:

$$E_{\text{coh}}^b = (E_{\text{tot}}^b - N_c E_I) / N_c$$

where E_{tot}^b is the total energy per unit cell, E_I is the energy of the isolated cluster and N_c is the number of clusters in the unit cell. Several bulk structures

were investigated: Simple Cubic (SC), DIAMond-type (DIA), Body Centered Cubic (BCC), Face Centered Cubic (FCC) and Hexagonal Close Packed (HCP). We placed 1 cluster per unit cell in the SC, BCC and FCC structures, and 2 in DIA and HCP. We have also tried to use supercells for the different lattices but the corrections in energy were found to be negligible. We have carefully chosen the k -point sampling in each calculation (particularly for small inter-cluster distances) in order to ensure well converged results. We used the following Monkhorst-Pack grids: $2 \times 2 \times 2$ for DIA, $4 \times 4 \times 4$ for SC, BCC and FCC and $3 \times 3 \times 2$ for HCP.

Subsequently we performed a full geometry relaxation of both atomic coordinates and lattice parameters taking as a starting point the configuration corresponding to the minimum of the cohesive energy per cluster as a function of distance between clusters for the different bulk structures we found before.

Pressure curve and bulk modulus

Given the cohesive energy per cluster as a function of the distance d between clusters, $E_{\text{coh}}(d)$, we can obtain the pressure as a function of inter-cage distance $P(d)$ by computing the numerical derivative from a cubic spline fit to the cohesive energy points:

$$P(d) = -\frac{\partial E}{\partial V} = -\frac{\partial E}{\partial d} \left(\frac{\partial V}{\partial d} \right)^{-1}$$

For a hexagonal lattice in the ideal packing structure (HCP), the volume of the primitive cell is $V = \sqrt{2}d^3$. Thus:

$$P(d) = -\frac{1}{3\sqrt{2}d^2} \frac{\partial E}{\partial d} = -\frac{254.845}{d^2} \frac{\partial E}{\partial d}, \quad (10.2)$$

which provides the pressure in GPa for lengths in Bohr and energies in eV. The Bulk modulus B is determined by fitting the cohesive energy points to the Birch-Murnaghan equation of state [35]:

$$E(V) = E_0 + \frac{9V_0B_0}{16} \left\{ \left[\left(\frac{V_0}{V} \right)^{2/3} - 1 \right]^3 B_0' + \left[\left(\frac{V_0}{V} \right)^{2/3} - 1 \right]^2 \left[6 - 4 \left(\frac{V_0}{V} \right)^{2/3} \right] \right\} \quad (10.3)$$

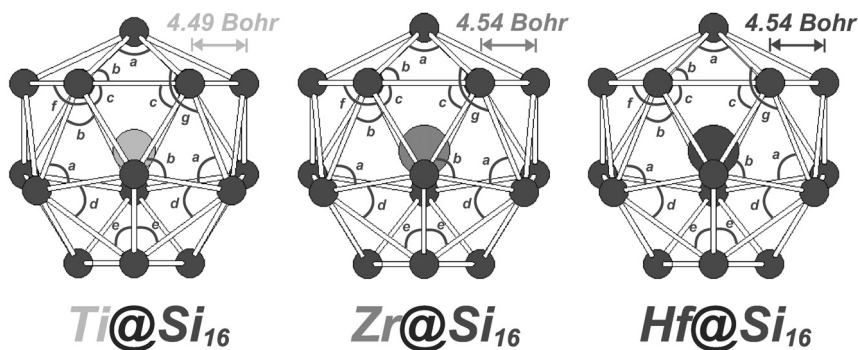


Figure 10.1. The Frank-Kasper [36] cage-structures, corresponding to the equilibrium of the $X@Si_{16}$ nano-particles. These highly symmetric structures, exhibiting several C_3 symmetry axes, will be used as building blocks of molecular solids. Selected bond angles are also represented. Angle values are given in Table 10.1.

Table 10.1. Selected bond angles depicted in Figure 10.1 for the $X@Si_{16}$ clusters ($X=Ti, Zr, Hf$). Similar values for the angles have been identified in amorphous Silicon [37].

$X@Si_{16}$	a	b	c	d	e	f	g
Ti	54.6°	62.7°	60.0°	53.1°	63.4°	120.0°	106.4°
Zr	54.0°	63.0°	60.0°	52.6°	63.7°	120.0°	108.4°
Hf	54.0°	63.0°	60.0°	52.6°	63.7°	120.0°	108.4°

10.3 Results and Discussion

10.3.1 Isolated Clusters

The structures of the isolated $X@Si_{16}$ nano-particles obtained using the procedure outlined in the previous section are shown in Figure 10.1.

All these nano-particles exhibit Frank-Kasper [36] cage structures with C_{3v} symmetry. In Table 10.2 the parameters characterizing the structural properties of these clusters are given. We choose three sets of distances: The distance from the metal atom to the four silicon atoms on the tetrahedral sites r_1 ; the distance from the metal atom to the remaining twelve silicon atoms r_2 , and the minimum nearest neighbour Si – Si distance r_{min}^{nn} . The $Zr@Si_{16}$ and $Hf@Si_{16}$ have larger dimensions than $Ti@Si_{16}$: r_1 and r_2 are $\sim 3\%$ and $\sim 1\%$ larger than the ones found for $Ti@Si_{16}$.

Once the ground state geometries have been determined, we computed their

Table 10.2. Structural parameters for the $X@Si_{16}$ clusters with $X=Ti, Zr, Hf$. r_1 is the distance from the metal atom to the four silicon atoms on the tetrahedral sites, r_2 is the distance of the metal atom to the remaining twelve silicon atoms and r_{min}^m is the minimum nearest neighbour Si-Si distance.

$X@Si_{16}$	r_1 (Bohr)	r_2 (Bohr)	r_{min}^m
Ti	4.93	5.34	4.49
Zr	5.09	5.40	4.54
Hf	5.09	5.40	4.54

Table 10.3. Cohesive energy per cluster and HOMO-LUMO gaps for the $X@Si_{16}$ clusters with $X = Ti, Zr, Hf$.

$X@Si_{16}$	$E_{cob}/Atom$ (eV)	$H - L$ Gap (eV)
Ti	-4.96	2.3
Zr	-4.99	2.4
Hf	-4.97	2.5

main electronic properties. In Table 10.3 we list the calculated cohesive energy per atom and HOMO-LUMO (Highest Occupied - Lowest Unoccupied Molecular Orbital) gap for these clusters. Whereas the cohesive energies are almost identical for all cages the Zr@Si₁₆ and Hf@Si₁₆ gaps are $\sim 6\%$ larger than the one found for Ti@Si₁₆.

In Figure 10.2 we show the radial electronic density of all the three clusters, which is remarkably similar. Besides their large HOMO-LUMO gaps, another indication of stability in these clusters is that almost all of the electronic density is concentrated inside the cage clusters. The vertical bars represent the outer limits of the cage-cluster, taking into account the cage radius and the silicon atomic radius (cf. Table 10.2). Approximately 96% of the electronic charge density is concentrated inside a sphere of radius 8 Bohr, suggesting a remarkable level of chemical inertia.

In Figure 10.3 we display the one-electron energy levels. The three nanoparticles exhibit energy level distributions which are qualitatively similar. The degeneracies of the energy levels can be qualitatively organized in the following

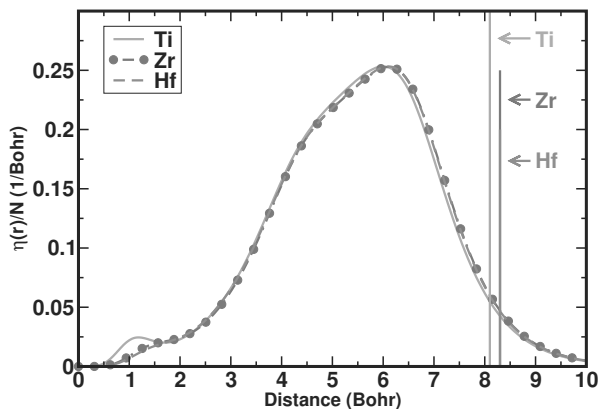


Figure 10.2. Normalized radial electronic densities $\eta(r) = 4\pi r^2 \rho(r)$ plotted as a function of the distance to the central metal atom for isolated clusters Ti@Si_{16} (solid line), Zr@Si_{16} (dash-dotted line) and Hf@Si_{16} (dashed line). The radial electronic density $\rho(r)$ is obtained from the calculated ground state total electronic density $\rho(\mathbf{r})$ taking its average over the solid angle Ω . See Eq. (10.1). The total area subtended by each curve is 1.

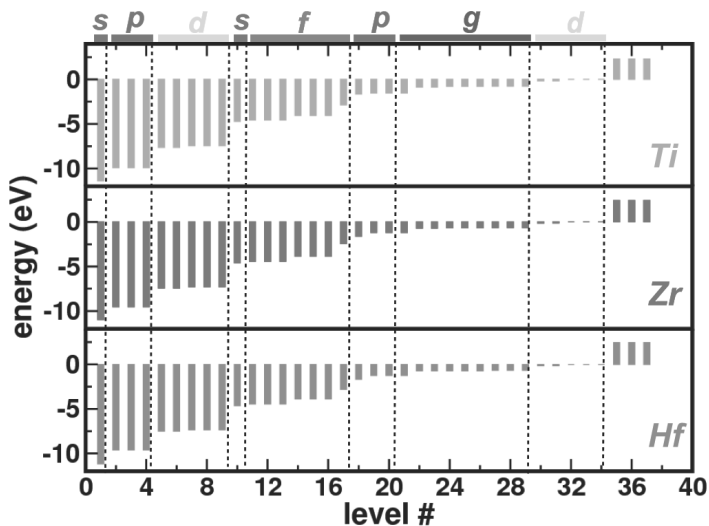


Figure 10.3. Energy levels for the $X@Si_{16}$ clusters with $X=\text{Ti, Zr, Hf}$. The electronic occupancy of each level is 2. The plotted levels are grouped according to their approximated degeneracies corresponding to levels in a spherical (jellium) shell structure with angular momenta s, p, d, s, f, p, g, d .

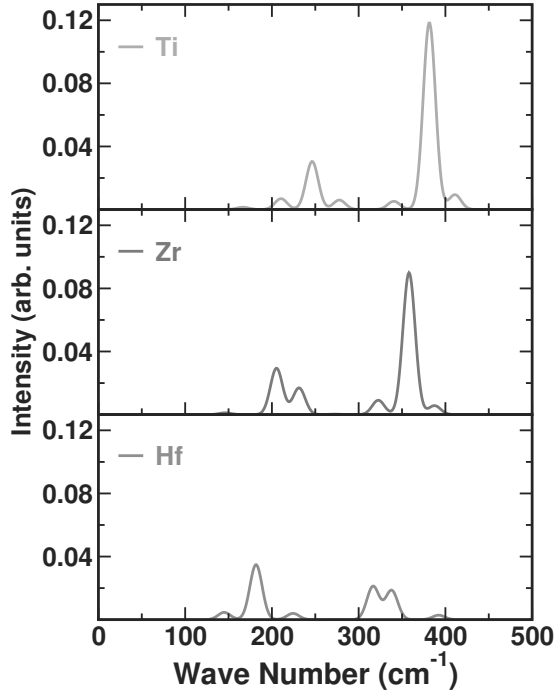


Figure 10.4. The calculated infrared spectrum of the $X@Si_{16}$ ($X=Ti, Zr$ and Hf) nanoparticles.

sequence:

$$2, 6, 10, 2, 14, 6, 18, 10.$$

This sequence is in excellent agreement with that resulting from a spherical-like (jellium) super-atom:

$$s, p, d, s, f, p, g, d.$$

Hence, and on top of a structurally stable and highly symmetric cluster, the 68 valence electrons of each cage cluster also organize into a spherical closed-shell electronic system. Consequently these cages qualify as “double magic”.

In Figure 10.4 we show the results of the calculation of the infrared spectrum using the procedure described in the previous section. In all three cases the normal modes have frequencies which are low compared to the fullerenes, exhibiting sizable intensity $\sim 200\text{ cm}^{-1}$. This picture is consistent with a weaker bonding of the silicon atoms in the $X@Si_{16}$ ($X=Ti, Zr$ and Hf) nanoparticles

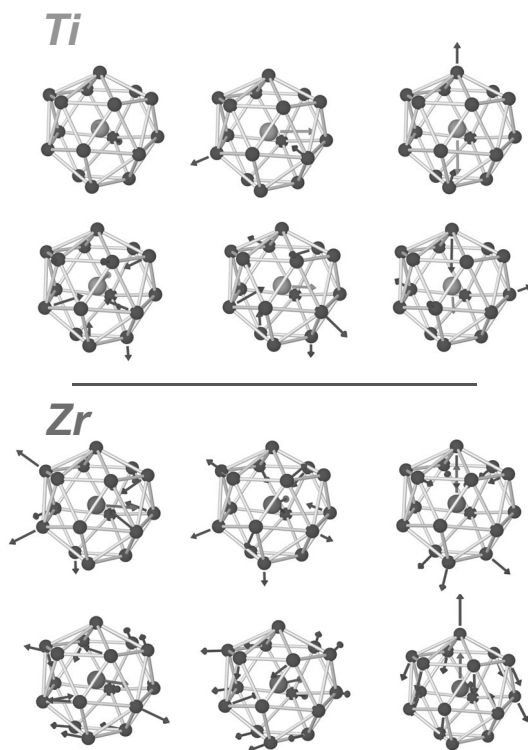


Figure 10.5. Selected normal modes for the Ti@Si_{16} (upper panel) and Zr@Si_{16} (lower panel) nanoparticles. In each panel the three top modes correspond to the peak of highest IR activity whereas the lower three modes correspond to second most intense peak.

compared to the carbon atoms in the fullerene clusters. The IR spectrum for Ti@Si_{16} depicted in the upper panel of Figure 10.4 is nearly identical to the one obtained by Nakajima and coworkers [14] using a localized basis set method. One interesting feature apparent in Figure 10.4 is a progressive softening of the frequency spectrum with the increasing mass of the central metal atom. This is accompanied with a simultaneous decrease in IR activity which is most pronounced for Hf@Si_{16} . The peaks of highest intensity at 380 cm^{-1} and 360 cm^{-1} for Ti@Si_{16} and Zr@Si_{16} respectively correspond to the three normal modes depicted in the upper part of each panel of Figure 10.5. In the case of Ti@Si_{16} these are essentially displacements of the central metal atom in the cluster with minor rearrangements of the surrounding silicon atoms. For the Zr@Si_{16} the

Hf

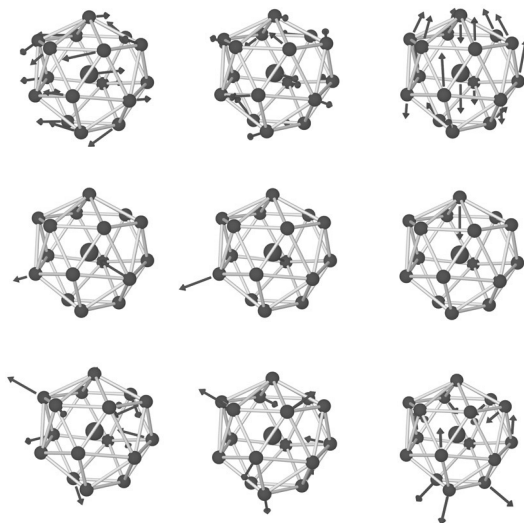


Figure 10.6. Selected normal modes for the Hf@Si_{16} nanoparticles. The three top modes correspond to the peak of highest IR activity whereas the lower six modes correspond to second most intense peaks.

movement of the central metal atom is accompanied by a more sizable distortion of the silicon cage. This is also the case for the three modes corresponding to the second most intense peak for both Ti@Si_{16} and Zr@Si_{16} at 246 cm^{-1} and 205 cm^{-1} respectively.

In the case of Hf@Si_{16} the peak of highest IR activity is located at 180 cm^{-1} . These modes are depicted in the upper part of Figure 10.6 whereas the second most intense peaks correspond to the six normal modes depicted in the lower part of Figure 10.6.

10.3.2 Bulk phase

We investigate now the possible stability of bulk forms of the cluster assembled materials. We restrict our analysis to the Frank-Kasper [36] cage structures even though we are aware that other isomers of $M@Si_{16}$ have been reported in the literature [16, 21, 22]. However no structure of comparable stability

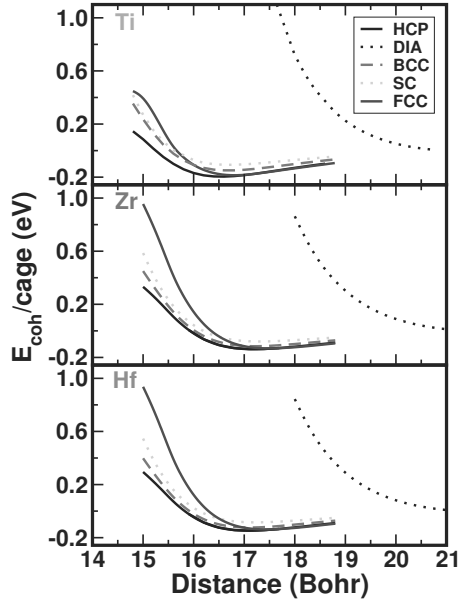


Figure 10.7. Cohesive energy as a function of inter-cage distance for bulk structures of $X@Si_{16}$ clusters with $X=Ti, Zr, Hf$. For all crystal structures, nearest neighbor cages are all at the same distance from any focal cage (for the HCP structure ($c/a = \sqrt{8/3}$), see main text for details). The curves for the HCP, FCC, BCC and SC are drawn with solid lower, solid upper, dashed and dotted lines, respectively. The only curve which exhibits no bound state corresponds to the DIA structure, drawn with a dotted line.

has been identified to date with stoichiometry $M@Si_{16}$. Hence we believe this choice is justified. The existence of a C_{3v} axis in the Frank-Kasper [36] structure may favour the HCP structure, since C_{3v} is the point symmetry group of the crystallographic $P3m1$ hexagonal group; nonetheless we investigated other possibilities. In Figure 10.7 we plot the cohesive energy per cluster as a function of cage-cage distance for the three cluster assembled materials in their different bulk structures - SC, DIA, BCC, FCC and HCP. In all cases, the cohesive energy curves for the SC, BCC, and FCC structures exhibit well defined minima around 17 Bohr. They are, however, less stable than the HCP structure. An entirely different behaviour is found for the DIAMond structure indicating that in all cases this structure is unstable. In Figure 10.8 we show in detail the cohesive energy

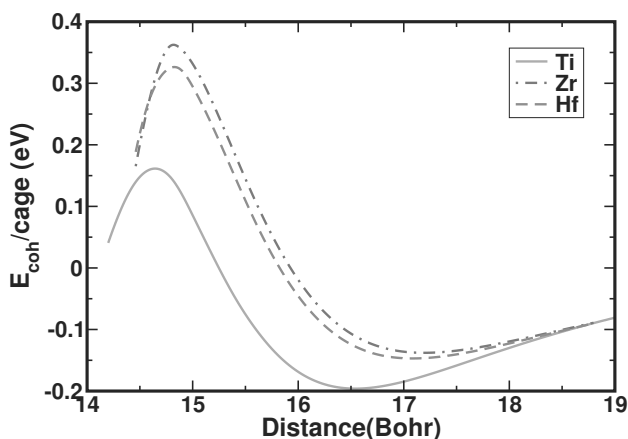


Figure 10.8. Cohesive energy as a function of inter-cage distance for the HCP molecular solids Ti@Si₁₆ (solid line), Zr@Si₁₆ (dashed-dotted line) and Hf@Si₁₆ (dashed line).

curves for the three cluster assembled materials in the HCP structure. The curve for HCP-Ti@Si₁₆ has a minimum for a cage-cage distance of 16.54 Bohr and a value at the minimum of only -0.2 eV indicating that the cages bind weakly. The significant reduction of the binding compared to fullerite [38] (cohesive energy per cluster of -1.6 eV) is related to the role played by the central metal atom which effectively pulls the valence charge density to within the cage, increasing not only the cluster structural stability but also the HOMO-LUMO gap therefore reducing its chemical reactivity. The curves for Zr@Si₁₆ and Hf@Si₁₆ have minima at cage-cage distances of 17.2 Bohr and 17.1 Bohr respectively. The inter-cage distance in these two structures is $\sim 4\%$ larger than the one found for HCP Ti@Si₁₆. The values of -0.14 eV and -0.15 eV at the minimum also indicate that the binding in these bulk materials is weaker than in the bulk Ti@Si₁₆. These results correlate with the fact that both Zr@Si₁₆ and Hf@Si₁₆ nanoparticles have a cage radius $\sim 3\%$ larger than Ti@Si₁₆. Indeed, a larger cage radius induces an increase of the inter-cage distance for the cluster assembled materials and also a decrease of the binding between clusters given that the same electronic charge is spread in a larger cluster volume.

Table 10.4. Lattice parameters for the $X@Si_{16}$ HCP molecular solids with $X=Ti, Zr, Hf$. Δ is the deviation of the ratio of lattice parameters c/a from the ideal packing value $\sqrt{8/3}$.

$X@Si_{16}$	a (Bohr)	c (Bohr)	Δ (%)
Ti	16.54	27.13	0.5
Zr	17.11	27.94	0.01
Hf	16.93	28.14	1.8

Relaxation of both the internal cluster coordinates and the lattice parameters starting at the minimum structures of Figure 10.8 leads to HCP structures characterized by the lattice parameters summarized in Table 10.4. The atomic rearrangements within each cluster are negligible compared to the isolated cluster geometry, the same applying to the overall changes in cohesive energies. The orientation of the clusters in the $Zr@Si_{16}$ and $Hf@Si_{16}$ HCP structures is compatible with the $p3m1$ crystallographic group and identical to that of $Ti@Si_{16}$ in Ref. 26 where it has been explicitly illustrated.

Figure 10.8 also reveals that, despite the well developed minima in the cohesive energy per cluster, these minima are separated by barriers from other equilibrium structures [26], which turn out to be more stable.

Similar to what was found for $Ti@Si_{16}$ [26] these systems will relax to an amorphous structure where silicon atoms of neighbouring cages bind covalently when subject, *e.g.*, to very high pressures. This covalent binding leads to an absolute increase of the cohesive energy per cluster to -2.2 eV. However from Figure 10.8 it is apparent that the values of the barrier maxima for both $Zr@Si_{16}$ and $Hf@Si_{16}$ are larger than the 0.16 eV found for $Ti@Si_{16}$. This translates into an increase in the applied pressure necessary to drive the Zr, Hf@ Si_{16} bulk materials away from their metastable equilibrium HCP structure. Fully unconstrained geometry relaxations, varying both the cluster coordinates and unit cell parameters, starting from a configuration significantly compressed with respect to the equilibrium HCP configuration show no sign of amorphous transition at normal temperature.

In Figure 10.9 we plot the pressure as a function of inter-cage distance for the three $X@Si_{16}$, $X=Ti, Zr, Hf$ bulk materials using the data from the cohesive

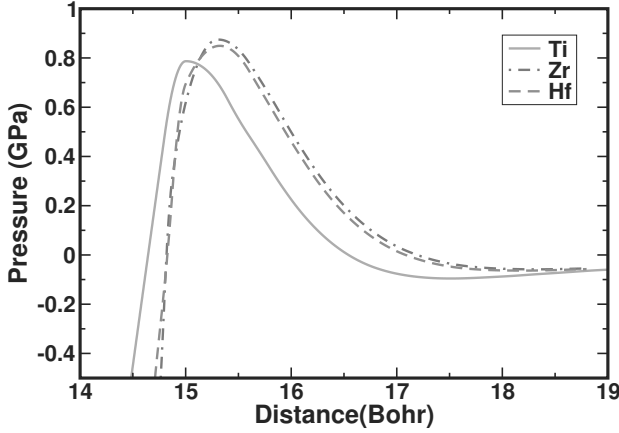


Figure 10.9. Computed pressure as a function of inter-cage distance for the HCP molecular solids Ti@Si_{16} (solid line), Zr@Si_{16} (dash-dotted line) and Hf@Si_{16} (dashed line). The curves were obtained by computing the numerical derivative of the cubic spline fit to the cohesive energy points used to plot Figure 10.8. See Eq. (10.2).

Table 10.5. Bulk modulus for the $X@Si_{16}$ HCP molecular solids with $X=\text{Ti, Zr, Hf}$.

$X@Si_{16}$	Bulk Modulus (GPa)
Ti	1.25
Zr	0.90
Hf	0.97

energy curves and Eq. (10.2). We found that the maxima of the pressure curves are 0.87 GPa for bulk Zr@Si_{16} and 0.85 GPa for bulk Hf@Si_{16} , values $\sim 8\%$ larger than the 0.79 GPa obtained for the bulk Ti@Si_{16} indicating that both bulk Zr@Si_{16} and Hf@Si_{16} are more stable than bulk Ti@Si_{16} against applied pressure. The values for the bulk modulus B , obtained by fitting the Birch-Murnaghan equation of state, Eq. (10.3), to the cohesive energy points are given in Table 10.5.

Quantum Langevin molecular dynamics (QLMD) simulations [31], starting at the Ti@Si_{16} HCP equilibrium structure, suggest that the HCP phase is probably stable at room temperature, as shown in Figure 10.10. QLMD simulations provide a very efficient test of the overall stability of the system, given the feasibility of observing the occurrence of structural phase transitions, whenever they

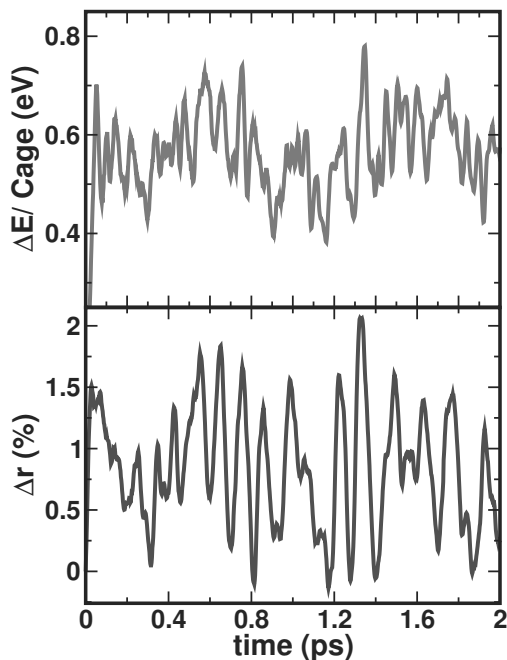


Figure 10.10. Upper Panel: Change of total energy per cage (with respect to equilibrium HCP configuration) as a function of time for a variable cell-shape quantum Langevin molecular dynamics of bulk-Ti@Si₁₆. Simulation started from the HCP structure at a temperature of 300 K. Lower Panel: Time dependence of the percentual deviation (with respect to the equilibrium value) of the average radius of each cage. The results show the small amplitude of the oscillations taking place at room temperature, and suggest the probable stability of this material. The time step used in each iteration is 2×10^{-15} sec, and the simulation ran for a total of 2×10^{-12} sec.

actually take place. QLMD combines some of the advantages of Metropolis Monte Carlo (MC) and MD simulations. By exploiting the energy gradient the atoms move collectively to the minima thereby efficiently sampling the configuration space. This is generally more efficient than a MC procedure where the position of a single atom is updated at each step, followed by a recalculation of the energy. The evaluation of the gradients of the energy, *i.e.*, atomic forces and stress are performed at almost no cost once the energy is determined.

The starting point of the simulation is the equilibrium HCP structure previously determined. Each atom was given an average initial kinetic energy corresponding to a temperature of 300 K. Throughout the simulation the system was in contact with a heat bath at a constant temperature of 300 K. In the top panel

we depict the energy difference (per cage, in eV) between the actual configuration at time t and the equilibrium configuration, where one can observe small oscillations around an average energy value reflecting the fact that the crystal is at finite temperature. In the lower panel we depict the time dependence of the deviation from the equilibrium value of the average cage radius (in percentage). Both numbers illustrate the small amplitude nature of the oscillations taking place [39].

Finally in Figure 10.11 we show the calculated band structures for the three bulk structures determined above. All three molecular solids are semiconductors with indirect band gaps of 1.3 eV (Ti@Si₁₆) and 1.6 eV (Zr@Si₁₆ and Hf@Si₁₆).

10.4 Conclusions

Making use of first principles computer simulations in the framework of DFT, we have investigated the main structural and electronic properties of the isovalent $X@Si_{16}$ ($X=Ti, Zr, Hf$) nano-particles. We showed the feasibility of using these remarkably stable clusters to synthesize molecular solids and we characterized their main structural and electronic properties. Similar to bulk Ti@Si₁₆, we found that bulk Zr@Si₁₆ and Hf@Si₁₆ also crystallize in HCP structures with $\sim 4\%$ larger inter-cage distance, compared to HCP-Ti@Si₁₆. These bulk materials have a phase stability under isotropic compression up to ~ 1 GPa and bulk modulus also ~ 1 GPa. Fully unconstrained QLMD simulations of the bulk structures suggest their stability at room temperature and normal pressure. Our calculations lead to band gaps of 1.6 eV for Zr@Si₁₆ and Hf@Si₁₆. Taking into account that GGA systematically underestimates semi-conductor band gaps it is likely that the true band gap is larger than 2 eV.

The results obtained here suggest an interesting hierarchical rationale for the design of cluster assembled materials. Starting from the well known properties of the atoms, one can design target nanoparticles with pre-defined properties which, as such, are the constituent elements of new bulk materials. Furthermore, as shown here, when the nano-cage nucleates around a central atom, one can use at profit the size of the nucleating atom - via isovalent replacement - to

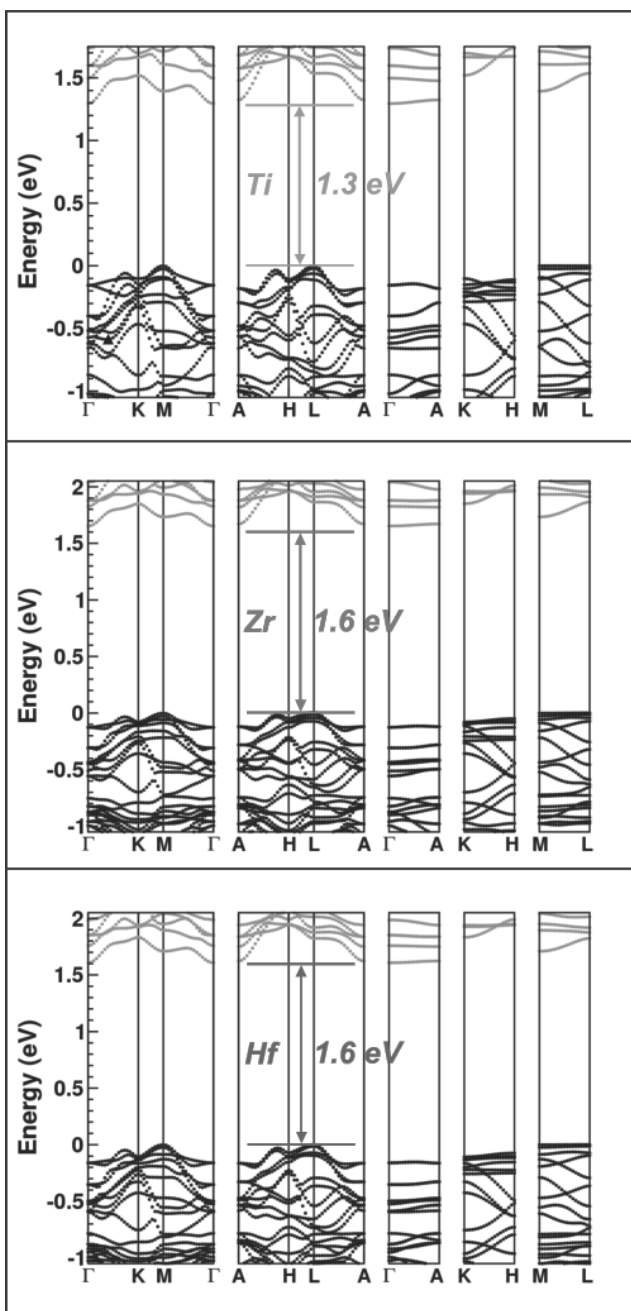


Figure 10.11. Calculated band structures of bulk $X@Si_{16}$ with $X = Ti, Zr, Hf$. These molecular materials are predicted to be indirect gap semiconductors. Both $Zr@Si_{16}$ and $Hf@Si_{16}$ have larger band gaps than $Ti@Si_{16}$.

manipulate the cage size and, consequently, the bulk lattice, with direct implications on the band gap. This provides an additional degree of freedom which may prove very useful in, *e.g.*, the quest for nano-designed, superconducting alloys. Taking fullerite as a model template, to the extent that doped bulk- $X@Si_{16}$ is superconducting, changing the doping element and the nucleating nano-cage atom may provide additional laboratory knobs to tune the superconducting gap. The existence of low frequency intramolecular modes is another strong indicator that appropriately doped bulk- $X@Si_{16}$ can exhibit a remarkable potential as possible high- T_c superconductors. Ongoing calculations of the electron-phonon coupling to these nodes seem to support this. Additionally, the superconducting transition temperature of hypothetical doped bulk materials based on the $X@Si_{16}$ nanoparticles can be accurately predicted by means of computer simulations within the framework of the Migdal-Eliashberg [40–42] theory of phonon mediated superconductivity coupled to DFT. Work along these lines is in progress. We further hope that our results stimulate experiments aiming at synthesizing these materials in the lab [13, 15].

Acknowledgments

Financial support from FCT-Portugal is gratefully acknowledged.

References

- [1] P. Hohenberg and W. Kohn, *Phys. Rev.* **136**, B864 (1964).
- [2] W. Kohn and L. J. Sham, *Phys. Rev.* **140**, A1133 (1965).
- [3] M. John, “Intel Says Chips Will Run Faster, Using Less Power” (New York Times, January 27, 2007).
- [4] M. Schulz, *Nature* **399**, 729 (1999).
- [5] *Clusters and Nanomaterials* Springer Series in Cluster Physics (Springer, Heidelberg, 2002), edited by Y. Kawazoe, T. Kondow, and K. Ohno.
- [6] S. M. Beck, *J. Chem. Phys.* **90**, 6306 (1989); **87**, 4233 (1987).
- [7] S. M. Beck, *Adv. Met. Semicond. Clusters* **1**, 241 (1993).
- [8] H. Hiura, T. Miyazaki, and T. Kanayama, *Phys. Rev. Lett.* **86**, 1733 (2001).

- [9] M. Ohara, K. Koyasu, A. Nakajima, and K. Kaya, *Chem. Phys. Lett.* **371**, 490 (2003).
- [10] K. Koyasu, M. Akutsu, M. Mitsui, and A. Nakajima, *J. Am. Chem. Soc.* **127**, 4998 (2005).
- [11] J. B. Jaeger, T. D. Jaeger, and M. A. Duncan, *J. Phys. Chem. A* **110**, 9310 (2006).
- [12] E. Janssens, P. Gruene, G. Meijer, L. Wste, P. Lievens, and A. Fielicke, *Phys. Rev. Lett.* **99**, 063401 (2007).
- [13] K. Koyasu, J. Atobe, M. Akutsu, M. Mitsui, and A. Nakajima, *J. Phys. Chem. A* **111**, 42 (2007).
- [14] S. Furuse, K. Koyasu, J. Atobe, and A. Nakajima, *J. Chem. Phys.* **129**, 064311 (2008).
- [15] J. T. Lau, K. Hirsch, Ph. Klar, A. Langenberg, F. Lofink, R. Richter, J. Rittmann, M. Vogel, V. Zamudio-Bayer, T. Möller, and B. v. Issendorff, *Phys. Rev. A* **79**, 053201 (2009).
- [16] V. Kumar and Y. Kawazoe, *Phys. Rev. Lett.* **87**, 045503 (2001).
- [17] V. Kumar and Y. Kawazoe, *Phys. Rev. Lett.* **88**, 235504 (2002).
- [18] J. Lu and S. Nagase, *Phys. Rev. Lett.* **90**, 115506 (2003).
- [19] J. U. Reveles and S. N. Khanna, *Phys. Rev. B* **74**, 035435 (2006).
- [20] P. Guo, Z. Y. Ren, A. P. Yang, J. G. Han, J. Bian, and G. H. Wang, *J. Phys. Chem. A* **110**, 7453 (2006).
- [21] M. B. Torres, E. M. Fernández, and L. C. Balbás, *Phys. Rev. B* **75**, 205425 (2007).
- [22] D. Bandyopadhyay, *J. Appl. Phys.* **104**, 084308 (2008).
- [23] G. K. Gueorguiev and J. M. Pacheco, *J. Chem. Phys.* **119**, 10313 (2003).
- [24] S. Zorriasatein, K. Joshi and D. G. Kanhere, *Phys. Rev. B* **75**, 045117 (2007).
- [25] J. M. Pacheco, G. K. Gueorguiev and J. L. Martins, *Phys. Rev. B* **66**, 033401 (2002).
- [26] C. L. Reis, J. L. Martins, and J. M. Pacheco, *Phys. Rev. B* **76**, 233406 (2007)
- [27] J. P. Perdew, K. Burke and M. Ernzerhof, *Phys. Rev. Lett.* **77**, 3865 (1996).
- [28] N. Troullier and J. L. Martins, *Phys. Rev. B* **43**, 1993 (1991).

- [29] X. Gonze, J.-M. Beuken, R. Caracas, F. Detraux, M. Fuchs, G.-M. Rignanese, L. Sindic, M. Verstraete, G. Zerah, F. Jollet, M. Torrent, A. Roy, M. Mikami, P. Ghosez, J.-Y. Raty, and D. C. Allan, *Comp. Mater. Sci.* **25**, 478 (2002).
- [30] X. Gonze, G.-M. Rignanese, M. Verstraete, J.-M. Beuken, Y. Pouillon, R. Caracas, F. Jollet, M. Torrent, G. Zerah, M. Mikami, Ph. Ghosez, M. Veithen, J.-Y. Raty, V. Olevano, F. Bruneval, L. Reining, R. Godby, G. Onida, D. R. Hamann, and D. C. Allan, *Zeit. Kristallogr.* **220**, 558 (2005).
- [31] N. Binggeli, J. L. Martins, and J. R. Chelikowsky, *Phys. Rev. Lett.* **68**, 2956 (1992).
- [32] D. Porezag and M. Pederson, *Phys. Rev. B* **54**, 7830 (1996).
- [33] X. Gonze, *Phys. Rev. B* **55**, 10337 (1997).
- [34] X. Gonze and C. Lee, *Phys. Rev. B* **55**, 10355 (1997).
- [35] F. Birch, *J. Geophys. Res.* **57**, 227 (1952).
- [36] F. C. Frank and J. S. Kasper, *Acta Crystallogr.* **11**, 184 (1958); **12**, 483 (1959).
- [37] S. Kugler, L. Pusztai, L. Rosta, P. Chieux, and R. Bellissent, *Phys. Rev. B* **48**, 7685 (1993)
- [38] N. Troullier and J. L. Martins, *Phys. Rev. B* **46**, 1754 (1992).
- [39] The very demanding nature of the computer simulations ultimately dictates the total QLMD simulation time. Besides the large energy cutoff of 30 Hartree required to ensure convergence of inter-atomic forces, no symmetry was enforced, such that both atomic coordinates and cell shape parameters were allowed to vary simultaneously. The total simulation time of 2 pico-second provides some evidence of the stability of this new molecular crystal. Nonetheless this does not fully warrant, however, its stability.
- [40] G. M. Eliashberg, *Sov. Phys. JETP* **11**, 696 (1960).
- [41] G. M. Eliashberg, *Zh. Eksp. Teor. Fiz.* **38**, 966 (1960).
- [42] D. J. Scalapino, J. R. Schrieffer, and J. W. Wilkins, *Phys. Rev.* **148**, 263 (1966).

(Página deixada propositadamente em branco)

Série
Documentos

•

Imprensa da Universidade de Coimbra
Coimbra University Press

2011

